

**SPATIAL MODELING TO EVALUATE THE IMPACT
INTENSITY OF LANDSLIDE AND FLASH FLOOD IN
HIGHLAND WATERSHED AREA: WITH REFERENCE
TO NAM LI WATERSHED, UTTARADIT, THAILAND**



**A Thesis Submitted in Partial Fulfillment of the Requirements for the
Degree of Doctor of Philosophy in Geoinformatics**

Suranaree University of Technology

Academic Year 2012

การสร้างแบบจำลองเชิงพื้นที่เพื่อประเมินความรุนแรงของผลกระทบ
จากดินถล่มและน้ำท่วมฉับพลันในพื้นที่ลุ่มน้ำบนที่สูง: อ่างอิงพื้นที่ลุ่มน้ำน้ำดี
อุตรดิตถ์ ประเทศไทย



นางสิริลักษณ์ ตะนัง

วิทยานิพนธ์นี้เป็นส่วนหนึ่งของการศึกษาตามหลักสูตรปริญญาวิทยาศาสตรดุษฎีบัณฑิต

สาขาวิชาภูมิสารสนเทศ

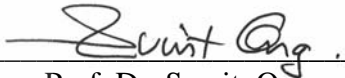
มหาวิทยาลัยเทคโนโลยีสุรนารี

ปีการศึกษา 2555

**SPATIAL MODELING TO EVALUATE THE IMPACT INTENSITY
OF LANDSLIDE AND FLASH FLOOD IN HIGHLAND
WATERSHED AREA: WITH REFERENCE TO NAM LI
WATERSHED, UTTARADIT, THAILAND**

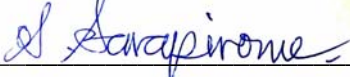
Suranaree University of Technology has approved this thesis submitted in partial fulfillment of the requirements for the Degree of Doctor of Philosophy.

Thesis Examining Committee




(Assoc. Prof. Dr. Suwit Ongsomwang)

Chairperson



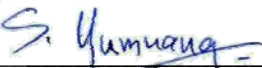
(Asst. Prof. Dr. Sunya Sarapirome)

Member (Thesis Advisor)



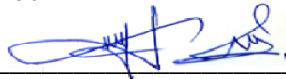
(Asst. Prof. Dr. Songkot Dasananda)

Member



(Asst. Prof. Dr. Sombat Yumuang)

Member




(Dr. Dusdi Chanlikit)

Member



(Prof. Dr. Sukit Limpijumnong)

Vice Rector for Academic Affairs
and Innovation



(Assoc. Prof. Dr. Prapun Manyum)

Dean of Institute of Science

ศิริลักษณ์ ตะนัง : การสร้างแบบจำลองเชิงพื้นที่เพื่อประเมินความรุนแรงของผลกระทบ
จากดินถล่มและน้ำท่วมฉับพลันในพื้นที่ลุ่มน้ำบนที่สูง: อ้างอิงพื้นที่ลุ่มน้ำน้ำลี อุดรดิตถ์
ประเทศไทย (SPATIAL MODELING TO EVALUATE THE IMPACT INTENSITY OF
LANDSLIDE AND FLASH FLOOD IN HIGHLAND WATERSHED AREA: WITH
REFERENCE TO NAM LI WATERSHED, UTTARADIT, THAILAND)

อาจารย์ที่ปรึกษา : ผู้ช่วยศาสตราจารย์ ดร.สัญญา สราภิรมย์, 190 หน้า.

เหตุการณ์ดินถล่มและน้ำท่วมฉับพลันในลุ่มน้ำน้ำลีก่อให้เกิดความเสียหายเป็นอย่างมาก
เนื่องจากลุ่มน้ำดังกล่าวเป็นลุ่มน้ำในที่สูง ไม่มีสถานีตรวจวัดระดับน้ำและปริมาณฝน จึงเป็นการ
ยากที่จะประเมินความรุนแรงจากเหตุการณ์ดังกล่าวได้ การศึกษานี้จึงมีวัตถุประสงค์เพื่อประเมิน
ความรุนแรงของภัยพิบัติดินถล่มและน้ำท่วมฉับพลันด้วยการบูรณาการวิธีทางวิศวกรรมธรณี อุทก
วิทยา และภูมิสารสนเทศ โดยใช้วิธีทางวิศวกรรมธรณีในการประเมิน โอกาสเกิดการพังทลาย
(Probability of Failure) ซึ่งครอบคลุมการวิเคราะห์เสถียรภาพของลาดดิน (Slope stability analysis)
โดยใช้ค่าความปลอดภัย (Factor of Safety, FS) และฟังก์ชันความน่าจะเป็นแบบต่อเนื่อง
(Probability Density Function, PDF) วิธีทางอุทกวิทยาได้ประยุกต์แนวคิดของ Horton โดยใช้
สมการคำนวณหาฝนส่วนเกิน และคำนวณค่าน้ำหลาก (Overland flow, Q) นอกจากนี้ได้ทำการ
ประมาณค่าดัชนีความรุนแรงจากน้ำท่วมฉับพลัน (Flash Flood Impact Intensity Index, FFII) ซึ่ง
เป็นผลรวมของค่าน้ำหลากสะสมและค่าความลึกของน้ำท่วมในพื้นที่เกิดน้ำท่วมฉับพลัน
ผลกระทบโดยรวมจากตะกอนไหล (Debris Flow Impact Intensity Index, DFII) ได้มาจากการ
รวมค่าโอกาสเกิดการพังทลาย ค่าน้ำหลาก และค่าความลึกของน้ำท่วม โดยใช้ฟังก์ชันการวิเคราะห์
เชิงพื้นที่ของโปรแกรม ArcGIS พื้นที่ที่มีค่า DFII สูงแสดงให้เห็นว่ามีศักยภาพในการถูกทำลายสูง
หลักฐานจากการสำรวจภาคสนามใช้เป็นข้อมูลตรวจสอบความถูกต้องและความสมเหตุสมผลของ
ผลการศึกษา

สาขาวิชาการรับรู้อาการระยะไกล
ปีการศึกษา 2555

ลายมือชื่อนักศึกษา

ลายมือชื่ออาจารย์ที่ปรึกษา

SIRILAK TANANG : SPATIAL MODELING TO EVALUATE THE
IMPACT INTENSITY OF LANDSLIDE AND FLASH FLOOD IN
HIGHLAND WATERSHED AREA: WITH REFERENCE TO NAM LI
WATERSHED, UTTARADIT, THAILAND. THESIS ADVISOR :
ASST. PROF. SUNYA SARAPIROME, Ph.D. 190 PP.

LANDSLIDE/ FLASH FLOOD/ SLOPE STABILITY ANALYSIS/ PROBABILITY
OF FAILURE/ INFILTRATION EXCESS/ IMPACT INTENSITY MODELING

Landslide and flash flood catastrophic phenomenon in Nam Li watershed caused severe damage to human lives and properties. It is difficult to evaluate hazardous intensity, because the Nam Li watershed is an unguage highland watershed. This study attempts to evaluate both landslide and flash flood hazardous intensity by integrated 3 techniques including geotechnical, hydrology, and geoinformatics. By geotechnical method, slope stability analysis applied the concept of Factor of Safety (FS) and Probability Density Function (PDF) to estimation of Probability of Failure Index (PFI). Horton's concept was applied to assess rainfall excess and overland flow (Q). Flood depth in flood area and Q were used to derive the flash flood impact intensity index (FFIII). Finally, Debris Flow Impact Intensity Index (DFIII) was incorporated from PFI, overland flow, and flood depth using ArcGIS spatial analytical functions. The area with higher DFIII indicated higher potential of damage capability. The study results were validated by evidences from field investigation.

School of Remote Sensing

Academic Year 2012

Student's Signature

S. Tanang

Advisor's Signature

S. Sarapirome

ACKNOWLEDGEMENTS

This work has been done with a great contribution from many people and their assistance must be extremely appreciated. It is a pleasure to convey my gratitude to them all.

In the first place I would like to express my deep gratitude to my Advisor, Asst. Prof. Dr. Sunya Sarapirome, for his supervision, advice, helps with valuable instructions, guidance and suggestions, for his effort to edit and to complete this dissertation, and his moral support during the study periods. Without his constructive devotion and support, this dissertation would not be finished successfully. Additionally, I would like to thank all of my SUT lecturers and Asst. Prof. Chatchai Tantasirin of Kasetsart University for their helpful instruction and recommendation.

I would also very grateful to the chairman and other members of the dissertation committee, Assoc. Prof. Dr. Suwit Ongsomwang, Asst. Prof. Dr. Songkot Dasananda, Asst. Prof. Dr. Sombat Yumuang, and Dr. Dusdi Chanlikhit for their constructive comments.

I would like to express thank to Suranaree University of Technology (SUT) and the Commission on Higher Education for providing the Royal Thai Government Scholarship for supporting my research during Ph.D. studying periods.

I would also like to appreciate the Geo-Informatics and Space Technology Development Agency (GISTDA), the Land Development Department (LDD), the Department of Mineral Resources (DMR), The Royal Thai Survey Department

(RTSD), and the Thailand Meteorological Department (TMD) for providing and supporting data. My special thanks also go to Mrs. Lucksawan Horsin and all officers of Nam Li Watershed Management Unit for their helps and supports on field surveying.

I would also like to thank all of my friends in school of Remote Sensing and all of my colleagues in Institute of Science, Geomachanic Research Unit, and the Center for Scientific and Technological Equipment at SUT for all their helps.

Last but not least, thanks to all of former, my relatives, and my friends for their great kindness and supporting. I whole-heartedly thank to my father, my mother, and my son for keeping their health, who have been great enduring source of inspiration to grow academically and professionally, and their undying love.

Sirilak Tanang



CONTENTS

	Page
ABSTRACT IN THAI.....	I
ABSTRACT IN ENGLISH	II
ACKNOWLEDGEMENTS.....	III
CONTENTS.....	V
LIST OF TABLES.....	XI
LIST OF FIGURES	XIII
LIST OF ABBREVIATIONS.....	XVII
CHAPTER	
I GENERAL INTRODUCTION.....	1
1.1 Background and significance of the study.....	1
1.2 Research objectives.....	6
1.3 Scope and limitations of the study	7
1.3.1 Scope of the study	7
1.3.2 Limitations of the study.....	8
1.4 Conceptual model of the study.....	9
1.5 Benefits of the results.....	10
1.6 Structure of the thesis.....	11
1.7 References	11

CONTENTS (Continued)

	Page
II LITERATURE REVIEW	16
2.1 Definition and terminology	16
2.1.1 Landslide	16
2.1.2 Slope stability and factor of safety	20
2.1.3 Probability of failure	22
2.1.4 Flash flood	23
2.1.5 Overland flow	25
2.1.6 Debris flow	26
2.1.7 Impact intensity	27
2.2 Landslide studies	28
2.2.1 Geotechnical engineering method	28
2.2.2 Spatial modeling	33
2.3 Flooding studies	37
2.3.1 Hydrological model	38
2.3.2 Other methods	41
2.4 Synthesis for the research approach	42
2.4.1 Landslide susceptibility assessment	42
2.4.2 Flash flood occurrence assessment	44
2.5 References	45
III CHARACTERISTICS OF THE STUDY AREA	57
3.1 Location	57

CONTENTS (Continued)

	Page
3.2 Climate and precipitation	58
3.3 Land use and land cover (LU/LC)	60
3.4 Slope	62
3.5 Geology	63
3.6 References	69
IV LANDSLIDE SUSCEPTIBILITY MODELING	70
4.1 Abstract	70
4.2 Introduction	71
4.3 Research methods	73
4.3.1 Research procedure	73
4.3.2 Slope stability analysis	74
4.3.3 Probability of failure assessment	77
4.4 Data collection and data preparation	79
4.4.1 SPOT imagery and landslide scars layer	79
4.4.2 Digital elevation model and slope layer	83
4.4.3 Rock properties data and geologic layer	84
4.5 Result and discussion	87
4.5.1 Landslide susceptibility index	87
4.5.2 Probability failure index	90
4.6 Conclusion	99
4.7 References	101

CONTENTS (Continued)

	Page
V FLASH FLOOD IMPACT INTENSITY MODELING	105
5.1 Abstract	105
5.2 Introduction	106
5.3 Research methods	107
5.3.1 Research procedure	107
5.3.2 Rainfall intensity analysis and infiltration measurement	108
5.3.3 Overland flow (Q) analysis	111
5.3.4 Flood scars surface estimation	113
5.3.5 Flash flood susceptibility assessment	114
5.3.6 Flash flood impact intensity assessment	115
5.4 Data collection and preparation	115
5.4.1 Rainfall input data	115
5.4.2 Infiltration input data	118
5.4.3 Land use and land cover map	123
5.4.4 Flash flood scars extraction	124
5.5 Results and discussion	128
5.5.1 Relation of infiltration and precipitation	128
5.5.2 Overland flow assessment	132
5.5.3 Flash flood scar surface and flood depth estimation	139
5.5.4 Flash flood susceptibility index	143
5.5.5 Flash flood impact intensity index	149

CONTENTS (Continued)

	Page
5.6 Conclusion	151
5.7 References	152
VI DEBRIS FLOW IMPACT INTENSITY INDEX.....	155
6.1 Abstract	155
6.2 Introduction.....	156
6.3 Research methods	157
6.3.1 Research procedure	157
6.3.2 Data preparation	158
6.3.3 Debris flow accumulated index evaluation	161
6.3.4 Debris flow impact intensity determination	161
6.4 Result and discussion	161
6.4.1 Debris flow accumulation index	161
6.4.2 Debris flow impact intensity index	163
6.5 Conclusion	172
6.6 References	172
VII CONCLUSION AND RECOMMENDATIONS	174
7.1 Conclusion	174
7.2 Recommendations	175
APPENDICES	176
APPENDIX A LANDSLIDE CLASSIFICATION	177

CONTENTS (Continued)

	Page
APPENDIX B INFINITE SLOPE STABILITY ANALYSYS	181
APPENDIX C ROCK MECHANICS TESTING.....	183
APPENDIX D THE FITTING RATIO CALCULATION.....	185
APPENDIX E RAINFALL DATA	188
CURRICULUM VITAE.....	190



LIST OF TABLES

Table	Page
1.1 Major landslide occurrences in Thailand during 1988-2006	2
1.2 Examples of previous landslide hazard studies in Thailand	3
1.3 Examples of previous flood hazard studies in Thailand	3
2.1 A classification of landslide mechanisms, compatible with Hutchinson (1988) and EPOCH (1993)	18
2.2 The examples of studies using the Geotechnical engineering method	33
3.1 The stratigraphy of the study area	64
4.1 Geotechnical properties of rocks of 4 geologic units in the study area	84
4.2 The classes of related rock and terrain properties used for LSI calculation ...	85
4.3 The LSIs associated and the ratio between sensitive cells and scar cells	89
4.4 The results of slake durability index testing	89
4.5 The LSIs become candidates to be a critical LSI	90
4.6 The fitting ratios of all candidate critical LSIs	95
5.1 The rainfall data during May 20-23, 2006	117
5.2 15 Horton equations of unique unit of LULC and geology	123
5.3 The 3 hours rainfall of the event during May 19-23, 2006	129
5.4 The 57 infiltration rate of 1 hour intervals in 15 sampling sites	131
5.5 The result of overland flow calculation	133

LIST OF TABLES (Continued)

Table	Page
5.6 The accumulated overland flow at the outlet of each duration and their increasing ratios	138
6.1 Q_{prob} in different LU_GU units of the study area	160
A.1 Classification of landslide suggested by Varnes (1978).....	178
A.2 Classification of landslide and down slope movements by Keller (2002)....	178
A.3 Classification of landslide suggested by Hutchinson (1988).....	179
A.4 Classification of landslide suggested by EPOCH (1993)	180
D.1 The fitting ratio calculation of C unit	185
D.2 The fitting ratio calculation of P1 unit.....	186
D.3 The fitting ratio calculation of gr unit.....	186
D.4 The fitting ratio calculation of Tr1 unit	187

LIST OF FIGURES

Figure	Page
1.1 The conceptual model of the study.....	10
2.1 The planar failure surface and translational movement.....	19
2.2 Definition of infinite slope stability.....	21
2.3 The plot of probability density function and safety margin.....	23
2.4 The flash flood occurred on May 23, 2006 in Nam Li watershed.....	25
3.1 Location of the study area.....	58
3.2 The precipitation intensity of Nam Li watershed during years 2005, 2006, and 2007.....	59
3.3 The land cover map in year 2004.....	60
3.4 The modified land cover map of the study area in year 2007.....	61
3.5 The characteristic scales of slope in the study area.....	62
3.6 The geologic units of the study area.....	63
3.7 Examples of field investigation outcrops.....	65
3.8 The modified geological map of the study area.....	68
4.1 The procedure framework of landslide susceptibility modeling.....	74
4.2 The procedure framework of slope stability analysis.....	76
4.3 The procedure framework of landslide impact intensity assessment.....	79
4.4 The landslide scars extraction from the SPOT5 imagery.....	81
4.5 The examples of landslide scar check points.....	82

LIST OF FIGURES (Continued)

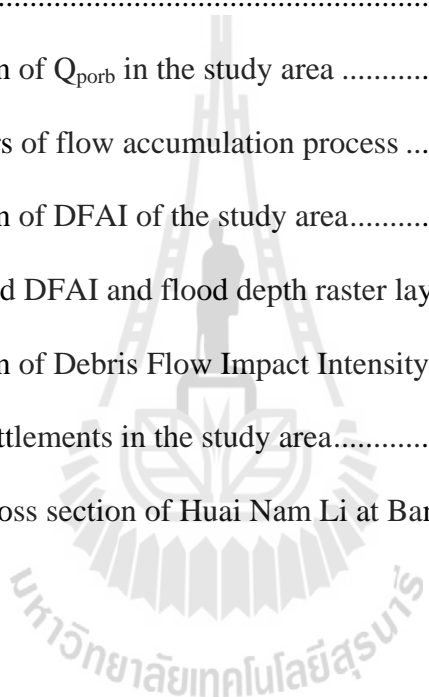
Figure	Page
4.6 Steps of slope layer preparation.....	83
4.7 Slope Layer	83
4.8 Geologic units layer	86
4.9 Frequency of sensitive and scar areas according to candidate critical LSIs	88
4.10 The candidates of a critical LSI and the PFI-1 raster layers	91
4.11 Variation of fitting ratios according to candidate critical LSIs.....	96
4.12 The distribution of landslide scars and PFI-1 of all critical LSIs.....	96
4.13 The distribution of Probability Failure Indexes (PFIs) classes in Nam Li watershed	97
4.14 The cell-based and percentage of scar and class areas including their associating ratio	98
5.1 The procedure framework of flash flood impact intensity modeling.....	108
5.2 The relation of $\log_{10} (f_t - f_c)$ and time.....	110
5.3 Hortonian concept of overland flow generation	111
5.4 The procedure to extract DEM of flash flood scar surface	114
5.5 The daily rainfall intensity duration curve in May 2006 from stations within the study area and the surroundings.....	116
5.6 The location of rain gauge stations around the study area.....	116
5.7 The equipment used for infiltration testing.....	118
5.8 The test procedure of single ring infiltrometer	119

LIST OF FIGURES (Continued)

Figure	Page
5.9 15 sampling sites of single ring infiltrometer tests	120
5.10 The combination units of LULC and geology of the study area	124
5.11 The flash flood scars extracted from SPOT5 imagery	125
5.12 Photographs illustrating the actual location of flash flood scars	126
5.13 Photographs illustrating the current mud traces of flash flood event.....	127
5.14 The 3 hours rainfall intensity duration curve on May 21-23, 2006.....	130
5.15 The relation between rainfall intensity and infiltration of 15 sampling sites in semi-logarithm scale	132
5.16 The raster layers of candidate suitable overland flow (Q).....	134
5.17 The accumulated overland flow raster layers	136
5.18 The increasing ratio of accumulated Q of 18 durations	138
5.19 The example of cross section of DEM in flood scars	140
5.20 The elevation of flood surface	141
5.21 The flood depth in flood scar area	142
5.22 The frequency of Q_{ac} cells corresponding to Q_{ac} values	144
5.23 The distribution of Q_{ac} of Nam Li watershed	145
5.24 The distribution of FFSI in Nam Li watershed.....	147
5.25 The 4 classes of Flash Flood Susceptibility index (FFSI)	148
5.26 The transformed layers before operated impact intensity accumulation	149
5.27 The distribution of FFIII	150

LIST OF FIGURES (Continued)

Figure	Page
6.1	The procedure framework of landslide and flash flood impact intensity evaluation 158
6.2	The PFIs layer 159
6.3	The distribution of Q_{porb} in the study area 160
6.4	The input layers of flow accumulation process 162
6.5	The distribution of DFAI of the study area..... 162
6.6	The interpolated DFAI and flood depth raster layers of the study area..... 163
6.7	The distribution of Debris Flow Impact Intensity Index (DFIII)..... 164
6.8	The 4 major settlements in the study area..... 165
6.9	The SE-NW cross section of Huai Nam Li at Ban Nam Ri..... 171



LIST OF ABBREVIATIONS

CR	=	Coefficient of Reliability
DEM	=	Digital Elevation Model
DFII	=	Debris Flow Impact Intensity
DFIII	=	Debris Flow Impact Intensity Index
DMR	=	Department of Mineral Resource
FFIII	=	Flash Flood Impact Intensity Index
FFSI	=	Flash Flood Susceptibility Index
FR	=	Fitting Ratio
FS	=	Factor of Safety
GIS	=	Geographic Information System
GISTDA	=	Geo-Informatics and Space Technology Development Agency (Public Organization)
LDD	=	Land Development Department
LIII	=	landslide Impact Intensity Index
LSI	=	Landslide Susceptibility Index
LU/LC	=	Land Use and Land Cover
PDF	=	Probability Density Function
PF	=	Probability of Failure
PFI	=	Probability of Failure Index
RID	=	Royal Irrigation Department

LIST OF ABBREVIATIONS (Continued)

MSL	=	Mean Sea Level
TIN	=	Triangulated Irregular Network
TMD	=	Thai Meteorological Department
TWI	=	Topographic Wetness Index
USGS	=	U.S. Geological Survey
UTM	=	Universal Transverse Mercator



CHAPTER I

GENERAL INTRODUCTION

1.1 Background and significance of the study

Most landslide occurrences in Thailand are debris flows, which cause severe damage to structures and infrastructure and often claim human lives. Suttisak Soralump and Wisut Chotikasathien (2007) showed an example of landslide of Thailand database in a Geographic Information System (GIS) format during years 1970 to 2006 which was developed by Geotechnical Engineering Research and Development center (GERD), Kasetsart University. Most events occurred in the northern and the southern of Thailand which are mountainous areas. Moreover, the record of the Department of Mineral Resource (DMR) during years 1988 to 2006 presented 17 landslide and muddy-debris flow events in which more than 1,000 people were killed and lost as listed in Table 1.1.

Debris flow is the mixture of water, mud, sand, rock and driftwood. The debris flow and flash flood usually occur together and are triggered by heavy rainfall. This results in severe damages on land. In general, existing researches on landslide and flash flood in Thailand have been studied separately. Most of the studies are different in methods, the utilization of factors, and types of model. Some examples of the studies from various agencies are shown in Tables 1.2 and 1.3.

Table 1.1 Major landslide occurrences in Thailand during 1988-2006.

Date	Site	Lost of life and property damage
22 Nov 1988	Ban Kratun Nua, Amphoe Phipun, Nakhon Si Thammarat	- 230 people dead and injured - 1500 houses damaged - 9.84 km ² agriculture areas damaged - 1,000 million baht approximately cost
22 Nov 1988	Ban Khiriwong, Amphoe LanSaka, Nakhon Si Thammarat	- 12 people dead - 152 houses damaged - 210 partial houses damaged
30 July 1999	King Amphoe Khao Khitchakut, Chanthaburi	- people were moved before happening - cattle and agriculture areas damaged
11 Sep 2000	Ban Than Tip, Amphoe LomSak and Ban Pho Ngoen, Amphoe Mueang, Phetchabun	- 10 people dead and 2 people lost - 363 houses damaged - cattle and agriculture areas damaged
4 May 2001	Amphoe Wang Chin, Phrae	- 43 people dead and 4 people lost - 18 houses damaged - cattle and agriculture areas damaged - 100 million baht approximately cost
11 Aug 2001	Tambon Nam Ko, Amphoe Lom Kao, Phetchabun	- 136 people dead - 109 people injured and 4 people lost - 188 houses damaged - 441 partial house damaged - 645 million baht approximately cost
15 Sep 2002	Ban Nam Mae Rak, Amphoe Mae Chaem, Chiang Mai	- 180 household were moved before - Mae Cham – Hot highway damaged
6 May 2004	Ban Kong Bod, Tambon Pang Hin Fon, Amphoe Mae Chaem, Chiang Mai	- 1 people dead - 3 houses damaged
20 May 2004	Mon Chong Tambon Mae Tuen and Tambon Yang Piang, Amphoe Om Koi, Chiang Mai	- 1 people dead - 100 people of 120 household in 4 Tambon 14 Muban were distressed
20 May 2004	Tambon Mae Tuen, Kha Na Chue and Mae Charao, Amphoe Mae Ramat, Tak	- 5 people dead and 391 people injured - 8,846 people of 2,135 household in 4 Tambon 16 Muban were distressed
22 May 2004	Ban Sop Khong, Tambon Mae Suad, Amphoe Sop Moei, Mae Hong Son	- 100 house damaged - 400 people of 120 household were distressed
17 Oct. 2004	Tambon Ao Nang, Amphoe Mueang, Krabi	- 14 guesthouse damaged - 10 million baht approximately cost
18 Oct 2004	Ban Huai Som Fai, Tambon Khao Kham, Amphoe Mueang, Krabi	- 3 people dead and 1 people injured - 25 houses damaged
12 Dec 2004	Amphoe Than To, Yala	- 2 people dead and 1 house damaged - Yala-Betong highway damage
20 Dec 2005	Tambon Da No Pu Te, Amphoe Bannang Sata, Yala	- 18 houses damaged - 55 partial house damaged
23 May 2006	Amphoe Laplae, Amphoe Tha Pla, Amphoe Mueang, Uttaradit, Amphoe Si Satchanalai, Sukhothai and Amphoe Mueang, Phrae	- Uttaradit, 71 people dead and 32 people lost - Sukhothai, 7 people dead and 1 people lost - Phrae, 5 people dead
9 Oct 2006	Ban Yang, Tambon Mae Ngon, Amphoe Fang, Chiang Mai	- 8 people dead - 29 houses damaged

Source: Department of Mineral Resource (2011).

Table 1.2 Examples of previous landslide hazard studies in Thailand.

Method/Organization	Year	Feature based	Factors related to landslide															
			1	2	3	4	5	6	7	8	9	10	11	12	13	14	15	16
1. Index model																		
1.1 LDD	2005	2		✓			✓					✓		✓	✓	✓		
1.2 DMR	2006	2		✓	✓				✓	✓		✓	✓	✓				
1.3 CU	2005	1	✓	✓				✓			✓	✓		✓				
1.4 FRC	2006	2	✓	✓							✓			✓		✓		
1.5 SUT	2006	1	✓	✓	✓	✓			✓		✓			✓				
2. Geotechnical method																		
2.1 LDD	2006	1	✓	✓	✓						✓		✓	✓	✓			
2.2 GERD	2007	3	✓	✓								✓	✓	✓	✓	✓		

Feature based 1. Cell-based 2. Polygon-based 3. Point-based

Factors used in the studies

- | | | | |
|----------------------|----------------------|---|-------------------------------|
| 1. Geology/lithology | 5. Morphology | 9. Soil type/soil series | 13. Land use/land cover |
| 2. Slope and aspect | 6. Stream proximity | 10. Soil thickness | 14. Watershed characteristics |
| 3. Elevation | 7. Flow direction | 11. Soil moisture/ liquid limit of soil | 15. Rainfall |
| 4. Lineament | 8. Flow accumulation | 12. Engineering soil properties | 16. Groundwater |
- Remark LDD = Land Development Department, DMR = Department of Mineral and Resources,
 CU = Chulalongkon University, SUT = Suranaree University of Technology,
 FRC = Forest Research Center, GERD = Geotechnical Engineering Research and Development Center

Table 1.3 Examples of previous flood hazard studies in Thailand.

Method/Organization	Year	Feature based	Factors/data													
			1	2	3	4	5	6	7	8	9	10	11	12	13	14
1. Weather monitoring																
1.1. LDD	2004	3		✓									✓	✓		
1.2. RID	2007	3	✓	✓										✓		
2. Index model																
2.1. RID	2006	2	✓		✓	✓	✓	✓		✓	✓	✓				
2.2. PSU	2007	2	✓		✓	✓	✓	✓			✓					
3. Hydraulic model																
3.1. KKU	2006	2								✓	✓	✓			✓	✓

Feature based 1. Cell-based 2. Polygon-based 3. Point-based

Factor related to flash flood/flood

- | | | | |
|----------------------|--------------------------------------|----------------------------|---------------------------|
| 1. Rainfall | 5. Drainage density | 9. Land use/land cover | 13. Channel cross section |
| 2. Runoff | 6. Soil Type/Soil texture | 10. Soil drainage | 14. Flow rate |
| 3. Slope | 7. Flow direction/ Flow accumulation | 11. Geomorphology | |
| 4. Size of watershed | 8. Infrastructures (road, dam) | 12. Radar/Satellite images | |
- Remark LDD = Land Development Department, RID = Royal Irrigation Department,
 PSU = Prince of Songkhla University, KKU = KhonKan University.

The existing researches on landslide in Thailand are carried out on different methods and concepts. In Table 1.2, more landslide hazards were studied by using index model (e.g. Land Development Department (กรมพัฒนาที่ดิน, 2547); Sree Teerarungsikul, 2006) and univariant probability method (e.g. Sombat Yumuang, 2005) which was later defined the relationship with relevant parameters. Some geotechnical methods were applied, e.g. Surin Waicharoen (สุรินทร์ ไวกจริญ, 2549), Suttisak Soralump and Wisut Chotikasathien (2007), and worked on more site investigation than on larger area evaluation. In other countries such as China, Korea, Malaysia, and Canada also used occurrence frequency ratio and logistic regression model to determine landslide susceptibility areas (Dai, Lee, Li, and Xu, 2000; Lee, 2004; Lee and Pradhan, 2006; Chen and Wang, 2007; Meisina and Scarabelli, 2007). In recent years, the application of simplified slope stability models has effectively proved as descriptive and predictive tools in temperate zones, allowing for rapid stability assessment over a wide area (Montgomery and Dietrich, 1994; Pack, Tarboton, Goodwin, and Prasad 1998; Zaitchik and Vas Es, 2003; Zaitchik, Van Es, and Sullivan, 2003; Mergili and Fellin, 2009).

From Table 1.3, the flood hazard maps in Thailand have been generally created by index model and hydrodynamic module such as MIKE 11 and HEC-GeoRAS. Weather monitoring is the simple method which was used to warn flooding as well. The existing research about spatial analysis in other countries such as Italy, Spain, USA, China, and Korea also used Hydrometeorological Analysis (Borga, Boscolo, Zanon, and Sangati, 2007), rain fall monitoring (Yates, Warner, and Leavesley, 2000; Cremonini and Bechini, 2010), rainfall-runoff model (Zhenghui, et. al,

2003; Zhan and Huang, 2004; Kim and Choi, 2011), numerical analysis (Martín, Romero, De Luque, Alonso, Rigo, and Llasat, 2007) and infiltration rate for water management (Talaat, 2009). The various methods have similar aim that is finding the flash flood sensitivity area prediction or forecasting.

The researches on landslide and flash flood in events are different in area characteristics and causes. Some areas have either landslide or flash flood occurrence but some the occurrence could be both. The association of both of landslide and flash flood occurrence is known as “debris flow”. In general, the relevant parameters, score, and weight of criteria for index calculation are more subjective or arbitrary and more likely to depend on the uncertain expert-claimed opinions.

A catastrophic phenomenon in Nam Hman Subdistrict, Tha Pla District of Uttaradit Province occurred on May 22, 2006. The Asian Disaster Preparedness Center (2006) and Uttaradit Provincial Office (จังหวัดอุตรดิตถ์, 2549) reported a 24 hours rainfall of 264 mm. As a result, 29 were killed, 24 lost, 20 injured, 106 houses damaged, and 56 partial houses damaged. The houses were swept away and other infrastructures, such as roads, bridge, drainage system, and agriculture areas were damaged. Nam Li watershed was another severe damaging place in this event which included both flash flood and landslide.

The landslide and flash flood in Nam Li watershed related to heavy rainfall. The landslides were triggered by heavy rainfall and flash floods were occurred by the surface water excess. The landslide and flash flood event are different processes but can occur together. When landslide and flash flood occurred, the material from landslide and water from flash flood become debris flow to downstream and impact on land surface along their movement path. Since landslide and flash flood frequently

occurred together, for a case like this, the intensity evaluation of catastrophe from both landslide and flash flood should be done together.

The author attempted to integrate 3 techniques including hydrologic, geotechnical, and geoinformatic approaches to study impact intensity of both landslide and flash flood occurrence in the study area. The objective of the study is other word to determine the landslide and flash flood impact intensity of these highland watersheds using cell-based analysis and their accumulation.

1.2 Research objectives

Main objective of the research is to evaluate the potential hazardous intensity of the study area caused by both flash flood and landslide using a GIS cell-based and the accumulation technique and this can be summarized as follows:

(1) to apply the factor of safety and probability of failure calculated using the slope stability model and probability density function to evaluate the landslide susceptibility of the study area;

(2) to apply the overland flow calculated using the infiltration excess model to evaluate the flash flood impact intensity of the study area; and

(3) to spatially model to evaluate the total index of flash flood and landslide impact intensity in terms of debris flow impact intensity using the cell-based GIS accumulation technique.

1.3 Scope and limitations of the study

This study attempted to integrate hydrology, geotechnology, and geoinformatics through the geospatial modeling. The real world process is simulated by geospatial modeling through the spatial input data sets. The spatial input data sets are the cell-based raster layers which contain the attribute data of each relevant theme. The efficiency of geospatial modeling for flash flood and landslide evaluation depends upon the limitations of remote sensing data, map data, non-spatial data, and models themselves.

1.3.1 Scope of the study

1.3.1.1 Spatial model

The study of landslide based on the factor of safety value estimated from the slope stability model that is the equations involved the Mohr-Coulomb failure criterion. The applied equations in flash flood modeling include infiltration excess and overland flow. The Horton's equation through the infiltration rate was used for infiltration excess calculation and the overland flow using Horton's concept.

1.3.1.2 Landslide and flash flood scars interpretation

The landslide and flash food scars were extracted from SPOT5 imagery on January 13, 2007, scene ID (K-J) 260-314 (Copyright 2007© GISTDA). The criterion for landslide scars visual interpretation was the false color composite image, set at the scale of 1:4,000, that displays the color representing white and bright color as scars and the scar cells of each has to be not less than 64 cells. The flash flood scars were extracted by comparison between SPOT5 imagery acquired after May 21, 2006 and orthophotograph acquired before May 21, 2006. The white and bright color in drainage channels and the vicinity which showed in

SPOT5 imagery but they were covered by vegetation and building in orthophotograph are the flash flood scars. The accuracy of landslide and flash flood scars were verified by field check.

1.3.1.3 Engineering properties of rock

The set of rock properties as input data for the analysis were adopted from the researches and the records of Goodman (1989), Wyllie and Mah (2004), and Alden (2010) by matching rock types and characteristics. The Mae Tha group was selected to be a sample for direct shear testing to determine cohesion and friction angle, because a number of landslide scars was obviously occurred in this unit. The rock hardness was classified by point load strength index testing. The weathering and degradation characteristics of rocks were determined by the slake durability index testing.

1.3.1.4 Infiltration rate testing

The single ring infiltrometer with 25 cm diameter and 20 cm height was used for initiated water height testing to determine the infiltration rate of each combination of geologic unit and land use. The testing step followed Farrell (2010)'s experiment.

1.3.1.5 Field investigation

The evidences from the field investigation included rocks outcrop, vegetation, and agricultural area were used to modify geologic map and LU/LC map. The landslide scars and flash flood scars were used to verify the scars interpretation.

1.3.2 Limitations of the study

1.3.2.1 Remote sensing data

The requirement of remote sensing data would show the clearer appearance of land cover, landslide scars, and flash flood scars. The SPOT5 imagery

with 5 meters resolution after May 21, 2006, and the digital color orthophotomaps, the Ministry of Agriculture and Co-operatives (MOAC), at the scale of 1:25,000 before flash flood and landslide occurrence (before May 21, 2006) are selected.

1.3.2.2 Map data

The map layers comprise LU/LC map from the LDD and geologic map from the DMR at the scale of 1:50,000. They will be collected and prepared to be vector layers of input variables. DEM layer with 5×5 cell size will be generated using contour data of the scale 1:4,000 and 5 meter contour data which are created by the LDD. This cell size will agree with resolution of SPOT5 imagery.

1.3.2.3 Non-spatial data

The non-spatial data are the variables and will be used in the slope stability analysis and overland flow analysis. These data will be obtained from various sources such as the Geomechanics Research Unit, Suranaree University of Technology, field measurements, exiting reports, and exiting records.

1.4 Conceptual model of the study

This research aims to combine 2 analyses, slope stability and overland flow, by using GIS cell-based accumulation technique to evaluate potentially hazardous intensity in highland watersheds. Most of landslide and flash flood phenomena are triggered by heavy rainfall. In nature, within the same spatial domain the impact intensity of landslide and flash flood will increase from upstream to downstream by their accumulation. Considering from cell to cell, the accumulation degree of each of their impacts should be performed and integrated towards downstream. It results in

providing indexes reflecting both flashflood and landslide impact intensity of the downstream areas as shown in Figure 1.1.

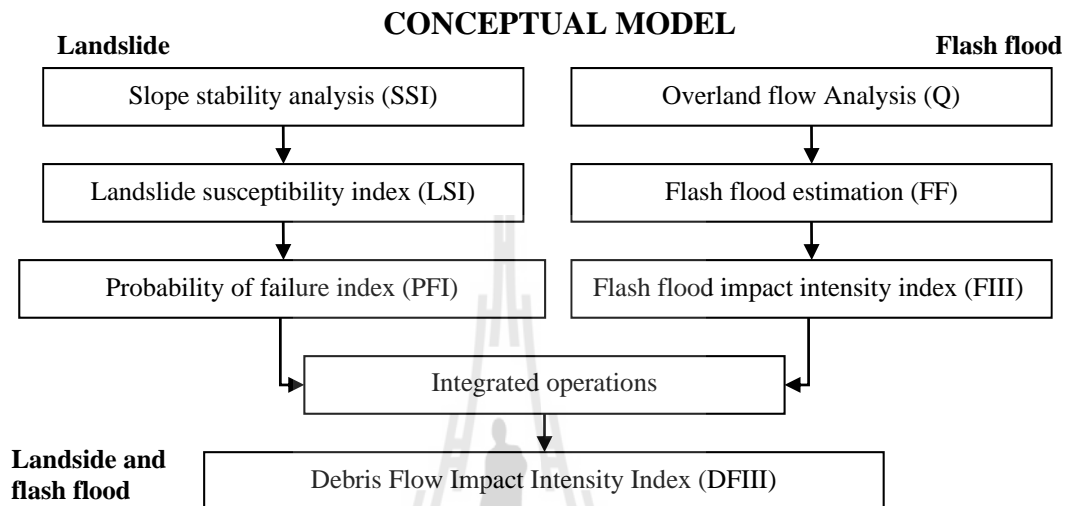


Figure 1.1 The conceptual model of the study.

1.5 Benefits of the results

(1) The procedure to evaluate impact intensity of both flash flood and landslide occurrence in highland watershed that can be applied to other areas with similar geographic characteristics.

(2) The raster layers of Debris Flow Impact Intensity Index (DFIII) indicating spatially impact intensity of both hazards in the study area. This can be further used for area management, warning and mitigation planning.

1.6 Structure of the thesis

This thesis comprises 7 chapters. The Chapter I is for introduction. Chapter II is literature reviews that are the basic concepts on landslide and flash flood occurrence and the previous literatures related to techniques for landslide and flash flood evaluation. The characteristics of the study area including location, climate and precipitation, land use and land cover, slope, and geology are given in Chapter III.

The landslide susceptibility modeling in Chapter IV presents the research method including slope stability analysis and probability of failure assessment. In this Chapter, input data preparation is presented including landslide scars, slope layer, and rock properties. For flash flood impact intensity modeling in Chapter V, the input data collection and preparation including rainfall intensity, infiltration rate, and flood scars are presented. The research method including infiltration analysis, overland flow analysis, flood surface estimation, flash flood susceptibility analysis, and flash flood impact intensity analysis are presented in Chapter V. The spatial analysis for the impact intensity caused by debris flow which is formed from landslide and flash flood is presented in Chapter VI.

1.7 References

กรมพัฒนาที่ดิน. (2547). **พื้นที่เสี่ยงต่อการเกิดดินถล่มและอุทกภัยในประเทศไทย**. กรมพัฒนาที่ดิน กระทรวงเกษตรและสหกรณ์.

จังหวัดอุตรดิตถ์. (2549). **สรุปสถานการณ์อุทกภัยและการช่วยเหลือผู้ประสบภัยจังหวัดอุตรดิตถ์ [ออนไลน์]**. ได้จาก: <http://ww.uttaradit.go.th/flood.doc>.

- สุรินทร์ ไวกเจริญ. (2549). การวิเคราะห์พื้นที่ที่มีความเสี่ยงจากดินถล่มในประเทศไทย. สถาบันวิจัยพัฒนาและป้องกันการเป็นทะเลทรายและการเตือนภัย กรมพัฒนาที่ดิน กระทรวงเกษตรและสหกรณ์.
- Alden, A. (2010). **Density of Common Rock Type** [On-line]. Available http://geology.about.com/cs/rock_types/a/aarockspeggrav.htm.
- Borga, M., Boscolo, P., Zanon, F., and Sangati, M. (2007). Hydrometeorological Analysis of the 29 August 2003 Flash Flood in the Eastern Italian Alps. **Journal of Hydrometeorology**. 8(5): 1049-1067.
- Chen, Z. and Wang, J. (2007). Landslide hazard mapping using logistic regression model in Mackenzie Valley, Canada. **Natural Hazard** 42(1): 75-89.
- Cremonini, R. and Bechini, R. (2010). Heavy rainfall monitoring by Polarimetric C-Band weather radars. **Water**. 2: 838-848.
- Dai, F. C., Lee, C. F., Li, J., and Xu, Z. W. (2000). Assessment of landslide susceptibility on the natural terrain of Lantau Island, Hong Kong. **Environmental Geology**. 40(3): 381-391.
- Department of Mineral Resource. (2011). **Landslide record** [On-line]. Available http://www.dmr.go.th/main.php?filename=landslide_record.
- Farrell, Z. (2010). Single ring falling head infiltrometer [On-line]. Available: <http://www.usyd.edu.au/agric/web04/Single%20ring%20final.htm>.
- Goodman, R. E. (1989). **Introduction to Rock Mechanics**. New York, John Wiley & Sons, pp. 80-83.
- Kim, E. S. and Choi, H. I. (2011). Assessment of vulnerability to extreme flash flood in design storms. **International Journal of Environmental Research and Public Health**. 8: 2907-2922.

- Lee, S. (2004). Application of likelihood ratio and logistic regression models to landslide susceptibility mapping using GIS. **Environmental Management**. 34(2): 223-232.
- Lee, S. and Pradhan, B. (2006). Landslide hazard mapping at Selangor, Malaysia using frequency ratio and logistic regression models. **Landslides**. 4: 33-41 (9).
- Martín, A., Romero, R., De Luque, A., Alonso, S., Rigo, T., and Llasat, M. C. (2007). Sensitivities of a Flash Flood Event over Catalonia: A Numerical Analysis. **Monthly Weather Review**. 135(2): 651-669.
- Meisina, C. and Scarabelli, S. (2007). A comparative analysis of terrain stability models for predicting shallow landslides in colluvial soils. **Geomorphology**. 87: 207-223.
- Mergili, M. and Fellin, W. (2009). Slope stability and geographic information systems: an advanced model versus the infinite slope stability approach. In: Russian Academy of Sciences, Problems of Decrease in Natural Hazards and Risks, **The International Scientifically-Practical Conference GEORISK 2009**. pp. 119-124.
- Montgomery, D. R. and Dietrich, W. E. (1994). A physically based model for the topographic control on shallow land sliding. **Water Resources Research**. 30(4): 1153-1171.
- Pack, R. T., Tarboton, D. G., Goodwin, C. N., and Prasad, A. (1998). SINMAP a Stability Index Approach to Terrain Stability Hazard Mapping. **SINMAP User's Manual**. Logan: Utah State University.

- Sombat Yumuang. (2005). **Evaluation of Potential for 2001 Debris Flow and Debris Flood in the Vicinity of Nam Ko Area, Amphoe Lom Sak, Changwat Phetchabun, Central Thailand.** Ph.D. Thesis, Chulalongkorn University, Thailand.
- Suree Teerarungsigul. (2006). **Landslide Prediction Model Using Remote Sensing, GIS and Field Geology: A Case Study of Wang Chin District, Phrae Province, Northern Thailand.** Ph.D. Geotechnology, Suranaree University of Technology, Thailand.
- Suttisak Soralump and Wisut Chotikasathien. (2007). Integration of Geotechnical Engineering and Rainfall Data into Landslide Hazard Map in Thailand. In Proceedings of **GEO THAI'07 the International Conference on Geology of Thailand: Towards Sustainable Development and Sufficiency Economy.** Bangkok, Thailand, 125-131.
- Talaat, A. M. (2009). Assessment of infiltration rate parameters for water management in reclaimed area. **Research Journal of Agriculture and Biological Sciences.** 5(3): 223-234.
- Wyllie, D. C. and Mah, C. W. (2004). **Rock slope engineering: Civil and mining** (4th ed). New York: Spon Press. p 81.
- Yates, D. N., Warner, T. T., and Leavesley, G. H. (2000). Prediction of a flash flood in complex terrain. Part II: A comparison of flood discharge simulations using rainfall input from radar, a dynamic model, and an automated algorithmic system. **Journal of Applied Meteorology.** 39: 815-825.

- Zaitchik, B. F. and Van Es, H. M. (2003). Apply a GIS slope-stability model to site-specific landslide prevention in Honduras. **Journal of Soil and Water Conservation**. 5(1): 45-53.
- Zaitchik, B. F., Van Es, H. M., and Sullivan, P. J. (2003). Modeling slope-stability in Honduras: Parameter Sensitivity and scale of aggregation. **Soil Science Society of America Journal**. 67: 268-278.
- Zhan, X. and Huang, M. L. (2004). ArcCN-Runoff: an ArcGIS tool for generating curve number and runoff maps. **Environmental Modelling & Software**. 19(10): 875-879.
- Zhenghui, X., Fengge, S., Xu, L., Qingcum, Z., Zhenghuri, X., and Yufu, G. (2003). Application of a surface runoff model with Horton and Dunne runoff for VIC. **Advance in Atmospheric Science**. 20(2): 165-172.



CHAPTER II

LITERATURE REVIEW

2.1 Definition and terminology

2.1.1 Landslide

The most widely used terms of denudation process whereby surface is displaced along slope by mainly gravitational force are slope movement, mass movement, mass wasting, and landslide. Cruden (1991) defined landslide as “the movement of a mass of rock, debris or earth down a slope.” Crozier (1986) defined mass movement as “the outward and downward gravitational movement of earth material without the aid of running water as transporting.” In addition, Keller (2002) mentioned the term landslide refers to a rapid movement of rock or soil as a more or less coherent mass. Other general term are “slope failure” and “mass wasting”.

Important variables in common classifying of slope movements are types of movement, slope material, amount of water present, and rate of movement. Many systems were proposed for landslide classification as described by Sharpe (1938), Crozier (1973), Coates (1977), Varnes (1978), Hutchinson (1988), Cruden (1991), and EPOCH (1993). The most widely used was a system developed by Varnes (1978) and showed in Table A.1 and Appendix A; the others by Varnes (1978) that were described in two terms: material type, and type of movement (e.g. Keller (2002), as showed in Table A.2). Besides, most definitions give a guide to the processes as well as the type of material involved in the displacement. Hutchinson (1988) classified slope movements

into 8 categories containing several subdivision based on morphology, mechanism, type of material, and rate of movement (Table A.3). The classification of EPOCH (1993) used the terms fall, topple, rotational, translational, lateral spreading, flow, and complex to recognize the mechanism of failure and the type of material divided into rock, debris, and soil as illustrated in Table A.4. Dikau, Brunsten, Schrott, and Ibsen (1996) suggested the reporting of geotechnical analysis across the landslide types will improve as modern investigations which are fulfilled on more slides. But for the present, the most important information required about a landslide is the correct recognition of the failure type, mechanisms, and causes. Thus, the 7 terms (fall, topple, rotational, translational, lateral spreading, flow, and complex) were used to recognize the mechanism of failure as presented in Table 2.1 (Dikau et al., 1996).

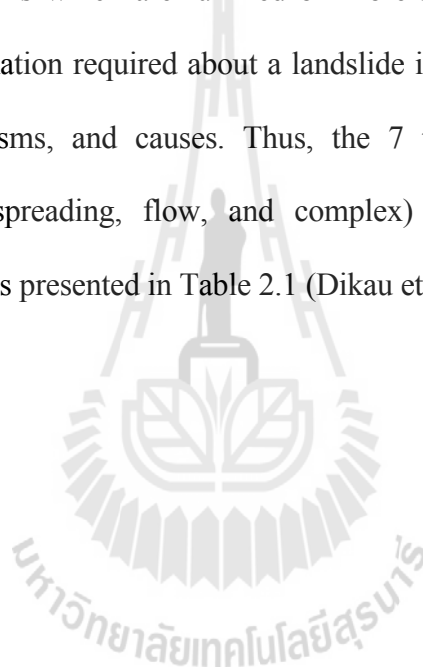
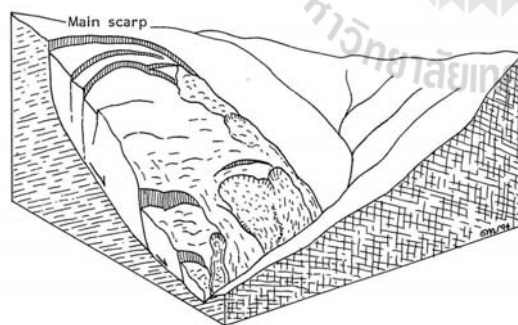


Table 2.1 A classification of landslide mechanisms, compatible with Hutchinson (1988) and EPOCH (1993).

Type	Form of failure surface	Subsequent deformation
Fall (rock or stiff soil) - Detachment from: pre-existing discontinuities or tension failure surfaces	a) Planar surface b) Wedge (two or more intersecting joints) c) Stepped surface d) Vertical surface	Free fall, may break up, bounce, slide or flow down slopes. May involve fluidisation, liquefaction, cohesionless grain flow, heat generation or other secondary effects on disintegration when failed rock hits the ground surface.
Topple (rock or stiff soil) - Detachment from: pre-existing discontinuities or tension failure surfaces	a) Single b) Multiple	As above
Slide - Rotational movement (failure surfaces essentially circular; occurs in soils) - Non-rotational compound movement (non-circular failure surface; may be listric or bi-planar; found in soils and rocks) - Translational movement (Often associated with discontinuity controlled failures in bedded or foliated rocks)	a) Single b) Multiple c) Successive a) Single b) Progressive c) Multi-stored a) Planar b) Stepped c) Wedge d) Non-rotational	Toe area may deform in a complex way. The ground may bulge, the slide may creep or even flow, possibly over existing failures. Failure might be retrogressive or progressive. Graben often develops at the head of the landslide. It may include a toe failure of a different type. May develop complex run-out forms after disintegrating (see falls and flows).
Spread (soils and weak rock) - Lateral spreading of ductile or soft material that deforms	a) Soft layer beneath a hard rock b) Weak interstratified layer c) Collapsing structure	Can develop sudden spreading failures in quick clays when the slope opens up in blocks and fissures followed by liquefaction. Might be a slow movement associated with denudational unloading. Can be represented by cambering and valley bulging.
Flow (usually associated with soils but rock flows do occur) - Debris movement by flow - Creep movement - Rock flow (sometimes referred to as sagging or sacking). Usually associated with mountain terrain or areas of rapid and deep incision.	a) Unconfined b) Channelized Failure surface rarely clearly defined a) Single-sided b) Double-sided c) Stepped (Failure surface may be rotational, compound, listric, bi-planar or intermittent)	Flow involves complex run-out mechanisms. It may be catastrophic in effect and it may move in sheets or lobes. The form of movement is a function of the rheological properties of the material. Creep may be superficial gravity movement, seasonal movements or it might represent pre-failure and progressive movements prior to a larger scale failure. May be slow gravity creep or the early stages of larger scale movements that only show as bulging in the topography without a clearly defined toe deformation. Where controlled by discontinuities it may involve toppling.
Complex a) Movements involving two or more of the above mechanisms (referred to as compound when two types of movement occur currently) b) Rock or debris avalanche	Dependant on the form of failure described above Often initiated as fall/slide of rock and/or debris	As described for the various categories above. Complex long run-out mechanisms, including fluidisation and cohesionless grain flow.

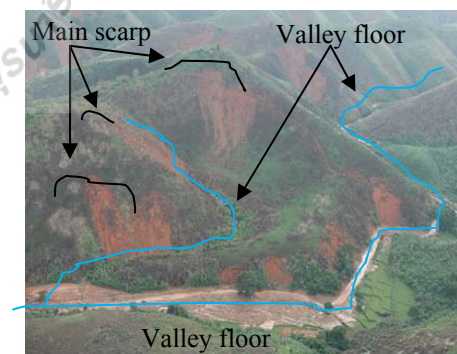
From: Dikau et al. (1996).

In this research, the term of landslide and slope failure were considered in type of movement and landslide mechanism based on Dikau et al. (1996). The movement type of this event is translational movement occurred on rock slide and the form of failure surface is planar as showed in Figure 1.2. Translational rock movement usually occurs along a more or less planar or gently undulating surface and the slope angle is close to or parallel to the dip of the rock. The classification determined by whether a pronounced change of behavior and run-out occurs when the material reaches the valley floor. The form and mode of movement is controlled by planar structure and its mode presence of weaker levels within the rock mass. The slope gradients and/or dip of slide surface are medium to high. The material moving are all intermediate forms between rock slide and rock block slide, as well as rock slide and debris flow. The scar on slope may persist for a long time and the occurrence as a single landslide surrounded by a wide unaffected area, or as a concentration of generally small slide that affect an extended zone.



a) Block diagram of planar translational slide.

From: Dikau et al. (1996)



b) Photograph of the Nam Li area.

From: จังหวัดอุดรดิตรดิตต์ (2549)

Figure 2.1 The planar failure surface and translational movement.

2.1.2 Slope stability and factor of safety

The slope stability is the relationship between driving force and resisting forces. The most common driving force is the down slope component of the slope material weight and the most common resisting forces is the shear strength of slope material acting along potential slip planes (Keller, 2002; Wyllie and Mah, 2004; Das, 2007).

The factor of safety is the process to evaluate slope stability. It is often calculated in engineering tasks. This evaluation defined as the ratio of the resisting forces divide by the driving forces. This process is called “slope stability analysis,” There are several different methods for analysis such as limit equilibrium method, the ordinary method of slices, the simplified Bishop method, the modified Swedish method, Spencer’s method, the wedge method, the infinite slope method, simple approximation, and chart solution (U.S. Army Corps of Engineers, 2003). All methods are based on equilibrium method which assumes the Factor of Safety (FS) to be constant along the slip surface, and it was defined with respect to the force or moment equilibrium. Cheng and Lau (2008) mentioned that the simplified method cannot fulfill both force and moment equilibrium simultaneously, whereas limit equilibrium method and finite slope method are most popular of geotechnical engineers because these methods fulfill the basic requirement from the soil/rock mechanic principle as well as the long-term performance of the slope. The assumption of equilibrium of force and moment to generate formula based on the failure mass is a rigid body, the base normal force acts at the middle of slice base, and the Mohr-Coulomb failure criterion is used. The use of FS for landslide potential may be done for either translational slides or rotational slide (Keller, 2002).

The infinite slope stability method is one method based on equilibrium to analyze non-circular failure surface which was selected in this study. This method assumes that the slope is infinite lateral extent and that sliding occurs along a plane surface parallel to the face of slope, where the effects of the head and toe portion of the slide are negligible.

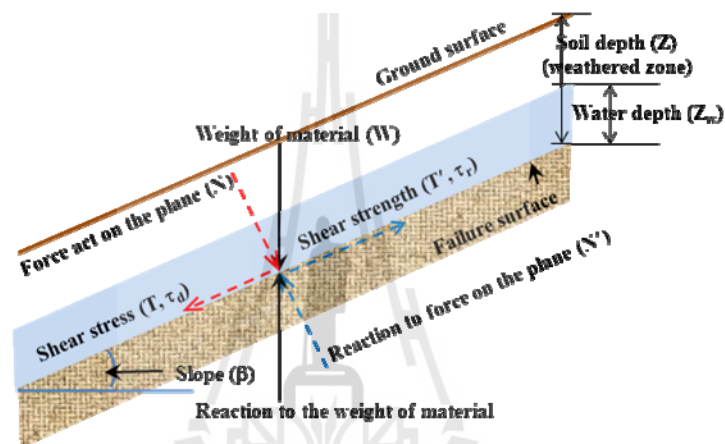


Figure 2.2 Definition of infinite slope stability.

Adapt from: U.S. Army Corps of Engineers (2003) and Das (2007).

Thus, the definition of factor of safety from Figure 2.2 can be calculated by the following equation.

$$FS = \frac{\text{shear strength}}{\text{shear stress}} = \frac{\tau_r}{\tau_d}, \quad (2.1)$$

or in terms of forces by,

$$FS = \frac{\text{Resisting force}}{\text{Driving force}} = \frac{T}{T'} \quad (2.2)$$

The definition of infinite slope stability and its theory was explained in Appendix B.

2.1.3 Probability of failure

Wyllie (1999) described the term “Probability of failure”, PF, is a term in reliability analysis method, which systematically examines the effect of the variability of each parameter on the stability of the foundation. The term “coefficient of reliability”, CR, which is related to PF which can be formulated by the following equation;

$$CR = (1 - PF) \quad (2.3)$$

In reliability analysis, the uncertainty parameters are assigned a range of values which is defined by a probability density function. The common type of function is the normal distribution as defined by,

$$f(x) = \frac{1}{SD\sqrt{2\pi}} \exp\left[-\frac{1}{2}\left(\frac{x - \bar{x}}{SD}\right)^2\right], \quad (2.4)$$

where x is a value, \bar{x} is the mean of values, and SD is the standard deviation of values.

The most often definition of Probability Density Function (PDF) is the equation used to describes a continuous probability distribution. It is a function of the relative for the continuous random variable to take on a given value (Kolmogorov, 1956; Feller, 1971; Billingsley, 1979; Ushakov, 2001). If x is a continuous variable within a defined range, the probability of x having precise value within that range is vanishingly small because a total probability of 1 must be distributed between an infinite numbers of values.

The method of Probability of failure determination in this research is the margin of safety method, which is the method of calculating the area under the curve of probability density function of safety margin which used the Equation (2.4) as shown in Figure 2.3. The area of the negative part is the PF and the area of the positive part is the CR.

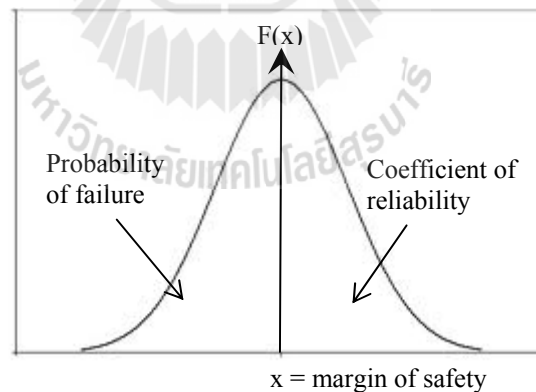


Figure 2.3 The plot of probability density function and safety margin.

2.1.4 Flash flood

The term of flash flood refers to the result of heavy or excessive amounts of rainfall within a short period of time, causing water to rise and fall quite rapidly (USGS, Kansas Water Science Center, 2005; National Weather Service

Forecast Office, 2010). The Thai Meteorological Department (TMD) defined the term of flashflood is a rapid flooding which occurred and terminated very fast by heavy rainfall. The event often occurs less than 6 hours in the highland area that steep slope and lower water storage area. It usually occurs in downstream that maybe not rainfall but the heavy rainfall in the headwater a long away (กรมอุตุนิยมวิทยา, 2553).

The flash floods occur when soil absorption, runoff or drainage cannot adequately disperse intense rainfall. The most frequent cause of flash flooding is slow-moving thunderstorms. These systems can deposit extraordinary amounts of water over a small area in a very short time. The strong updrafts of air within thunderstorms can suspend huge amounts of rain before releasing a deluge onto the ground. Such rain can reach intensities of more than 100 mm per hour, provided the environment is humid enough to feed sufficient moisture to the storm. Often topography acts to focus thunderstorm development over a particular location, further accentuating rainfall accumulation (Bureau of Meteorology, 2011). Takio Kinoshita indicated 2 important essentials of flash flood causes are climate and topography. The heavy rain over 1,800 mm. fall in 20-30 minute and the 80% of mountainous areas contain short streams and steep gradient could occurrence flash flood (Barnes, 1975). Besides, the cause of flooding can separate to be natural cause and manmade cause. The types of flooding in natural cause are classified by appearance of floods that are flash floods, steady floods, drainage floods, and river mouth floods. For manmade cause, there are 3 causes such as collapse of dam, road barrier and flood in urban area.

In this event, the flash flood occurred in the mountainous areas with short streams, steep slope, and low water storage areas. The heavy rainfall was over 500

mm in 3 hours, and the rainfall accumulated before flash flood in 39 hours was approximately 150 mm. This event occurred on May 23, 2006 as showed in Figure 2.4.



Figure 2.4 The flash flood occurred on May 23, 2006 in Nam Li watershed.

From: Vinai Dithajohn (2006).

2.1.5 Overland flow

Overland flow is water flowing over the ground surface because the soil or rock which it flows over has become saturated. The overland flow occurs when the rainfall intensity exceeds the infiltration capacity of the ground surface (Davie, 2002). The term ‘overland flow’, Q , that referred to the flow of water over a hill slope surface. It can occur in one of two ways which are unsaturated and saturated areas. Firstly, it is generated when the rainfall intensity exceeds the surface infiltration rate. The excess rainfall then accumulates on the soil surface in small depressions. Once these depressions are filled, the water spills out and flows downslope as overland flow. Overland flow originating in this way is called “Horton overland flow.” For a given rainfall intensity, the occurrence of Horton overland flow and the rate at which

it takes place are functions of the infiltration rate. Many factors influence the infiltration rate, including soil type, vegetation, and land use. In desert landscapes with their thin vegetation covers, shallow soils, and abundant outcrops of bedrock, infiltration rates are low and Horton overland flow is widespread. It is much less common in humid landscapes where thick vegetation and deep soils favor high infiltration rates. Exceptions occur where the natural vegetation cover has been thinned or removed, as in farmland. Destruction of the vegetation permits raindrop impact to seal the soil surface and lower infiltration rates without saturating the soil. Secondly, overland flow is generated when a rising water table intersects the soil surface. Subsurface water then escapes from the soil and flows downslope over the soil surface, this exfiltrating water is termed “return flow.” That portion of the hill slope over which return flow emerges is saturated, so any rain falling on to it is unable to penetrate the surface and also flow downslope. Direct precipitation on to saturated areas and return flow together constitute saturation overland flow. This type of overland flow is rare in desert landscapes but is common in humid ones. It typically occurs on valley floors and concave foot slopes, in valley-head and valley-side hollows, and in areas where the underlying geology directs subsurface flow to the surface. The extent of the saturated area varies both between storms and within storms, and controls the rate of overland flow.

2.1.6 Debris flow

The term “debris flow”, is form of rapid mass movement in which a combination of loose mud, sand, soil, rock, water, and air mobilize as slurry that flow downslope under the influence of gravity (Highland and Bobrowsky, 2008). In Table 2.1, debris flow is one type of landslide which is debris movement by flow. Flow

involves complex run-out mechanisms. It may be catastrophic in effect and it may move in sheets or lobes. The form of movement is a function of the rheological properties of the material (Dikau et al., 1996). Debris flow usually occurs on hilly area and intense rainfall. In this study landslide that mobilize into debris flow occurred along topographic concavity which was triggered by overland flow from heavy rainfall.

2.1.7 Impact intensity

The term “impact intensity” in the thesis refers to the physical environment changing in the area which effected from catastrophic event. This physical environment changing related to the land surface damaged such as land cover areas, infrastructure, stream, and settlement. WHO (2002) described that the human impacts of natural disasters were contingent on economic, cultural, and social relations, but the human impacts in this study were not considered. Inbar (1997) mentioned the results of catastrophic events, like flood, drought, forest fire, erosion, and landslide, affect to human directly. Whereas, Malet and Maquaire (2010) proposed the impact of landslide did not generally present risk for the human lives when a landslide occurred slow, progressive movement, and far from settlement but there were large impacts on infrastructures such as building, road, etc. A case of Nam Li watershed, the landslide and flash flood occurred in the upstream areas and the mass movement down to the settlement area in a downstream. Although the people were affected from this event in a downstream but the large impacts were acted on the large area which did not act to human directly. Consequently, the term “impact intensity” should be focused on land surface damaged.

2.2 Landslide studies

There are plenty of methods, model types, and factors applied to the studies on landslide. The weighting model and the logistic regression model are also exercised in spatial analysis, and slope stability analysis is based on geotechnical engineering method. The geotechnical engineering method is a civil engineering process concerned with the engineering behavior of earth materials. The landslide study in term “slope stability analysis” is used to evaluate landslide susceptibility in Nam Li watershed. The reviewing focuses on the geotechnical engineering method and its result as follow.

2.2.1 Geotechnical engineering method

Landslide susceptibility can assessed through geotechnical engineering method by the slope stability analysis. The slope failure of soil commonly occurs on curved surface. Bishop Method and Swedish Method are considered as the improved methods for slope stability analysis on a regional scale (Mergili and Fellin, 2009). The infinite slope method can be simplified and easily applied for preparing regional hazard zonation (Udas, 2005; Warakorn Mairaing, 2006). It is a 1 direction (1D) model which was selected because it is the most widely used (Das, 2007; Mergili and Fellin, 2009). There are many different methods for Factor of Safety (FS) calculation.

Many research studies were employed the FS values in landslide susceptibility and landslide risk area evaluation in Thailand, such as Sutep Junkhiaw (2003), สุรินทร์ ไวกะริญ (2549), Warakorn Mairaing and Nonglak Thaijeamaree (2004), and Suttisak Soralump and Wisut Chotikasathien (2007). Sutep Junkhiaw’s research in Phuket Province selected equation from Coppin and Richards (1990) to calculate FS values. The factors in this equation include shear strength and shear stress of both

soil and root reinforcement. The FS values were classified into 4 classes, including <1 (high risk), 1.01-1.05 (moderate risk), 1.51-2.00 (low risk), and >2.00 (no risk); and the landslide risk area map was generated from the classes of FS. Beyond that the weighting model was used in this thesis. The factors applied in weighting model consist of geology, landform, surface drainage zone, land use and land cover, soil characteristics, rainfall intensity, and root type. The scores were classified into 4 classes, namely, high risk, moderate risk, low risk, and no risk. Both of FS calculation and weighting model showed the consistent results. However, the values of variables in the equation were derived from the research in other areas that have the same characteristics as the study area. The FS raster layer was operated on slope raster layer with 1,000 m × 1,000 m. It was very coarse for slope stability analysis. If the cell size of slope layer was smaller than this, the accuracy of landslide risk map might be better.

สุรินทร์ ไวกิจ (2549) exploited SINMAP model (Pack, Tarboton, Goodwin, and Prasad, 1998) to determine landslide susceptibility of 255 watersheds in Thailand. The equation of infinite slope stability in SINMAP was modified by Hammond, Hall, Miller, and Swetik (1992). The water depth and soil thickness were difficult to measure in the field, then Pack et al. (1998) proposed the Topographic Wetness Index (TWI) from TOPMODEL that created by Beven and Kirkby (1979) to replace the water depth and soil thickness. The TWI defined as upslope area (m²) per unit contour length (m), it was one of the landmark developments in recent hydrology. The variables of several raster layers with 30 m × 30 m were used in this research, concurrently the slope layer was extracted from DEM with the same resolution. The landslide risk map was presented at 1:50,000 map scale. The cohesion and friction angle of soil and root plant were derived from Pack et al. (1998) which used maximum and

minimum value of variables for calculation. The output values from SINMAP were lower bound from minimum values and upper bound from maximum values. สุรินทร์ ไวกวี (2549) classified stability index into 3 classes as High, moderate, and low risk landslide occurrence ($FS < 0.5$, $0.5 < FS < 1.0$, and $FS > 1.0$, respectively).

Generally, the geotechnical engineering method is used for small sites stability analysis. Warakorn Mairaing and Nonglak Thaijeamaree (2004) and Suttisak Soralump and Wisut Chotikasathien (2007) used FS values from geotechnical engineering method as one factor in the index model. The first research evaluated mountain slope stability from unsaturated soil strength in Nam Kor watershed area, Phetchabun Province. The second research integrated geotechnical engineering method with weighting factors method in Phuket Province. The soil properties of 2 researches were derived from laboratory and in situ testing. Consolidate drained direct shear test was selected to evaluate water content. And the soil strength was represent by 3-D plan similar to Mohr-Coulomb envelop with the saturate ratio as the additional axis. The topographic data, unsaturated soil properties, and rainfall data were used to evaluate water content in each storm period. As soil cohesion was evaluated from water content in each geologic unit, the result showed that more than 85% of water content gave a negligible cohesion of soil. Finally, it was concluded that the heavy rainfall was the main cause of landslide occurrence which the high water content in soil pore made insignificant soil cohesion. This research suggested that landslide prediction and warning should be done by using critical rainfall from various pattern of possible rainfall associated with slope stability analysis on the location. Suttisak Soralump and Wisut Chotikasathien (2007) selected the method for engineering soil properties determination in the same way with

the first research. The engineering properties as Strength Reduction Index (SRI), plastic index, and grain size distribution were used as an index to quantify the landslide potential of residual soil. The weathering intensity levels were determined from these engineering properties to be a criterion of weight rating model for landslide hazard map creation. While Warakorn Mairaing (2006) suggested that the analysis for FS in the large area was in need of the geographic information system to provide the FS values in the cells of FS raster layer. The warning level index in his research was established from both FS raster layer and rainfall raster layer. The slope stability analysis is a difficult method to prepare the soil or rock properties approach to the real properties in small site. But all of the researches discussed it was a best method to assess small site stability. The researchers tried to separate study area to be small using grid cells such as Sutep Junkhiaw used $1 \text{ km} \times 1 \text{ km}$, Suttisak Soralump and Wisut Chotikasathien (2007) used $50 \text{ m} \times 50 \text{ m}$, and Surin Waicharoen used $30 \text{ m} \times 30 \text{ m}$ based on DEM cell size.

The geotechnical engineering method for slope stability analysis was widely used in other countries during year 1998 to 2011 such as Kilpala watershed, Rose Creek watershed, and Burnt watershed in British Columbia (Pack et al., 1998; Pack, Tarboton, and Goodwin, 2001), the central high land of Honduras (Zaitchik and van Es, 2003; Zaitchik, van Es, and Sullivan, 2003), the high relief area of Cincinnati metropolitan in Ohio, USA (Ritter, 2004), along Chungju lake in Korea (Kim, Park, Lee, and Woo, 2004), Okayama prefecture in Japan (Greif, Sassa, and Fukuoka, 2006), Karak Highway in Kuala Lumpur, Malaysia (Omar, Ibrahim, and Hashim, 2007), Oltrepo Pavese, Northern Apennines, Italy (Meisina and Scaravelli, 2007), the Bowenvale Reserve catchment in New Zealand (Acharya and Cochrane, 2009), along the Storfjorden in western Norway (Groneng, Nilsen, and Sandven, 2009), and the left bank

of Canelles reservoir in Spain (Pinyol, Alonso, Corominas, and Moya, 2011). The examples of studies were shown in Table 2.2.

The factor of safety is a famous model for landslide susceptibility areas assessment. Even though the researchers used difference variable in the FS equation, the landslide susceptibility maps from FS values, it correspond to inventory landslide scars and landslide scars extracted from satellite images. The infinite slope stability was used to calculate FS value in order to get landslide susceptibility indices. The application of simplified slope stability models has proved effective as descriptive and predictive tool, allowing for rapid slope stability assessment over a wide area.

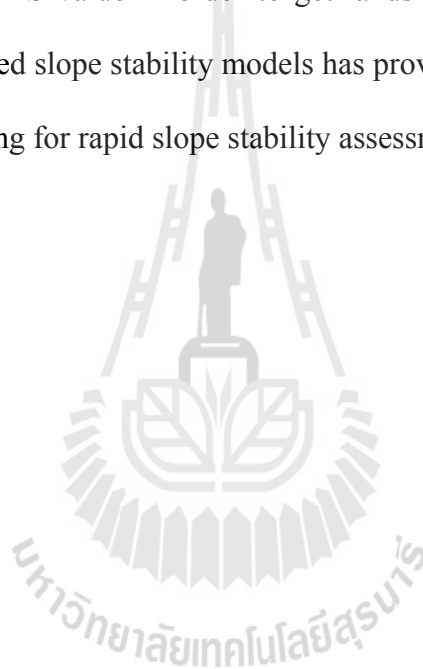


Table 2.2 The examples of studies using the Geotechnical engineering method.

Authors	Year	Method/Model	Factors/Variables
Pack, et al.	1998	GIS based, SINMAP	} TWI, rock properties (C_s , ϕ), slope.
Pack, et al.	2001	GIS based, SINMAP	
Zaitchik and vas Es	2003	GIS based, SINMAP	
Zaitchik, et al.	2003	GIS based, SINMAP	
Ritter	2004	GIS based, FS by infinite slope stability analysis	} Rock properties (C_s , ϕ , γ), slope.
Kim, et al.	2004	GIS based, FS by infinite slope stability analysis	
Greif, et al.	2006	Physical modeling	
Omar, et al.	2007	GIS based, FS by infinite slope stability analysis	Rock properties (C_s , ϕ , γ), slope.
Meisina and Scaravelli	2007	SINMAP and SHALSTAB	TWI, rock properties (C_s , ϕ), slope.
Acharya and Cochrane	2009	GIS based, FS for shallow landslide by infinite slope stability analysis	Rock properties (D , C_s , C_r , ϕ , γ_e , γ_w), slope.
Groneng, et al.	2009	Triaxial testing, shear strengths assessment	Water, Rock properties (e.g. C_s , ϕ , density, porosity, permeability).
Pinyol, et al.	2011	FS by limit equilibrium analysis	Rock properties (C_s , ϕ , γ_e , pore water pressure), landslide geometry.

Remark: TWI is topographic wetness index, C_s is soil cohesion, C_r is root cohesion, ϕ is friction angle, γ and γ_e is unit weight of soil, γ_w is unit weight of water, and D is soil thickness.

2.2.2 Spatial modeling

The application of weighting index model to landslide is quite popular method in Thailand. Many studies on landslide are different in methods, factors used and model types. More landslide hazards were studied using weighting index model e.g. the studies of the Land Development Department (กรมพัฒนาที่ดิน, 2547; รุ่งนภา ตะวันรอน และ ประทุมพร ฟั่นเพ็ง, 2547; ประทุมพร ฟั่นเพ็ง, 2548; สมพร ผาตินาวิน, 2548;

กรมพัฒนาที่ดิน, 2550), Sombat Yumuang (2006), and Suree Teerarungsigul (2006).

Score and weight of criteria for index calculation are more subjective or arbitrary and more likely to depend on the uncertain expert-claimed opinions.

The LDD was carried out many studied on landslides and floods in many parts of Thailand during year 2004 to 2007 by means of overlay techniques using a GIS approach (กรมพัฒนาที่ดิน, 2547; รุ่งนภา ตะวันรอน และ ประทุมพร พันเพ็ญ, 2547; ประทุมพร พันเพ็ญ, 2548; สมพร ผาดินาวิน, 2548; กรมพัฒนาที่ดิน, 2550). Five factors used for evaluating hazardous areas were LU/LC, liquidity of soil, slope, size of catchments area, and rainfall. All factors for soil movement studies were used to examine the movement probability of soil at 30 cm depth. All of these depend on soil type and LU/LC. The LDD indicated that the percentage of slope >35 would face the high probability of landslide occurrence. The saturation probability of soil were grouped into 3 classes using daily rainfall amount (>100 mm/day, >200 mm/day, and >300 mm/day). The percentage of slope was grouped into 2 classes as $\leq 35\%$ for low probability and $>35\%$ for high probability. The size of catchment area was grouped into 2 classes, ≤ 32 km² and >32 km². The LDD considered that the serious hazardous soil movement in mountainous area should be >32 km². Areas with slope $>35\%$ and catchment area >32 km² were selected to divided into 3 zones of soil movement probability according to 3 zones of daily rainfall. Although, this method can predict soil movement area but it can only predict in small scale such as provincial scale but none of the regional scale. It was insufficient accuracy for predicting local hazardous area in large area. Then, this method is suitable for soil movement management.

Sombat Yumuang (2006) presented debris flow-flood susceptibility analysis using univariant probability method similar to Suree Teerarungsigul (2006) proposed the landslide hazard or susceptibility analysis based on the bivariate probability and weighting method. The difference of the studies was the factors used. The univariant probability method was a correlation ratios were performed on the relationship between a number of scar-scouring cells and each range of parameters. The ratio calculated was the probability of flow-flood susceptibility in each parameter's range. As well as, the bivariate probability with weighting method was the statistical correlations were relationships between the probabilities of landslide occurrence and several factors' classes. The results of two studies, landslide susceptibility maps, had been verified by geotechnical technique. Sombat Yumuang had done a point load testing for verifying a rock strength index and geotechnical engineering study of soil properties for evaluating shear strength. A result of Flow-Flood Susceptibility Index (FFSI) was agreed with the test. As well as, Suree Teerarungsigul compared her bivariate weighting method with rock slope stability model which created from RSS-GIS program suite and its result in the factors of safety. This result shows the slope stability map which agrees with the existing landslide location data. These probably depend on the accuracy of DEM data with $30\text{ m} \times 30\text{ m}$.

Other method for predicting and evaluating landslide susceptibility area is a logistic regression model. It is a multivariate technique that considers several parameters which affect probability of landslide occurrence. The examples of landslide studies using this method are Dai, Lee, and Xu (2000), Lee (2004), Lee and Pradhan (2006), and Chen and Wang (2007). Most examples determined the important factors that relate to topography and material. Lee (2004) added factors that

relate to land cover. Dai, Lee, Li, and Xu (2000) mentioned that the drainage lines are important factor controlling debris flow susceptibility. In addition, Lee (2004) mentioned about the relationship between the drainage and average wetness or dryness of soil. It considers as a clue to soil permeability. When the prediction accuracy of the studies were compared, they found the studies using frequency ratio presented the accuracy higher than the logistic regression models, and the using of logistic regression models showed the accuracy higher than the likelihood ratio (Lee and Pradhan, 2006). The study of Cheng and Wang (2007) used the logistic regression model in Mackenzie Valley, Canada. They concluded that the logistic regression was effectively used to establish the relationship between the landslides and related environmental conditions that cause of the landslides. The importance environmental conditions were ranked and predicted future landslide probabilities. Nelson, Connors, and Suárez (2007) used GIS and modeling technique to analyze risk of slope failure in Chuquicamata mine in northern Chile. They presented the sensitivity analysis model to select the component layers such as training points, and classification and ranking of categorical parameters. The result presented high degree of correspondence with recent, post-model failures. Such modeling techniques could provide a powerful tool for predictive modeling in a vast array of large-scale-map applications requiring similar data integration and evaluation.

2.3 Flooding studies

The GIS technique and Remote Sensing data are widely used in other countries (Pradas, 2009; Saini and Kaushik, 2012). But this research focuses on the hydrologic method for water balance calculation. Therefore, the reviewing focuses on the hydrologic equipment and the result from the method. The hydrologic model or hydraulic model is the models that related to rainfall-runoff model. The example models are HEC-RAS, NAM, MIKE, SWAT, and URBS. The HEC-RAS is a 1D hydrodynamic modeling. The NAM model is a sub-catchment scale model which consists of physical based and rainfall-runoff model. The MIKE is a hydrodynamic modeling that simulates flow and water level, water quality and sediment transport in rivers, flood plains, irrigation canals, reservoirs and other inland water bodies (DHI, 2003). The URBS is a distributed nonlinear rainfall runoff routing model which account for the spatial and temporal variation in rainfall (Malone, 1999). The SWAT model has proven to be an effective tool for assessing water resource and nonpoint source pollution problems for a wide range of scales and environmental condition (Gassman, Reyes, Green, and Arnold, 2007). The infiltration excess model was involved in applying flash flood occurrence prediction. In the hydraulic models, normally the infiltration is neglected. For flat areas the water levels are very low and maybe similar to the infiltration amount. The flooding front perhaps is necessary to consider the infiltration effects over flat areas. The antecedent rainfall situation that necessary for the water infiltration will depend on the previous rain. If the area is saturated, the effect over the flooding propagation will be completely unexpected (Bateman, Medina, and Velasco, 2010). The overland flow or runoff is the result of

infiltration excess model. The term “infiltration excess” was used for flood assessment.

2.3.1 Hydrological model

Naruemol Taragsa, Charat Mongkolsawat, Chalermchai Pawattana, and Rasamee Suwanweerakamtorn (2004) applied GIS and hydraulic model to create floodplain inundation for representing flood extent and flood depth of Chi Basin in parts of Mahasarakham, Kalasin, and Roiet. The data were prepared as a cross section including elevation, water body, land use, stream center line, bank line, flow path, river profile and river cross section. The water surface profile was calculated using input of the cross section, stream center line and flow rate into HEC-RAS programme. The obtained output was water surface profile layer. It was overlaid on digital terrain model to evaluate flood depth and flood extent. Finally, flood extent was checked against the data acquired by RADARSAT. The fitting percentage is about 52%. This study suggested that this was not a time consuming method in the way of preparing data input and data analysis. Spatial factors which were roughness coefficients and cross section were as well easy to prepare.

Punpim Puttaraksa Mapiam, and Nuchanart Sriwongsitanon (2009) used URBS and NAM to estimate the parameter for flood estimation in ungauged catchments in the upper Ping river. The physical based analysis of rainfall-runoff model routed through the catchment characteristic which it is composed of channel length, channel slope, and percent of land used consisting agricultural and forest. The URBS give a rainfall excess; rainfall depth, there are 7 model parameters necessary for the model application; the channel lag parameter, the catchment nonlinear parameter, the Muskingum translation parameter, the catchment lag parameter, the

initial loss, the proportional amount of runoff, and the maximum infiltration rate. The results revealed the relationship between URBS model and catchment characteristic can be confidently applied for flood estimation of ungauged catchment. Moreover, MIKE11 and NAM were used in hydrodynamic model to simulate flood inundation in the Yom River (Tawatchai Tingsanchali and Karim, 2010) and URBS model was used in flood forecasting in the Upper Ping River Basin (Nutchanart Sriwongsitanon, 2010).

Sumangala (2005) studied flood frequency in order to understand behavior of flood over the Delta region of Puri District, Orissa state, India. A flood inundation map was created from water surface profile which was calculated by 1D hydrodynamic model. Several software used for this study were ILWIS for image processing, ArcView 3.2 with HEC-GeoRAS for creating geographic data, RAS-GIS for importing field data, and HEC-RAS for 1D hydrodynamic modeling. This study compared flood inundation map from 1D hydrodynamic model and RADARSAT. The results showed good agreement. The study suggested that the HEC-RAS was a powerful tool for hydraulic simulation, and the model stability problem of HEC-RAS was affected by too many factors and the model accuracy depended more on surveyed cross section data and accurate DEM.

Chowdhury (2000) reported that the Flood Forecasting and Warning Center (FFWC) of Bangladesh Water Development Board (BWDB) used MIKE 11 for flood simulation at the national scale. The discussion suggested the high resolution and accurate data are important for any numerical model. Moreover, Apirymanekul and Mark (2001) used MIKE11 and GIS technique for urban flooding in Dhaka city. DEM resolution at 50 m was used to estimated storage volume and water level.

Drainage system and road network was used for flood area consideration. Ballesteros-Cánovas, Eguibar, Bodoque, Díez-Herrero, Stoffel, and Gutiérrez-Pérez (2011) estimated the peak discharge of flash flood event in year 1997 in ungauged mountain catchment. They integrated dendrogeomorphic techniques to obtain observation point and to define hypothetical scenarios as well as hydraulic and topographic approaches to gather simulated water surface values. The sampling strategy has been designed to analyze and check flash flood scars from tree trunk. The terrestrial laser scanner was used for the acquisition of topographic data. The MIKE21 was selected to operate water depth, velocity as well as stream bed shear stress. The water depth simulation from dendrogeomorphic techniques was corresponding to the simulation from MIKE21.

The concept of Robert E. Horton is Hortonian overland flow or infiltration excess overland flow (Beven, 2004). It was used for runoff/overland flow assessment. Ogden, Sharif, Senarath, Smith, Baeck, and Richardson (2000) simulated infiltration excess runoff from CASC2D model. The original CASC2D formulation has been significantly enhanced with the addition of continuous soil moisture accounting, a variety of channel cross-sections and Green and Ampt infiltration with redistribution. The surface water was accumulated in each grid cell until specified retention depth for the cell is exceeded. Thereafter, the overland flow is routed in two orthogonal directions. When overland flow reaches a grid cell that contains a defined channel. Bateman, Medina, and Velasco (2010) used 2D shallow water equation (2D-SWE) to flood front propagation on dry bed river. The modeling was improved by infiltration calculation which Green and Ampt equation and SCS method were selected to calculate infiltration. The FLATModel was selected to simulate flooding

based on topographic data derived from 1 m resolution LIDAR data. The result showed the influence of infiltration in the flood area extension. All infiltration models are based on the Hortonian concept and its influence in water balance equation also.

2.3.2 Other methods

Numerous of researches (e.g. กรมพัฒนาที่ดิน, 2547; รุ่งนภา ตะวันรอน และ ประทุมพร พันเพ็ญ, 2547; กรมชลประทาน, 2549; Charlchai Tanavud, Chao Yongchalermchai, Abdollah Bennui, and Omthip Densreeserekul, 2004; Phiraphit Phutmongkhon et al., 2007; Rawee Rattanakom and Suwit Ongsomwang, 2008) used GIS overlay technique and weighting model for flood assessment and flood risk map during year 2004-2008. Factors used in the model comprised of rainfall, floodplain size, watershed size, soil texture, drainage ability, drainage density, slope, road, LU/LC. The rainfall indicated an important factor that causes flood occurrence. Then, the rainfall data must be used in the model. The group of Land Development Department considered the rainfall per day related to the floodplain area which extracted from soil group. The rainfall (R) was classified into 3 classes as $>100 \leq 200$ mm/day, $>200 \leq 300$ mm/day, and >300 mm/day. The floodplain was classified into 2 groups: flash flood hazard which occurs in the boundary of mountainous areas within 10 km of the radius; and flood inundation hazard which occurs outside mountainous areas. The major aim of this map was to warning, protecting, and relieving distress in provincial planning level. The RID (กรมชลประทาน, 2549) created flood hazard map in Huai Pong Sub-watershed, Loeng Nok Tha District, Yasothon Province, using weighting index model. The factors consisted of rainfall, soil texture, drainage ability,

drainage density, slope, road, LU/LC. Those factors were weighted. The flood hazard map was checked by comparing with the flood areas previously occurred. For University group, the orders of weighting of factors were rainfall, watershed area, drainage density, slope area, slope of main stream, soil texture, soil depth and land use. They concluded that the most important factor was rainfall whereas the least important factor was land use. Rawee Rattanakom and Suwit Ongsomwang (2008) described the factor weighting were derived from pairwise comparison method, Although, index model is a simple method and factors of the model related to flood event, but the highly hazardous flooded areas can occur outside the rainfall area. For flood monitoring in Thailand, the Geo-Informatics and Space Technology Development Agency used the real-time rainfall data from MTSAT2 and imageries from satellite as RADARSAT-1, RADARSAT-2, COSMO-SkyMed-2, and COSMO-SkyMed-3 to evaluate flood area during year 2005-2012 (GISTDA, 2012).

2.4 Synthesis for the research approach

2.4.1 Landslide susceptibility assessment

The geotechnical engineering method is a method that concerned with the engineering behavior of earth materials. The materials properties were used to evaluate slope stability through the ratio of resisting force to driving force which is factor of safety. In general, the resisting force was derived from shear strength of earth material which were included weight, material cohesion, and internal friction that related the normal stress of material (Wyllie, 1999; Cheng and Lau, 2008). Moreover, Abe and Iwamoto (1985) mentioned the tree roots on soil material affected the soil shearing strength. Sutep Junkhiaw (2003) and สุรินทร์ ไวกิจิณญ์ (2549), derived the

material properties from reviewing existing research matching with their material and classes units. For the research in other countries, the FS values were derived from SINMAP, SHALSTAB, and GIS based calculation. The SINMAP and SHALSTAB transfer the weight of material to be TWI (Topographic Wetness Index), it was developed by TOPMODEL (Beven and Kirkby, 1979).

Slope stability analysis was reviewed based on equilibrium theory. The infinite slope method was mostly chosen to calculate FS. Generally, the slope failure of soil occurs on curved surface. The approved methods of slope stability analysis on the regional scale are Bishop Method and Swedish Method. The infinite slope method can be simplified and easily applied for preparing regional hazard zonation (Udas, 2005). The slope stability analysis, which includes the variables that relates to rock properties and slope characteristic, was applied for FS calculation. There are many different methods for FS calculation. But the infinite is a 1D model that is most commonly employed for the purpose (Warakorn, 2006; Omar et al., 2007; Das, 2007; Mergili and Fellin, 2009). Many researches discussed the accurate landslide maps should be derived from certain value of material properties (e.g., weight, material cohesion, and internal friction), high resolution DEM and cell size of the study area; especially they should be in the same cell size. For these reasons, FS calculation for each slope polygon derived from DEM was exercised the infinite slope stability, and it was based on Bishop Method. The slope stability model was performed to predict landslide susceptibility in large area through the spatial analysis which its result could be more reliable.

Various rock properties in the study area were reviewed and sampling tested by engineering method. The reliable result was assumed with a revision of rock

properties. Besides, the ranges of rock properties were divided into the possibility of rock properties, and then FS can be calculated. After that the probability of failure was computed using a probability density function. Consequently, the landslide impact intensity was assessed from the probability of failure.

2.4.2 Flash flood occurrence assessment

Barnes (1975) discussed the causes of flash flood were short duration of high intensity rainfall on steep gradient and short river. Watershed characteristics, particularly water control structures, were a very significant impact on the flood discharge downstream from the large detention basin formed. Therefore, the important input data of hydrologic model is not only rainfall intensity but various characteristics of watersheds, especially drainage system, material, and land used are also important. For package models (e.g., HEC-RAS, NAM, MIKE, SWAT, and URBS), the water depth and water surface simulation data input acquired from the characteristics of drainage channels such as elevation, channel length, channel density, channel slope, flow path, stream center line, bank line, stream bed shear stress, river profile, and river cross section. Normally, the data input obtained from observed station and field measurement which were difficult for ungauged basin. On the other hand, Ballesteros-Cánovas et al. (2011) proposed flash flood scars on tree to simulate peak water depth of flash flood discharge event. From those researches provided the knowledge of water depth and water surface which were important parameters for flood surface simulation.

This research proposed the method for water depth and flash flood surface evaluation from DEM and flood scars. According to Sumangala (2005) suggested that the water depth at stream center line should be derived from closely

frequently stream cross section which can be operated on high resolution DEM and flood scars. Similarly, flood scars should be derived from high resolution satellite images. In addition, flooding was effected by soil capacity and land use types. The same as weighting index model, land use types were used as one of their criteria due to it related to soil drainage ability and soil infiltration. Then, the Horton's infiltration excess equation was selected to evaluate overland flow for flash flood impact intensity assessment.

2.5 References

- กรมชลประทาน. (2549). รายงานการศึกษาแผนหลัก/แผนแก้ไขปัญหาน้ำแล้งและน้ำท่วม. กรมชลประทาน กระทรวงเกษตรและสหกรณ์.
- กรมพัฒนาที่ดิน. (2547). พื้นที่เสี่ยงต่อการเกิดดินถล่มและอุทกภัยในประเทศไทย. กรมพัฒนาที่ดิน กระทรวงเกษตรและสหกรณ์.
- กรมพัฒนาที่ดิน. (2550). การวิเคราะห์พื้นที่ที่มีความเสี่ยงจากดินถล่มในประเทศไทย [ออนไลน์].
ได้จาก: http://www.idd.go.th/web_irw/landslide.html.
- จังหวัดอุดรดิตถ์. (2549). สรุปสถานการณ์อุทกภัยและการช่วยเหลือผู้ประสบภัยจังหวัดอุดรดิตถ์ [ออนไลน์].
ได้จาก: <http://ww.uttaradit.go.th/flood.doc>.
- กรมอุตุนิยมวิทยา. (2553). **อุทกภัย (Flood)** [ออนไลน์].
ได้จาก: <http://www.tmd.go.th/info/info.php?FileID=70>.
- ประทุมพร พินพิง. (2548). พื้นที่เสี่ยงต่อการเกิดดินถล่มและอุทกภัยภาคเหนือของประเทศไทย. สำนักสำรวจดินและวางแผนการใช้ที่ดิน กรมพัฒนาที่ดิน กระทรวงเกษตรและสหกรณ์.
- รุ่งนภา ตะวันรอน และ ประทุมพร พินพิง. (2547). วิธีการแจ้งเตือนภัยพื้นที่ที่มีโอกาสเสี่ยงภัยต่อการเกิดดินถล่มและอุทกภัย. สำนักสำรวจดินและวางแผนการใช้ที่ดิน กรมพัฒนาที่ดิน กระทรวงเกษตรและสหกรณ์.

สมพร ผาตินาวิน. (2548). **พื้นที่เสี่ยงต่อการเกิดดินถล่มและอุทกภัยภาคใต้ ภาคตะวันออก และภาคกลาง ของประเทศไทย**. สำนักสำรวจดินและวางแผนการใช้ที่ดิน กรมพัฒนาที่ดิน กระทรวงเกษตรและสหกรณ์.

สุรินทร์ ไวกะริญ. (2549). **การวิเคราะห์พื้นที่ที่มีความเสี่ยงจากดินถล่มในประเทศไทย**. สถาบันวิจัยพัฒนาและป้องกันการเป็นทะเลทรายและการเตือนภัย กรมพัฒนาที่ดิน กระทรวงเกษตรและสหกรณ์.

Abe, K. and Iwamoto, M. (1985). **Effects of tree roots on shearing strength**, pp. 341-346. Proc. Int. Symp. On erosion, debris flow and disaster prevention. Quote in Sutep Junkhiaw. (2003). **Flash Flood and Landslide Risk Area in Phuket Province using Geographic Information System**. M.Sc. Thesis, Watershed Management, Kasetsart University, Thailand.

Acharya, G., and Cochrane, T. A. (2009). Development of an integrated model for water induced top soil erosion and shallow landslides. Paper presented at **the 18th World IMACS Congress and MODSIM09 International Congress on Modelling and Simulation**, Cairns, Australia, 13-17 July. pp 1908-1914.

Apirymanekul, C. and Mark, O. (2001). Modeling of urban flooding in Dhaka city. In **the 4th DHI Software Conference**, 6-8 June, Bangkok, Thailand. 101-108.

Barnes, H. H. (1975). Inventory of flash floods - method for computing, protection, forecasting networks; economical consequences, disasters. **Hydrological Science Bulletin**. 20(1): 35-46.

Ballesteros-Cánovas, J. A., Eguibar, M., Bodoque, J. M., Díez-Herrero, A., Stoffel, M., and Gutiérrez-Pérez, I. (2011). Estimating flash flood discharge in an ungauged mountain catchment with 2D hydraulic models and dendrogeomorphic palaeostage indicators. **Hydrological Processes**. 25: 970-979.

- Bateman, A., Medina, V., and Velasco, D. (2010). Soil infiltration effect in flat areas floods simulation. In J. Carrera (eds.). **XVIII International Conference on Water Resources** (pp 1-8). Barcelona: CIMNE.
- Beven, K. (2004). Robert E. Horton's perceptual model of infiltration processes. **Hydrological Processes**. 18: 3447-3460.
- Beven, K. J. and Kirkby, M. J. (1979). A physically based variable contributing area model of basin hydrology. **Hydrological Sciences Bulletin**. 24(1): 43-69.
- Billingsley, P. (1979). **Probability and Measure**. New York: John Wiley and Sons.
- Bureau of Meteorology, Commonwealth of Australia. (2011). **Facts on Flash Floods in NSW** [On-line]. Available: <http://www.bom.gov.au/nsw/sevwx/flashfact.shtml>.
- Chanchai Tanavud, Chao Yongchalermchai, Abdollah Bennui, and Omthip Densreeserkul. (2004). Assessment of flood risk in Hat Yai Municipality, Southern Thailand, using GIS. **Journal of Natural Disaster Science**. 2(1): 1-14.
- Chen, Z. and Wang, J. (2007). Landslide hazard mapping using logistic regression model in Mackenzie Valley, Canada. **Natural Hazard** 42(1): 75-89.
- Cheng, Y. M., and Lau, C. K. (2008). **Slope Stability Analysis and Stabilization**. New York: Routledge.
- Chowdhury, R. (2000). An Assessment of flood forecasting in Bangladesh: The experience of the 1998 flood. **Natural Hazard**. 22: 139-163.
- Coates, D. R. (1977). Landslide. In D. R. Coates (ed.). **Reviews in Engineering Geology Vol. 3** (pp 3-38). Boulder, Colorado: Geological Society of America.

- Coppin, N. J. and Richards, I. J. (1990). **Use of Vegetation in Civil Engineering. Construction Industry Research and Information Association.** Cambridge: Great Britain at the University Press. Quote in Sutep Junkhiaw. (2003). **Flash Flood and Landslide Risk Area in Phuket Province using Geographic Information System.** M.Sc. Thesis, Watershed Management, Kasetsart University, Thailand
- Crozier, M. J. (1973). Techniques for the morphometric analysis of landslps. *Zeitschrift fur Geomorphologie N.F.* 17(1): 78-101. Quoted in Intarawichian, N. (2008). **A comparative study of analytical hierarchy process and probability analysis for landslide susceptibility zonation in lower Mae Chaem Watershed, Northern Thailand.** Ph.D. Thesis, Suranaree University of Technology, Thailand.
- Cruden, D. M. (1991). A simple definition of a landslide. **Bulletin of International Association of Engineering Geology.** 43: 27-29.
- Dai, F. C., Lee, C. F., Li, J., and Xu, Z. W. (2000). Assessment of landslide susceptibility on the natural terrain of Lantau Island, Hong Kong. **Environmental Geology.** 40(3):381-391.
- Das, B. M. (2007). **Principles of Geotechnical Engineering.** Toronto: Nelson, pp 309-315.
- Davie, T. (2002). **Fundamentals of Hydrology.** London: Routledge.
- Dikau, R., Brunsten, D., Schrott, L., and M. L. Ibsen (eds.). (1996). **Landslide Recognition: Identification, Movement and Causes.** Chichester: Wiley & Sons.

- DHI (Danish hydraulic Institute). (2003). **User guide to MIKE 11: A modeling system for rivers and channels**. Software Manual, DHI, Denmark.
- EPOCH. (1993). **The temporal occurrence and forecasting of landslides in the European community**. In J. C. Flageollet (ed.). Contract No. 90 0025, Vol. 3. Quoted in Engineering Group Working Party on Geological Hazards. **Landslide & Slope Instability Geohazards: Classification Schemes - EPOCH** [On-line]. Available: http://www.ukgeohazards.info/pages/eng_geol/landslide_geohazard/eng_geol_landslides_classification_epoch.htm.
- Feller, W. (1971). **An introduction to probability theory and its applications**. Vol II. 2nd ed. Wiley Series in Probability and Mathematical Statistics. New York: John Wiley and Sons, 669 p.
- Gassman, P. W., Reyes, M. R., Green, C. H., and Arnold, J. G. (2007). The soil and water assessment tool: Historical development, applications, and future research directions. **Transaction of the ASABE**. 50(4): 1211-1250.
- GISTDA. (2012). Thailand Flood Monitoring System [On-line]. Available: <http://flood.gistda.or.th/>.
- Greif, V., Sassa, K., and Fukuoka, H. (2006). Failure mechanism in an extremely slow rock slide at Bitchu-Matsuyama castle site (Japan). **Landslides**. 3(1): 22-38.
- Groneng, G., Nilsen, B., and Sandven, R. (2009). Shear strength estimation for Åknes sliding area in western Norway. **International Journal of Rock Mechanics & Mining Sciences**. 46(2009): 479-488.
- Hammond, C., Hall, D., Miller, S., and Swetik, P. (1992). **Level I Stability Analysis (LISA) Documentation for Version 2.0**. General Technical Report INT-285, USDA Forest Service Intermountain Research Station.

- Highland, L. M. and Bobrowsky, P. (2008). **The Landslide Handbook –A guide to Understanding Landslides**. Reston, Virginia: U.S. Geological Survey Circular 1325, Section I Part B. Page 16.
- Hutchinson, J. N. (1988). General Report: Morphological and geotechnical parameters of landslides in relation to geology and hydrogeology. In C. Bonnard (ed.). Proceedings of **the 5th International Symposium on Landslides** (No.1, pp 3-35). Rotterdam: Balkema.
- Inbar, M. M. (1997). Geomorphic catastrophic events and human impact in a Mediterranean-type climate. **Méditerranée**. 86: 53-59.
- Keller, E. A. (2002). **Introduction to environmental geology** (2nd ed). Upper Saddle River, New Jersey: Prentice Hall.
- Kim, K. S., Park, H. J., Lee, S., and Woo, I. (2004). Geographic Information System (GIS) based stability analysis of rock cut slopes. **Geosciences Journal**. 8(4): 391-400.
- Kolmogorov, A. N. (1956). **Foundation of the Theory of Probability**. 2nd edition. New York: Chelsea.
- Lee, S. (2004). Application of likelihood ratio and logistic regression models to landslide susceptibility mapping using GIS. **Environmental Management**. 34(2): 223-232.
- Lee, S. and Pradhan, B. (2006). Landslide hazard mapping at Selangor, Malaysia using frequency ratio and logistic regression models. **Landslides**. 4: 33-41 (9).
- Malet, J. P. and Maquaire, O. (2010). **Risk Assessment Methods of Landslides**. Project Report 2.2, RAMSOIL. Alterra, Soil Science Centre, UK.

- Malone, T. (1999). **Using URBS for real time flood modeling**. Water 99 Joint Congress, Institution of Engineers, Australia. Quoted in Punpim Puttaraksa Mapiam, and Nutchant Sriwongsitanon. (2009). Estimation of the URBS model parameters for flood estimation of ungauged catchments in the upper Ping river basin, Thailand. **SciencAsia**. 35: 49-56.
- Meisina, C. and Scarabelli, S. (2007). A comparative analysis of terrain stability models for predicting shallow landslides in colluvial soils. **Geomorphology**. 87: 207-223.
- Mergili, M. and Fellin, W. (2009). Slope stability and geographic information systems: an advanced model versus the infinite slope stability approach. In: Russian Academy of Sciences, Problems of Decrease in Natural Hazards and Risks, **The Internationally-Practical Conference GEORISK 2009**. pp. 119-124.
- Naruemol Taragsa, Charat Mongkolsawat, Chalermchai Pawattana and Rasamee Suwanweerakamtorn. (2004). An Application of GIS and Hydraulic Model to Flood Plain Inundation. **Journal of Remote Sensing and GIS Association of Thailand**. 5(3): 47-60.
- National Weather Service Weather Forecast Office, Morristown. (2010). **Flash flood** [On-line]. Available: <http://www.srh.noaa.gov/mrx/hydro/flooddef.php>.
- Nelson, E. P., Connors, K. A., and Suárez, S. C. (2007). GIS-Based Slope Stability Analysis, Chuquicamata Open Pit Copper Mine, Chile. **Natural Resources Research**. 16(2): 171-190.
- Nutchant Sriwongsitanon. (2010). Flood forecasting system development for the Upper Ping River basin. **Kasetsart Journal (Natural Science)**. 44(4): 717-731.

- Ogden, F. L., Sharif, H. O., Senarath, S. U. S., Smith, J. A., Baeck, M. L., and Richardson, J. R. (2000). Hydrologic analysis of the Fort Collins, Colorado, flash flood of 1997. **Journal of Hydrology**. 228: 82-100.
- Omar, H., Ibrahim, A. L., and Hashim, M. (2007). Slope stability analysis using remote sensing data. Paper presented at **the 28th Asian conference on Remote Sensing (ACRS 2007)**, Putra World Trade Center, Kuala Lumpur, Malaysia [On-line]. Available: <http://www.a-a-r-s.org/acrs/proceeding/ACRS2007/Papers/PS1.G2.3.pdf>.
- Pradhan, B. (2009). Flood susceptible mapping and risk area delineation using logistic regression, GIS and remote sensing. **Journal of Spatial Hydrology**. 9(2): 1-18.
- Pack, R. T., Tarboton, D. G., and Goodwin C. N. (2001). Assessing Terrain Stability in a GIS using SINMAP. Paper presented at **the 15th annual GIS conference, GIS 2001**, Vancouver, British Columbia.
- Pack, R. T., Tarboton, D. G., Goodwin, C. N., and Prasad, A. (1998). SINMAP a Stability Index Approach to Terrain Stability Hazard Mapping. **SINMAP User's Manual**. Logan: Utah State University.
- Pinyol, N. M., Alonso, E. E., Corominas, J., and Moya, J. (2011). Canelles landslide: modelling rapid drawdown and fast potential sliding. **Landslides**. 9(1): 33-51.
- Phiraphit Phutmongkhon, Thirada Yongsatisak, Nattaya Jungcharoentham, Anan Khampeera, Ratana Tongyoi, Adul Bennui, and Chao Yongchalermchai. (2007). Delineation of flood hazard areas in the Lower Eastern Area of Southern Thailand by Using Geo-informatics. **Journal of Remote Sensing and GIS Association of Thailand**. 8(3): 47-57.

- Punpim Puttaraksa Mapiam, and Nuchanart Sriwongsitanon. (2009). Estimation of the URBS model parameters for flood estimation of ungauged catchments in the upper Ping river basin, Thailand. **SciencAsia**. 35: 49-56.
- Rawee Rattanakom and Suwit Ongsomwang. (2008). The application of GIS for risk Area Analysis in Ubon Ratchathani Province. **Journal of Remote Sensing and GIS Association of Thailand**. 9(2): 42-48.
- Ritter, J. B. (2004). **Landslides and Slope Stability Analysis: using an infinite slope model to delineate areas susceptibility to translational sliding in the Cincinnati, OH area**. Department of Geology, Wittenberg University.
- Saini, S. S. and Kaushik, S. P. (2012). Risk and vulnerability assessment of flood hazard in part of Ghaggar Basin: A case study of Guhla block, Kaithal, Haryana, India. **International Journal of Geomatics and Geosciences**. 3(1): 42-54).
- Shape, C. F. S. (1938). **Landslides and related features - a study of mass movement of soil and rocks**. New York: Columbia University Press. Quoted in Yumuang, S. (2005). **Evaluation of potential for 2001 debris flow and debris flood in the vicinity of Nam Ko area, Amphoe Lom Sak, Changwat Phetchabun, Central Thailand**. Ph.D. Thesis, Chulalongkorn University, Thailand.
- Sombat Yumuang. (2006). 2001 debris flow and debris flood in Nam Ko area, Phetchabun province, central Thailand. **Environmental Geology**. 51:545-564.
- Sumangala. A. (2005). **Flood Inundation Mapping and 1-D Hydrodynamic Modelling Using Remote Sensing and GIS Technique**. Center of Space

Science and Technology Education in Asia and the Pacific, IIRS Campus, India.

Suree Teerarungsikul. (2006). **Landslide Prediction Model Using Remote Sensing, GIS and Field Geology: A Case Study of Wang Chin District, Phrae Province, Northern Thailand**. Ph.D. Geotechnology, Suranaree University of Technology, Thailand.

Sutep Junkhiaw. (2003). **Flash Flood and Landslide Risk Area in Phuket Province using Geographic Information System**. M.Sc. Thesis, Watershed Management, Kasetsart University, Thailand.

Suttisak Soralump and Wisut Chotikasathien. (2007). Integration of Geotechnical Engineering and Rainfall Data into Landslide Hazard Map in Thailand. In Proceedings of **GEOTHAI'07 the International Conference on Geology of Thailand: Towards Sustainable Development and Sufficiency Economy**. Bangkok, Thailand, 125-131.

Tawatchai Tingsanchali and Karim, F. (2010). Flood-hazard assessment and risk-based zoning of a tropical flood plain: case study of the Yom River, Thailand. **Hydrological Sciences Journal**. 55(2): 145-161.

U.S. Army Corps of Engineers. (2003). Engineering and Design: Slope Stability. **Engineer Manual**. Department of the Army, U.S. Army Corps of Engineers, Washington, DC.

Udas, A. (2005). **Slope stability analysis using GIS on a regional scale: a case study of Narayanghat-Mungling highway section, Nepal**. M.Sc. Thesis, Unimersiteit Gent Vrije Universiteit Brussel, Belgium.

- U.S. Army Corps of Engineers. (2003). Engineering and Design: Slope Stability. **Engineer Manual**. Department of the Army, U.S. Army Corps of Engineers, Washington, DC.
- USGS, Kansas Water Science Center. (2005). **Flood Definitions** [On-line]. Available: <http://ks.water.usgs.gov/Kansas/waterwatch/flood/definition.html>.
- Ushakov, N. G. (2001). Density of a probability distribution. **Encyclopedia of Mathematics** [On-line]. Available: http://www.encyclopediaofmath.org/index.php?title=Density_of_a_probability_distribution&oldid=25939.
- Varnes, D. J. (1978). Slope movement types and processes. In R.L. Schuster and R.J. Krizek (eds.). **Special Report 176: Landslides: Analysis and Control** (11-33). Washington D.C.: Transportation Research Board, National Academy Press.
- Vinai Dithajohn. (2006). **OnAsia** [On-line]. Available: <http://www.onasia.com/system/compview.aspx?Filename=vdi0155911.50>.
- Warakorn Mairaing and Nonglak Tajjeamaree. (2004). **Unsaturated Soil Strength for Mountain Slope Stability Analysis**. Proceedings of the 9th National Convention on Civil Engineering. Petburi, Thailand, 1-7.
- Warakorn Mairaing. (2006). Landslide Problems and Warning by Geotechnical Methods. In Proceedings of **The 5th International Symposium on New echnology for Urban Safety of Mega Cities in Asia**, AIT&ICUS, Phuket, Thailand.
- WHO. (2002). **Gender and Health in disasters**. Geneva: World Health Organization.
- Wyllie, D. C. (1999). **Foundations on Rock**. 2nd edition. London: E & FN Spon, pp 19-22.

Wyllie, D. C. and Mah, C. W. (2004). **Rock slope engineering: Civil and mining** (4th ed). New York: Spon Press. p 81.

Zaitchik, B. F. and Van Es, H. M. (2003). Apply a GIS slope-stability model to site-specific landslide prevention in Honduras. **Journal of Soil and Water Conservation**. 5(1): 45-53.

Zaitchik, B. F., Van Es, H. M., and Sullivan, P. J. (2003). Modeling slope-stability in Honduras: Parameter Sensitivity and scale of aggregation. **Soil Science Society of America Journal**. 67: 268-278.



CHAPTER III

CHARACTERISTICS OF THE STUDY AREA

In the thesis, Nam Li Watershed is chosen as a study area which was experienced severe damage in a big catastrophic event in Thailand. The characteristics mentioned in this Chapter included location, climate, topography, geology, and engineering properties of rocks.

3.1 Location

The Nam Li watershed is located in the northwestern of Tha Pla District, Uttaradit Province. It covers 3 villages of Nam Hman Subdistrict which are Ban Nam Ta, Ban Nam Ri, and Ban Sai Ngam. It contains 434 households and 1,565 people living in (ลักษณะวรรณ หอศิลป์, 2546). The extent of the study area is bounded by the grid lines 1985000 N, 625000 E at the upper left corner and 1969000 N, 640000 E at the lower right corner of the UTM coordinate system of zone 47 N. Its datum is WGS 1984. Its area is approximately 200 square kilometers. The study area encompasses:

Northern part: Cho Hae Subdistrict of Mueang Phrae District and Hua Fai Subdistrict of Sung Men District, Phrae Province,

Southern part: Khun Fang Subdistrict and Ban Dan Na Kham Subdistrict of Mueang Uttaradit District, Uttaradit Province,

Eastern part: Nam Mhun Subdistrict and Cha Rim Subdistrict of Tha Pla District, Uttaradit Province,

Western part: Huai Rai Subdistrict of Den Chai District, Phrae Province and Ban Dan Na Kham Subdistrict of Mueang Uttaradit District.

The watershed is officially taken care by the Nam Li watershed Management Unit which is an organization of the Right of Lam Nam Nan National Park. The whole study area is one of the catchments of Nan River. The location and grid DEM data of the study area is shown in Figure 3.1.

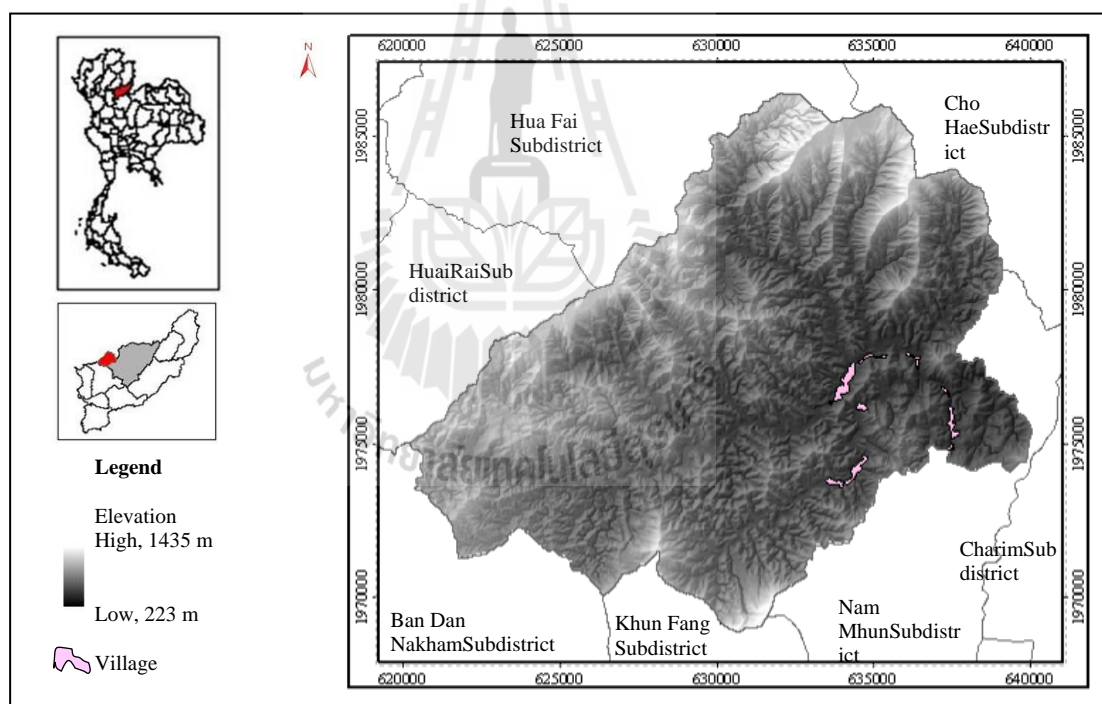


Figure 3.1 Location of the study area.

3.2 Climate and precipitation

The climate of the study area is tropical. The average annual temperature is 27°C. The lowest temperature is 9°C in January, and the highest is 42°C in April. The

mean annual rainfall is usually from 1,350 mm to 1,600 mm. The average annual relative humidity is about 55% (ลักษณะวรรณ หอศิลป์, 2546). The monthly precipitation data of years 2005, 2006, and 2007 from the TMD were plotted and displayed in Figure 3.2.

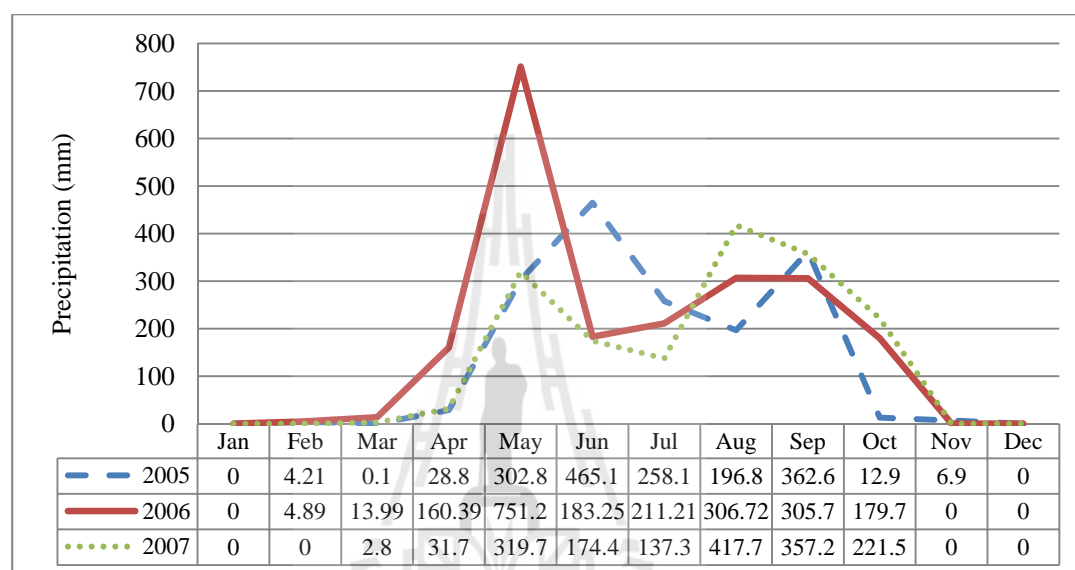


Figure 3.2 The precipitation intensity of Nam Li watershed during years 2005, 2006, and 2007.

From: Thai Meteorological Department (2009).

In Figure 3.2, during 2005-2007, the highest precipitation of the year was represented in June, May, and August, respectively. It is noted that the rain of the year 2006 which associated with a catastrophic event of landslide and flashflood started in April. The cause of the occurrence was the relatively very low pressure moved to cover the lower part of the country. Akapon Sumongkol (2006) reported that the heavy rainfall of this event was a return period occurrence of 500 years.

3.3 Land use and land cover (LU/LC)

The LU/LC of the area was classified by the LDD (2004) into 7 classes including paddy, corn (swidden cultivation area), perennial, mixed orchards, deciduous forest, village, and water body. Most area was forest and swidden cultivation area. Vector-based land cover map of the LDD (copyright 1994 @ Department of Land Development) is shown in Figure 3.3.

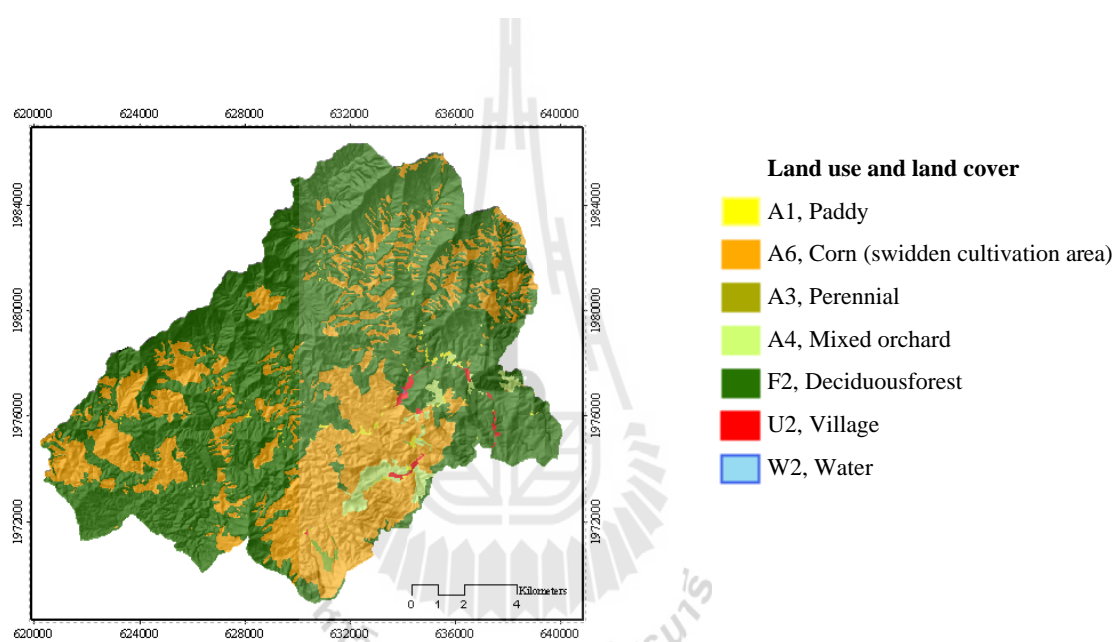


Figure 3.3 The land cover map in year 2004.

Source: Land Development Department (2004).

From field investigation, the forest consisted of hill evergreen forest, dry evergreen forest, and mix deciduous forest. The hill evergreen forest was situated on the high ridge of the northern part of the area, at Phu Phraya Pho which is connected to the boundary of Phrae province. Several species of the hill evergreen forest are included, e.g. Fagaceae (Thai name is Ko), *Schima wallichii* (DC.) Korth. (Thai name is Mangtan), Iron wood (Thai name is Takean Tong) etc. The hill evergreen forest was located in high

humidity areas which were on hill slope and valleys along streams. The vegetation included teak, bamboo, and swidden cultivation area. The swidden cultivation area was covered by grasses, *Alpiniamalaccensis* (Thai name is Kha), and corn. The forest plantation was located in the upstream of Huai Nam Rid and near the villages. The trees such as teaks, *Irvingiamalayanus* (Thai name is Krabok), and many types of dipterocarpaceae (Thai name is Yang) were planted by the Nam Li watershed Management Unit. The mixing orchards include drambehs (Thai name is Ma Fai), langsats, mangoes, bananas, jackfruits, pomeloes, durians, and cashew nuts planted near the villages. The small paddies were located along the valley flat of Nam Rid and the Nam Li. Vector-based land cover map of the LDD was modified by information from field investigation in year 2007 into 7 classes including paddies, corns (swidden cultivation area), mixed orchards, old growth forest, forest plantation, village, and water. The modified LU/LC map was shown in Figure 3.4.

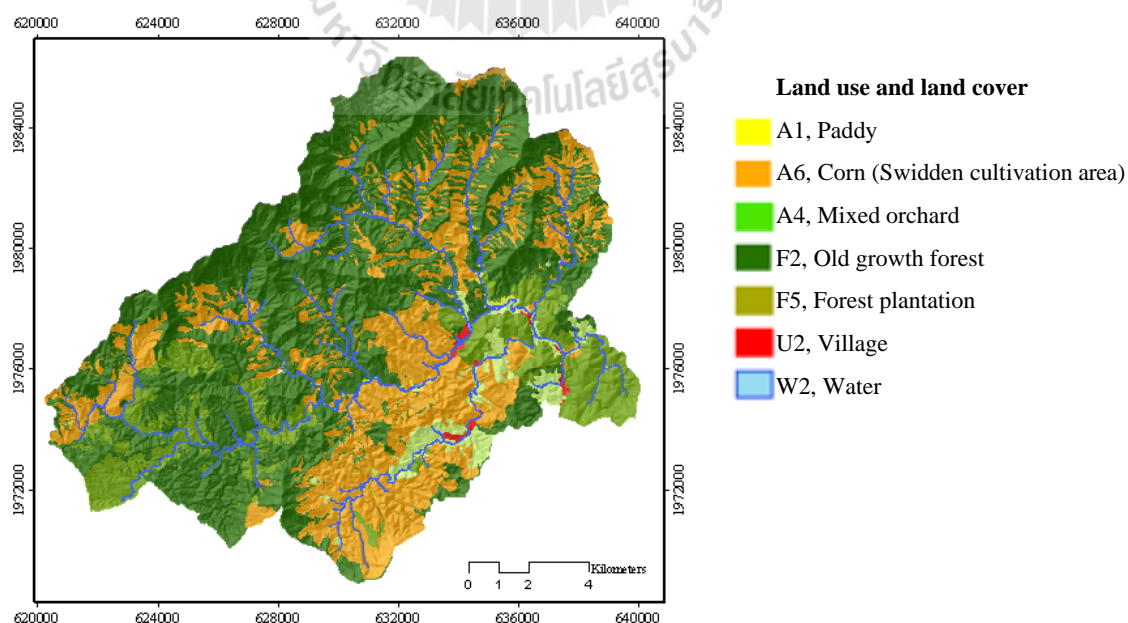


Figure 3.4 The modified land cover map of the study area in year 2007.

3.4 Slope

From field investigation and Digital Elevation Model data (DEM) data, the landform of the area is highland which consists of complex high hills and valleys. The drainage patterns are parallel and dendritic. The main drainage sub-basins include Huai Nam Rid and many streams, such as Huai Nam Ta, HuaiHin, Huai Sai Ngam and Huai Chem Toem. The upstream rim is bounded by the steep slope. The maximum altitude of the area is 1,447 m above mean sea level (MSL) down to the narrow flat area at altitude about 200 m MSL (see elevation or DEM data in Figure 3.1). The highest mountain range is Phu Phraya Pho located in the north of the area. Some mountains run north-east to south-west; others run north to south. The slope angles of the area are in range of 0.49 to 52.05degrees depicting on DEM with 5 m \times 5 m spatial resolution. The steep slopes are located in the northern upstream part of the area. The characteristic of slope in the area is depicted in Figure 3.5.

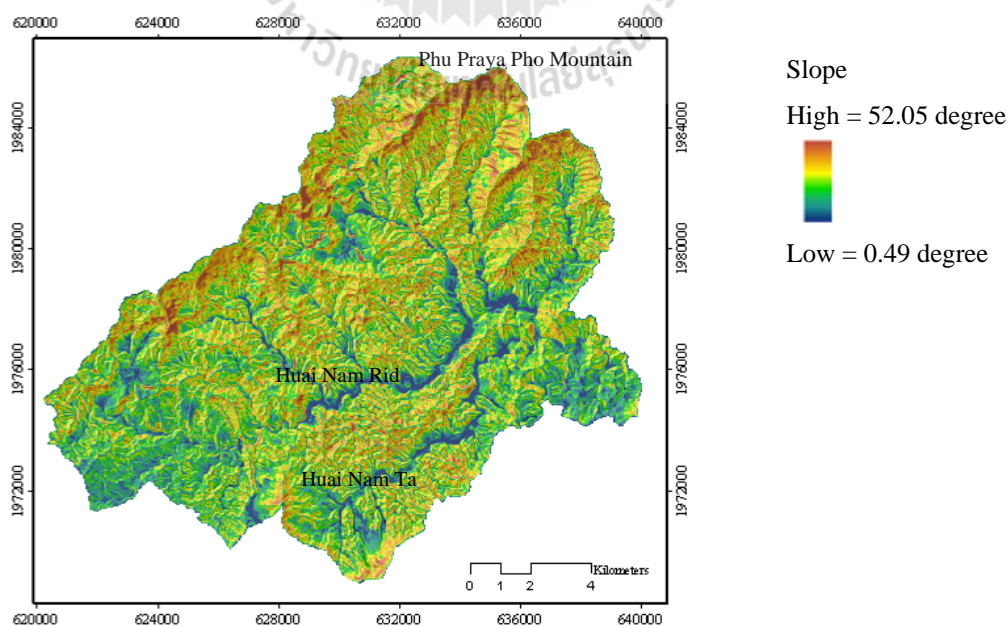


Figure 3.5 The characteristic scales of slope in the study area.

3.5 Geology

The geology of the area was previously mapped and described by Apichat Lamchuan and Suchai Sinpunanan (อภิชาติ ลำจวน และ สุชัย สิ้นพูนอนันต์, 2530) and presented in the series of geological maps of Thailand 1:50,000 by the Department of Mineral Resources, DMR (2006) as shown in Figure 3.6. The study area is underlain by rocks ranging in age from Carboniferous to Triassic. The stratigraphic sequences consist of meta-sedimentary rocks in northern part, known as the Mae Tha Group (C). The parts of eastern, central and southern consist mainly of sedimentary rocks in age Permian, known as the Kiu Lom Formation (P1). The western part consists of sedimentary rocks in age Triassic, known as the Phra That Formation (Tr1). The description of these rock units are shown in Table 3.1.

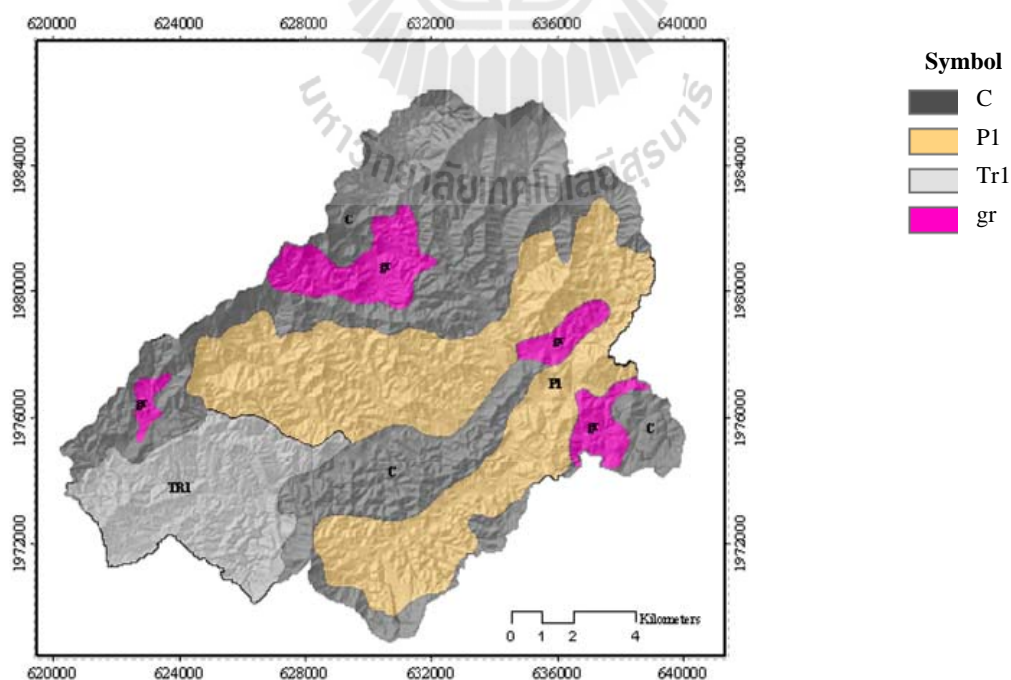


Figure 3.6 The geologic units of the study area.

Source: Department of Mineral Resources (2006).

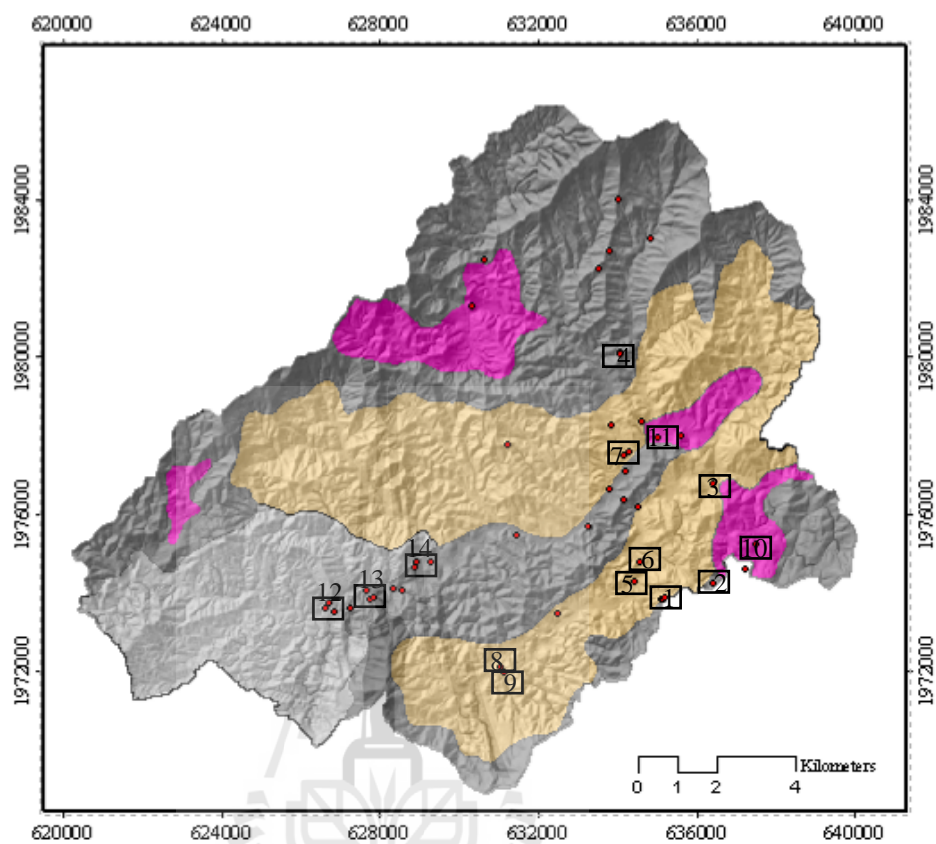
Table 3.1 The stratigraphy of the study area.

Age	Group	Formatio	Symbol	Lithology
Triassic	Lampang	Phra That	Tr1	Reddish-brown conglomerate, rhyolite, andesite tuffaceous sandstone, gray to brown shale with limestone lenses.
	Intrusive Igneous rock		gr	Hornblende-biotite granite, white to gray biotite granite.
Permian	Ratburi	KiuLom	P1	Sandstone, shale, graywacke, conglomerate, agglomerate and tuff with limestone lenses.
Carboniferous	Mae Tha		C	Phyllitic shale, slaty shale, phyllite, schist and phyllite with augenchert

Source: อภิชาติ ลำจวน และ สุชัย สีนพูนอนันต์ (2530).

อภิชาติ ลำจวน และ สุชัย สีนพูนอนันต์ (2530) reported no fossils found in this area, furthermore the rocks were metamorphosed and deformed and made them hard to identify the stratigraphy and age. The C unit consists of phyllitic shale, slaty shale, phyllite, schist, and phyllite with augenchert. From field investigation, weathered phyllitic shale and slaty shale were found the most. The P1 unit consists of sandstone, shale, graywacke, conglomerate, agglomerate, and tuff with limestone lenses. The fine-grained tuffaceous sandstone (weak rock) and metamudstone are the outcrops found in the field. The gr unit consists of moderately weathered rocks and float rock which are mainly medium-grained biotite granite and medium- to fine-grained granite. At a part of the contact, silicified siltstone was found. The rocks of Tr1 unit are mainly reddish-brown sandstone with being moderately weathered.

From field investigation, as examples, photos of rock outcrops of various stratigraphic units are displayed in Figure 3.7.



(a) The field investigation sites visited.



(b) The site No.1: bedded chert.



(c) The site No.2: meta-siltstone.

Figure 3.7 Examples of field investigation outcrops.



(d) The site No.3: silty shale.



(e) The site No.4: phyllitic shale/bedded chert interbedded.



(f) The site No.5: fine-grained tuffaceous sandstone.



(g) The site No.6: rhyolite.



(h) The site No.7: fine-grained tuffaceous sandstone (weak rock).



(i) The site No.8: meta-mudstone.

Figure 3.7 Examples of field investigation outcrops (Continued).



(j) The site No.9: tuffaceous sandstone/
meta-mudstone complex.



(k) The site No.10: medium-grained
biotite granite.



(l) The site No.11: medium-fine-grain
granite contact silicified siltstone.



(m) The site No.12: reddish-brown
sandstone.



(n) The site No.13: reddish-brown
sandstone.



(o) The site No.14: reddish-brown
sandstone.

Figure 3.7 Examples of field investigation outcrops (Continued).

The hillshade image showing topographic pattern together with information from field investigation or outcrop examination (as examples shown in Figure 3.7) were used to modify geologic unit boundaries. For example, at the site No.12 and No.13 the rocks are reddish-brown sandstone and conglomerate of the unit Tr1 while in geologic map they were mapped as the C unit of which the main rock type is phyllitic shale. Therefore, the boundary between Tr1 unit and C unit near site No.12 and No.13 was modified by image interpretation. As a result, the geologic map was modified as shown in Figure 3.8 with the unit description in Table 3.1.

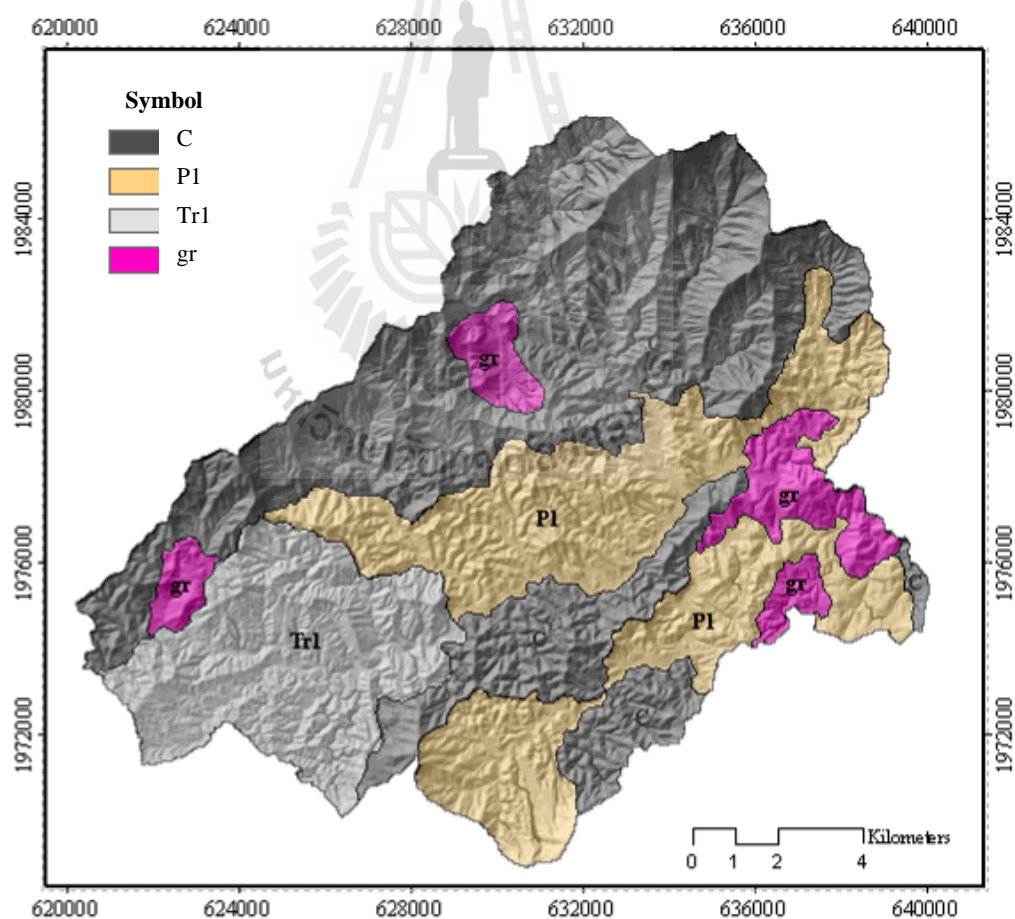


Figure 3.8 The modified geological map of the study area.

3.6 References

- ลักษณะวรรณ หอศิลป์. (2546). หน่วยจัดการต้นน้ำน้ำดี อำเภอท่าปลา จังหวัดอุตรดิตถ์. สำนักบริหารจัดการพื้นที่ป่าอนุรักษ์ 11 กรมอุทยานแห่งชาติ สัตว์ป่า และพันธุ์พืช. (เอกสารที่ไม่ได้พิมพ์เผยแพร่).
- อภิชาติ ลำจวน และ สุชัย สิ้นพูนอนันต์. (2530). **ธรณีวิทยาระวางเขื่อนสิริกิติ์ และระวางอำเภอท่าปลา**. กองธรณีวิทยา กรมทรัพยากรธรณี. (เอกสารที่ไม่ได้พิมพ์เผยแพร่).
- Akapon Sumongkol. (2006). **Inundation and Landslide of Uttaradit Province 2549 B.E.**.The Department of Public works and Town & Country PlanningUttaradit Province [On-line]. Available: <http://www.dpt.go.th/stbd/files/uataradit1-10.pdf>.
- Department of Mineral Resource. (2006). **Geological map of Thailand scale 1:50,000, map sheet 5144 IV and 5044 I** [Shape file]. Bangkok: DMR.
- Land Development Department. (2004). **DinThai** [Computer programme]. Bangkok: LDD.
- Thai Meteorological Department. (2009). **Rainfall data** [Excel file]. Bangkok: TMD.

CHAPTER IV

LANDSLIDE SUSCEPTIBILITY MODELING

4.1 Abstract

The purpose of the research is to evaluate landslide impact intensity in Nam Li watershed, Uttaradit, Thailand. The infinite slope stability analysis with the concept of Factor of Safety (FS) was applied to determining landslide susceptibility index (LSI) indicating comparatively potential landslide risk area. The less LSI indicates the more unsafe area. The FS calculation requires the weight of material on slope failure (W), slope angle (β) and rock properties such as cohesion (c), internal friction angle (ϕ), and unit weight of rock (γ). These variables could be provided under the domains of geologic units and slope characteristics in the form of GIS vector layers for mathematical operation. The geological map layer contains the attributes of those rock properties while the slope map layer derived from TIN (Triangulated Irregular Network) contains slope angle and slope height. The union of these two layers resulted in the layer containing polygons with identical combination attributes for LSI calculation.

Due to the spatial complexity of mixed kinds of rocks in a geological mapping unit and their structure, quantitative engineering properties which were related to landslide were existed in specific range of number. This could lead to the existence of range for calculating LSI at a certain TIN polygon. Therefore, the probability of landslide occurrence was determined in each TIN polygon using Probability Density

Function (PDF). The range of LSIs of each geologic unit associated with landslide scars was extracted. The LSIs of C, P1, gr, and Tr1 units were sliced into 12, 17, 23, and 18 ranges, respectively. Each LSI was considered as a candidate for each TIN polygon to determine a final critical LSI. Then, the slope of each polygon, mean and standard deviation of LSI from the possible composite properties of the rock unit were input to PDF to estimate the probability of failure indexes (PFIs). The candidate LSI of the layer depicting the highest fitting ratio between ratio and candidate LSI was identified as the critical LSI. PFIs from the critical LSI between 0-1 were classified to be 5 classes using equal ranging including 0-0.2, 0.2-0.4, 0.4-0.6, 0.6-0.8, and 0.8-1.0 corresponding to very low, low, moderate, high, and very high landslide susceptibility, respectively.

Keywords: GIS/FS/PDF/landslide/Uttaradit

4.2 Introduction

Many landslide hazards were studied using index model (e.g. กรมพัฒนาที่ดิน, 2547; Suree Teerarungsigul, 2006). Score and weight of criteria for index calculation seem to be more subjective or arbitrary and more likely depend on the uncertain expert-claimed opinions. Some used geotechnical method (e.g. Warakorn Mairaing and Nonglak Taijeamaree, 2004; สุรินทร์ ไวกเจริญ, 2549; Soralump et al., 2010) which more concentrate on site investigation than large area evaluation. In recent year, the application of simplified slope stability models has been proven as effective as the descriptive and predictive tools in temperate zones, led to rapid stability assessment over a wide area (e.g. Montgomery and Dietrich, 1994; Pack et al., 1998; Zaitchik and

van Es, 2003, Zaitchik, van Es, and Sullivan, 2003; Mergili and Fellin, 2009). The slope stability analysis in term of factor of safety (FS) was chosen to determine landslide susceptibility index (LSI) in TIN (Triangulated Irregular Network) polygons represented slope surface.

The big event of landslide was occurred in Nam Li watershed during 20-22 May 2006. Plenty of scars could be easily recognized on SPOT imagery dated 13 January 2007. From the geological map prepared by Lamchuan and Sinpunanan (อภิชาติ ถ้ำจวน และ สุชัย สีนพูนอนันต์, 2530), this mountainous area consists of 4 geologic units and was selected as the study area for this research. Spatial analysis of landslide scars appeared in the SPOT imagery was performed. The scars were visually extracted and converted to be a raster layer of 5 m × 5 m cell size for overlay analysis in the study. The slope failure occurred in all geologic units of the study area as shallow landslide with mainly circular sliding plane. The radius of the circular was so big that the failure is close to be plain type. To calculate LSIs of each TIN polygon in the study area, engineering properties input in the equation were mainly based on mapping rock units. The mean, a single value, was used to represent each property. In fact, by geological mapping, the rock unit was classified and mapped according to rock types and time period when the unit was formed. The result showed that the mapped rock unit could contain many kinds of rocks. Moreover, by nature, each engineering property of a certain kind of rock varies in a range, not a single value. Therefore, the LSIs of TIN polygons derived from single values of rock properties cannot as much practically reflect the probability of landslide occurrences as it should be.

To cover engineering properties existing in a certain kind of rock as much as possible, the input for LSI calculation should be varied to various values in a range. Then all possible combinations of these properties and slope can be used as representative inputs into the Probability Density Function (PDF) (Wyllie, 1999). The PDF is a relative for the continuous random variable to take on a given value (Kolmogorov, 1956; Feller, 1971; Billingsley, 1979). The results in Probability of Failure Indexes (PFIs) are further used to indicate the probability of landslide occurrence. Therefore, the purpose of this study is to analyze the probability of landslide occurrence of the Nam Li watershed in term of PFI using PDF.

4.3 Research methods

4.3.1 Research procedure

The 2 main steps of the research procedure of the part: (1) slope stability analysis and (2) probability of failure analysis are shown in Figure 4.1. All data were prepared in GIS vector layer and analyses were operated on raster-based GIS data. The details of these steps can be explained as the followings.

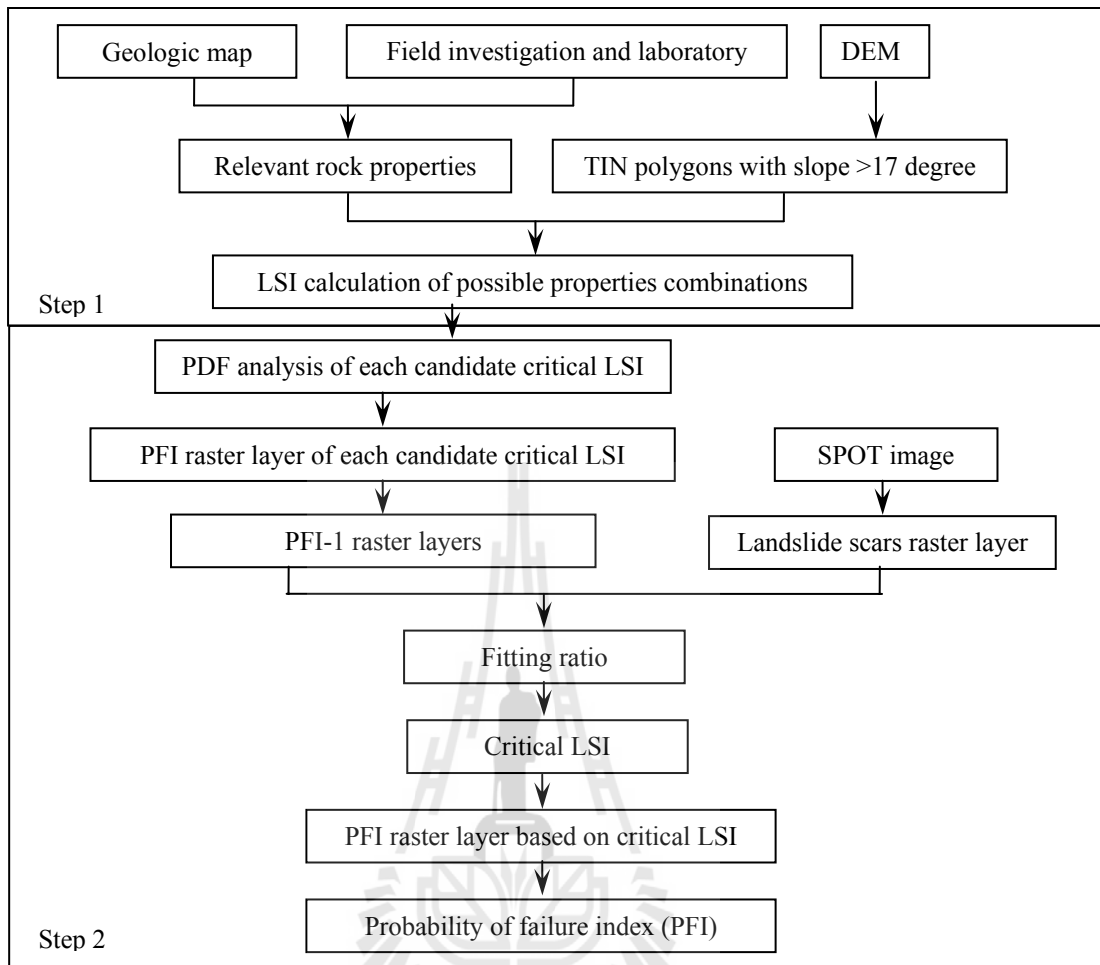


Figure 4.1 The procedure framework of landslide susceptibility modeling.

4.3.2 Slope stability analysis

The high resolution DEM data in form of contour with 5 m interval of the Land Development Department (LDD) of Thailand, the grid DEM (5 m × 5 m) and TIN were generated. The TIN polygons were considered as the representative of slope surfaces of the area. The slope angle appeared in attribute of each TIN polygon was later estimated. The intersection of TIN and the geologic polygons could result in TIN polygons of the rock unit with identical slope. Only polygons with slope angle bigger than 17 degree (approximately 30%) were extracted for further LSI analysis and the rest was identified as insensitive area. This is because, in general, the critical

angle of repose of material was approximately set up at 30% (Coe, Michael, Crovelli, and Savage, 2000; Mahidol University, 2003). It means that the material with surface slope bigger than this angle is not stable and more likely to slide down.

The Factor of Safety (FS) value was calculated by infinite slope stability method in 1D model which is most commonly employed for the purpose of slope failure (Das, 2007; Mergili and Fellin, 2009). The FS is the ratio between resisting and driving force. The resisting force is the shear strength (τ_r) and the driving force is the shear stress (τ_d). The equations involved the Mohr-Coulomb failure criterion as shown Equation (2.1) and (2.2) in the Chapter II.

The landslide susceptibility index (LSI) was created on the basis of the factor of safety (FS) but the result is not as accurate as the site investigation to which FS is practically applied. The indexes obtained by this method are considered more objective and relying on geotechnical concept and theory, which are more related to the landslide occurrence than the conventional index model. The equation of calculation the LSI involves Mohr-Coulomb failure criterion (Keller, 2002; U.S. Army Corps of Engineers, 2003; Wyllie and Mah, 2004; Das, 2007; Cheng and Lau, 2008; Mergili and Fellin, 2009) as shown in Equation (4.1):

$$FS = \frac{c + (\gamma \cdot Z - \gamma_w \cdot Z_w) \cdot \cos^2 \beta \cdot \tan \phi}{\gamma \cdot Z \cdot \sin \beta \cdot \cos \beta}, \quad (4.1)$$

where FS is the factor of safety which was represented to be the LSI, c is the cohesion of material (kN/m^2), γ is the unit weight of material (kN/m^3), γ_w is the unit weight of water (9.81 kN/m^3), Z is the thickness of slope material above sliding plane (m), Z_w is the thickness of saturated slope material above sliding plane (m), β is slope angle

(degree), and ϕ is the internal friction angle of material (degree). The detail of equation was expanded in Appendix B.

The all LSIs of each geologic unit were compared with the land slide scars. The LSIs which falling in scars were keep to be active LSIs for probability of failure assessment. The procedure of step 1 was expanded in Figure 4.2.

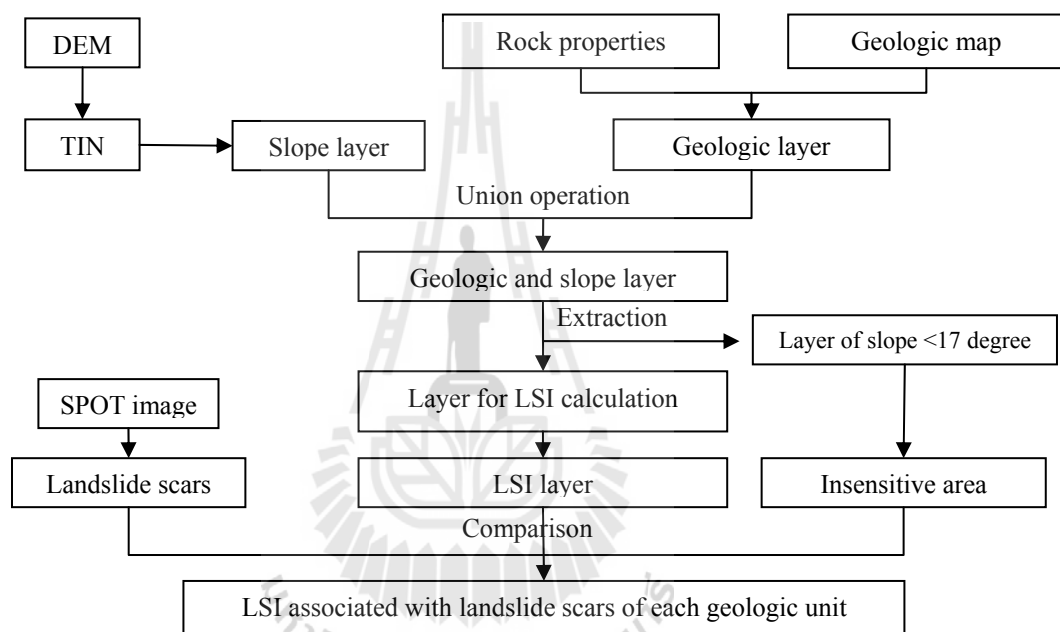


Figure 4.2 The procedure framework of slope stability analysis.

In the first test of LSI (Sirilak Tanang, Sunya Sarapirome, and Sasikan Pliklang, 2010), the LSIs were calculated from the average of rock properties. The LSIs were considered to be index relative to frequency of landslide scars occurrence. Even though the result of LSI values was apparently reasonable in the overall, it is not reasonable when LSI values of each geological unit were considered. Some geologic unit showed the frequency of landslide scar in the wide range and some unit showed narrow range. Using the lowest to the highest of LSI from all geologic units was

unreasonable. Then, this thesis proposed the rock properties categorization into classes and calculation of LSI from all combination of rock properties.

4.3.3 Probability of failure assessment

All possible combinations of these properties and slope can be used as representative inputs into the Probability Density Function (PDF). The result in Probability of Failure Indexes (PFIs) was further used to indicate probability of landslide occurrence. Therefore, the purpose of this study is to analyze the probability of landslide occurrence of the Nam Li watershed in terms of PFI using PDF. As an example studied by Sarapirome and Tanang (2012), the PFI of the C rock unit was determined using PDF. The result showed acceptable result.

The rock properties were categorized into 6 classes, and 216 possible combinations of rock properties of each TIN polygon can be set up as input into Equation (4.1). Considering the sensitive area of the rock unit, excluding the insensitive area, only slope angle can be varied among polygons and each polygon can end up with 216 LSIs. All polygons of the sensitive area were transformed to be cell-based. With raster-based overlay analysis, the range of LSIs from cells associated scars was able to be extracted. A number of sub-ranges were applied to slide the range of LSIs and all sub-ranges were captured by a number of LSIs. Each of which became a candidate of critical LSI that could provide the most accurate prediction of probability of landslide occurrences.

Together with each candidate LSI (x), the mean (\bar{x}) and standard deviation (SD) of LSIs of each TIN polygon were calculated and put into Equation (4.2), the PDF for PFI calculation (Wyllie, 1999), as shown below:

$$f(x) = \frac{1}{SD\sqrt{2\pi}} \exp\left[-\frac{1}{2}\left(\frac{x-\bar{x}}{SD}\right)^2\right], \quad (4.2)$$

where x is a candidate LSI, \bar{x} and SD is the mean and the standard deviation of LSIs in each TIN polygon.

Then, for each TIN polygon, PFI of each candidate LSI was achieved. The values of calculated PFIs were between 0 and 1.

To find out the actual critical LSI, the layer of TIN polygons could be transformed to be raster layers of all candidates with PFI of any cell equal to 1 when it was 1 or 0 otherwise. A number of raster layers obtained was equal to a number of the candidates. Overlay analysis using Equation (4.3) of each raster layer of a candidate and the raster layer of landslide scars was performed to find the candidate capability to provide the most fitting ratio:

$$FR = \frac{A \cap B}{(A \cup B) - (A \cap B)}, \quad (4.3)$$

where FR is the fitting ratio of a number of cells obtained from the intersect of PFI-1 and scars cells ($A \cap B$) and the difference number of cells between the union of all PFI-1 and scar cells and the intersect of PFI-1 and scar cells ($(A \cup B) - (A \cap B)$). ($A \cap B$) is a number of PFI-1 cells falling in landslide scars which indicated the accuracy of the prediction while $(A \cup B) - (A \cap B)$ is the disagreement number of PFI-1 and landslide scar cells which indicated their discrepancy. The candidate LSI layer that could provide the best fitting ratio or the highest ratio was identified to be the critical LSI.

The raster layer of the critical LSI with the original PFI of each cell was then classified into 5 classes from very low to very high probability of landslide occurrence. The frequency of scar cells in each class was then checked to see the prediction capability of the landslide occurrence map. The procedure of step 2 was expanded in Figure 4.3.

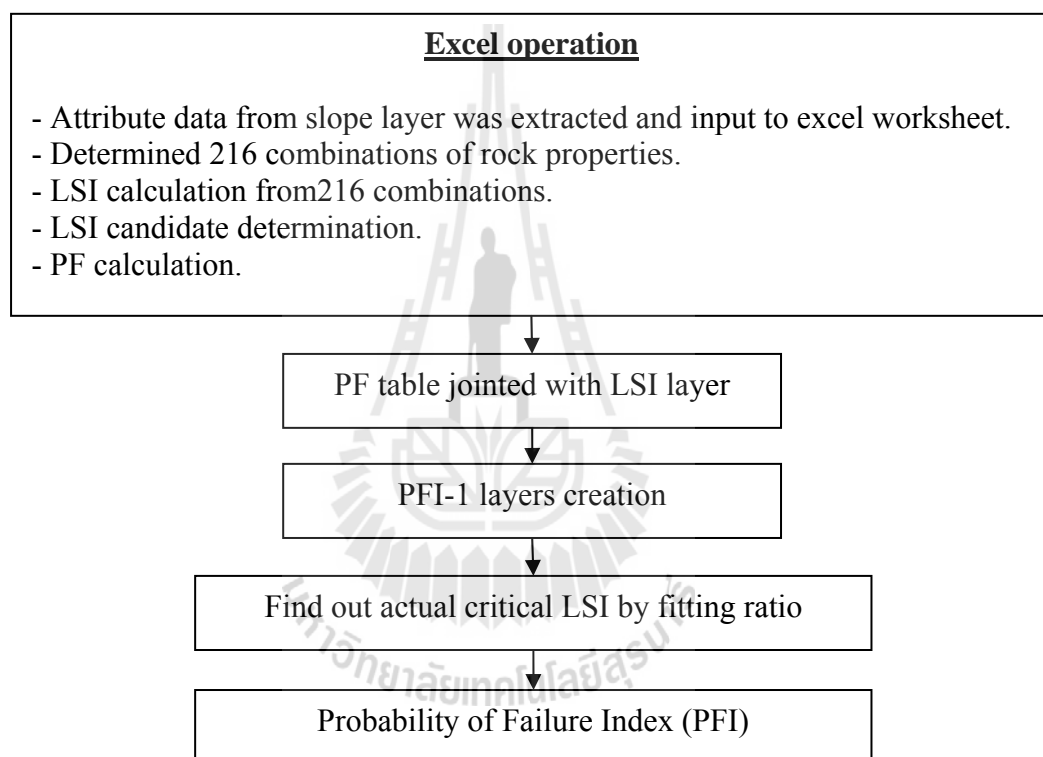


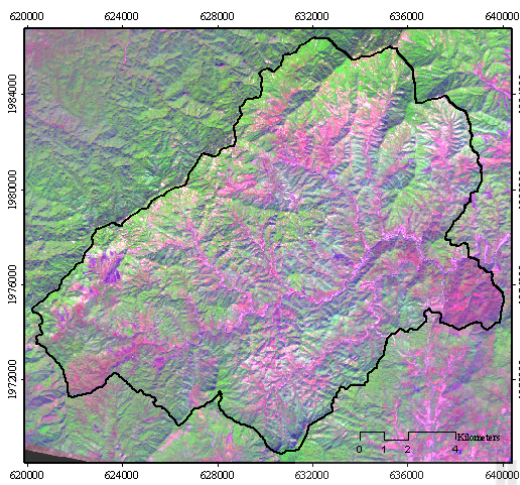
Figure 4.3 The procedure framework of landslide impact intensity assessment.

4.4 Data collection and data preparation

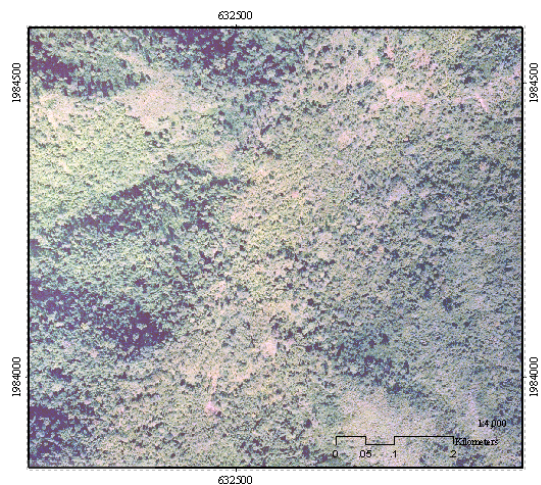
4.4.1 SPOT imagery and landslide scars layer

Satellite imageries were obtained SPOT5 imagery on January 13, 2007, scene ID (K-J) 260-314 (Copyright 2007 © GISTDA). The SPOT5 product has been used for landslide scars and flash flood extraction by visual interpretation. The HM+HJ

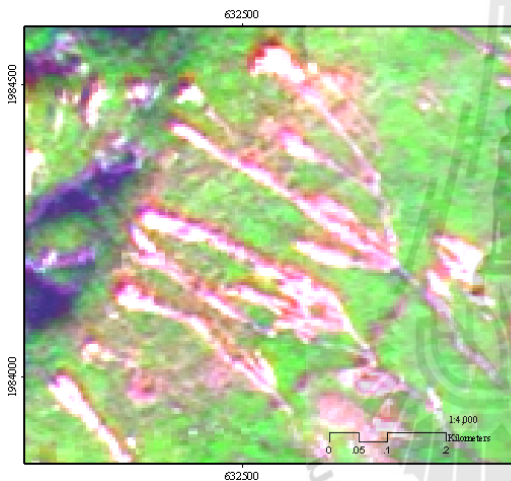
mode (4 spectral bands with 5 m resolution) was selected in the study which consist of 4 spectral bands (green = 0.43-0.47 μm , red = 0.61-0.68 μm , NIR = 0.78-0.89 μm , SWIR = 1.58-1.75 μm) and pan sharpening (0.48-0.71 μm). They are obtained by merging two separate images acquired simultaneously by the same HRG instrument, one in panchromatic mode at 5 m resolution and the other in 4 bands multispectral mode at 10 m resolution. Images thus obtained are similar to a 4 bands color image, with a resolution of 5 meters and panchromatic viewing geometry. For scars extraction, the false color composite image (RGB = bands 4, 1, 3) and scale of 1:4,000 displaying were used. Hence the 3 bands have contained spectral characteristic of vegetation (Jensen, 2007), then the colors in an image is the vegetation except white and bright color. The criterion for visual interpretation was the white and bright cells that it was adjacent cells not less than 64 cells. The meaning of 64 cells was the area size equal 1 rai or 1,600 m^2 which is the minimum mapping unit scale clearly displayed on map scale of 1:50,000. The white and bright cells were compared with orthophotographs which acquired in 2004 before landslide occurrence. The white and bright cells appeared as bare land in orthophotographs and in SPOT5 imagery were not considered to be landslide scars. On the other hand, if they were vegetation or building in orthophotographs, then they were landslide scars in SPOT5 image (Figure 4.4). The 1,813 polygons of scars were verified by 433 points by field check. The examples of check point selection were based on the landslide scars extraction which was more convenient to access as shown Figure 4.5. From field investigation, no landslide scars was found in the insensitive area which slope is <17 degree.



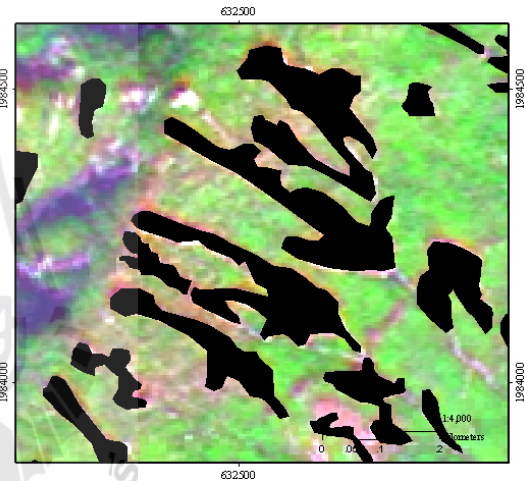
(a) SPOT5 imagery (RGB = bands 4, 1, 3).



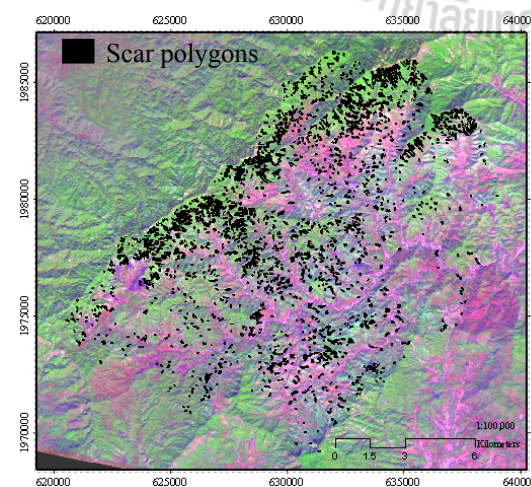
(b) Orthophotograph acquired on year 2004.



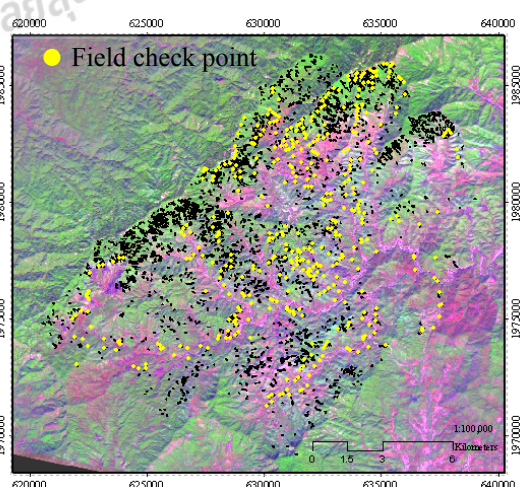
(c) The white and bright colors are scars.



(d) Landslide scars extracted (black color).

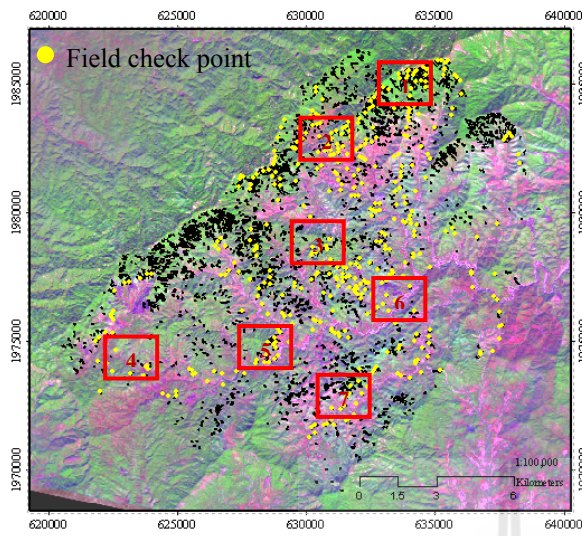


(e) The 1,813 landslide scars extracted.



(f) The 433 field check points.

Figure 4.4 The landslide scars extraction from the SPOT5 imagery.



(a) The 433 field check points.



(b) The example No.1.



(c) The example No.2.



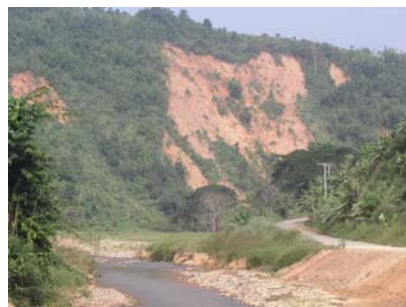
(d) The example No.3.



(e) The example No.4.



(f) The example No.5



(g) The example No.6.



(h) The example No.7

Figure 4.5 The examples of landslide scar check points.

4.4.2 Digital elevation model and slope layer

Spatial varying slope angles were derived from DEM through TIN generation. The contour line from LDD was used to generate DEM raster data with cell size of $5\text{ m} \times 5\text{ m}$. Triangle polygons of TIN were extracted to represent each slope surface in the area. The slope angles of the study area are in range 0.49 to 52.05 degree that the preparation step showed in Figure 4.6. The slope layer was derived from TIN as showed in Figure 4.7.

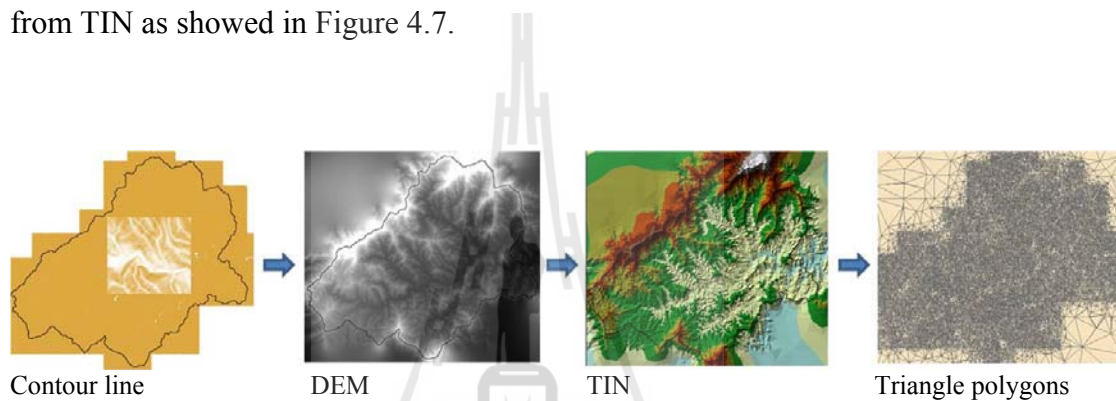


Figure 4.6 Steps of slope layer preparation.

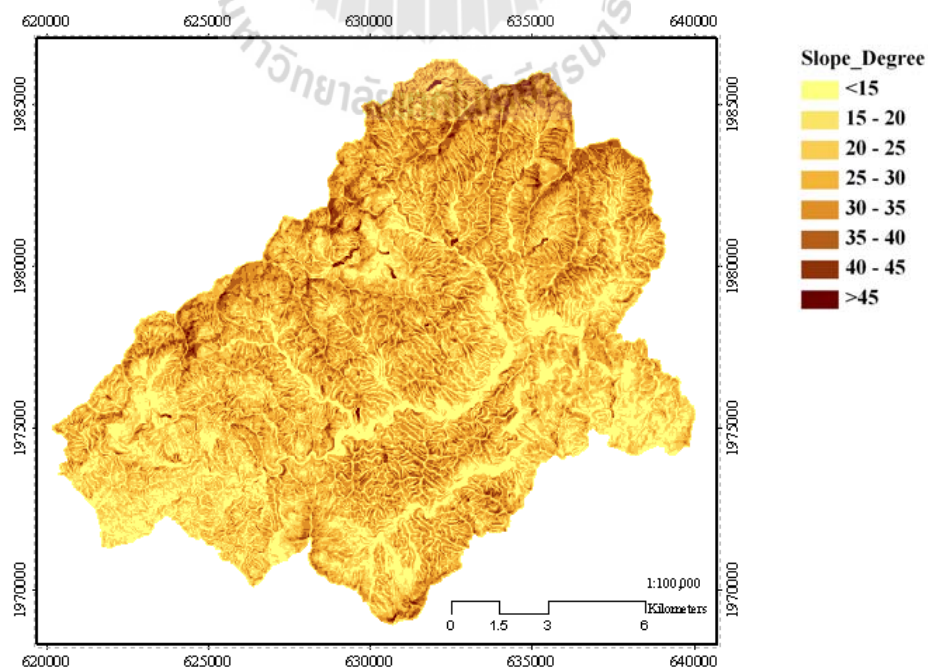


Figure 4.7 Slope Layer.

4.4.3 Rock properties data and geologic layer

The geotechnical properties of rocks used in this research depended on shear failure surface and the rocks were assumed to be a Mohr-Coulomb material (Wyllie, 1999). These properties consist of cohesion, average unit weight, and tangent of average friction angle. The rock mechanic testing of Point Load Strength Index Testing, Slake Durability Index Testing, and Direct Shear Testing were used for rock properties extraction, the details were described in Appendix C. The C unit was selected to be samples for Direct Shear Testing, because the highest landslide scars were occurred in this unit. The result of direct shear testing matched with the rock properties in the reviewing. Hence, rock properties of 4 units were adopted from the researches and records of Goodman (1989), Wyllie and Mah (2004), and Alden (2010) by matching rock types and characteristics. Thus, a set of rock properties as input data for the analysis are listed in Table 4.1.

Table 4.1 Geotechnical properties of rocks of 4 geologic units in the study area.

Geologic units	Group/ Formation	Rock Classification	Cohesion, c (kN/m ²)	Unit weight, γ (kN/m ³)	Friction angle, ϕ (degree)
C	Mae Tha	Phyllitic shale	5.0×10^3	23.54×10^3 - 27.47×10^3	20-27
gr	Intrusive Igneous rock	Biotite granite	55.2×10^3	25.51×10^3 - 26.49×10^3	34-40
P1	Ratburi/ Kiu Lom	Tuffaceous sandstone	38.4×10^3	21.58×10^3 - 27.47×10^3	27-34
Tr1	Lampang/ Phra That	Red sandstone	27.2×10^3	23.54×10^3 - 25.51×10^3	27-34

Source: Goodman (1989), Wyllie and Mah (2004), and Alden (2010).

The modified geologic map in the Chapter III was used to be input geologic unit layer. The 4 geologic units contain attributes of rock properties which consist of cohesion, average unit weight, and tangent of average friction angle as shown in Table 4.2. This layer was used to calculate LSIs that were associated with landslide scars and considered as candidate critical LSIs. The rock properties in ranges categorized into 6 classes by equal interval as shown in Table 4.2 for the LSIs calculation. Since Z_w and Z appear to be the same and the cohesion is considered stable, each TIN polygon falling into the rock unit contains 216 possible combinations of γ , ϕ , and Z . The geologic unit layer was shown in Figure 4.8.

Table 4.2 The classes of related rock and terrain properties used for LSI calculation.

Class	C unit ($c = 5.0 \times 10^3 \text{ kN/m}^2$)			P1 unit ($c = 38.4 \times 10^3 \text{ kN/m}^2$)		
	$\gamma \text{ (kN/m}^3\text{)}$	$\phi \text{ (degree)}$	Z (m)	$\gamma \text{ (kN/m}^3\text{)}$	$\phi \text{ (degree)}$	Z (m)
1	23540	13.0	1.0	21580	27.0	1.00
2	23804	14.0	1.4	22758	28.4	1.40
3	24068	15.0	1.8	23936	29.8	1.80
4	24332	16.0	2.2	25114	31.2	2.20
5	24596	17.0	2.6	26292	32.6	2.60
6	24860	18.0	3.0	27470	34.0	3.00
Average	21200	15.5	2.0	24525	30.5	2.0
Class	gr unit ($c = 55.2 \times 10^3 \text{ kN/m}^2$)			Tr1 unit ($c = 27.2 \times 10^3 \text{ kN/m}^2$)		
	$\gamma \text{ (kN/m}^3\text{)}$	$\phi \text{ (degree)}$	Z (m)	$\gamma \text{ (kN/m}^3\text{)}$	$\phi \text{ (degree)}$	Z (m)
1	25510	34.0	1.00	23540	27.0	1.00
2	25706	35.2	1.40	23934	28.4	1.40
3	25902	36.4	1.80	24328	29.8	1.80
4	26098	37.6	2.20	24722	31.2	2.20
5	26294	38.8	2.60	25116	32.6	2.60
6	26490	40.0	3.00	25510	34.0	3.00
Average	26000	37.0	2.0	24525	30.5	2.0

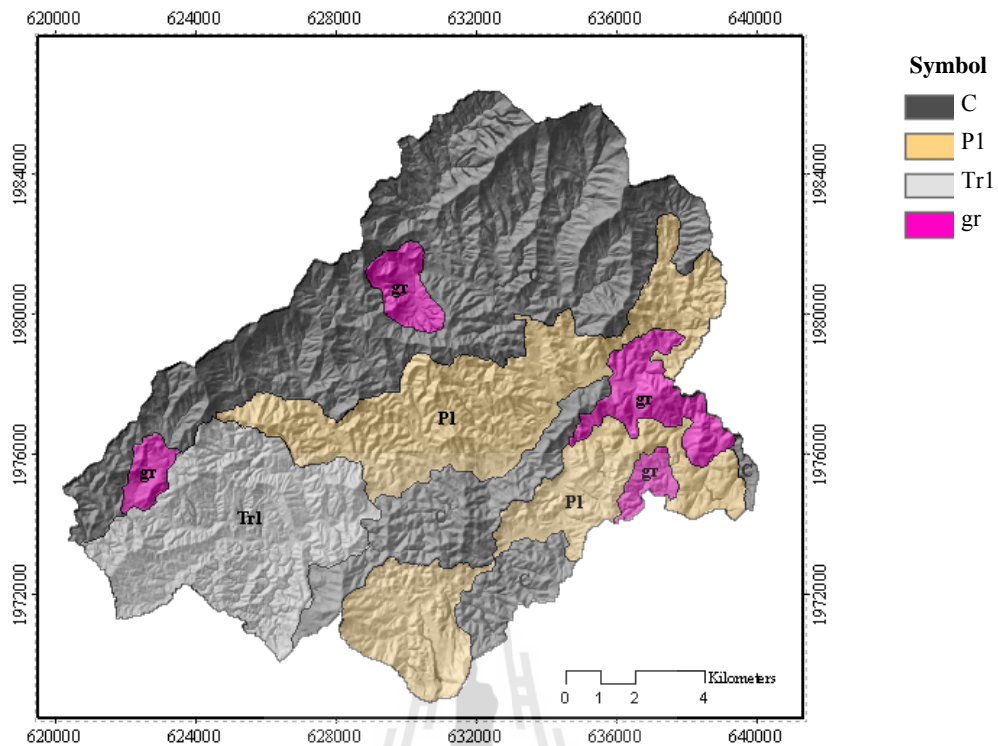


Figure 4.8 Geologic units layer.

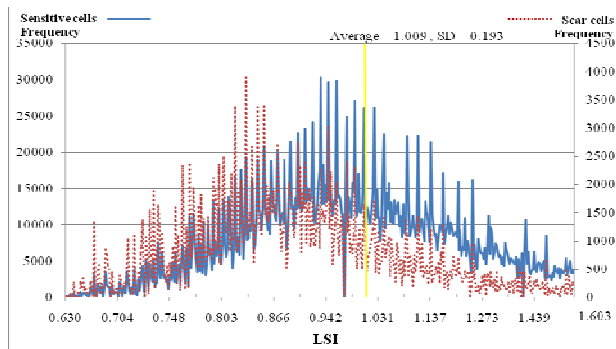
The rock hardness was classified by Point Load Strength Index Testing. Brown (1981) suggested the uniaxial compressive strength (σ_c) can be used to classify rock hardness level in field classification. The point load strength index (I_s) is correlated to σ_c . The result of testing from 7 points with a minimum of 20 samples for each point showed that the rock hardness level was weak to moderate hard that the details were described in Appendix C.

4.5 Result and discussion

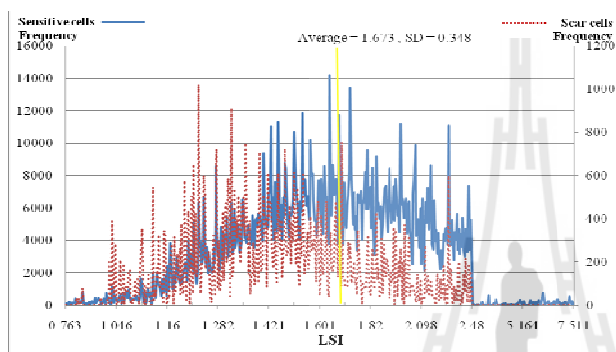
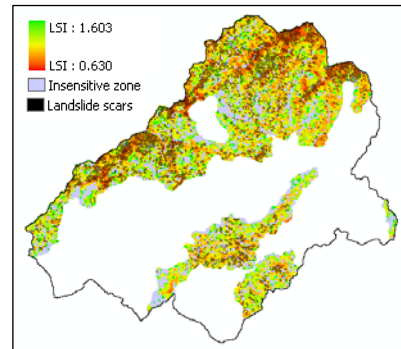
4.5.1 Landslide susceptibility index

As a raster layer with $5\text{ m} \times 5\text{ m}$ cell size, all scars and sensitive cell showed the frequency curve corresponding to LSI in Figure 4.9. The plot shows the relationship of the frequencies of all scar cells and sensitive cells according to varying LSIs and their spatial distribution in the map of the rock unit. The frequency curves of C unit show fair corresponding in the shape of the normal distribution. Whereas the curves of P1 unit and Tr1 unit shows the same shape that their right tails were cut, because the right tails were the LSIs cells no scar cells falling in. For gr unit, the frequency curve pattern show the mostly of scar cells fall in small LSIs and mostly of sensitive cells were fall in the large LSIs that corresponding with the highest durability and the definition of factor of safety.

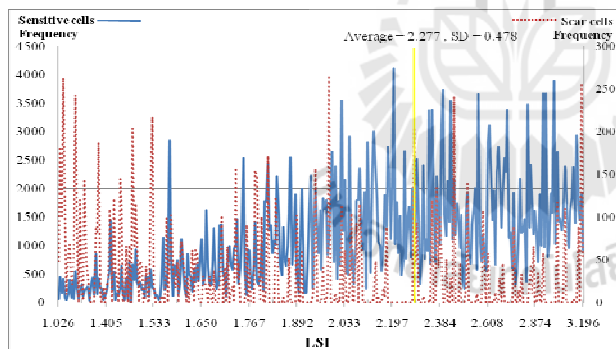
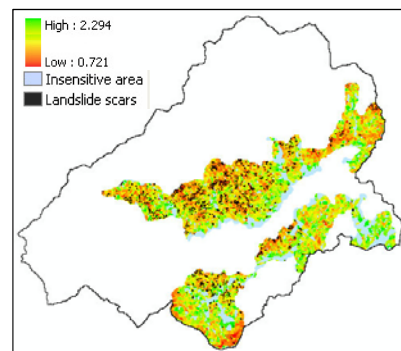
The ratio between sensitive cells and scar cells of rock is showed in Table 4.3, C unit was 10.211, P1 unit was 23.056, Tr1 unit was 23.849, and gr unit was 37.256. These ratios are related to the durability of rocks in which the high ratio was the low weathered rock and the low ratio was the highly weathered rock. The gr unit is composed of moderately weathered rocks which was the highest durability of 4 units. The C unit is composed of highly weathered rocks which was the lowest of 4 units. The P1 and Tr1 were composed of highly to moderately weathered rocks which was the moderate of 4 units.



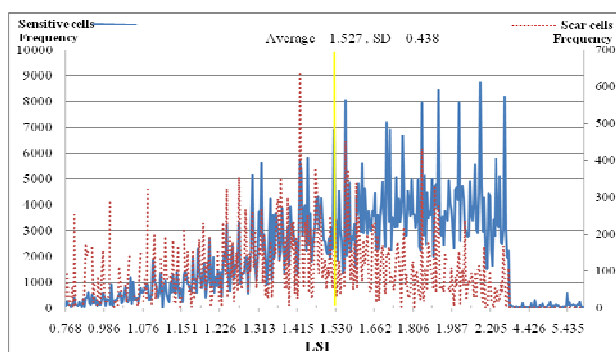
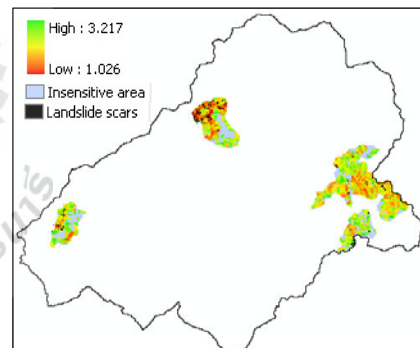
(a) C unit



(b) P1 unit



(c) gr unit



(d) Tr1 unit

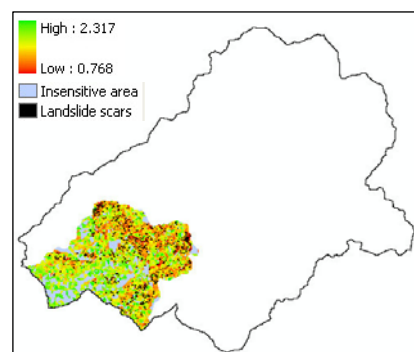


Figure 4.9 Frequency of sensitive and scar areas according to candidate critical LSIs.

Table 4.3 The LSIs associated and the ratio between sensitive cells and scar cells.

Geologic units	LSIs associated	Sensitive cells	Scar cells	Ratio (sensitive : scar)
C	0.630-1.603	3,311,172	324,245	10.211
P1	0.926-2.480	614,944	70,044	23.056
gr	1.026-3.196	386,282	10,383	37.256
Tr1	0.768-2.317	845,787	35,464	23.849

The results were approved with the Slake Durability Index tested by Geomachanic Research Unit, Suranaree University of Technology. It is the method that can predict long-term durability of rock specimens and assess the impact of water on the rock degradation (Fuenkajorn, 2008). The results are the evidence of the rock types deteriorate rapidly when exposed to the atmosphere and can be shaped through the weathering process. Water and fluctuation of temperatures accelerate the strength of the degradation. Under wet condition, rocks change from high durability rock to very low durability within 2 months. The result of Slake Durability Index tested was shown in Table 4.4.

Table 4.4 The results of slake durability index testing.

Samples	Rock Type	Slake Durability Index (I_d , %)		Δ SDI (%)	Weathering ratio
		Cycle I	Cycle II		
C-PS	Phyllitic shale	82.74	70.06	12.68	Low durability
C-MS	Meta siltstone	96.19	93.59	2.6	High durability
C-SS	Silty shale	95.21	91.07	4.14	Moderate durability
P1-01	Fine grain tuffaceous sandstone	96.88	95.44	1.44	High durability
P1-02	Rhyolite	97.88	97.05	0.83	Very high durability
P1-03	Fine grain tuffaceous sandstone (weak rock)	75.92	68.52	7.4	Low durability
P1-04	Meta Mudstone	95.55	92.42	3.13	Moderate durability
gr	Medium Grain Biotite Granite	90.48	85.47	5.01	Moderate durability

Note: Weathering ratio of Fuenkajorn's classification

<1= very high durability, 1-3= high durability, 3-7= moderate durability, 7-15= low durability, and >15 very low durability

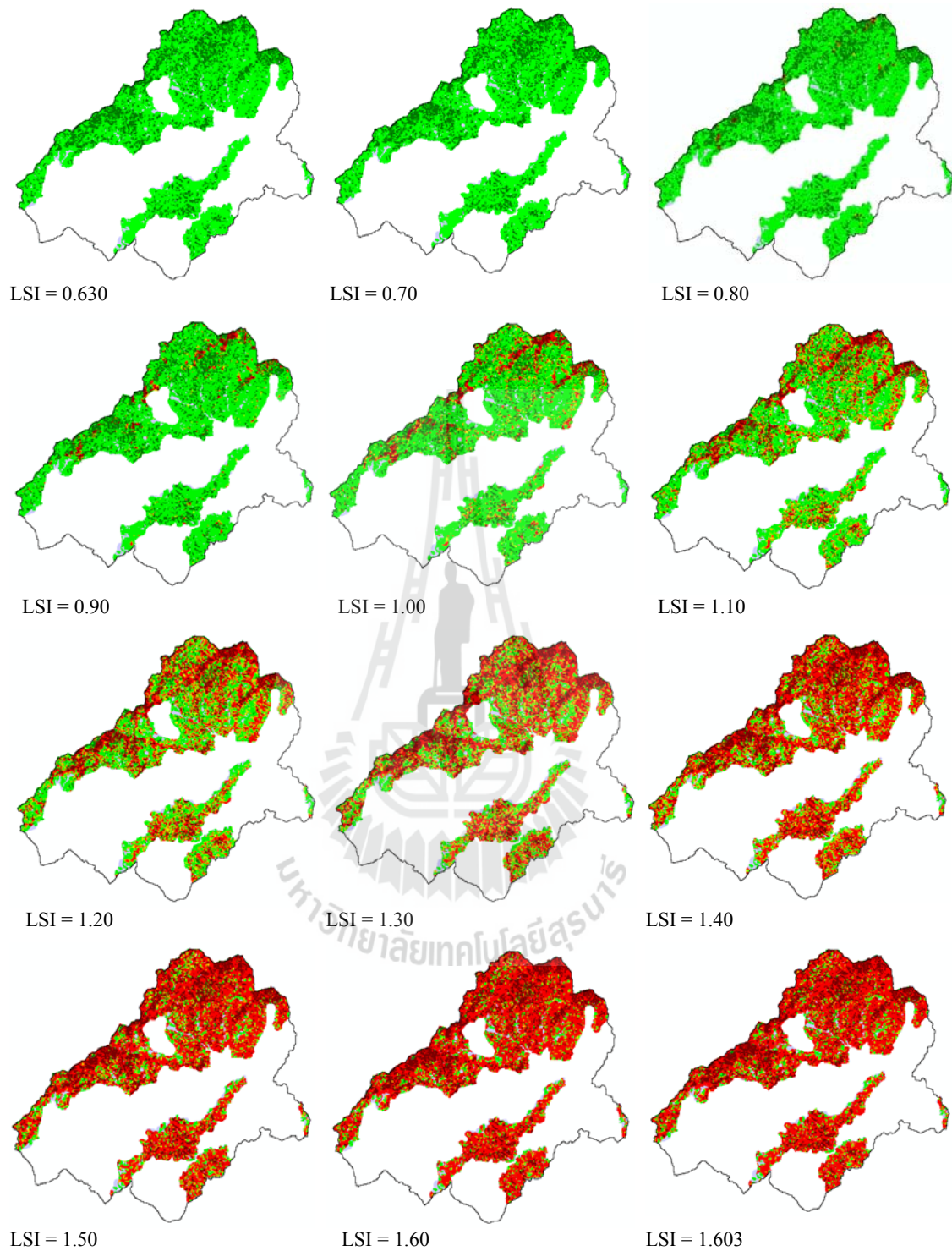
4.5.2 Probability failure index

The range of active LSIs of 4 units was sliced into the ranges captured by the lowest LSI values, the upper boundary values of the ranges, and the highest LSI values. The class intervals of all were 0.10. The LSIs of C, P1, gr, and Tr1 units were sliced into 12 values of 11 ranges, 17 values of 16 ranges, 23 values of 22 ranges, and 18 values of 17 ranges, respectively. These LSIs become candidates to be a critical LSI that shown in Table 4.5. It means that one of them can be the most sensitive LSI indicating the highest probability of landslide occurrences in the rock unit area.

Table 4.5 The LSIs become candidates to be a critical LSI.

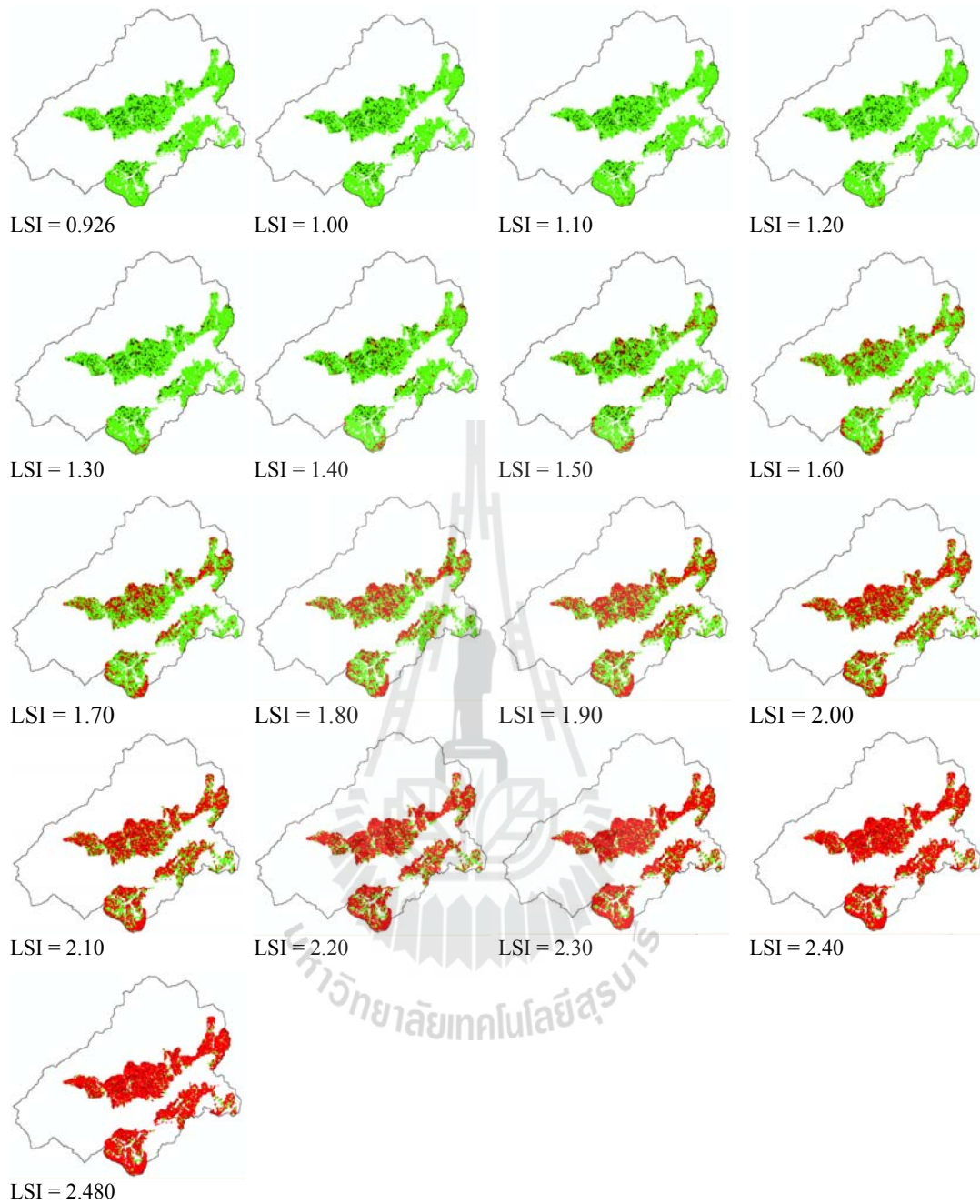
Geologic units	LSIs associated	Candidate critical LSI
C	0.630-1.603	0.63, 0.70, 0.80, 0.90, 1.00, 1.10, 1.20, 1.30, 1.40, 1.50, 1.60, and 1.603
P1	0.926-2.480	0.926, 1.00, 1.10, 1.20, 1.30, 1.40, 1.50, 1.60, 1.70, 1.80, 1.90, 2.00, 2.10, 2.20, 2.30, 2.40, and 2.480
gr	1.026-3.196	1.026, 1.10, 1.20, 1.30, 1.40, 1.50, 1.60, 1.70, 1.80, 1.90, 2.00, 2.10, 2.20, 2.30, 2.40, 2.50, 2.60, 2.70, 2.80, 2.90, 3.00, 3.10, and 3.196
Tr1	0.768-2.317	0.768, 0.80, 0.90, 1.00, 1.10, 1.20, 1.30, 1.40, 1.50, 1.60, 1.70, 1.80, 1.90, 2.00, 2.10, 2.20, 2.30, and 2.317

The PFIs of all TIN polygons were calculated under each candidate LSI and presented as raster layers shown in Figure 4.10. The cells with PFI equal to 1 are depicted in red while the ones with PFI less than 1 are in green. The scar cells are illustrated in black.



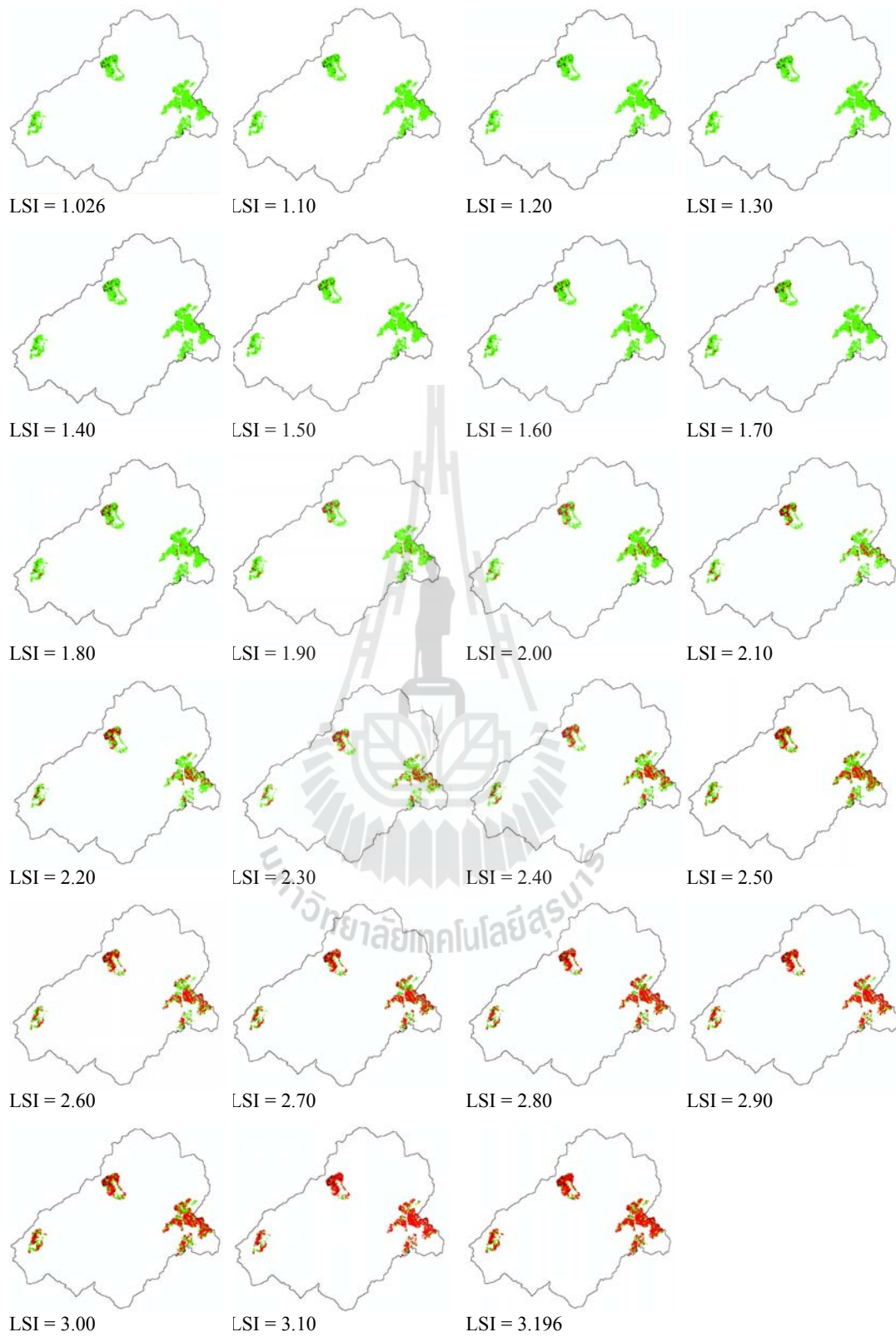
(a) The 12 PFI-1 raster layers of C unit.

Figure 4.10 The candidates of a critical LSI and the PFI-1 raster layers.



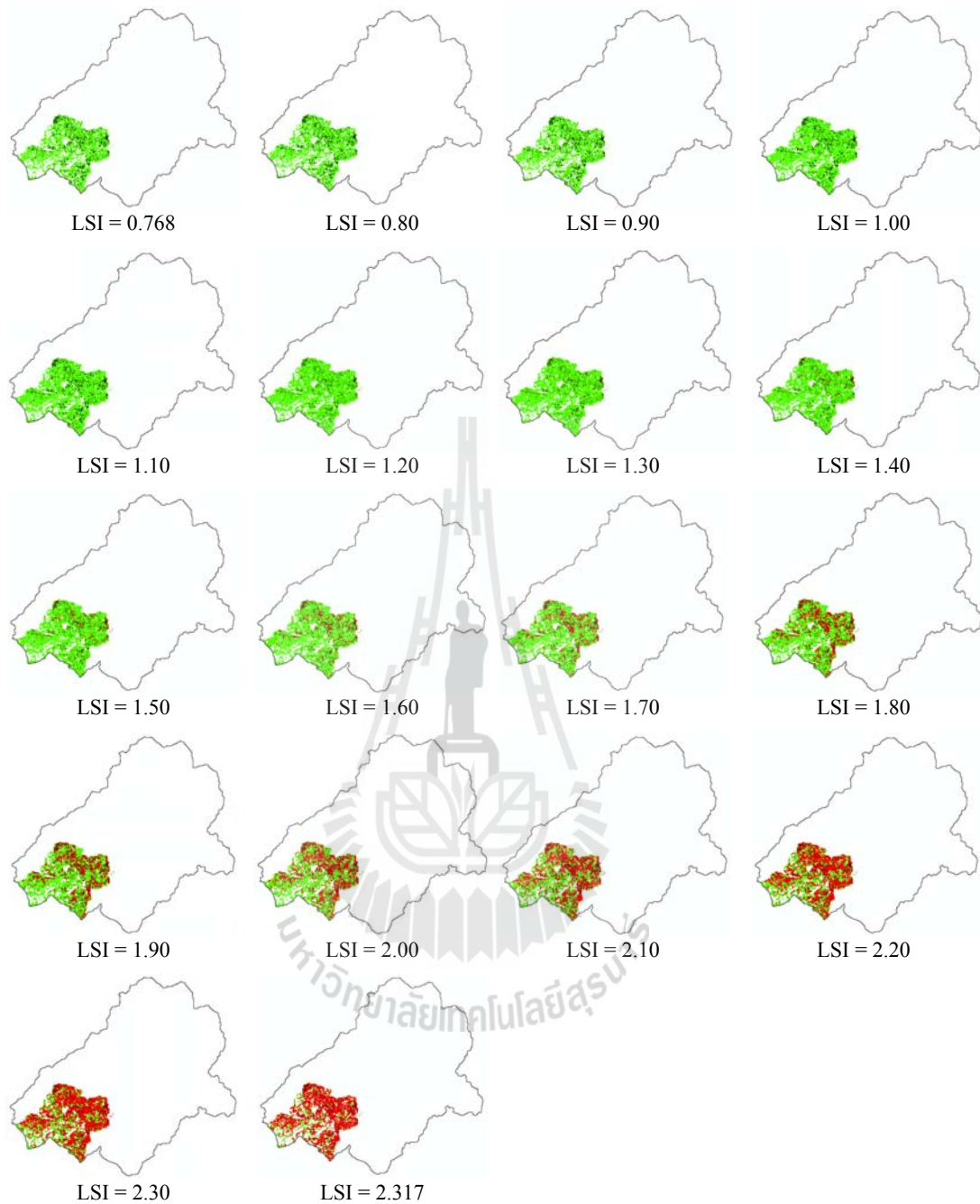
(b) The 17 PFI-1 raster layers of P1 unit.

Figure 4.10 The candidates of a critical LSI and the PFI-1 raster layers (Continued).



(c) The 23 PFI-1 raster layers of gr unit.

Figure 4.10 The candidates of a critical LSI and the PFI-1 raster layers (Continued).



(d) The 18 PFI-1 raster layers of Tr1 unit.

Figure 4.10 The candidates of a critical LSI and the PFI-1 raster layers (Continued).

Obviously, a number of red cells and their association with the scar cells are increased with increasing candidate LSI. In contrast, a number of green cells and their association with the scar cells are increased with decreasing LSI as well.

Therefore, the fitting ratio (FR) of each candidate raster layer was calculated (detail of FR calculation was shown in Appendix D) and the results are shown in Table 4.6 and Figure 4.11. From the results, the critical LSI of C, P1, gr, and Tr1 unit were 1.2, 1.7, 1.8, and 1.6 respectively provided the best fitting ratio as 0.143, 0.082, 0.159, and 0.095. The overlaid landslide scars and PFI-1 layer of all critical LSI is shown in Figure 4.12. Thus, the critical LSI from which calculated PFIs will best reflect the most accurate probability landslide occurrences of the rock unit when compared to the landslide scars of the big event. Although, Wyllie (1999), Keller (2002), U.S. Army Corps of Engineers (2003), Wyllie and Mah (2004), Das (2007), Cheng and Lau (2008), and Mergili and Fellin (2009) mentioned the theory of critical point of FS is equaled 1.

Table 4.6 The fitting ratios of all candidate critical LSIs.

C unit		P1 unit		gr unit		Tr1 unit	
Candidate LSI	FR	Candidate LSI	FR	Candidate LSI	FR	Candidate LSI	FR
0.900	0.019	1.200	0.002	1.200	0.005	1.000	0.003
1.000	0.093	1.300	0.019	1.300	0.064	1.100	0.014
1.100	0.137	1.400	0.004	1.400	0.074	1.200	0.046
<u>1.200</u>	<u>0.143</u>	1.500	0.068	1.500	0.113	1.300	0.072
1.300	0.132	1.600	0.078	1.600	0.152	1.400	0.087
1.400	0.121	<u>1.700</u>	<u>0.082</u>	1.700	0.157	1.500	0.095
1.500	0.114	1.800	0.074	<u>1.800</u>	<u>0.159</u>	<u>1.600</u>	<u>0.096</u>
1.600	0.108	1.900	0.069	1.900	0.129	1.700	0.087
1.603	0.108	2.000	0.065	2.000	0.103	1.800	0.081
		2.100	0.060	2.100	0.073	1.900	0.072
		2.200	0.057	2.200	0.060	2.000	0.069
		2.300	0.053	2.300	0.054	2.100	0.064
		2.400	0.051	2.400	0.049	2.200	0.058
		2.480	0.050	2.500	0.048	2.300	0.056
				2.600	0.038	2.317	0.050
				2.700	0.037		
				2.800	0.035		
				2.900	0.034		
				3.000	0.035		
				3.100	0.031		
				3.196	0.032		

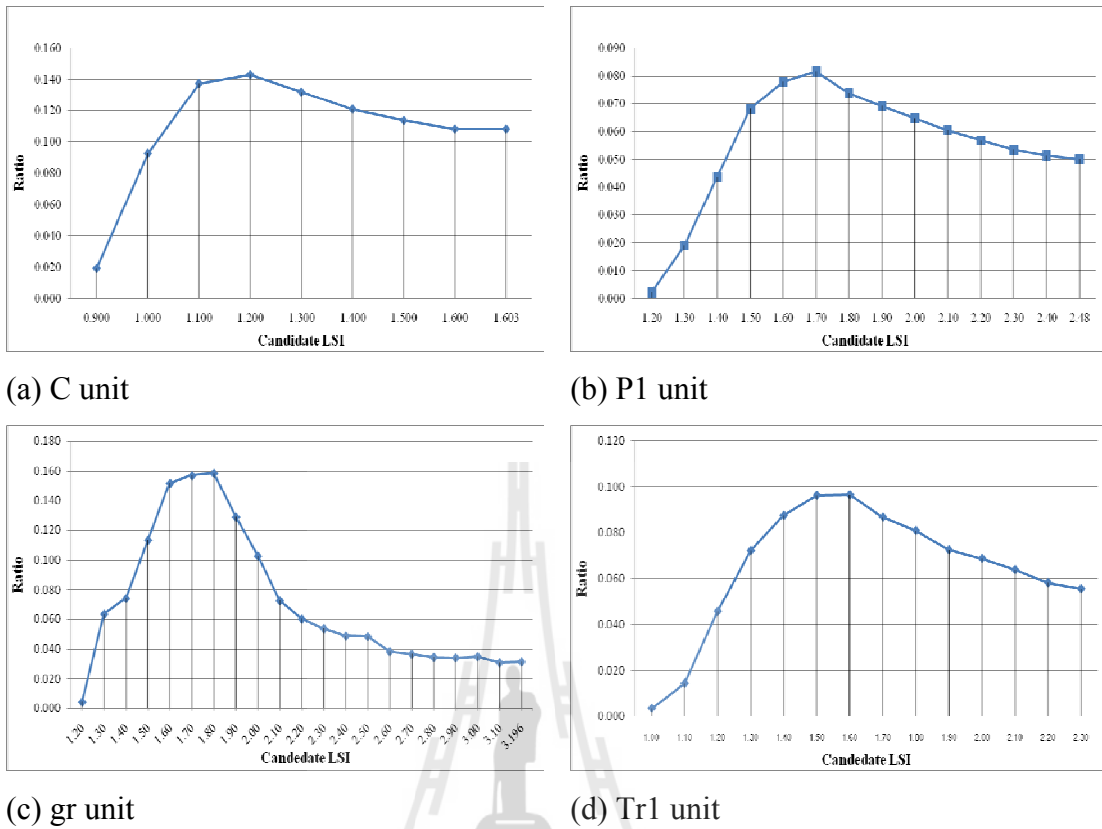


Figure 4.11 Variation of fitting ratios according to candidate critical LSIs.

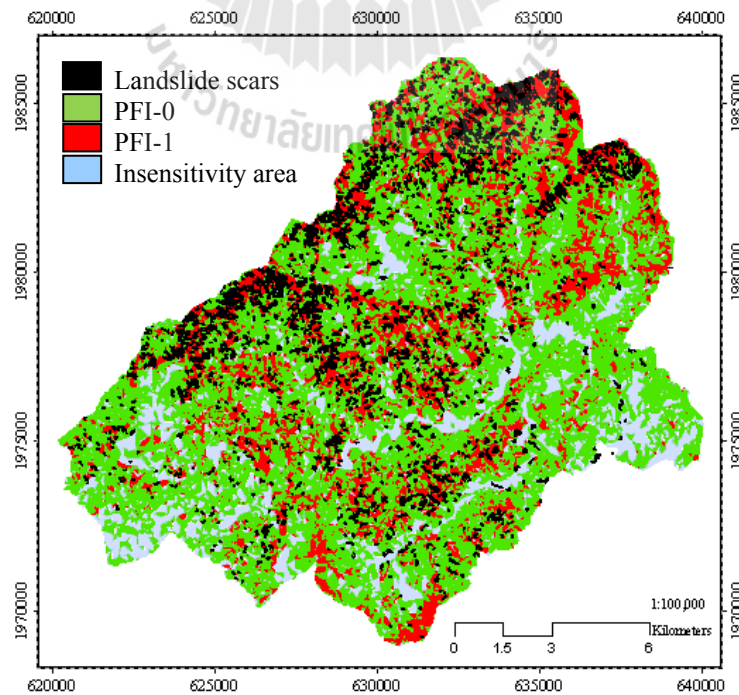


Figure 4.12 The distribution of landslide scars and PFI-1 of all critical LSIs.

The original calculated PFIs raster layer of the 4 critical LSIs consisted of 1.2, 1.7, 1.8, and 1.6, were merged to be PFI layer of the study area. The original PFIs between 0-1 were classified to be 5 classes using equal ranging including very low (0-0.2), low (0.2-0.4), moderate (0.4-0.6), high (0.6-0.8), and very high (0.8-1.0). The result is shown in Figure 4.13. The graph depicting the percentages of classes and scar areas of every class including their associating ratio is displayed in Figure 4.14.

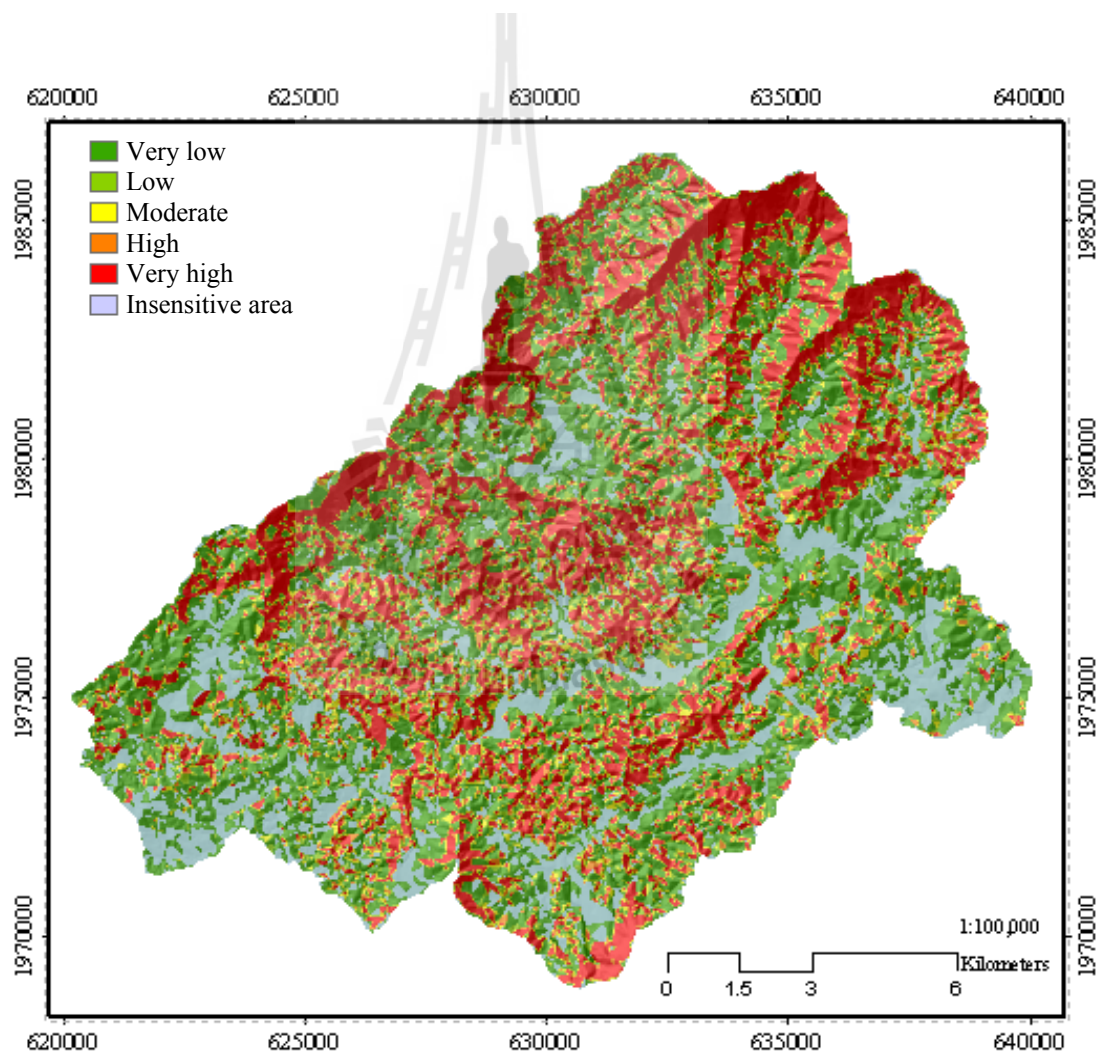


Figure 4.13 The distribution of Probability Failure Indexes (PFIs) classes in Nam Li watershed.

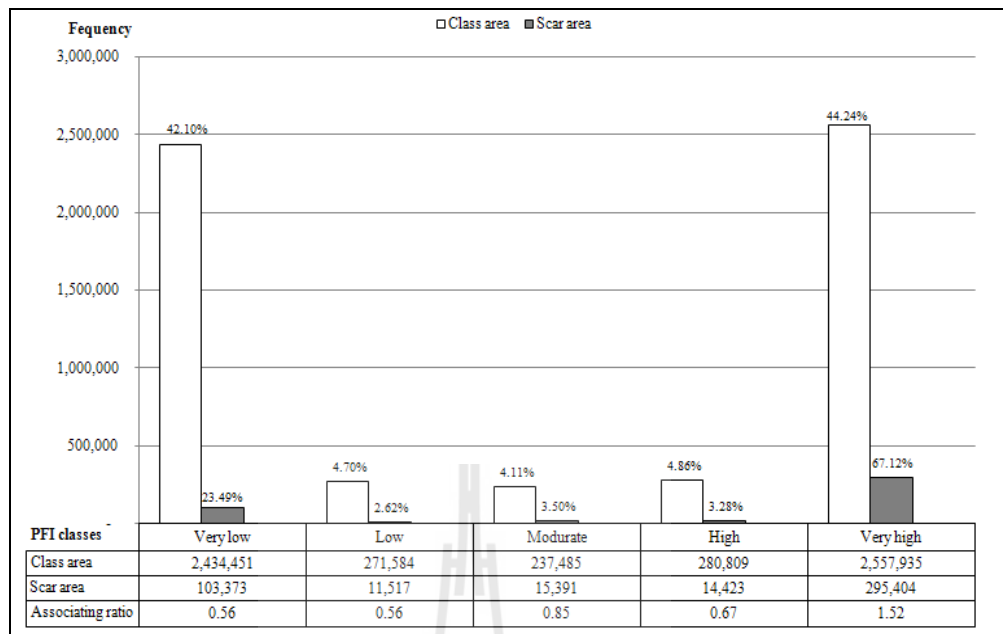


Figure 4.14 The cell-based and percentage of scar and class areas including their associating ratio.

The classes of very high and very low cover the main part of the study area with almost equal area (44.24% and 42.10%, respectively). Big numbers of scars fall into these two classes while the rests show little existence percentage of both scars and areas. This can misunderstand that landslide scars have more relation to the very low class than the other classes except the very high one. This result seems to be not supported by the theory. But when the associating ratio of scars and class area is considered as shown in Figure 4.14, it reveals that the proportion of scars existing in class area strongly agrees with theory. The higher associating ratio is increased with the higher PFI class. The area of very high class has higher chance of landslide occurrence which is confirmed by the higher associating ratio.

A little conflict can be observed between the moderate and high classes. The scar existing in the moderate class or its associating ratio is a bit higher

than that of the high one. This could happen because the existing areas of these two classes in the rock unit are a bit too small, only 2.62-3.28% to express the good representation.

4.6 Conclusion

The landslide susceptibility modeling is a spatial model which based on the slope stability analysis and GIS technique. The approach is the evaluation of the landslide susceptibility area in the connection of spatial distribution of slope characteristic and geoenvironmental properties of rock. The infinite slope stability method in 1 dimensional model was applied to calculate Landslide Susceptibility Index (LSI) for critical LSI determination. The data input which are the weight of material on slope failure (W), that related to the thickness of slope material above sliding plane (Z) and the thickness of saturated slope material above sliding plane (Z_w), slope angle (β), and rock properties i.e. cohesion (c), internal friction angle (ϕ), and unit weight of rock (γ) were prepared under the domain of geologic unit and slope characteristics in form of GIS vector layer. The geological map layer contains the attribute of those rock properties while the slope map layer derived from TIN (Triangulated Irregular Network) contains the slope angle. All LSIs which related to landslide scars in each geologic unit were slice to be candidate critical LSIs. The probability of landslide occurrence was determined from 216 LSIs in each TIN polygon which calculated from 216 combinations of rock properties. The probability of landslide occurrence in term of Probability of Failure Indexes (PFIs) was calculated in each TIN polygon using Probability Density Function (PDF). Then, slope of each polygon, mean and standard deviation of LSI from the possible composite properties

of the rock unit were put into PDF to estimate PFIs. For each candidate, a raster map layer was generated with each cell containing PFI. PFI less than 1 was changed to 0 while PFI equals to 1 was kept as 1. Then, overlay analysis of a raster layer containing 0 and 1 of each candidate and landslide scar layer was operated to obtain the optimum ratio. The candidate LSI of the layer depicting the highest optimum ratio was identified as the critical LSI which herein the critical LSI of C, P1, gr, and Tr1 were 1.2, 1.7, 1.8, and 1.5, respectively. The original PFIs between 0-1 were classified into 5 classes using equal ranging including very low (0-0.2), low (0.2-0.4), moderate (0.4-0.6), high (0.6-0.8), and very high (0.8-1.0). Finally, the distribution of PFIs classes was established.

The application of infinite slope stability models together with GIS technique can rapidly evaluate landslide susceptibility in large area. Even though the LSIs used to classify the landslide susceptibility were obtained by using equation for FS calculation and the input data are not as accurate as the data from site investigation, the result of the study is apparently reasonable. More accurate result could be obtained if the details of geotechnical properties from the field are used as input data for the analysis. In addition, the Probability of Failure (PF) by using the probability density function (PDF) could be applied to improve fuzzy input data.

The study developed the systematic procedure to classify probability of landslide occurrence in the high risk area that had the case of big landslide event. The geological engineering properties of the rock unit appearing in nature and map, engineering laboratory and practice, and the inferred statistic method such as probability density function were agglomerated in the classification method. Full

functions of GIS techniques were also applied and enable the study to achieve the fruitful results with good spatial presentation.

The study took the insensitive area out at the beginning, plus associating ratio was applied to validating each class of classification result. This makes validation method and results be more reasonable and scientific.

4.7 References

- กรมพัฒนาที่ดิน. (2547). **พื้นที่เสี่ยงต่อการเกิดดินถล่มและอุทกภัยในประเทศไทย**. กรมพัฒนาที่ดิน กระทรวงเกษตรและสหกรณ์.
- สุรินทร์ ไวจริญ. (2549). **การวิเคราะห์พื้นที่ที่มีความเสี่ยงจากดินถล่มในประเทศไทย**. สถาบันวิจัยพัฒนาและป้องกันการเป็นทะเลทรายและการเตือนภัย กรมพัฒนาที่ดิน กระทรวงเกษตรและสหกรณ์.
- อภิชาติ ลำจวน และ สุชัย สีนพูนอนันต์. (2530). **ธรณีวิทยาระวางเขื่อนสิริกิติ์ และระวางอำเภอท่าปลา**. กองธรณีวิทยา กรมทรัพยากรธรณี. (เอกสารที่ไม่ได้พิมพ์เผยแพร่).
- Alden, A. (2010). Density of Common Rock Type [On-line]. Available http://geology.about.com/cs/rock_types/a/aarockspeggrav.htm.
- Billingsley, P. (1979). **Probability and Measure**. New York: John Wiley and Sons.
- Brown, E. T. (Ed). (1981). **Rock characterization, testing and monitoring – ISRM suggested methods**. Oxford: Pergamon.
- Cheng, Y. M. and Lau, C. K. (2008). **Slope Stability Analysis and Stabilization**. New York: Routledge.
- Coe, J. A., Michael, J. A., Crovelli, R. A., and Savage, W. Z., 2000. **Preliminary map showing landslide densities, mean recurrence intervals and exceedance probabilities as determined from historic records**. Seattle, Washington. Open-file report 00-303, U.S. Geological Survey.

- Das, B. M. (2007). **Principles of Geotechnical Engineering**. Toronto: Nelson, pp 309-315.
- Feller, W. (1971). **An introduction to probability theory and its applications**. Vol II. 2nd ed. Wiley Series in Probability and Mathematical Statistics. New York: John Wiley and Sons, 669 p.
- Fuenkajorn, K. (2008). Prediction of Long-Term Strength of Some Weak Rocks in Thailand. Proceedings of **the First Southern Hemisphere Rock Mechanics Symposium**, September 16-19, Perth, Western Australia.
- Goodman, R. E. (1989). **Introduction to Rock Mechanics**. New York, John Wiley & Sons, pp. 80-83.
- Jensen, J. R. (2007). **Remote Sensing of the Environment** (2nd ed.). Upper Saddle River, NJ: Pearson Education.
- Keller, E. A. (2002). **Introduction to environmental geology** (2nd ed.). Upper Saddle River, New Jersey: Prentice Hall.
- Kolmogorov, A. N. (1956). **Foundation of the Theory of Probability**. 2nd edition. New York: Chelsea.
- Land Development Department. (2004). **DinThai** [Computer programme]. Bangkok: LDD.
- Mahidol University. (2003). **The study of landslide risk area** (final report). Engineering Data and Research Center, Faculty of Engineering, Mahidol University, Thailand.

- Mergili, M. and Fellin, W. (2009). Slope stability and geographic information systems: an advanced model versus the infinite slope stability approach. In: **Russian Academy of Sciences, Problems of Decrease in Natural Hazards and Risks**, The International Scientifically-Practical Conference GEORISK 2009. pp. 119-124.
- Montgomery, D. R. and Dietrich, W. E. (1994). A physically based model for the topographic control on shallow land sliding. **Water Resources Research**. 30(4): 1153-1171.
- Pack, R. T., Tarboton, D. G., Goodwin, C. N., and Prasad, A. (1998). SINMAP a Stability Index Approach to Terrain Stability Hazard Mapping. **SINMAP User's Manual**. Logan: Utah State University.
- Sirilak Tanang, Sunya Sarapirome, and Sasikan Pliklang. (2010). Landslide susceptibility map of Nam Li watershed, Uttaradit, Thailand. In proceedings of **the 31th Asian Conference on Remote Sensing 2010**, Nov 01-05. Hanoi, Vietnam, TS11-5, 6 p.
- Soralump, S., Isaroranit, R., Kulsuwan, B., and Yangsanphu, S. (2010). Weak plane failure of philitic sandstone: slope stabilization of the access road of Mae Mao Dam. In **International Conference on Slope 2010: Geotechnique and Geosynthetics for Slopes**. Chiangmai, Thailand.
- Sunya Sarapirome and Sirilak Tanang. (2012). Probability of landslide occurrence mapping using probability density function: A case study of the Mae Tha Group in Nam Li watershed, Thailand. In **Proceedings of the 33rd Asian Conference on Remote Sensing 2012**, Nov 25-30, Pattaya, Thailand.

- Suree Teerarungsikul. (2006). **Landslide Prediction Model Using Remote Sensing, GIS and Field Geology: A Case Study of Wang Chin District, Phrae Province, Northern Thailand**. Ph.D. Geotechnology, Suranaree University of Technology, Thailand.
- U.S. Army Corps of Engineers. (2003). Engineering and Design: Slope Stability. **Engineer Manual**. Department of the Army, U.S. Army Corps of Engineers, Washington, DC.
- Warakorn Mairaing and Nonglak Taijeamaree. (2004). Unsaturated Soil Strength for Mountain Slope Stability Analysis. **Proceedings of the 9th National Convention on Civil Engineering**. Petburi, Thailand, 1-7.
- Wyllie, D.C., 1999. Foundations on Rock. 2nd edition. London, E & FN Spon, pp. 19-22.
- Wyllie, D. C. (1999). **Foundations on Rock**. 2nd edition. London: E & FN Spon, pp 19-22.
- Wyllie, D. C. and Mah, C. W. (2004). Rock slope engineering: Civil and mining 4th ed. New York; Spon Press, p.81.
- Zaitchik, B. F. and van Es, H. M. (2003). Apply a GIS slope-stability model to site-specific landslide prevention in Honduras. **Journal of Soil and Water Conservation**. 5(1): 45-53.
- Zaitchik, B. F., van Es, H. M., and Sullivan, P. J. (2003). Modeling slope-stability in Honduras: Parameter Sensitivity and scale of aggregation. **Soil Science Society of America Journal**. 67: 268-278.

CHAPTER V

FLASH FLOOD IMPACT INTENSITY MODELING

5.1 Abstract

The study develops the systematic procedure to evaluate flash flood impact intensity index (FFIII) in the high risk area. The 3 hours rainfall intensity, infiltration ability, flood depth, and accumulated overland flow were used for flash flood impact intensity evaluation. The 3 hours rainfall was interpolated from daily rainfall of the study area based on the 3 hours rainfall pattern of a nearest station. The infiltration ability assessment was derived from infiltration rates which calculated from infiltrometer in situ testing and Horton's equation. The rainfall excess of each LU/LC and geologic unit combinations were overland flow which affect to the flash flood occurrence area. Therefore, the flash flood impact intensity was assessed by overland flow and water depth when the event occurred. The water depth was calculated by the difference of stream elevation from DEM and flash flood surface elevation which generated from cross section data. The boundary of flash flood area was extracted from flash flood scars which appeared on SPOT5 imagery. The study determined the risk flood area was occurrence in flood scar. Then, the overland flow was accumulated to be flash flood susceptibility index (FFSI). The FFIII was operated from FFSI and water depth. The result showed location of the high FFIII in the downstream.

Keywords: GIS/Infiltration/Overland flow/Flash flood/Uttaradit

5.2 Introduction

The flood hazard maps and risk area maps in Thailand have been created generally by index model (e.g. Tanavud, Yongchalemchai, Bennui, and Densreeserkul, 2004; Phutmongkhon, Yongsatisak, Jungcharoentham, Khampeera, Tongyoi, and Bennui, 2007; Rattanakom, and Ongsomwang, 2008) and hydrodynamic module such as NAM, MIKE 11 and HEC-GeoRAS (e.g. Taragsa, Mongkolsawat, Pawattana, and Suwanweerakamtorn, 2004; Mapiam and Sriwongsitanon, 2009). The input datasets in hydrodynamic model should be accurate and high resolution data (Chowdhury, 2000; Sumangala, 2005). Therefore, the parameters calibration in hydrodynamic model has been provided from observe station or gauge station. It is difficult to observe rainfall and runoff within an ungauge basin. Weather monitoring is another simple method used to warn flooding as well in local area.

From the Hortonian mechanism (Beven, 2004), the runoff/overland flow can be defined from rainfall and soil capacity related to infiltrate ability. For the flash flood assessment, the Hortonian mechanism is one of the hydrological theories that define overland flow as water excess of infiltration (กীরติ ลีวัจนกุล, 2543; Davie, 2002; Beven, 2004; Department of Natural Resource and Water, 2007). Once the water comes down to the surface, it could be separated into 3 parts i.e. evaporation, infiltration, and overland flow. Therefore the flash flood potential can be determined using the volume of overland flow from infiltration excess model (ซัชชัย ตันตะสิรินทร์, 2550).

The Horton equation is selected to work as infiltration excess model. The important factors of this model are rainfall intensity and infiltration rate. In the event

of Nam Li, the evaporation could be neglected from the model because the relative humidity is as high as 90-92% (Thai Meteorological Department, 2009). According to the infiltration theory in Chapter II, many factors affect infiltration rate, e.g. soil moisture, vegetal cover, and available storage in soil stratum. It is necessary to include these factors in the assessment. Besides, this event occurred on an area with very thin soil cover and saturated thick weathering rock. Therefore, the sampling sites of infiltration rate testing were prepared to represent geologic units and land cover in the study area. All variables were prepared as GIS raster layers. The input layers were mathematically incorporated for overland flow estimation. The overland flow in each cell was accumulated by watershed analysis using the hydrologic module in ArcGIS. The impact intensity of flash flood occurrence was estimated by correlating accumulative overland flow in cells to flood scars extracted from SPOT5 imagery. The output of this model is a cell-based layer which contains impact intensity of flash flood in each cell.

5.3 Research methods

5.3.1 Research procedure

There are 5 main steps within this research procedure which are rainfall intensity analysis and infiltration measurement, overland flow analysis, overland flow accumulation and flash flood area determination, flood depth estimation from flood scars, and flash flood impact intensity assessment. The analyses were operated on cell-based GIS data. The diagram showing steps in methodology can be displayed in Figure 5.1.

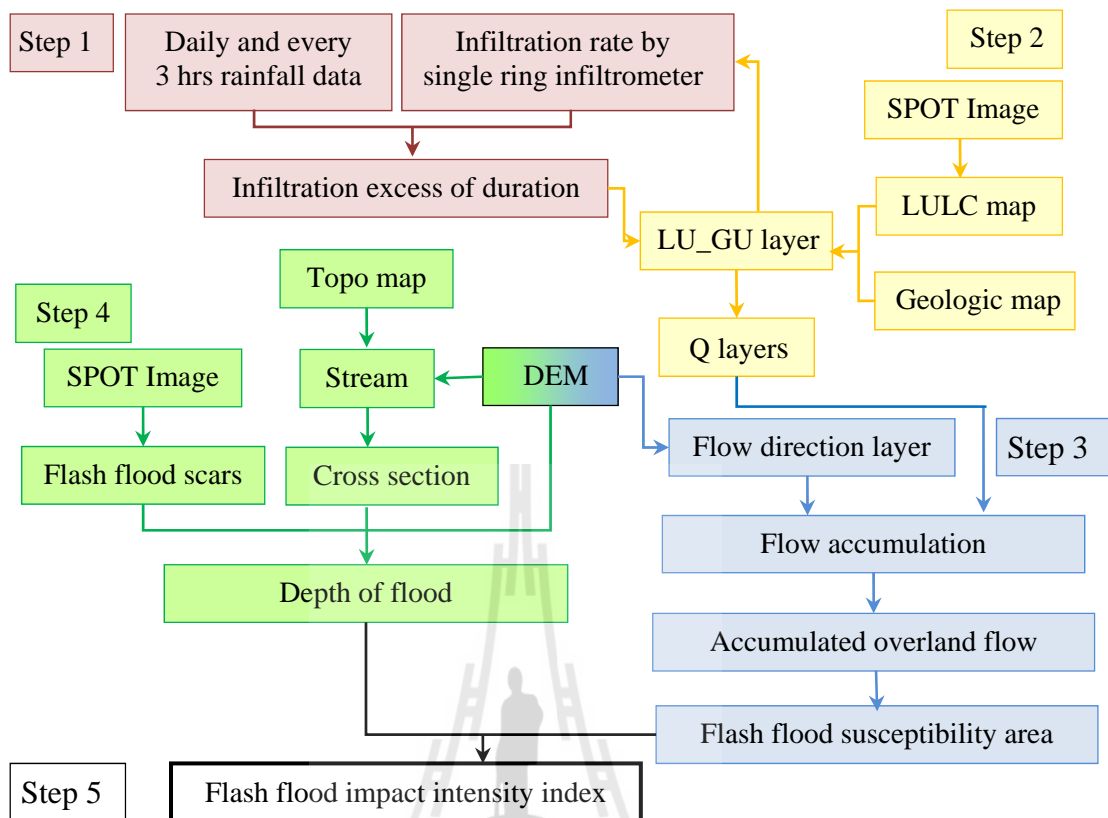


Figure 5.1 The procedure framework of flash flood impact intensity modeling.

5.3.2 Rainfall intensity analysis and infiltration measurement

The area of Nam Li watershed is approximately 200 km². It is a small and ungauged watershed. The Nam Li Watershed Management Unit records daily rainfall at 07:00 AM using simple rain gauge made from small bucket. However, the 3 hours rainfall data are required for accurate rainfall intensity analysis. The 3 hours rainfall data close to Nam Li watershed are available at Uttaradit which is the nearest TMD station (approximately 30 kms away). Fortunately, during the period that event occurred, the area fell into the same big rainstorm. Therefore, the rainfall pattern at the Uttaradit station can be used to represent at Nam Li. Using this pattern, the daily rainfall recorded at Nam Li was temporally interpolated to be 3 hours rainfall data.

The daily rainfall data is the rainfall accumulated in 24 hours. The relation of known 3 hours rainfall data at Uttaradit station and unknown 3 hours data of Nam Li at t duration can be stated mathematically as follows:

$$R3hr_{Aac(t)} = \frac{(RD_A \times R3hr_{Bac(t)})}{R3hr_{Bac}}, \quad (5.1)$$

where the $R3hr_{Aac(t)}$ is the 3 hours rainfall at t duration of A station, the RD_A is daily rainfall of A station, the $R3hr_{Bac}$ is 3 hours rainfall accumulated in 1 day of B station, and $R3hr_{Bac(t)}$ is 3 hours rainfall accumulated at t duration of B station.

The infiltration excess was calculated using Horton equation through the infiltration rate. The Horton equation as defined in equation (5.2) (เกียรติ ลีวัจนกุล, 2543; Davie, 2002) was chosen for infiltration rate calculation.

$$f_t = f_c + (f_0 - f_c)e^{-kt}, \quad (5.2)$$

or $(f_t - f_c) = (f_0 - f_c)e^{-kt}$

where f_t = infiltration rate (depth/time), f_c = infiltration capacity (depth/time), f_0 = initial infiltration rate at initial time (depth/time), $e = 2.71$ (the base of natural log), k is a constant value of infiltration rate which is measurement of the rate of decrease in infiltration rate, and t is duration of infiltration.

From equation (5.2), the data of initial infiltration rate (f_0) and infiltration capacity (f_c) were derived from single ring infiltrometer which was operated on unique units of LULC and geology in the study area. The f_0 was calculated from initial infiltrated

value per time, mm/sec in this case, at constant water infiltrated. The f_c was calculated from the last rate when water stops infiltrating. The k value was derived from the slope of semi-logarithm curve in the relation of infiltration rate and time.

The linear equation was used to create fitting curve in semi-logarithm graph. The fitting curve can be expressed as equation (5.3) and displayed in Figure 5.2:

$$\log(f_t - f_c) = \log(f_0 - f_c) - k t (\log e),$$

or

$$\log(f_t - f_c) = -k (\log e) t + \log(f_0 - f_c). \quad (5.3)$$

where $-k (\log e)$ is an coefficient and $\log(f_0 - f_c)$ is a constant.

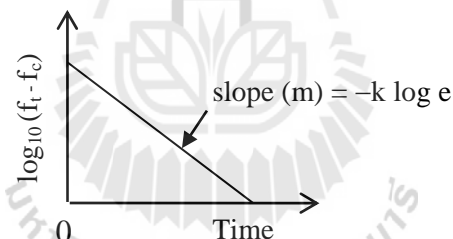


Figure 5.2 The relation of $\log_{10}(f_t - f_c)$ and time.

Modified from: กীরติ สิวัจจนกุล (2543).

Then, k can calculate by equation below:

$$k = -\frac{1}{\log_{10} e} \times \text{slope},$$

or

$$k = -\frac{1}{0.4343} \times \text{slope}. \quad (5.4)$$

5.3.3 Overland flow (Q) analysis

The equation (5.2) was used again to specify infiltration rate of rainfall duration. The 3 hours rainfall intensity and the infiltration of rainfall duration were used to calculate infiltration excess using Hortonian concept. Horton defines the infiltration capacity (f_c) at the maximum rate at which rain can be absorbed by the soil. When the rainfall intensity (P) falling on the ground is less than f_c , all rain water will infiltrate. When $P > f_c$, then only f_c will infiltrate and the excess of P over f_c becomes overland flow (Q). It can be stated mathematically as displayed in Figure 5.3 and equation (5.5).

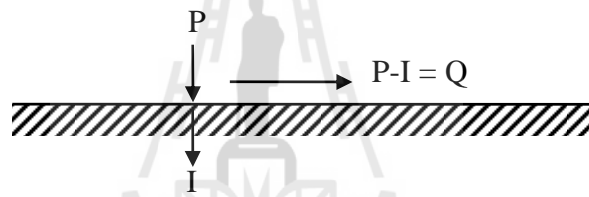


Figure 5.3 Hortonian concept of overland flow generation.

Source: Davie (2002).

Let I be the actual rate of infiltration during rain. Then,

$$I = P \quad \text{if } P < f_c,$$

$$I = f_c \quad \text{if } P > f_c.$$

Correspondingly, denoting the rate of overland flow by Q , it was stated equivalently;

$$Q = 0 \quad \text{if } P < f_c,$$

$$Q = P - f_c \quad \text{if } P > f_c. \quad (5.5)$$

According to the Chapter II, some researches (e.g., กรมพัฒนาที่ดิน, 2547; กรมชลประทาน, 2549; Rattanakom and Ongsomwang, 2008) discussed that soil drainage ability, land use, and slope affect the flood potential assessment. Hence the Q of sampling points in unique LULC and geologic units were calculated. The LULC vector layer was extracted from SPOT5 imagery by visual interpretation incorporating with data from LULC 2007 of the LDD, and field investigation. The LULC and geologic layers were combined by UNION operation to be LU_GU layer which contains Q value in each unique unit of all rainfall durations resulted from infiltration excess analysis. The Q vector layers were converted to be Q raster layers for all rainfall durations.

Q in each layer of rainfall duration was accumulated through the flow accumulation tool in ArcGIS to be overland flow (Q_{ac}) layers. To find out the flash flood area, the highest Q_{ac} of all layers were compared to the increase ratio as follow,

$$\text{Increase ratio} = (Q_{ac(n+1)} / Q_{ac(n)}), \quad (5.6)$$

where Q_{ac} is accumulated overland flow and n is the duration number of accumulated overland flow.

The highest flash flood is associated with the highest increase ratio. Therefore, the flash flood area of the event can be obtained from the Q_{ac} layer with the highest increasing ratio.

5.3.4 Flood scars surface estimation

The flood scars are the evident of the impact areas from the catastrophe which appear on SPOT5 imagery. They were extracted and considered as boundary of flood surface. The intensity of flood is related to water depth in impacted area and it can be evaluated from flood scar (Ballesteros-Cánovas et. al, 2011). Therefore, when peak of flash flood occurred (flood scar occurring) the elevation of flood surface should be associated with the scar boundary.

The flash flood surface can be interpolated from elevation of flood water at scar boundary and above streambed. Flood depths at stream (H_w) of sampling cross-sections were the difference between elevation at flood surface (E_S) above the streambed, interpolated from elevation of scar boundary at both sides, and elevation at streambed (E_B). It can be stated mathematically as:

$$H_w = E_S - E_B. \quad (5.7)$$

Then spot heights of flood water surface over streambed (S_E) can be calculated by:

$$S_E = E_B + H_w, \quad (5.8)$$

Thereafter, the flash flood surface was generated from sampling spot heights over stream and elevation along the boundary of flood scar.

The procedure of this step can be displayed in Figure 5.4.

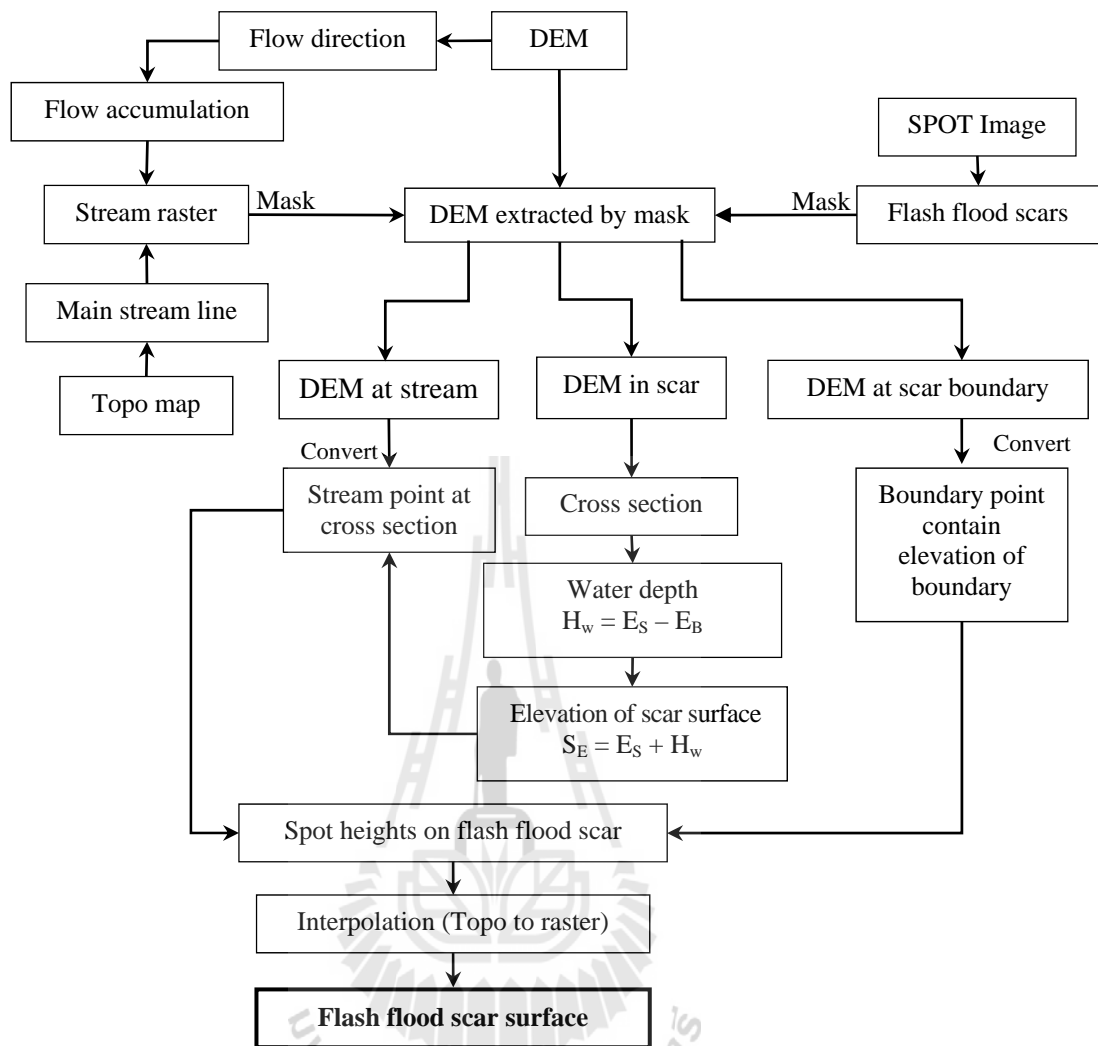


Figure 5.4 The procedure to extract DEM of flash flood scar surface.

5.3.5 Flash flood susceptibility assessment

The Q_{ac} of each cell in the selected raster layer was used to construct flash flood susceptibility indexes (FSI) indicating comparative susceptibility to flash flood of the area. They were classified into 3 classes based on logarithm scale for the frequency of occurrence.

5.3.6 Flash flood impact intensity assessment

The FSI was added to varying normalized depths (0-1) in flood scar. These are indexes reflecting flash flood impact intensity (FII) of the event. The FII layer was classified into 5 classes from very low to very high based on logarithm scale for the frequency of occurrence.

5.4 Data collection and preparation

The input data for flash flood impact intensity assessment consist of rainfall intensity and infiltration rate of the combined unit of geology and LULC. The rainfall intensity was prepared from rainfall record. The infiltration rates were prepared from the field in situ testing. The result of data collection and preparation are as follows:

5.4.1 Rainfall input data

The rainfall data in May 2006 from Thai Meteorological Department (TMD) at Uttaradit station were recorded every 3 hours together with the daily rainfall data at Nam Li Watershed Management Unit were used in the study. Their details were shown in Appendix E. The daily rainfall pattern in May 2006 at Uttaradit station was shown in Figure 5.5. The 6 rain gauge stations around Nam Li watershed in Figure 5.6 showed the similar daily rainfall pattern. The heavy rainfall occurred during May 20-24, 2006. Mostly rain gauge stations reported only daily rainfall. Not similarly, TMD station at Mueang district, Uttaradit records rainfall every 3 hours. Therefore, the data from Mueang Uttaradit station was used as 3 hours rainfall pattern of this event. The daily rainfall data from Nam Li Watershed Management Unit was interpolated to be 3 hours data based on TMD rain pattern and were used for overland flow assessment in

short duration of the event. The short temporal scale of rainfall data were shown to be useful in flash flood forecasting of mountainous watershed (Yates et al., 2000).

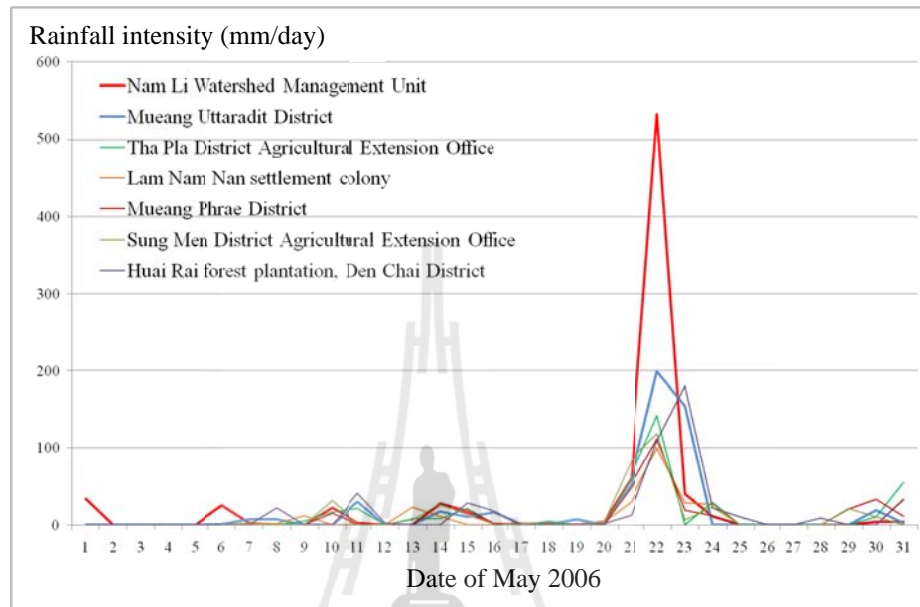


Figure 5.5 The daily rainfall intensity duration curve in May 2006 from stations within the study area and the surroundings.

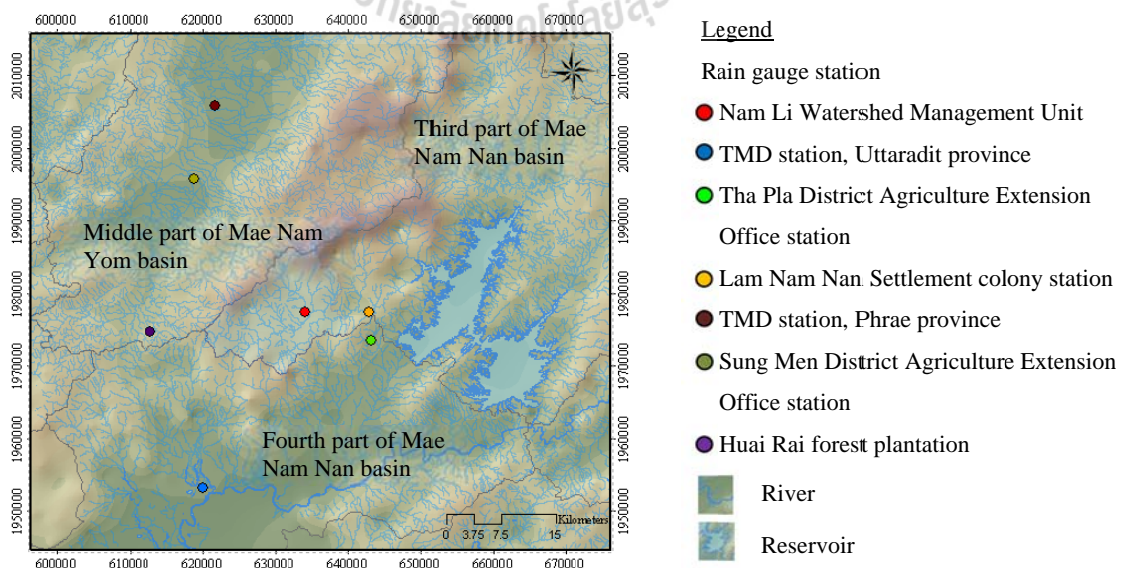


Figure 5.6 The location of rain gauge stations around the study area.

The catastrophic event occurred on May 22, 2006 which was corresponding to peak rainfall intensity (Figure 5.5). The antecedent rainfall of the event started on May 19, 2006 and an officer of Nam Li Watershed Management Unit informed that the deluge occurred on May 22, 2006 at 02:00 AM. The duration of rainfall was daily recorded from 01:00 AM to 10:00 PM to find out the exact time when overland flow occurred and effected to flash flood occurrence at 01:00 on May 22, 2006. Then the daily rainfall data were interpolated to be 3 hours rainfall. The rainfall data of TMD Uttaradit station and at Nam Li station using for interpolation were shown in Table 5.1.

Table 5.1 The rainfall data during May 20-23, 2006.

Date	TMD Uttaradit station (mm/3 hrs)									Nam Li Unit (mm/24hrs)
	1:00	4:00	7:00	10:00	13:00	16:00	19:00	22:00	Total	7:00
19	3	3.6	0.3	0	0	0	0	0	6.9	0
20	0	0	0	0	0	0	0	0	0	3.70
21	T	12	2.5	7	4.3	10.6	16	0.4	52.8	60.08
22	41.9	39	1.2	4.8	5.7	11.8	35.2	59.7	199.3	533.60
23	50.4	41.1	55	8.1	0	0	0	0	154.6	40.00
Total									413.6	637.38

According to the interview of officers of the Nam Li Watershed Management Unit, the daily rainfall is regularly recorded at 7:00AM. With an exception, the rainfall on May 22, 2006 was postponed to be 1:00PM. The trace amount of rainfall which cannot be measured and recorded as T was represented by 0.001 mm for rainfall accumulated calculation.

5.4.2 Infiltration input data

The field infiltration rate was measured in situ using the single ring infiltrometer. According to Farrell (2010), the measurement involves driving a ring (25 cm diameter and 20 cm height) into the soil and supplying water into the ring either at constant head or falling head condition. Constant head refers to condition when the amount of water in the ring is always held constant because infiltration capacity reaches to maximum infiltration rate. If rainfall exceeds the infiltration capacity, overland flow will occur. Therefore maintaining constant head means the rate of water supplied corresponds to the infiltration capacity. Falling head refers to condition when water is supplied into the ring and its level drops with time. The operator records the amount of water goes into the soil for a given time period. Equipment used is displayed in in Figure 5.7 and Figure 5.8 shows steps operated in the field.



Figure 5.7 The equipment used for infiltration testing.

1) Clearing and making flat area before test.



2) Keeping the ring vertical and hammer it into soil ~2-3 cm.



3) Preparing infiltrrometer ~20 cm height.



4) Sealing with a plastic sheet, pouring water over plastic sheet, and pulling out plastic sheet slowly.



5) Recording time initiated and the initial height when water is released from the plastic sheet.

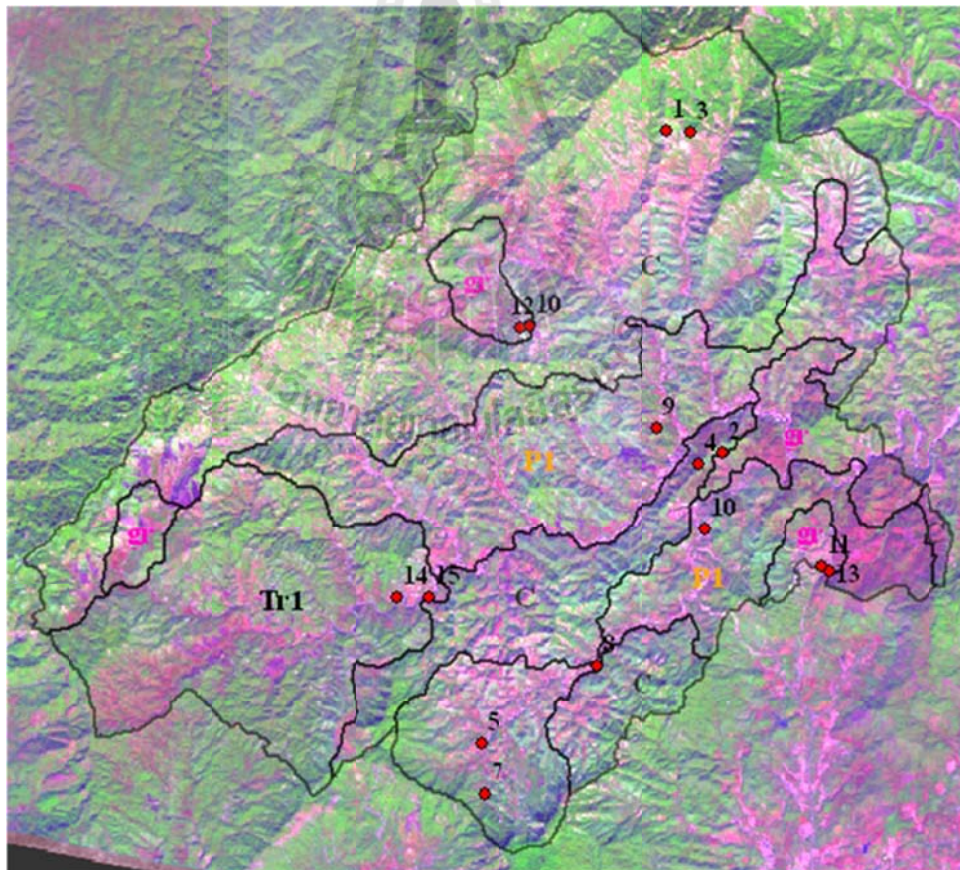


6) Recording water height at 15 second intervals for the first 2 minutes and every 1 minute after that until all water infiltrated.



Figure 5.8 The test procedure of single ring infiltrrometer.

The sampling sites shown in Figure 5.9 (a) were selected to represent unique units of LU/LC and geology. The paddy field, village, and water body were ignored. Total 15 sampling sites consisted of 4 from C unit, 5 from P1 unit, 4 from gr unit, and 2 from Tr1 unit. They were combined with various LU/LC units. f_c , (f_0-f_c) , and k in Horton equation were determined for 15 equations of sampling sites from water height changing with time and measured in single ring infiltrometer. These equations were listed in Table 5.2. They were used to calculate the infiltration rate of 3 hours duration of the event in each unique unit.



(a) The sampling sites of single ring infiltrometer tests

Figure 5.9 15 sampling sites of single ring infiltrometer tests.



(b) Site No.1, bare land in C unit



(c) Site No.2, mixed orchards in C unit



(d) Site No.3, forest in C unit



(e) Site No.4, forest plantation in C unit



(f) Site No.5, forest plantation P1 unit



(g) Site No.6, forest in P1 unit



(h) Site No.7, mixed orchard in P1 unit



(i) Site No.8, forest in P1 unit

Figure 5.9 15 sampling sites of single ring infiltrometer tests (Continued).



(j) Site No.9, forest plantation in P1 unit



(k) Site No.10, swidden cultivation area in gr unit



(l) Site No.11, mixed orchards in gr unit



(m) Site No.12, forest in gr unit



(n) Site No.13, forest plantation in gr unit



(o) Site No.14, forest in Tr1 unit



(p) Site No.15, plantation in Tr1 unit

Figure 5.9 15 sampling sites of single ring infiltrometer tests (Continued).

Table 5.2 15 Horton equations of unique unit of LULC and geology.

Sites	Geologic Units	LULC	Horton Equation
1	C	A6	$f_t = 0.3+(307-0.3)e^{-6.079t}$
2	C	A4	$f_t = 0.75+(552-0.75)e^{-4.237t}$
3	C	F	$f_t = 0.72+(330-0.72)e^{-4.029t}$
4	C	F5	$f_t = 0.48+(30-0.48)e^{-3.108t}$
5	P1	A2	$f_t = 0.3+(306-0.3)e^{-6.079t}$
6	P1	A3	$f_t = 0.27+(288-0.27)e^{-4.6281t}$
7	P1	A4	$f_t = 0.75+(552-0.75)e^{-4.237t}$
8	P1	F	$f_t = 0.48+(617-0.48)e^{-4.676t}$
9	P1	F5	$f_t = 0.40+(618-0.40)e^{-4.674t}$
10	gr	A6	$f_t = 0.36+(66-0.36)e^{-3.569t}$
11	gr	A4	$f_t = 0.48+(318-0.48)e^{-4.559t}$
12	gr	F	$f_t = 0.36+(156-0.36)e^{-3.9834t}$
13	gr	F5	$f_t = 0.46+(152-0.46)e^{-3.609t}$
14	Tr1	F	$f_t = 0.24+(180-0.24)e^{-4.306t}$
15	Tr1	F5	$f_t = 0.48+(150-0.48)e^{-3.799t}$

Note: Horton Equation is $f_t = f_c + (f_0 - f_c)e^{-kt}$

5.4.3 Land use and land cover map

The LULC map of year 2004 was interpreted by visual interpretation from SPOT5 imagery of May 27, 2006, and proved by field check on January 3-8, 2007. There were 10 types of LULC containing rice paddy (A1), perennial (A3), mixed orchards (A4), swidden cultivation area (A6), evergreen forest (F1), deciduous forest (F2), forest plantation (F5), village (U), and water body (W). Most of A1 and W were located in valley flat along streams, where were inundated during the event. The village area was ignored because it comprises asphaltic roads, concrete-paved roads, and crowded houses with no infiltration. Most of forest in the Nam Li watershed is hill evergreen forest. There is a small area of deciduous forest and all forest areas are primitive forest. They were merged to be F type. The layer showing combination units of LULC and geology (LU_GU layer) was displayed in Figure 5.10.

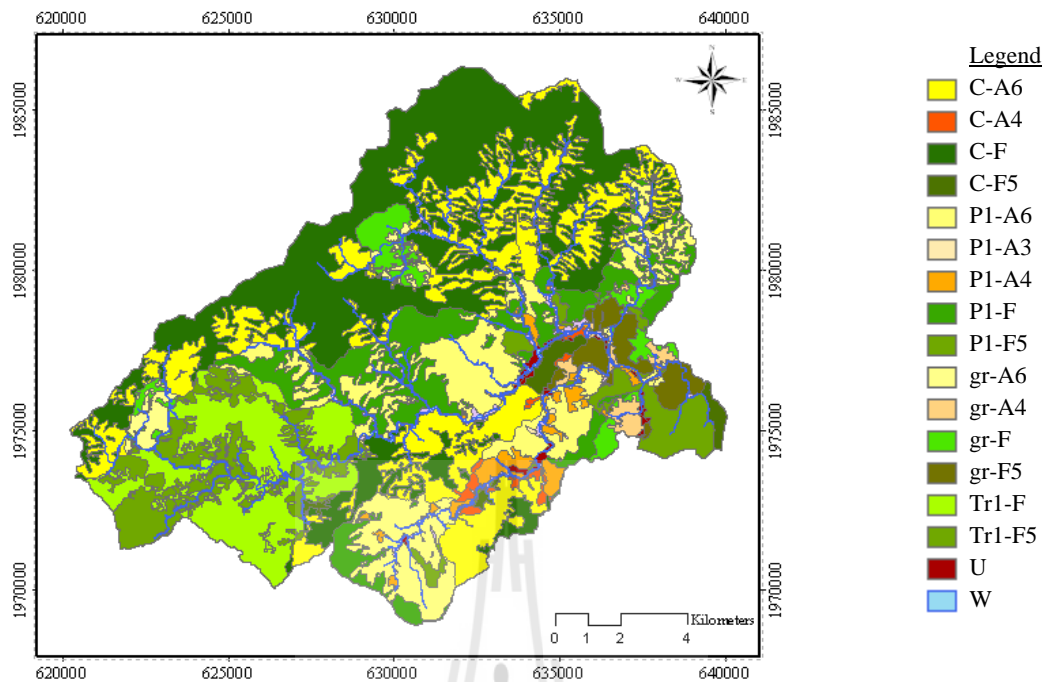
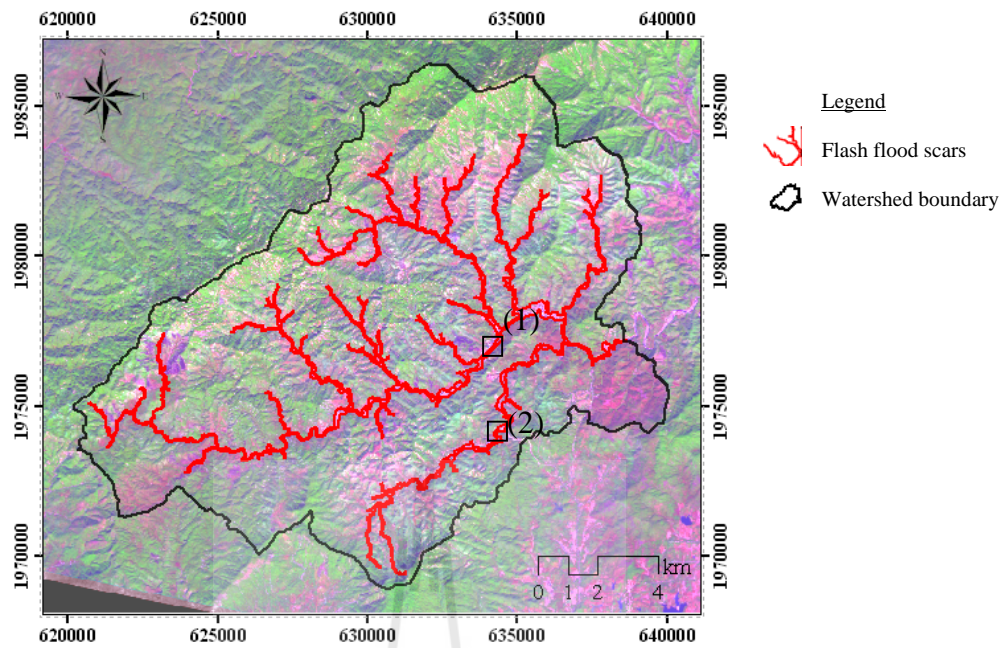


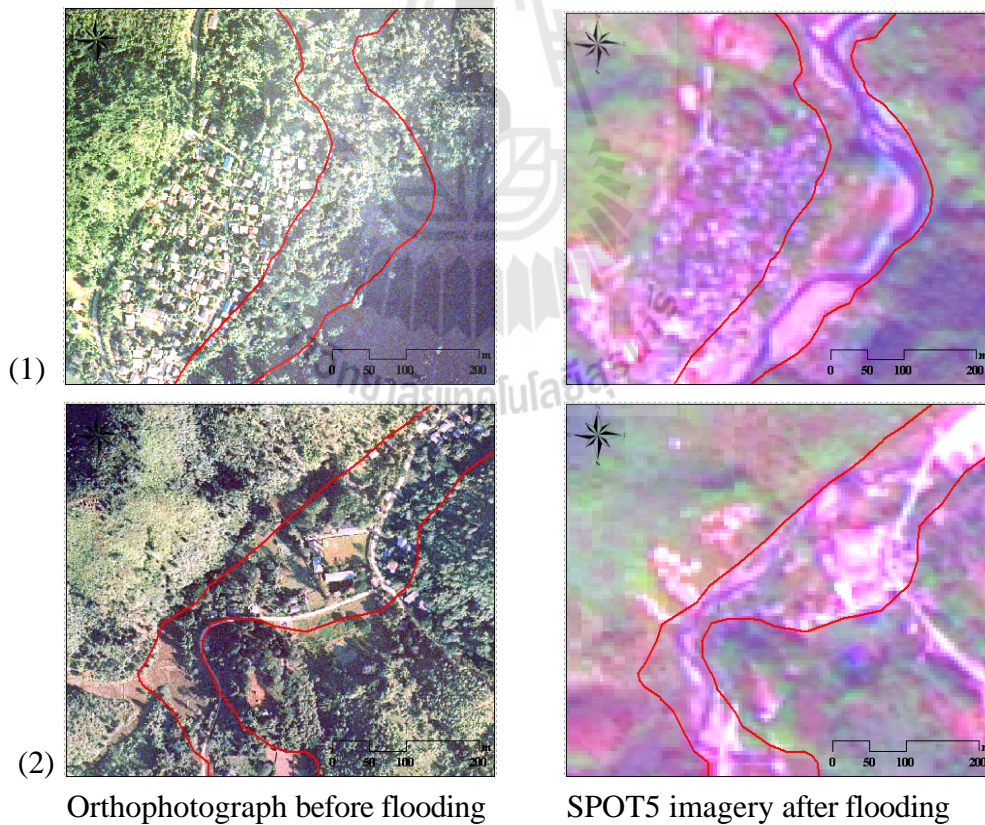
Figure 5.10 The combination units of LULC and geology of the study area.

5.4.4 Flash flood scars extraction

The boundary of flash flood scars was extracted from SPOT5 imagery of May 27, 2006 (Copyright 2006 © GISTDA) (Figure 5.11 (a)). The flood scar was defined from the different land covers which appear in false color composite (RGB = bands 4, 1, 3) of SPOT5 imagery and orthophotograph which acquired before flash flood occurrence. For example in Figure 5.11 (b), the dense vegetation both sides of the river appears in orthophotograph of year 2004 (Copyright 2004 © Department of Land Development) and became bare land as shown as bright pink color in SPOT5 imagery. The extracted flash flood scars were proved by field check on January 1-4, 2007 as field photos shown in Figures 5.12 and 5.13. The evidence of flash flood event can be seen in the actual locations which appear as a sequence of recent sediments of debris flow deposit cut at the top of river bank, mud traces on tree and house wall, and the clear away land.



(a) The extracted flash flood scars from SPOT5 imagery.



(b) Two examples of zoom-in different land covers in orthophotograph and SPOT5 imagery.

Figure 5.11 The flash flood scars extracted from SPOT5 imagery.

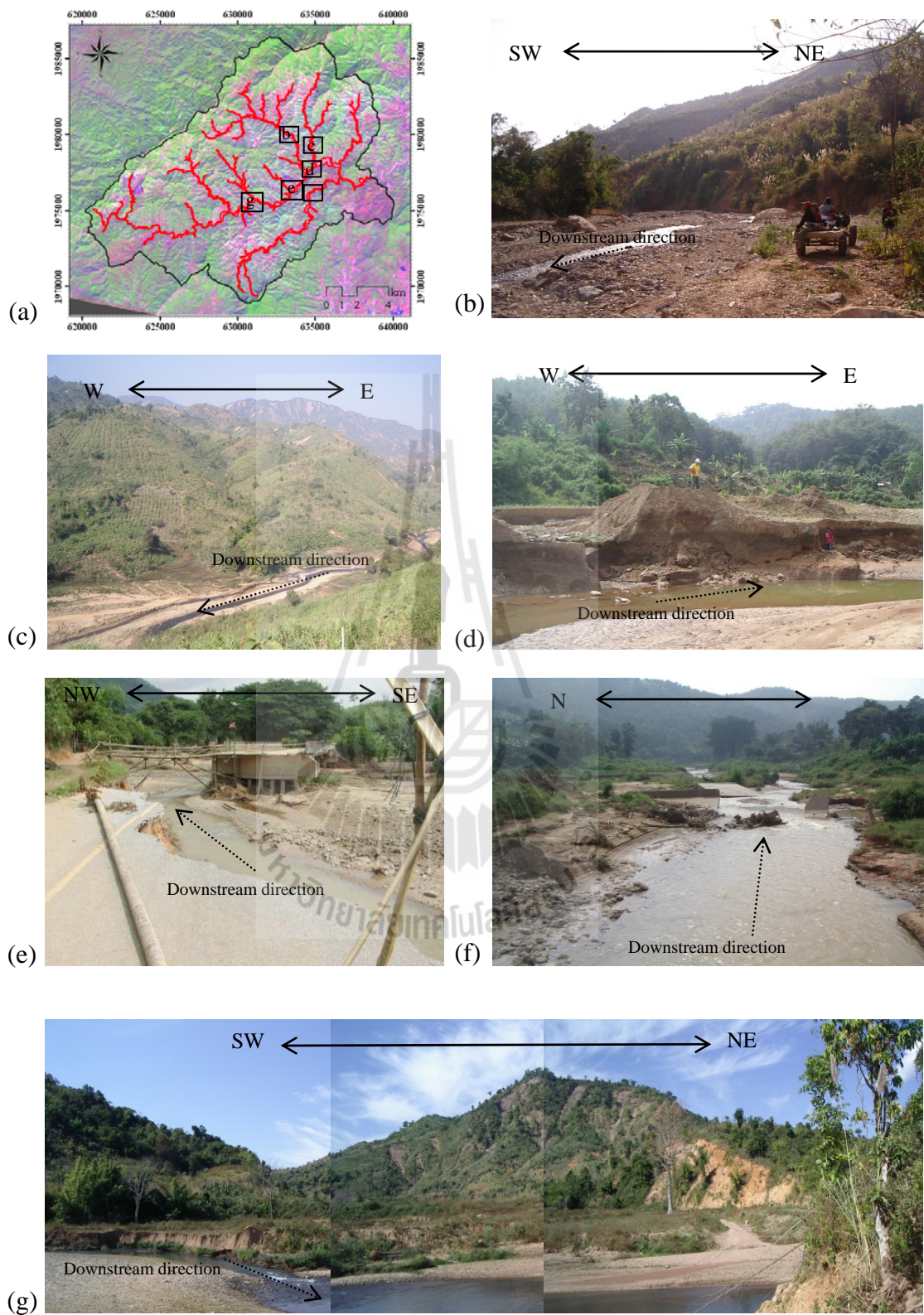


Figure 5.12 Photographs illustrating the actual location of flash flood scars.



Figure 5.13 Photographs illustrating the current mud traces of flash flood event.

5.5 Results and discussion

5.5.1 Relation of infiltration and precipitation

From Figure 5.5, the rainfall patterns depict the rain curve during May 19-23, 2006, but the antecedent rainfall is trace to slight rain. Therefore the antecedent rainfall on May 19, 2006 is negligible. Using equation (5.1), 3 hours rainfall of Nam Li watershed was calculated as results shown in Table 5.3. The 3 hours rainfall pattern of Nam Li watershed and Uttaradit station, during 1:00AM, May 20, 2006 to 10:00PM, May 23, 2006, were shown in Figure 5.14. The pattern of 3 hours rainfall intensity during 04:00AM, May 20, 2006 to 10:00AM, May 23, 2006 (57 hours) of two stations are identical in the period of antecedent and the peak rainfall of the event. These results were used to determine the excess water of 3 hours duration.

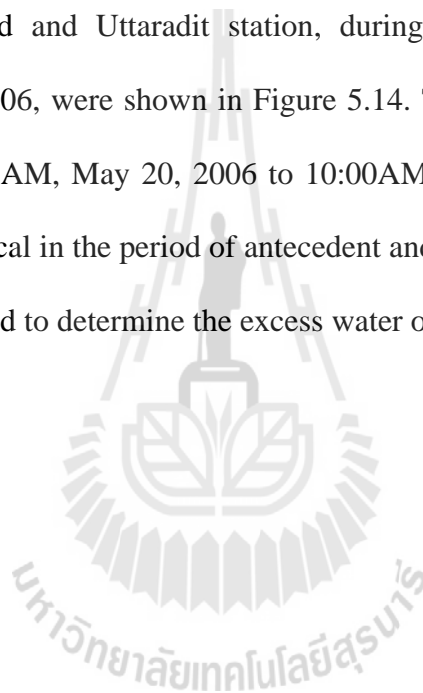


Table 5.3 The 3 hours rainfall of the event during May 19-23, 2006.

Date/Time	Stations				
	Uttaradit (B)		Daily rainfall (RD _A)	Nam Li (A)	
	R3hrs (R3hr _B)	R3hrs accumulated (R3hr _{Bacc})		R3hr accumulated simulation $R3hr_{Acc(t)} = \frac{(RD_A \times R3hr_{Bacc(t)})}{R3hr_{Bacc}}$	R3hrs _A = (R3hr _{Acc(t)} - R3hr _{Acc(t)before})
19/5/2006 1:00 PM	T	0.001		0.0	0.0
4:00 PM	0.3	0.301		0.1	0.1
7:00 PM	0.7	1.001		0.3	0.2
10:00 PM	0.0	1.001		0.3	0.0
19/5/2006 1:00 AM	3	4.001		1.0	0.7
4:00 AM	3.6	7.601		1.9	0.9
7:00 AM	0.3	7.901	2.00	2.0	0.1
10:00 AM	0.0	0.0		0.0	0.0
1:00 PM	0.0	0.0		0.0	0.0
4:00 PM	0.0	0.0		0.0	0.0
7:00 PM	0.0	0.0		0.0	0.0
10:00 PM	0.0	0.0		0.0	0.0
20/5/2006 1:00 AM	T	0.001		3.7	3.7
4:00 AM	0.0	0.001		3.7	0.0
7:00 AM	0.0	0.001	3.70	3.7	0.0
10:00 AM	0.0	0.0		0.0	0.0
1:00 PM	0.0	0.0		0.0	0.0
4:00 PM	0.0	0.0		0.0	0.0
7:00 PM	0.0	0.0		0.0	0.0
10:00 PM	0.0	0.0		0.0	0.0
21/5/2006 1:00 AM	T	0.001		0.0	0.0
4:00 AM	12	12.001		49.7	49.7
7:00 AM	2.5	14.501	60.08	60.1	10.4
10:00 AM	7.0	7.0		28.5	28.5
1:00 PM	4.3	11.3		46.1	17.5
4:00 PM	10.6	21.9		89.3	43.2
7:00 PM	16.0	37.9		154.5	65.2
10:00 PM	0.4	38.3		156.1	1.6
22/5/2006 1:00 AM	41.9	80.2		326.9	170.8
4:00 AM	39.0	119.2		485.9	159.0
7:00 AM	1.2	120.4		490.8	4.9
10:00 AM	4.8	125.2		510.4	19.6
1:00 PM	5.7	130.9	533.60	533.6	23.2
4:00 PM	11.8	22.3		3.4	3.4
7:00 PM	35.2	57.5		8.7	5.3
10:00 PM	59.7	117.2		17.8	9.1
23/5/2006 1:00 AM	50.4	167.6		25.4	7.6
4:00 AM	41.1	208.7		31.7	6.2
7:00 AM	55.0	263.7	40.00	40.0	8.3
10:00 AM	8.1	8.1		11.1	11.1
1:00 PM	0.0	8.1		11.1	0.0
4:00 PM	0.0	8.1		11.1	0.0
7:00 PM	0.0	8.1		11.1	0.0
10:00 PM	0.0	8.1		11.1	0.0

Note: T = 0.001, Unit = mm

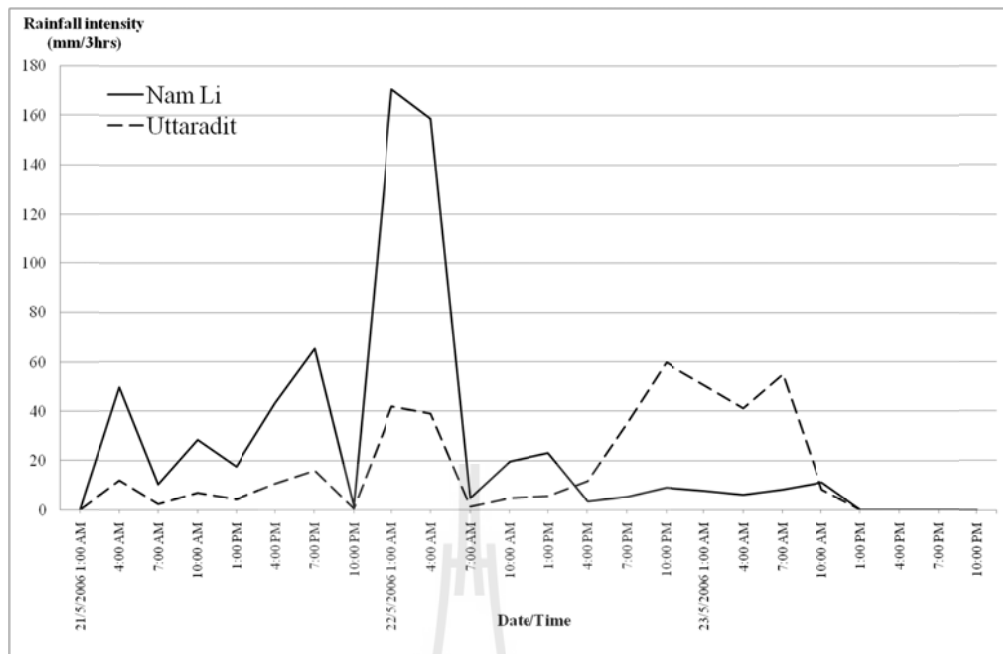


Figure 5.14 The 3 hours rainfall intensity duration curve on May 21-23, 2006.

The infiltration rate of 1 hour intervals was derived from rainfall interpolation in Table 5.3 through equations in Table 5.2 and the results are shown in Table 5.4. The curves of 3-hours rainfall intensity and 1-hour infiltration rates from 15 sampling sites are plotted as shown in Figure 5.15. From the Figure, the area of the rainfall over infiltration curve is the excess water which became overland flow of the event. This research does not use rainfall data from the stations around Nam Li watershed because there is rain gauge in the watershed and this watershed is a small area. Moreover the event was a torrential rain which could be constantly widespread over the watershed.

Table 5.4 The 57 infiltration rate of 1 hour intervals in 15 sampling sites.

t(hr)	Site 1	Site 2	Site 3	Site 4	Site 5	Site 6	Site 7	Site	Site 9	Site 10	Site	Site 12	Site 13	Site 14	Site 15
f _c	0.30	0.75	0.72	0.48	0.30	0.27	0.75	0.48	0.40	0.36	0.48	0.36	0.46	0.24	0.48
f ₀	307	552	330	30	306	288	552	617	618	66	318	156	152	180	150
k	6.079	4.237	4.029	3.108	6.079	4.628	4.237	4.674	4.674	3.569	4.559	3.98	3.609	4.306	3.799
1	7.32	80.41	59.31	13.67	7.30	28.39	80.41	58.03	58.05	18.86	33.73	29.44	41.50	24.37	33.96
2	0.32	1.90	1.76	1.07	0.32	0.54	1.90	1.02	0.94	0.88	0.83	0.90	1.57	0.78	1.23
3	0.30	0.77	0.74	0.51	0.30	0.27	0.77	0.49	0.41	0.37	0.48	0.37	0.49	0.25	0.50
4	0.30	0.75	0.72	0.48	0.30	0.27	0.75	0.48	0.40	0.36	0.48	0.36	0.46	0.24	0.48
5	0.30	0.75	0.72	0.48	0.30	0.27	0.75	0.48	0.40	0.36	0.48	0.36	0.46	0.24	0.48
6	0.30	0.75	0.72	0.48	0.30	0.27	0.75	0.48	0.40	0.36	0.48	0.36	0.46	0.24	0.48
7	0.30	0.75	0.72	0.48	0.30	0.27	0.75	0.48	0.40	0.36	0.48	0.36	0.46	0.24	0.48
8	0.30	0.75	0.72	0.48	0.30	0.27	0.75	0.48	0.40	0.36	0.48	0.36	0.46	0.24	0.48
9	0.30	0.75	0.72	0.48	0.30	0.27	0.75	0.48	0.40	0.36	0.48	0.36	0.46	0.24	0.48
10	0.30	0.75	0.72	0.48	0.30	0.27	0.75	0.48	0.40	0.36	0.48	0.36	0.46	0.24	0.48
11	0.30	0.75	0.72	0.48	0.30	0.27	0.75	0.48	0.40	0.36	0.48	0.36	0.46	0.24	0.48
12	0.30	0.75	0.72	0.48	0.30	0.27	0.75	0.48	0.40	0.36	0.48	0.36	0.46	0.24	0.48
13	0.30	0.75	0.72	0.48	0.30	0.27	0.75	0.48	0.40	0.36	0.48	0.36	0.46	0.24	0.48
14	0.30	0.75	0.72	0.48	0.30	0.27	0.75	0.48	0.40	0.36	0.48	0.36	0.46	0.24	0.48
15	0.30	0.75	0.72	0.48	0.30	0.27	0.75	0.48	0.40	0.36	0.48	0.36	0.46	0.24	0.48
16	0.30	0.75	0.72	0.48	0.30	0.27	0.75	0.48	0.40	0.36	0.48	0.36	0.46	0.24	0.48
17	0.30	0.75	0.72	0.48	0.30	0.27	0.75	0.48	0.40	0.36	0.48	0.36	0.46	0.24	0.48
18	0.30	0.75	0.72	0.48	0.30	0.27	0.75	0.48	0.40	0.36	0.48	0.36	0.46	0.24	0.48
19	0.30	0.75	0.72	0.48	0.30	0.27	0.75	0.48	0.40	0.36	0.48	0.36	0.46	0.24	0.48
20	0.30	0.75	0.72	0.48	0.30	0.27	0.75	0.48	0.40	0.36	0.48	0.36	0.46	0.24	0.48
21	0.30	0.75	0.72	0.48	0.30	0.27	0.75	0.48	0.40	0.36	0.48	0.36	0.46	0.24	0.48
22	0.30	0.75	0.72	0.48	0.30	0.27	0.75	0.48	0.40	0.36	0.48	0.36	0.46	0.24	0.48
23	0.30	0.75	0.72	0.48	0.30	0.27	0.75	0.48	0.40	0.36	0.48	0.36	0.46	0.24	0.48
24	0.30	0.75	0.72	0.48	0.30	0.27	0.75	0.48	0.40	0.36	0.48	0.36	0.46	0.24	0.48
25	0.30	0.75	0.72	0.48	0.30	0.27	0.75	0.48	0.40	0.36	0.48	0.36	0.46	0.24	0.48
26	0.30	0.75	0.72	0.48	0.30	0.27	0.75	0.48	0.40	0.36	0.48	0.36	0.46	0.24	0.48
27	0.30	0.75	0.72	0.48	0.30	0.27	0.75	0.48	0.40	0.36	0.48	0.36	0.46	0.24	0.48
28	0.30	0.75	0.72	0.48	0.30	0.27	0.75	0.48	0.40	0.36	0.48	0.36	0.46	0.24	0.48
29	0.30	0.75	0.72	0.48	0.30	0.27	0.75	0.48	0.40	0.36	0.48	0.36	0.46	0.24	0.48
30	0.30	0.75	0.72	0.48	0.30	0.27	0.75	0.48	0.40	0.36	0.48	0.36	0.46	0.24	0.48
31	0.30	0.75	0.72	0.48	0.30	0.27	0.75	0.48	0.40	0.36	0.48	0.36	0.46	0.24	0.48
32	0.30	0.75	0.72	0.48	0.30	0.27	0.75	0.48	0.40	0.36	0.48	0.36	0.46	0.24	0.48
33	0.30	0.75	0.72	0.48	0.30	0.27	0.75	0.48	0.40	0.36	0.48	0.36	0.46	0.24	0.48
34	0.30	0.75	0.72	0.48	0.30	0.27	0.75	0.48	0.40	0.36	0.48	0.36	0.46	0.24	0.48
35	0.30	0.75	0.72	0.48	0.30	0.27	0.75	0.48	0.40	0.36	0.48	0.36	0.46	0.24	0.48
36	0.30	0.75	0.72	0.48	0.30	0.27	0.75	0.48	0.40	0.36	0.48	0.36	0.46	0.24	0.48
37	0.30	0.75	0.72	0.48	0.30	0.27	0.75	0.48	0.40	0.36	0.48	0.36	0.46	0.24	0.48
38	0.30	0.75	0.72	0.48	0.30	0.27	0.75	0.48	0.40	0.36	0.48	0.36	0.46	0.24	0.48
39	0.30	0.75	0.72	0.48	0.30	0.27	0.75	0.48	0.40	0.36	0.48	0.36	0.46	0.24	0.48
40	0.30	0.75	0.72	0.48	0.30	0.27	0.75	0.48	0.40	0.36	0.48	0.36	0.46	0.24	0.48
41	0.30	0.75	0.72	0.48	0.30	0.27	0.75	0.48	0.40	0.36	0.48	0.36	0.46	0.24	0.48
42	0.30	0.75	0.72	0.48	0.30	0.27	0.75	0.48	0.40	0.36	0.48	0.36	0.46	0.24	0.48
43	0.30	0.75	0.72	0.48	0.30	0.27	0.75	0.48	0.40	0.36	0.48	0.36	0.46	0.24	0.48
44	0.30	0.75	0.72	0.48	0.30	0.27	0.75	0.48	0.40	0.36	0.48	0.36	0.46	0.24	0.48
45	0.30	0.75	0.72	0.48	0.30	0.27	0.75	0.48	0.40	0.36	0.48	0.36	0.46	0.24	0.48
46	0.30	0.75	0.72	0.48	0.30	0.27	0.75	0.48	0.40	0.36	0.48	0.36	0.46	0.24	0.48
47	0.30	0.75	0.72	0.48	0.30	0.27	0.75	0.48	0.40	0.36	0.48	0.36	0.46	0.24	0.48
48	0.30	0.75	0.72	0.48	0.30	0.27	0.75	0.48	0.40	0.36	0.48	0.36	0.46	0.24	0.48
49	0.30	0.75	0.72	0.48	0.30	0.27	0.75	0.48	0.40	0.36	0.48	0.36	0.46	0.24	0.48
50	0.30	0.75	0.72	0.48	0.30	0.27	0.75	0.48	0.40	0.36	0.48	0.36	0.46	0.24	0.48
51	0.30	0.75	0.72	0.48	0.30	0.27	0.75	0.48	0.40	0.36	0.48	0.36	0.46	0.24	0.48
52	0.30	0.75	0.72	0.48	0.30	0.27	0.75	0.48	0.40	0.36	0.48	0.36	0.46	0.24	0.48
53	0.30	0.75	0.72	0.48	0.30	0.27	0.75	0.48	0.40	0.36	0.48	0.36	0.46	0.24	0.48
54	0.30	0.75	0.72	0.48	0.30	0.27	0.75	0.48	0.40	0.36	0.48	0.36	0.46	0.24	0.48
55	0.30	0.75	0.72	0.48	0.30	0.27	0.75	0.48	0.40	0.36	0.48	0.36	0.46	0.24	0.48
56	0.30	0.75	0.72	0.48	0.30	0.27	0.75	0.48	0.40	0.36	0.48	0.36	0.46	0.24	0.48
57	0.30	0.75	0.72	0.48	0.30	0.27	0.75	0.48	0.40	0.36	0.48	0.36	0.46	0.24	0.48

Note: Unit = mm

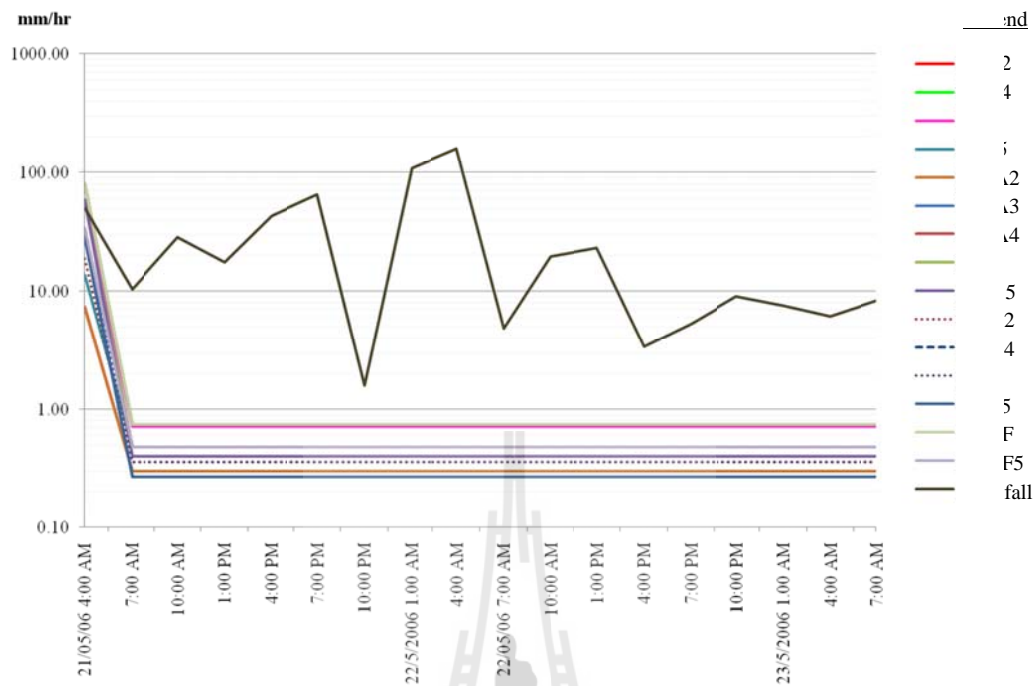


Figure 5.15 The relation between rainfall intensity and infiltration of 15 sampling sites in semi-logarithm scale.

5.5.2 Overland flow assessment.

From the curves in Figure 5.15, they reveal that $P > f_c$, then the excess water of each LU_GU unit can be calculated using equation (5.5) as results shown in Table 5.5. Nineteen raster layers of Q representing every 3-hour interval were constructed. The candidate suitable Q layers display the lowest in C unit with mixed orchard and the highest in P1 unit with crop as shown in Figure 5.16.



Table 5.5 The result of overland flow calculation.

Date/Time	21/5/2006								22/5/2006								23/5/2006							
	1:00 AM	4:00 AM	7:00 AM	10:00 AM	1:00 PM	4:00 PM	7:00 PM	10:00 PM	1:00 AM	4:00 AM	7:00 AM	10:00 AM	1:00 PM	4:00 PM	7:00 PM	10:00 PM	1:00 AM	4:00 AM	7:00 AM	10:00 AM				
Rainfall	P	0.00	49.70	60.10	88.60	106.10	149.30	214.50	216.10	323.90	482.90	487.80	507.40	530.60	534.00	539.30	548.40	556.00	562.20	570.50	581.60			
Site 1 CA2	I	0.00	7.32	8.24	9.14	10.04	10.94	11.84	12.74	13.64	14.54	15.44	16.34	17.24	18.14	19.04	19.94	20.84	21.74	22.64	23.54			
	Q	0.00	42.38	51.86	79.46	96.06	138.36	202.66	203.36	310.26	468.36	472.36	491.06	513.36	515.86	520.26	528.46	535.16	540.46	547.86	558.06			
Site 2 CA4	I	0.00	80.41	83.83	86.08	88.33	90.58	92.83	95.08	97.33	99.58	101.83	104.08	106.33	108.58	110.83	113.08	115.33	117.58	119.83	122.08			
	Q	0.00	-30.71	-23.73	2.52	17.77	58.72	121.67	121.02	226.57	383.32	385.97	403.32	424.27	425.42	428.47	435.32	440.67	444.62	450.67	459.52			
Site 3 CF	I	0.00	59.31	62.53	64.69	66.85	69.01	71.17	73.33	75.49	77.65	79.81	81.97	84.13	86.29	88.45	90.61	92.77	94.93	97.09	99.25			
	Q	0.00	-9.61	-2.43	23.91	39.25	80.29	143.33	142.77	248.41	405.25	407.99	425.43	446.47	447.71	450.85	457.79	463.23	467.27	473.41	482.35			
Site 4 CF5	I	0.00	13.67	15.73	17.17	18.61	20.05	21.49	22.93	24.37	25.81	27.25	28.69	30.13	31.57	33.01	34.45	35.89	37.33	38.77	40.21			
	Q	0.00	36.03	44.37	71.43	87.49	129.25	193.01	193.17	299.53	457.09	460.55	478.71	500.47	502.43	506.29	513.95	520.11	524.87	531.73	541.39			
Site 5 P1A2	I	0.00	7.30	8.22	9.12	10.02	10.92	11.82	12.72	13.62	14.52	15.42	16.32	17.22	18.12	19.02	19.92	20.82	21.72	22.62	23.52			
	Q	0.00	42.40	51.88	79.48	96.08	138.38	202.68	203.38	310.28	468.38	472.38	491.08	513.38	515.88	520.28	528.48	535.18	540.48	547.88	558.08			
Site 6 P1A3	I	0.00	28.39	29.48	30.29	31.10	31.91	32.72	33.53	34.34	35.15	35.96	36.77	37.58	38.39	39.20	40.01	40.82	41.63	42.44	43.25			
	Q	0.00	21.31	30.62	58.31	75.00	117.39	181.78	182.57	289.56	447.75	451.84	470.63	493.02	495.61	500.10	508.39	515.18	520.57	528.06	538.35			
Site 7 P1A4	I	0.00	80.41	83.83	86.08	88.33	90.58	92.83	95.08	97.33	99.58	101.83	104.08	106.33	108.58	110.83	113.08	115.33	117.58	119.83	122.08			
	Q	0.00	-30.71	-23.73	2.52	17.77	58.72	121.67	121.02	226.57	383.32	385.97	403.32	424.27	425.42	428.47	435.32	440.67	444.62	450.67	459.52			
Site 8 P1F	I	0.00	58.03	60.01	61.45	62.89	64.33	65.77	67.21	68.65	70.09	71.53	72.97	74.41	75.85	77.29	78.73	80.17	81.61	83.05	84.49			
	Q	0.00	-8.33	0.09	27.15	43.21	84.97	148.73	148.89	255.25	412.81	416.27	434.43	456.19	458.15	462.01	469.67	475.83	480.59	487.45	497.11			
Site 9 P1F5	I	0.00	58.05	59.80	61.00	62.20	63.40	64.60	65.80	67.00	68.20	69.40	70.60	71.80	73.00	74.20	75.40	76.60	77.80	79.00	80.20			
	Q	0.00	-8.35	0.30	27.60	43.90	85.90	149.90	150.30	256.90	414.70	418.40	436.80	458.80	461.00	465.10	473.00	479.40	484.40	491.50	501.40			
Site 10 grA2	I	0.00	18.86	20.48	21.56	22.64	23.72	24.80	25.88	26.96	28.04	29.12	30.20	31.28	32.36	33.44	34.52	35.60	36.68	37.76	38.84			
	Q	0.00	30.84	39.62	67.04	83.46	125.58	189.70	190.22	296.94	454.86	458.68	477.20	499.32	501.64	505.86	513.88	520.40	525.52	532.74	542.76			
Site 11 grA4	I	0.00	33.73	35.52	36.96	38.40	39.84	41.28	42.72	44.16	45.60	47.04	48.48	49.92	51.36	52.80	54.24	55.68	57.12	58.56	60.00			
	Q	0.00	15.97	24.58	51.64	67.70	109.46	173.22	173.38	279.74	437.30	440.76	458.92	480.68	482.64	486.50	494.16	500.32	505.08	511.94	521.60			
Site 12 grF	I	0.00	29.44	31.08	32.16	33.24	34.32	35.40	36.48	37.56	38.64	39.72	40.80	41.88	42.96	44.04	45.12	46.20	47.28	48.36	49.44			
	Q	0.00	20.26	29.02	56.44	72.86	114.98	179.10	179.62	286.34	444.26	448.08	466.60	488.72	491.04	495.26	503.28	509.80	514.92	522.14	532.16			
Site 13 grF5	I	0.00	41.50	44.02	45.40	46.78	48.16	49.54	50.92	52.30	53.68	55.06	56.44	57.82	59.20	60.58	61.96	63.34	64.72	66.10	67.48			
	Q	0.00	8.20	16.08	43.20	59.32	101.14	164.96	165.18	271.60	429.22	432.74	450.96	472.78	474.80	478.72	486.44	492.66	497.48	504.40	514.12			
Site 14 Tr1F	I	0.00	24.37	25.64	26.36	27.08	27.80	28.52	29.24	29.96	30.68	31.40	32.12	32.84	33.56	34.28	35.00	35.72	36.44	37.16	37.88			
	Q	0.00	25.33	34.46	62.24	79.02	121.50	185.98	186.86	293.94	452.22	456.40	475.28	497.76	500.44	505.02	513.40	520.28	525.76	533.34	543.72			
Site 15 Tr1F5	I	0.00	33.96	36.17	37.61	39.05	40.49	41.93	43.37	44.81	46.25	47.69	49.13	50.57	52.01	53.45	54.89	56.33	57.77	59.21	60.65			
	Q	0.00	15.74	23.93	50.99	67.05	108.81	172.57	172.73	279.09	436.65	440.11	458.27	480.03	481.99	485.85	493.51	499.67	504.43	511.29	520.95			

Note: P = Rainfall intensity, I = Infiltration rate, Q = Overland flow, Unit = mm.



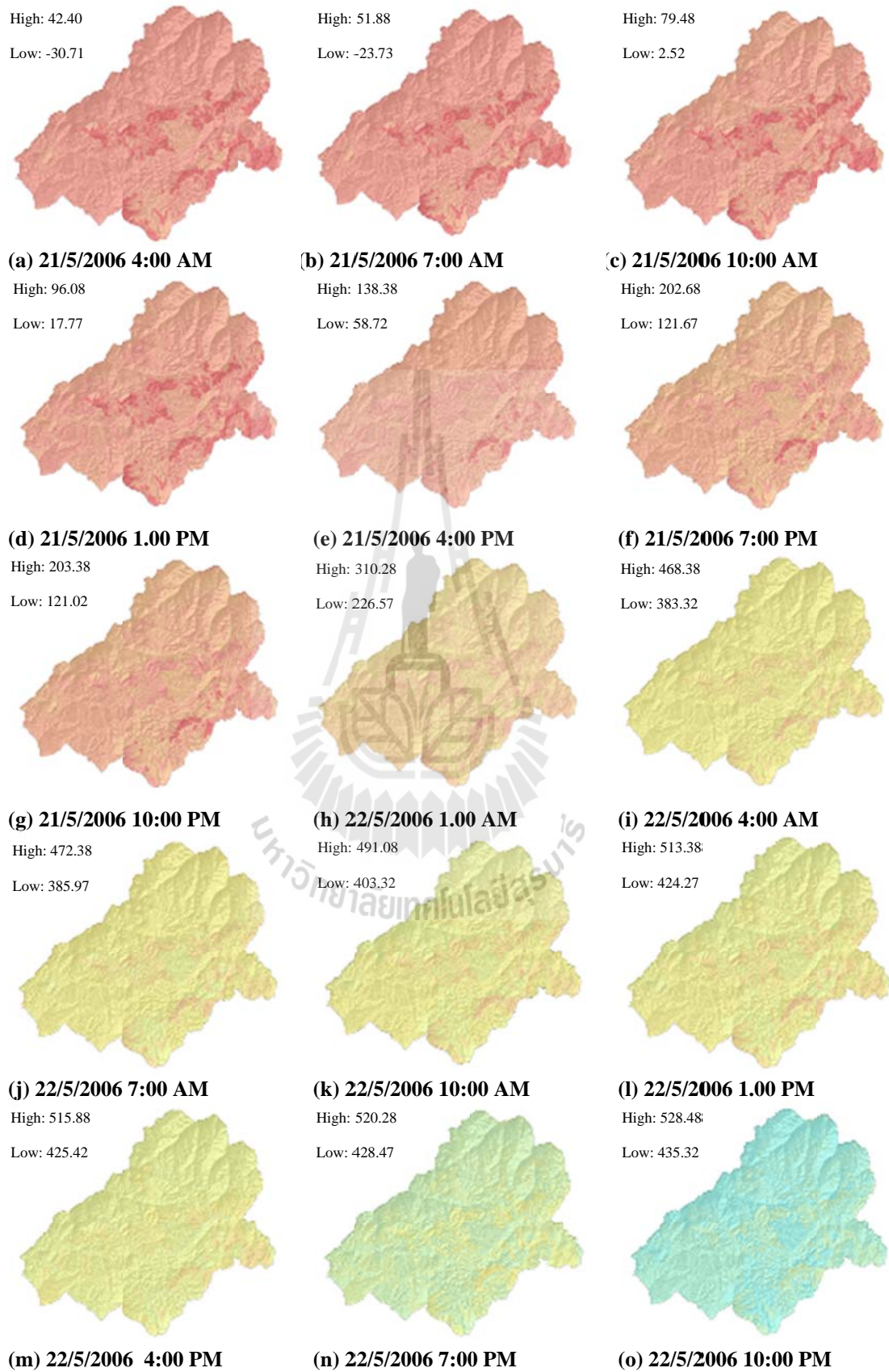


Figure 5.16 The raster layers of candidate suitable overland flow (Q).

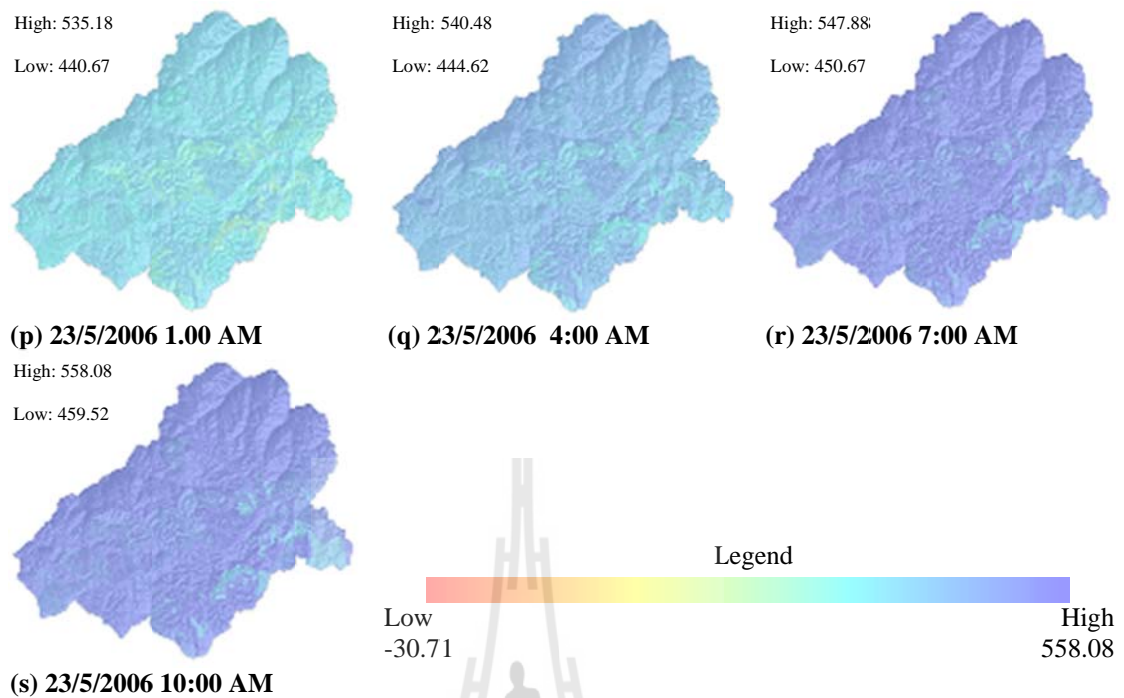


Figure 5.16 The raster layers of candidate suitable overland flow (Q) (Continued).

From the study it can be concluded that the land use/land cover and soil drainage ability affect to overland flow as same as the researches of Rawee Rattanakom and Suwit Ongsomwang (2008) and Saini and Kaushik (2012). In the mixed orchard and C unit which consists of phyllitic shale and silty shale with abundant fracture allow more water to infiltrate and less overland flow. On the other hand, the crop and P1 unit which consists of tuffaceous sandstone with less fracture allow less water to infiltrate and more overland flow.

To find out the time interval indicating the highest increasing rate of Q in the event, the flow accumulation of Q layer of each 3-hour interval was performed to achieve accumulated overland flow (Q_{ac}) at the outlet of the watershed (Figure 5.14). The highest ratio between Q_{ac} of n+1 time interval and of n time interval indicates time interval with the highest increasing rate of Q in the event. As shown in

Table 5.6 and Figure 5.18, the highest ratio is 3.01, indicating that the highest increasing rate of Q occurred at 10:00 PM - 1:00 AM on May 22, 2006. This Q_{ac} layer was further used for assessing flash flood susceptibility of the area. The Q_{ac} values of this layer (Figure 5.17 (h)) are continuous values from 0 to 705,934,902 mm.

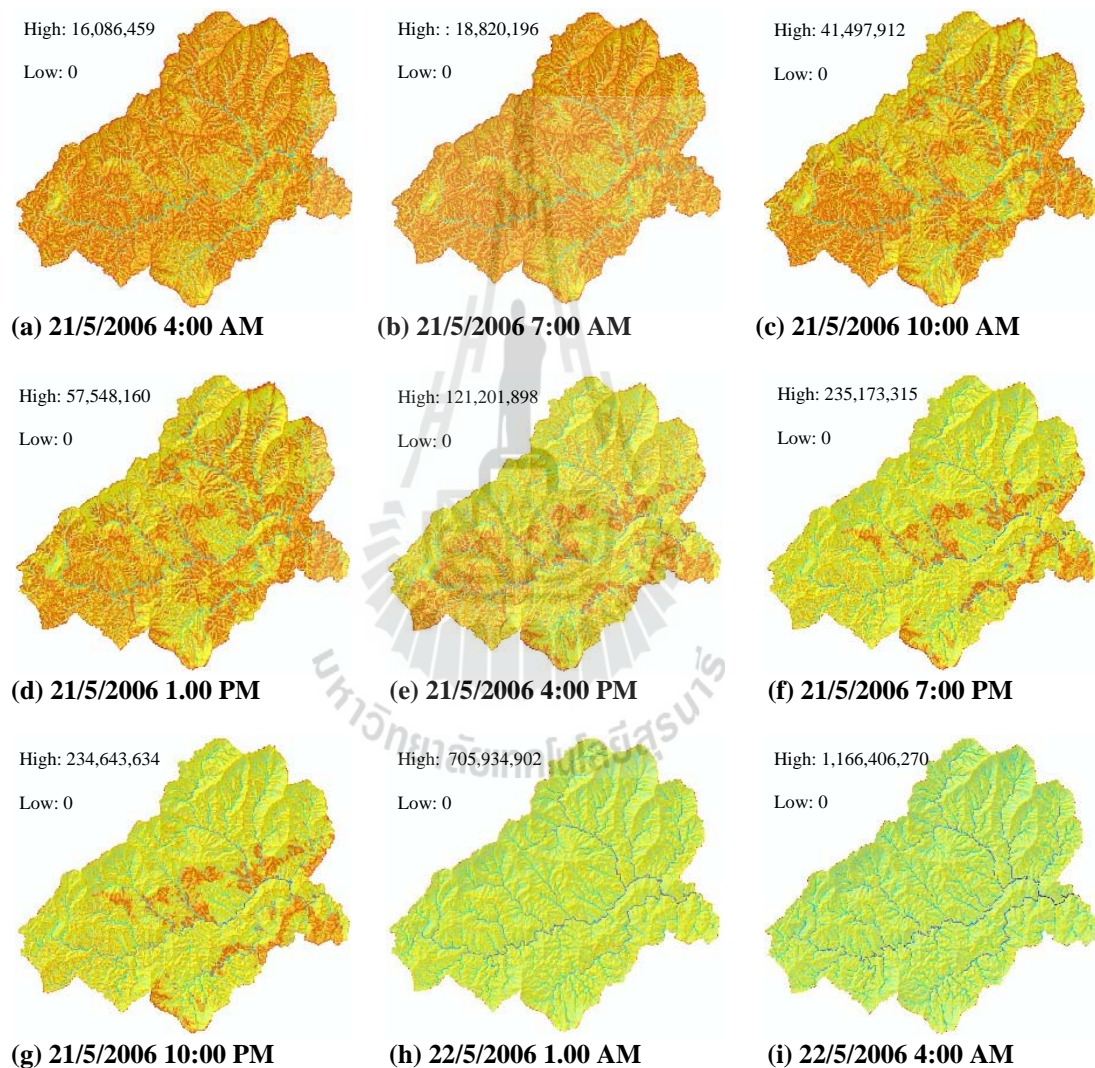


Figure 5.17 The accumulated overland flow raster layers.

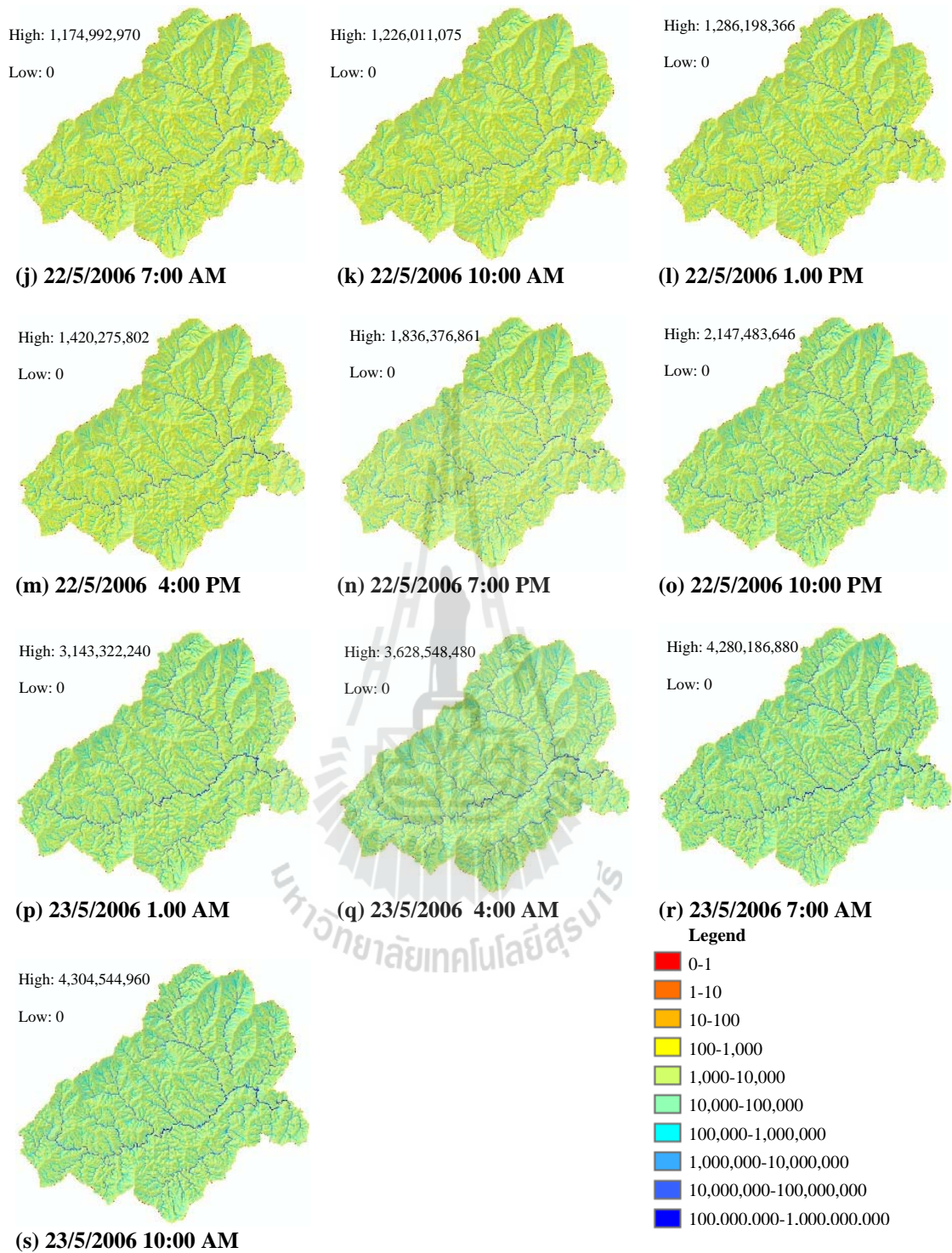


Figure 5.17 The accumulated overland flow raster layers (Continued).

Table 5.6 The accumulated overland flow at the outlet of each duration and their increasing ratios.

Date	Duration	Duration number (n)	Accumulated overland flow at the outlet (Q_{ac} , mm)	Ratio ($Q_{ac(n+1)}/Q_{ac(n)}$)
21/5/2006	1:00AM - 4:00 AM	1	16,086,459	
	4:00AM - 7:00 AM	2	18,820,196	1.17
	7:00AM - 10:00 AM	3	41,497,912	2.20
	10:00 AM - 1:00 PM	4	57,547,160	1.39
	1:00 PM - 4:00 PM	5	121,201,898	2.11
	4:00 PM - 7:00 PM	6	235,173,315	1.94
	7:00 PM - 10:00 PM	7	234,643,634	1.00
21/5/2006	10:00 PM - 1:00 AM	8	705,934,902	3.01
	1:00AM - 4:00 AM	9	1,166,406,270	1.65
	4:00AM - 7:00 AM	10	1,174,992,970	1.01
	7:00AM - 10:00 AM	11	1,226,011,075	1.04
	10:00 AM - 1:00 PM	12	1,286,198,366	1.05
	1:00 PM - 4:00 PM	13	1,420,275,802	1.10
	4:00 PM - 7:00 PM	14	1,836,376,861	1.29
	7:00 PM - 10:00 PM	15	2,147,483,646	1.17
23/5/2006	10:00 PM - 1:00 AM	16	3,143,322,420	1.46
	1:00AM - 4:00 AM	17	3,628,548,480	1.15
	4:00AM - 7:00 AM	18	4,280,186,880	1.18
	7:00AM - 10:00 AM	19	4,304,544,960	1.01

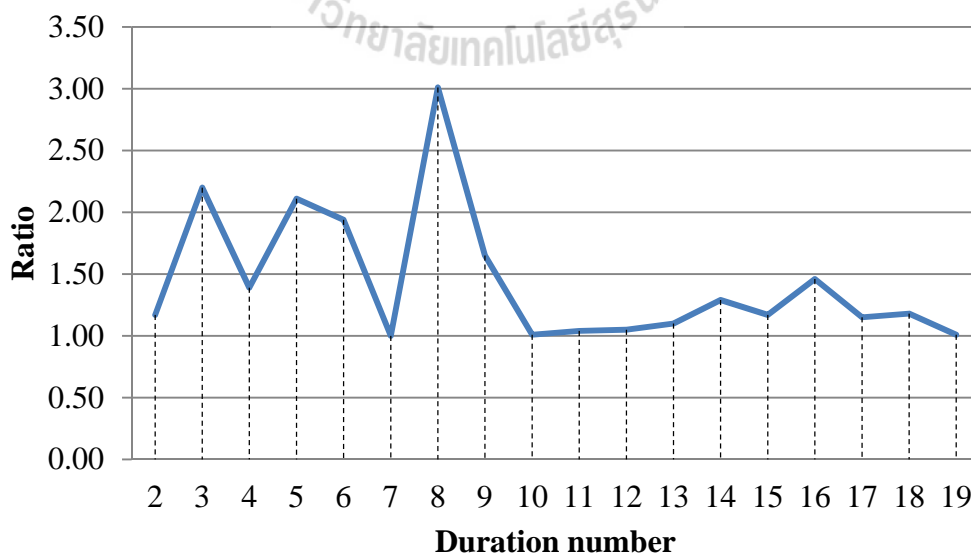
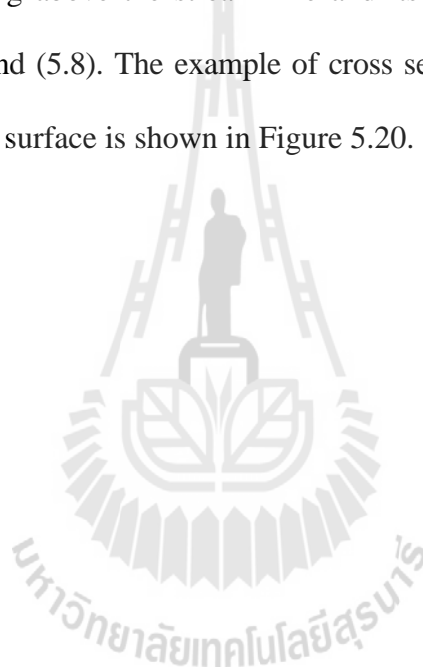


Figure 5.18 The increasing ratio of accumulated Q of 18 durations.

5.5.3 Flash flood scar surface and flood depth estimation

The boundary of flash flood scar was extracted from SPOT5 image as described in 5.4.4. The scar was located both sides of the streams. It represents the area subjected to high intensity impact from overland flow. To estimate elevation of the scar surface, elevations at the scar boundary and flood depth at the stream line are required for interpolation. Elevation at the scar boundary was extracted from DEM. Flood depth at every 100 m spacing above the stream line and its spot elevation were estimated using equation (5.7) and (5.8). The example of cross section is shown in Figure 5.19. The elevation of flood surface is shown in Figure 5.20.



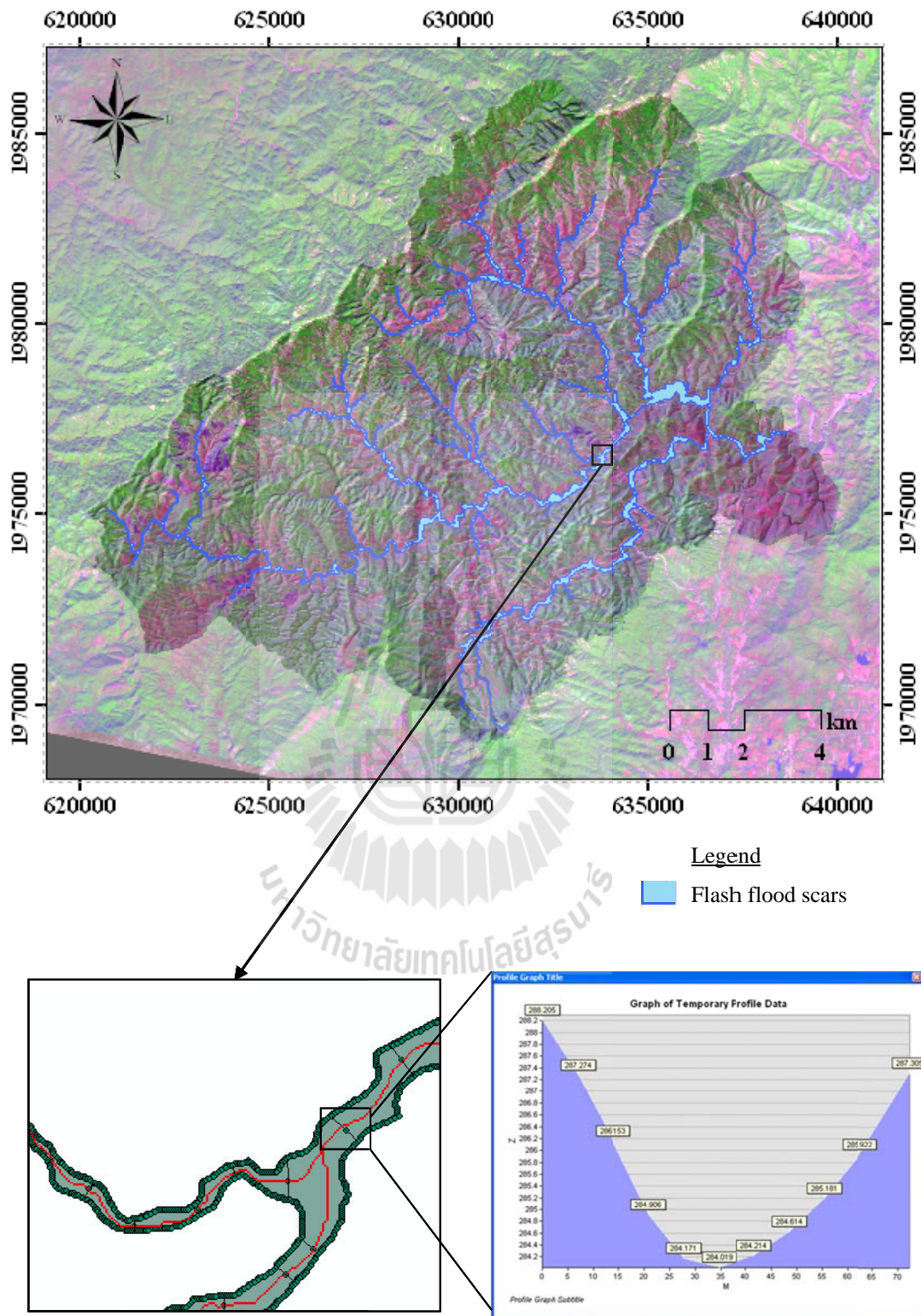


Figure 5.19 The example of cross section of DEM in flood scars.

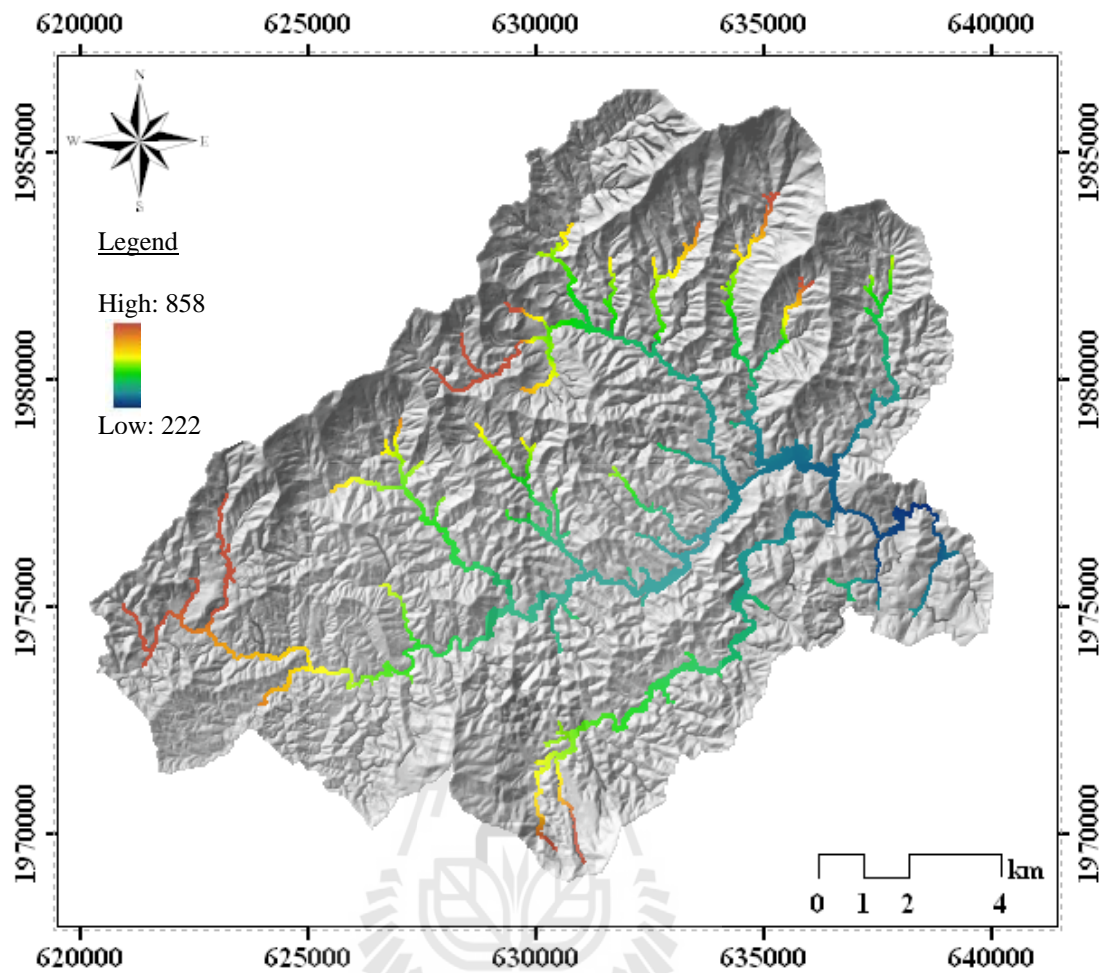


Figure 5.20 The elevation of flood surface.

The elevations of flood surface are approximately between 222-858 m above MSL. The flood depth of the event is between 0 m to 134 m as shown in Figure 5.21. The highest flood depth (134 m) was located near the junction of Nam Li and Nam Ta.

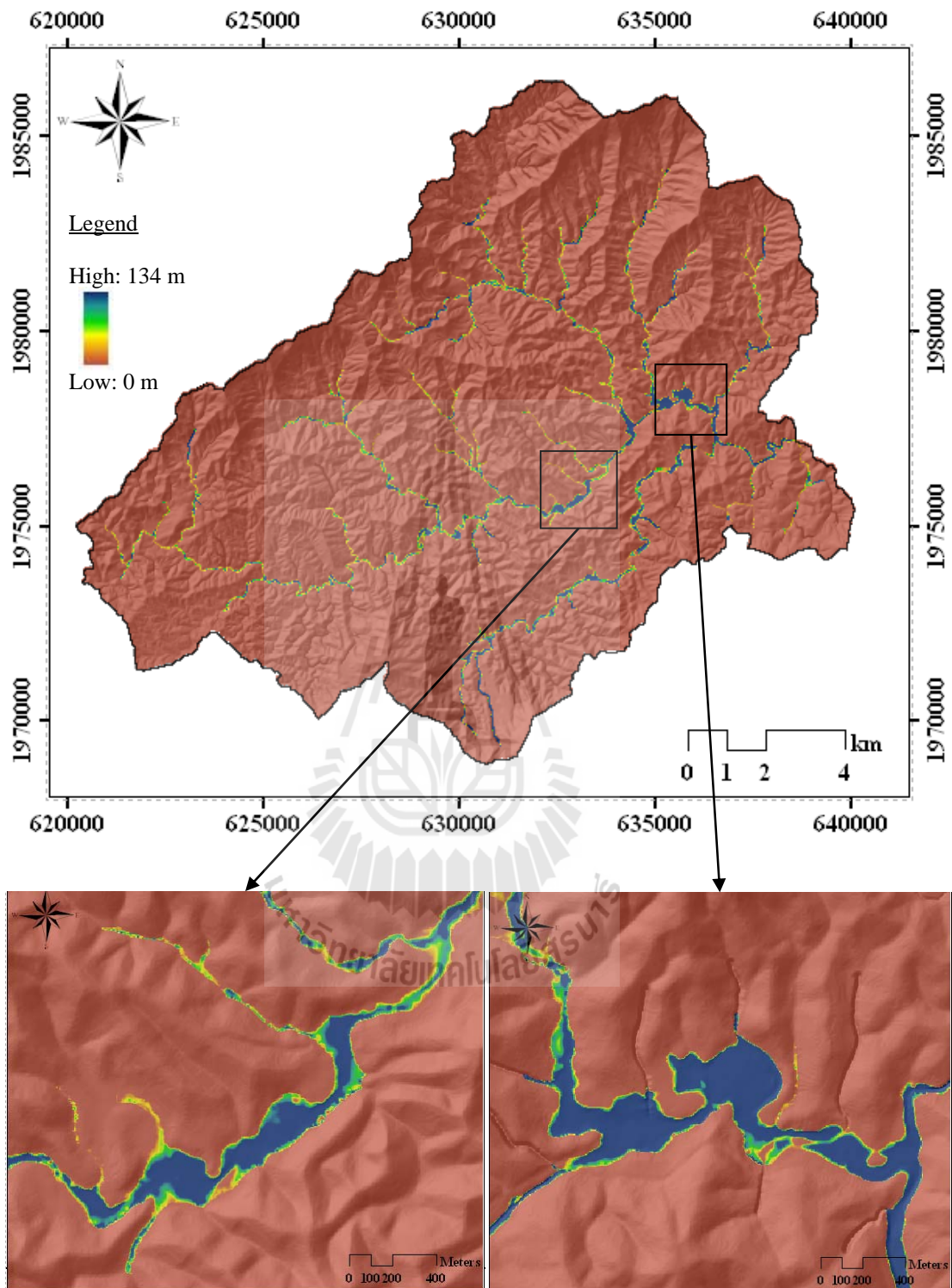
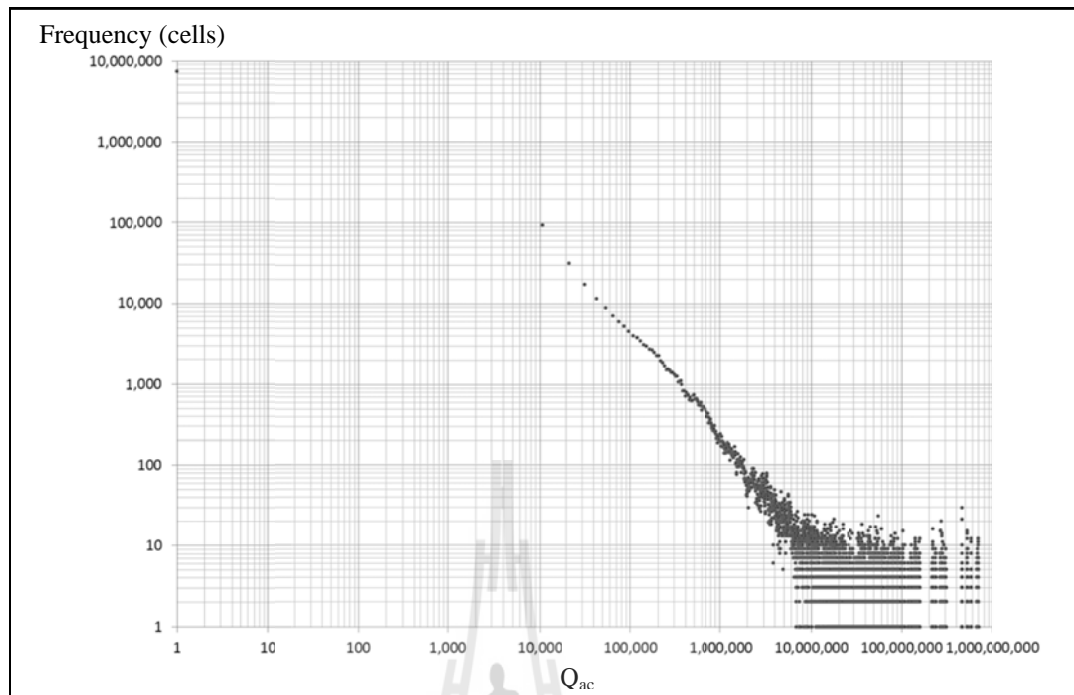


Figure 5.21 The flood depth in flood scar area.

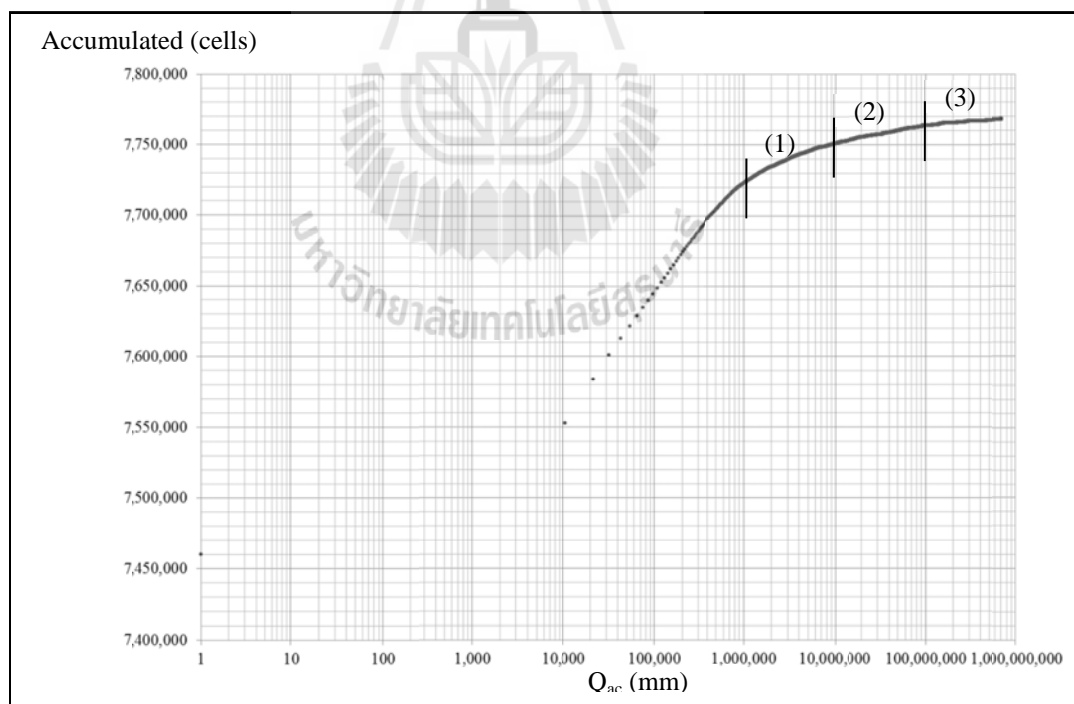
5.5.4 Flash flood susceptibility index

Based on the event occurred on May 22, 2006 at 1:00 AM when having the peak of rainfall intensity (about 170 mm), the range of estimated Q_{ac} values was 0-705,934,902 mm. The wide-range data could be displayed using logarithmic scale so that it can reflect the change proportion of data better than linear scale (Dehaene, Izard, Spelke, and Pica, 2008). The calculated Q_{ac} of cells in the study area were plotted against frequency and accumulated frequency as shown in Figure 5.20 (a) and 5.20 (b). From Figure 5.20 (a), the continuous frequency starts from Q_{ac} of 10,000 mm, indicating the continuous flow over the area containing Q_{ac} more than 10,000 mm. From Figure 5.20 (b), the accumulated frequency shows less increasing at Q_{ac} of 1,000,000 mm. This should indicate the area where the overland flow turns to be flash flood and have more potential to experience very high flood depth and causing damage. It means that during the peak of the event the Q_{ac} causing flash flood flew through cells in stream lines with the amount bigger than 1,000,000 mm in 3 hours period. These Q_{ac} values were normalized and incorporated with flood depth to determine flash flood impact intensity index (FFIII) of cells in flood scars occurred in this event.

For the result displaying purpose, the Q_{ac} values were divided into 4 classes based on the curve slope changing as very low (<1,000,000), low (1,000,000-10,000,000), moderate (10,000,000-100,000,000), and high (>100,000,000) as shown in Figure 5.20 (b). The Q_{ac} along the stream lines is displayed in Figure 5.21.

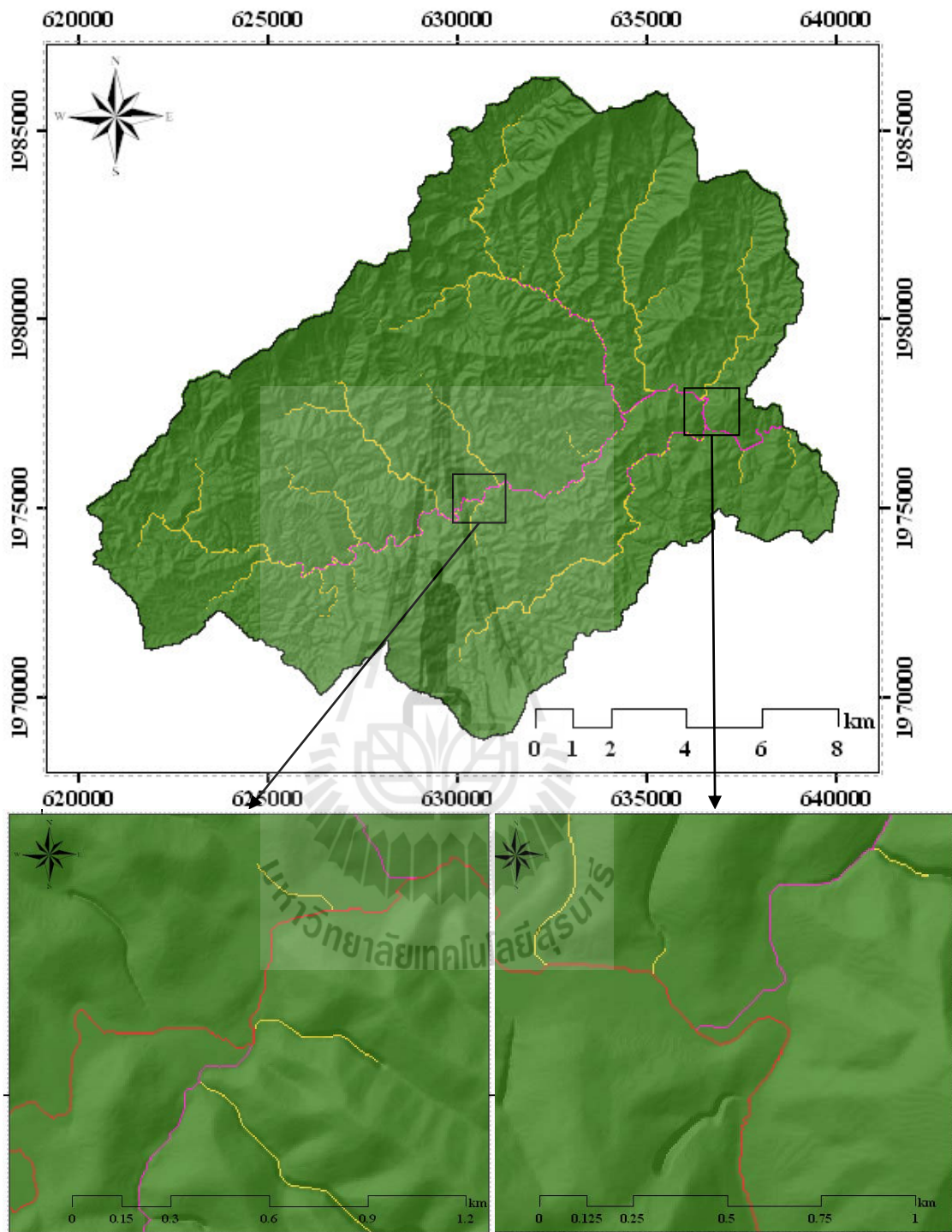


(a) The frequency of Q_{ac} cells corresponding to Q_{ac} values in logarithmic scale graph.



(b) The accumulated frequency of Q_{ac} cells corresponding to Q_{ac} values in logarithmic scale graph.

Figure 5.22 The frequency of Q_{ac} cells corresponding to Q_{ac} values.



Legend

- <1,000,000, Very low
- 1,000,000-10,000,000, Low
- 10,000,000-100,000,000, Moderate
- >100,000,000, High

Figure 5.23 The distribution of Q_{ac} of Nam Li watershed.

These high Q_{ac} values ($> 1,000,000$ mm) were mainly situated on the stream line and caused flooding. The actual flood area covered both sides of streams. The distribution of Q_{ac} in flood area (scar) was interpolated and represented in grid (5m \times 5m). The distribution of Q_{ac} in the flood scar or so called flash flood susceptibility index (FFSI) is displayed in Figure 5.24. They are divided into 4 classes as shown in Figure 5.25. FFSI was further normalized and incorporated with flood depth to determine flash flood impact intensity index (FFIII).



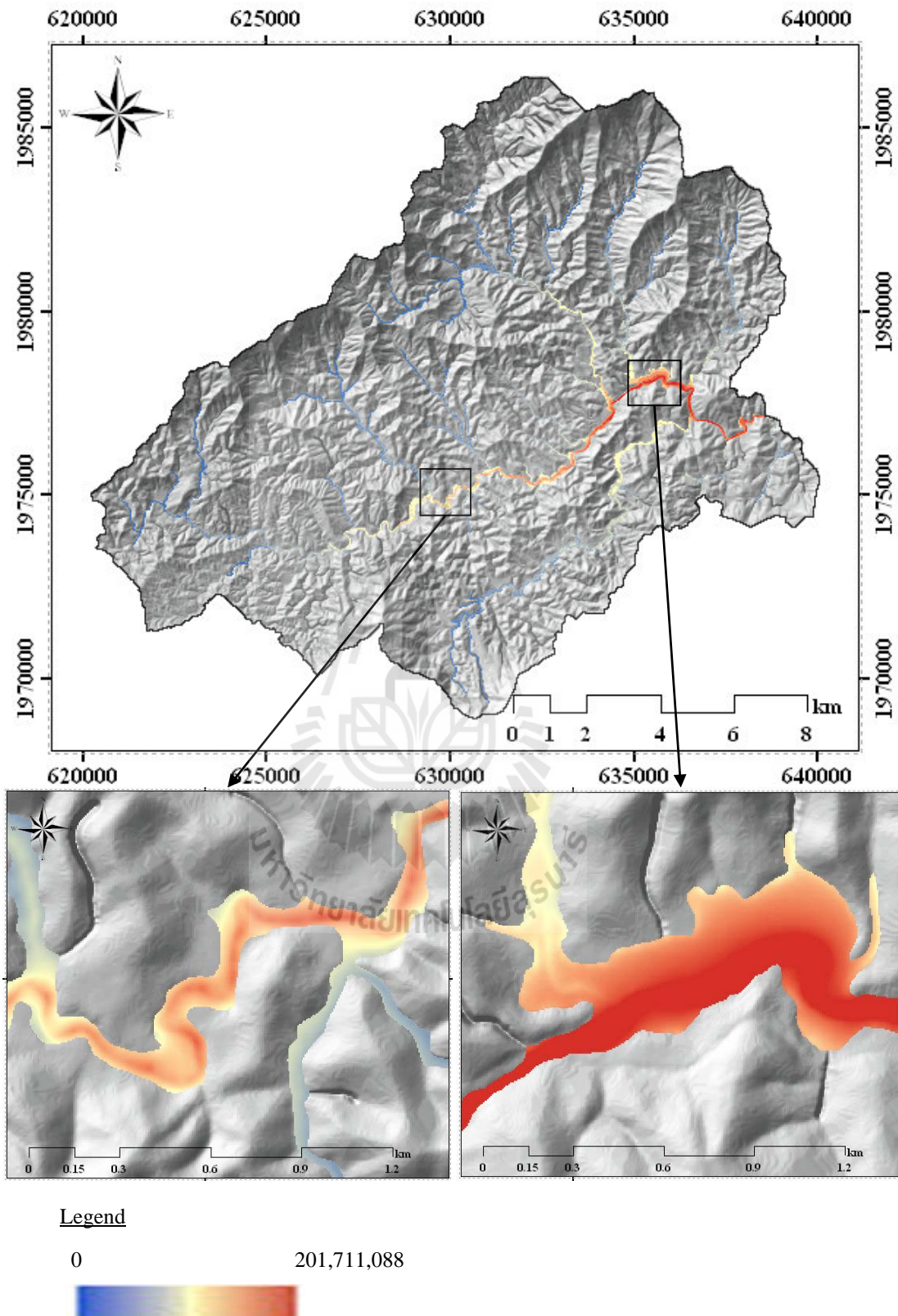
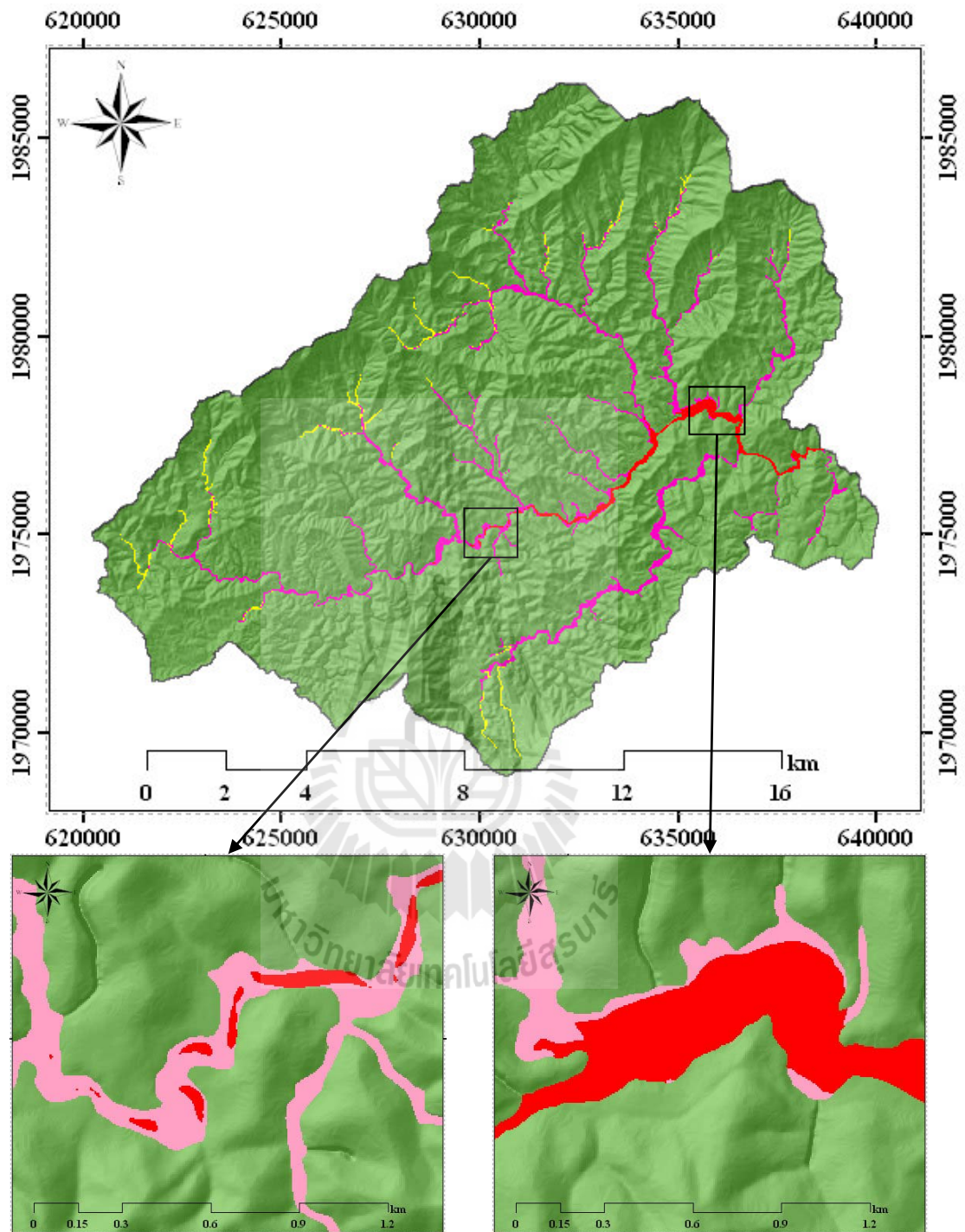


Figure 5.24 The distribution of FFSI in Nam Li watershed.



Legend

- <1,000,000, Very low
- 1,000,000-10,000,000, Low
- 10,000,000-100,000,000, Moderate
- >100,000,000, High

Figure 5.25 The 4 classes of Flash Flood Susceptibility index (FFSI).

5.5.5 Flash flood impact intensity index

The FFSI and the flood depth were normalized to be between 0-100 (as shown in Figure 5.26) before incorporated by cell-based multiplication to obtain FFIII. The FFIII map of the flood area is shown in Figure 5.27. The FFIII would be further normalized before incorporating with PFI so that the total index indicating the combination of landslide susceptibility and flash flood impact intensity can be determined.

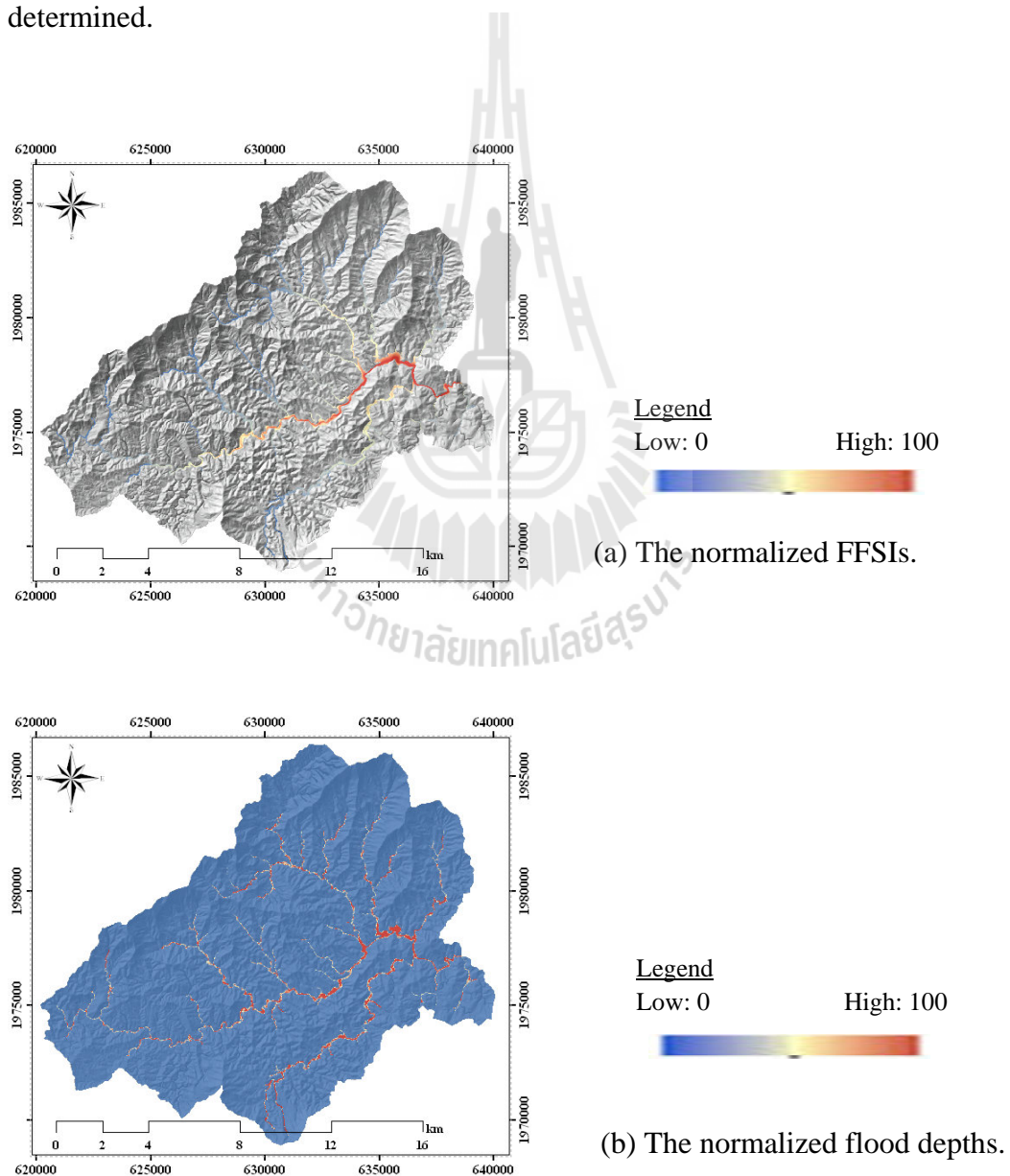


Figure 5.26 The transformed layers before operated impact intensity accumulation.

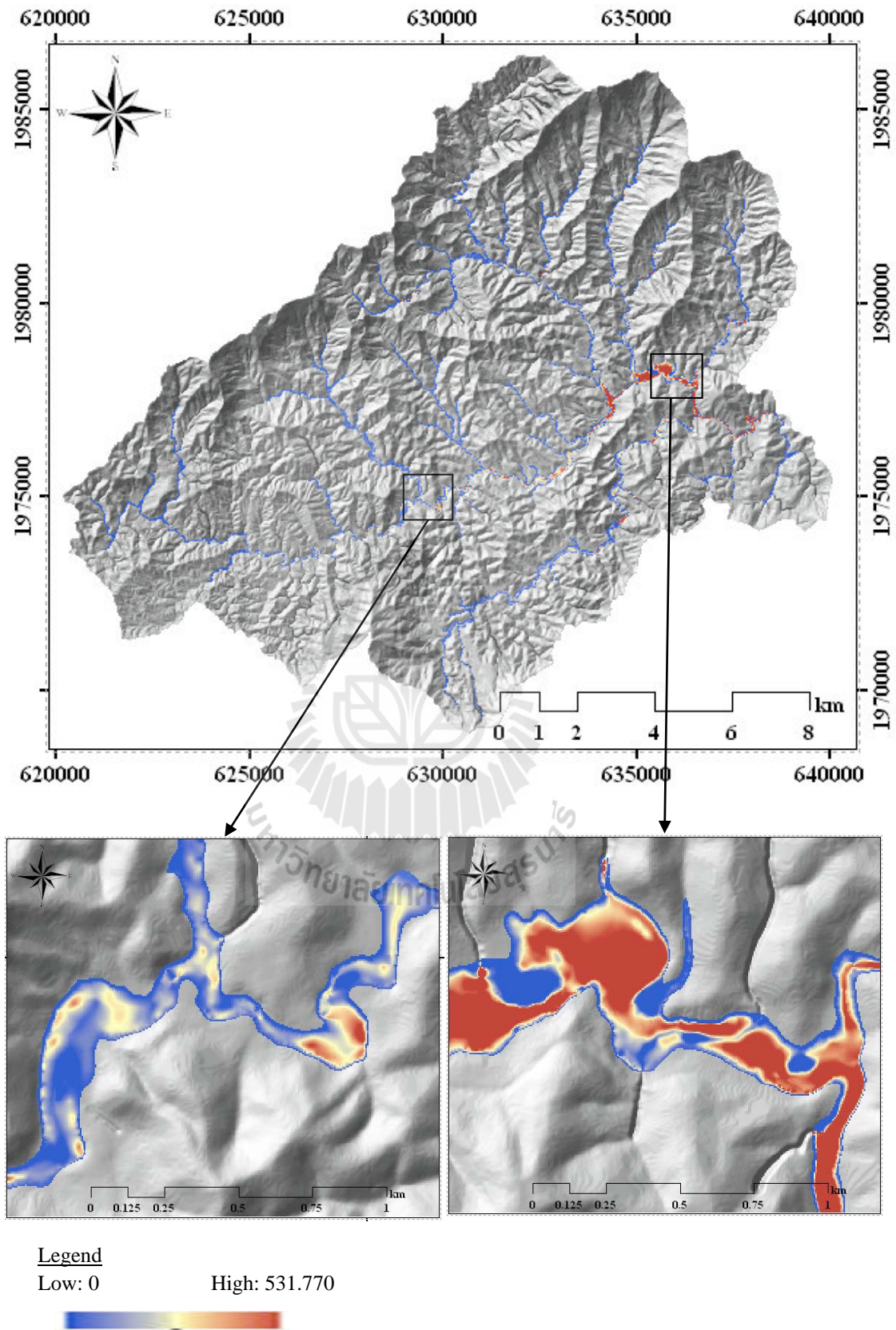


Figure 5.27 The distribution of FFIII.

5.6 Conclusion

The flash flood impact intensity modeling is a model which based on the Hortonian concept and GIS technique. The aim is the evaluation of flash flood impact intensity in the watershed by using data including 3-hours rainfall intensity, infiltration ability, flood depth, and accumulated technique. The Hortonian concept was applied to calculate overland flow (Q_{ex}) for flash flood susceptibility area assessment. The highest Q_{ex} layer was selected for flash flood susceptibility assessment by accumulated technique. The flash flood susceptibility area was determined from Q_{ex} accumulated (Q_{ac}) in flood scar. Flood depth in flood scar was estimated from flood surface and DEM. In this event, the peak period should indicate the highest water depth and overland flow turns to be flash flood. The Q_{ac} cells of peak period are bigger than 1,000,000 mm causing flash flood flow through cells in stream lines. In the fact, the flood area covered both sides of the stream. The Q_{ac} in flood scar was interpolated. The distribution of interpolated Q_{ac} in the flood scar or so called flash flood susceptibility index (FFSI). The FFSI was separated in to 4 classes using logarithmic scale including very low (<1,000,000), low (1,000,000-10,000,000), moderate (10,000,000-100,000,000) and high (>100,000,000). The very low FFSI is a mainly area and 3 classes are covered both side of the stream in flood scar. The highest FFSI is situated in the downstream near the village which was severe damage area.

The flash flood impact intensity is determined from the water through the flood area. The accumulated overland flow value (Q_{ac}), which was interpolated in flood scar, is related with flood depth in flood scar. The height flood depth is related with the height Q_{ac} and the lowest flood depth is related with lowest Q_{ac} at the

boundary of flood scar. The flash flood impact intensity index (FFIII) is incorporated by cell-based multiplication from normalized flood depth and FFSI (1-100). The FFIII displayed the potential of high impact intensity clearer than FFSI. The distribution of FFIII depicted the highest impact intensity on Huai Nam Rid near the outlet which Ban Nam Ri is located.

5.7 References

- กรมชลประทาน. (2549). รายงานการศึกษาแผนหลัก/แผนแก้ไขปัญหาน้ำท่วมและน้ำท่วม. กรมชลประทาน กระทรวงเกษตรและสหกรณ์.
- กรมพัฒนาที่ดิน. (2547). พื้นที่เสี่ยงต่อการเกิดดินถล่มและอุทกภัยในประเทศไทย. กรมพัฒนาที่ดิน กระทรวงเกษตรและสหกรณ์.
- กิริติ ลีวัจนกุล. (2543). อุทกวิทยา. ปทุมธานี: มหาวิทยาลัยรังสิต.
- ซัชชัย ตันตสิรินทร์. (2550). การจำลองแบบเพื่อเตือนภัยน้ำท่วมฉับพลันและดินถล่ม. เอกสารประกอบรายวิชา 301523 การจำลองแบบการจัดการลุ่มน้ำและระบบสิ่งแวดล้อม ภาควิชาอนุรักษ์วิทยา คณะวนศาสตร์ มหาวิทยาลัยเกษตรศาสตร์. (เอกสารที่ไม่ได้พิมพ์เผยแพร่).
- Ballesteros-Cánovas, J. A., Eguibar, M., Bodoque, J. M., Díez-Herrero, A., Stoffel, M., and Gutiérrez-Pérez, I. (2011). Estimating flash flood discharge in an ungauged mountain catchment with 2D hydraulic models and dendrogeomorphic palaeostage indicators. **Hydrological Processes**. 25: 970-979.
- Beven, K. (2004). Robert E. Horton's perceptual model of infiltration processes. **Hydrological Processes**. 18: 3447-3460.
- Chowdhury, R. (2000). An Assessment of flood forecasting in Bangladesh: The experience of the 1998 flood. **Natural Hazard**. 22: 139-163.
- Davie, T. (2002). **Fundamentals of Hydrology**. London: Routledge.

- Dehaene, S., Izard, V., Spelke, E., and Pica, P. (2008). Log or Linear? Distinct Intuitions of the Number Scale in Western and Amazonian Indigenous Cultures. **Science**. 320(5880): 1217
- Department of Natural Resources and Water. (2007). **Water management** [On-line]. Available: http://www.nrw.qld.gov.au/water/management/overland_flow/index.html.
- Farrell, Z. (2010). Single ring falling head infiltrometer [On-line]. Available: <http://www.usyd.edu.au/agric/web04/Single%20ring%20final.htm>.
- Taragsa, N., Mongkolsawat, C., Pawattana, C., and Suwanweerakamtorn, S. (2004). An Application of GIS and Hydraulic Model to Flood Plain Inundation. **Journal of Remote Sensing and GIS Association of Thailand**. 5(3): 47-60.
- Phutmongkhon, P., Yongsatisak, T., Jungcharoentham, N., Khampeera, A., Tongyoi, R., and Bennui, A. (2007). Delineation of flood hazard areas in the Lower Eastern Area of Southern Thailand by Using Geo-informatics. **Journal of Remote Sensing and GIS Association of Thailand**. 8(3):47-57.
- Mapiam, P. P. and Sriwongsitanon, N. (2009). Estimation of the URBS model parameters for flood estimation of ungauged catchments in the upper Ping river basin, Thailand. **SciencAsia**. 35: 49-56.
- Rattanakom, R. and Ongsomwang, S. (2008). The application of GIS for risk Area Analysis in Ubon Ratchathani Province. **Journal of Remote Sensing and GIS Association of Thailand**. 9(2): 42-48.

- Saini, S. S. and Kaushik, S. P. (2012). Risk and vulnerability assessment of flood hazard in part of Ghaggar Basin: A case study of Guhla block, Kaithal, Haryana, India. **International Journal of Geomatics and Geosciences**. 3(1): 42-54).
- Sumangala, A. (2005). **Flood Inundation Mapping and 1-D Hydrodynamic Modelling Using Remote Sensing and GIS Technique**. Center of Space Science and Technology Education in Asia and the Pacific, IIRS Campus, India.
- Tanavud, C., Yongchalermchai, C., Bennui, A., and Densreeserkul, O. (2004). Assessment of flood risk in Hat Yai Municipality, Southern Thailand, using GIS. **Journal of Natural Disaster Science**. 2(1): 1-14.
- Thai Meteorological Department. (2009). Climatological data for 2001-2009 [Computer file]. Bangkok: Thai Meteorological Department.
- Yates, D. N., Warner, T. T., and Leavesley, G. H. (2000). Prediction of a flash flood in complex terrain. Part II: A comparison of flood discharge simulations using rainfall input from radar, a dynamic model, and an automated algorithmic system. **Journal of Applied Meteorology**. 39: 815-825.

CHAPTER VI

DEBRIS FLOW IMPACT INTENSITY INDEX

6.1 Abstract

Landslide and flash flood impact intensity was determined in term Debris Flow Impact Intensity Index (DFIII) using ArcGIS spatial analytical functions. The accumulation of incorporation of Probability Failure Index (PFI) and overland flow (Q) was operated to indicate cell-based debris flow accumulation index (DFAI) Flood scars after the event show the area extent subject to be damaged by debris flow products. The potential damage in flood scars was proportionally related to DFAI and flood depth. Therefore, Debris Flow Impact Intensity Index (DFIII) was determined from the incorporation of DFAI and flood depth. The area with higher DFIII indicated higher potential of damage capability. This was validated by data from field investigation.

Keywords: Debris flow/Impact Intensity Index/GIS/Uttaradit

6.2 Introduction

A big catastrophic landslide and flash flood in Nam Li watershed occurred on heavy rainfall event which has a recurrence period of 500 years (Akapon Sumongkol, 2006). The land surface was damaged by landslide and debris flow. The damage caused by landslide was in situ. The debris flow occurred when landslide and overland flow were associated and worked toward downstream. The term “debris flow” is the form of rapid mass movement in which a combination of loose mud, sand, soil, rock, water, and air mobilize as slurry that flow downslope under the influence of gravity. Debris flow occurs in steep gullies caused by intense surface water due to heavy precipitation (Highland and Bobrowsky, 2008). Therefore, the potential of debris flow impact intensity (DFII) can be evaluated from the incorporation of potential of landslide and overland flow. The potential of landslide is expressed in term of PFI determined in the Chapter IV. The overland flow which occurred by heavy rainfall will be expressed in term of probability of overland flow (Q_{prob}).

The aim of Chapter VI is to estimate DFII in the study area of the event. From previous studies, many researchers (e.g. Chanchai et al., 2004; Lee, 2004; Sumangala, 2005; Sombat Yumuang, 2005; Suree Teerarungsigul, 2006; Nuchanart Sriwongsitanon, 2010; Narumon Intarawichien and Songkot Dasananda, 2011) are more likely to concentrate on land classification in term of landslide susceptibility, not debris flow impact. In this study, DFII was carried out. The DFII toward downstream area was determined using the weight from PFI and Q_{prob} through flow accumulation function of ArcMap hydrology tool. The land surface damage is occurred by debris flow which is formed by the association or interaction of landslide and flash flood.

Therefore, impact intensity on land surface can be evaluated from the combination of debris flow accumulation index and water depth in the flash flooded area.

6.3 Research methods

6.3.1 Research procedure

Three steps of the research procedure include data preparation, debris flow accumulation evaluation, and debris flow impact intensity index determination. The Debris Flow Impact Intensity Index (DFIII) was determined from Probability of Failure Index (PFI) and overland flow which was occurred in the event. The input data are PFI values from Chapter IV, overland flow (Q) from Chapter V and flow direction from DEM. The logistic function and accumulation technique was used for debris flow evaluation. The steps of landslide and flash flood impact intensity (FFII) determination can be displayed in Figure 6.1.

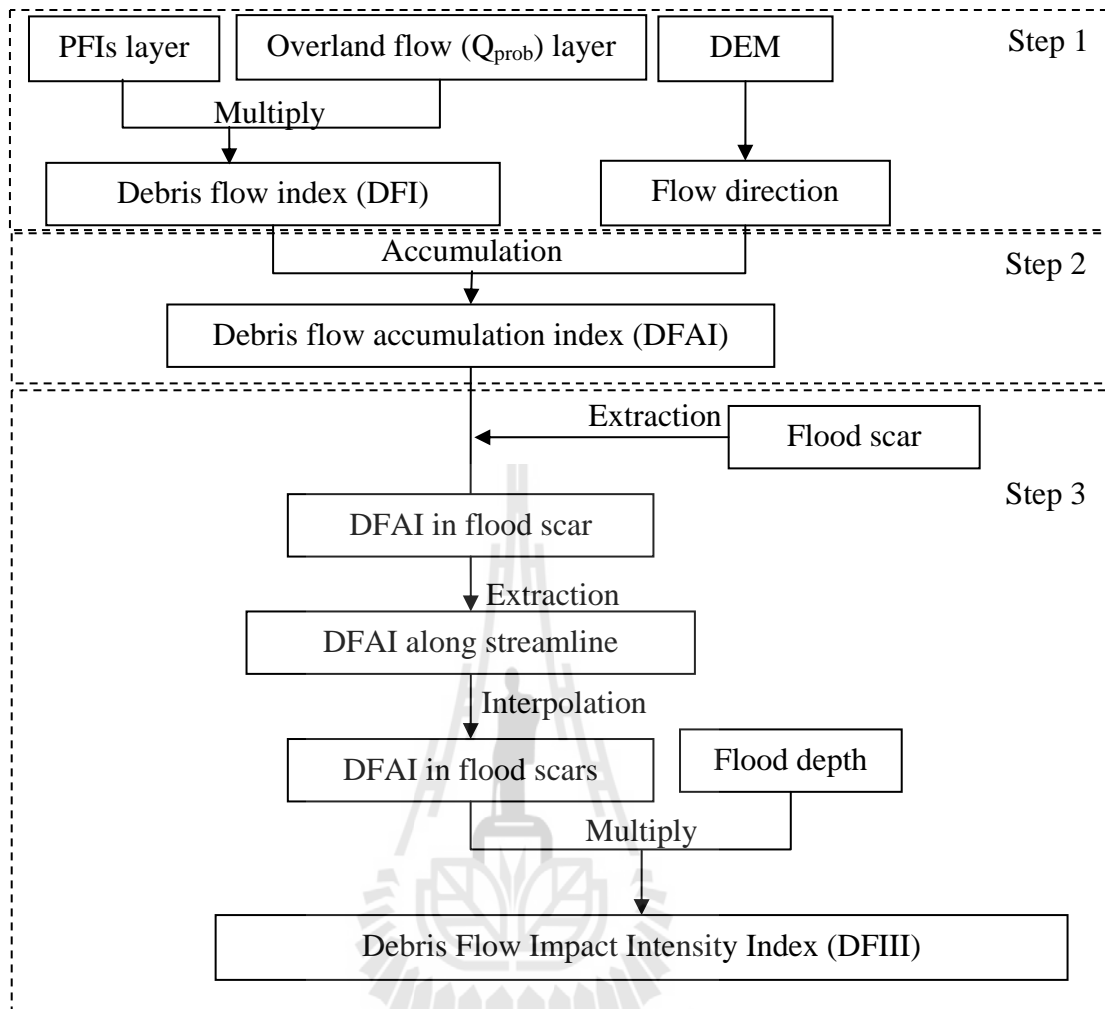


Figure 6.1 The procedure framework of landslide and flash flood impact intensity evaluation.

6.3.2 Data preparation

The PFIs raster-based layer was derived from land slide susceptibility index (LSI) using probability density function, discussed in Chapter IV and the result is shown in Figure 6.2. The PFI values are represented landslide impact intensity which each cell is contained values 0-1.

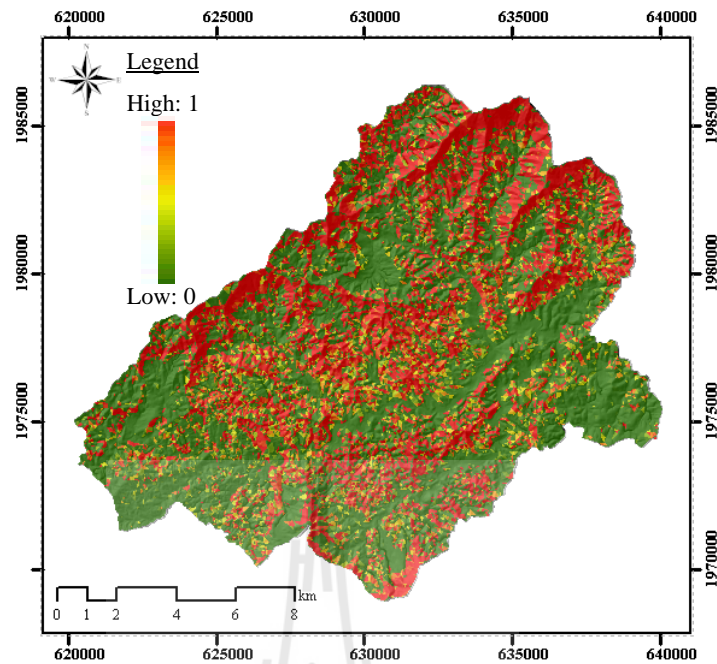


Figure 6.2 The PFIs layer.

The overland flow (Q) layer of the area was carried out and discussed in Chapter V. It has to be transformed into the probability scale as same as PFI (0-1) before their incorporation can be performed. The probability of overland flow (Q_{prob}) was estimated using logistic function as follows:

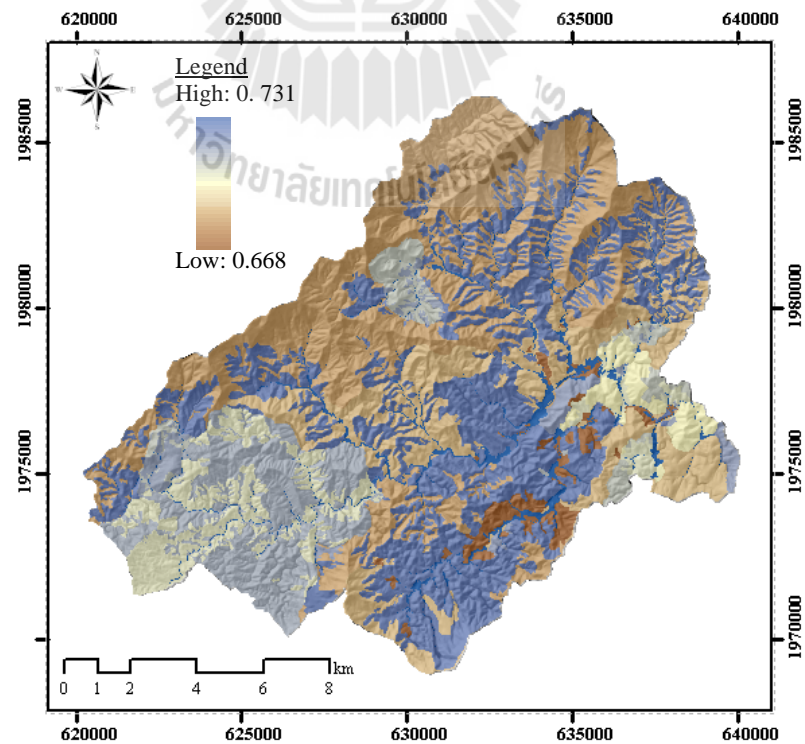
$$Q_{prob} = \frac{1}{1 + e^{-Q_{norm}}} , \quad (6.1)$$

where Q_{prob} is the probability of overland flow, Q_{norm} is the normalized overland flow, and e is exponential function ($e = 2.71828$).

Q_{prob} in different LU_GU units of the study area was calculated as shown in Table 6.1 and displayed as raster-based layer in Figure 6.3.

Table 6.1 Q_{prob} in different LU_GU units of the study area.

LU_GU unit	Q (mm)	Q_{norm}	Q_{prob}
CA2	310.26	0.96	0.722699
CA4	226.57	0.70	0.668078
CF	248.41	0.77	0.682857
CF5	299.53	0.92	0.716011
P1A2	310.28	0.96	0.722711
P1A3	289.56	0.89	0.709711
P1A4	226.57	0.70	0.668078
P1F	255.25	0.79	0.687413
P1F5	256.90	0.79	0.688506
grA2	296.94	0.92	0.714382
grA4	279.74	0.86	0.703425
grF	286.34	0.88	0.707658
grF5	271.60	0.84	0.698155
Tr1F	293.94	0.91	0.712489
Tr1F5	279.09	0.86	0.703006
Stream	323.90	1.00	0.731058

**Figure 6.3** The distribution of Q_{prob} in the study area.

6.3.3 Debris flow accumulated index evaluation

Debris flow accumulation index (DFAI) is an accumulation of DFI which is the multiplication product of PFI and Q_{prob} . The performance of accumulation is from upstream to downstream following the flow direction derived from grid DEM data. Those 2 parameters were weights in flow accumulation process of ArcGIS spatial analysis tool.

6.3.4 Debris flow impact intensity determination

The distribution of DFAI covers the whole area, both flash flood and non-flash flood area. The flash flood area is always associated with highly accumulated DFAI along the streams and both sides when over bank flow occurs. The land surface damage can be evaluated based on the cooperation of DFAI and flood depth in the flash flood area. Flood depth and interpolated DFAI were multiplied to obtain debris flow impact intensity index (DFIII). The impact occurs when there is human settlement in the flood area. The higher index indicates more damage.

6.4 Result and discussion

6.4.1 Debris flow accumulation index

The input layers of flow accumulation function are debris flow index and flow direction layers as shown in Figure 6.4. The result of accumulation process is the distribution of DFAI as shown in Figure 6.5. The DFAI is very high along stream network and increased from upstream to downstream. The index is immediately increased at junctions of tributaries. Together with flood depth, DFAI affects land surface damage in flash flood area.

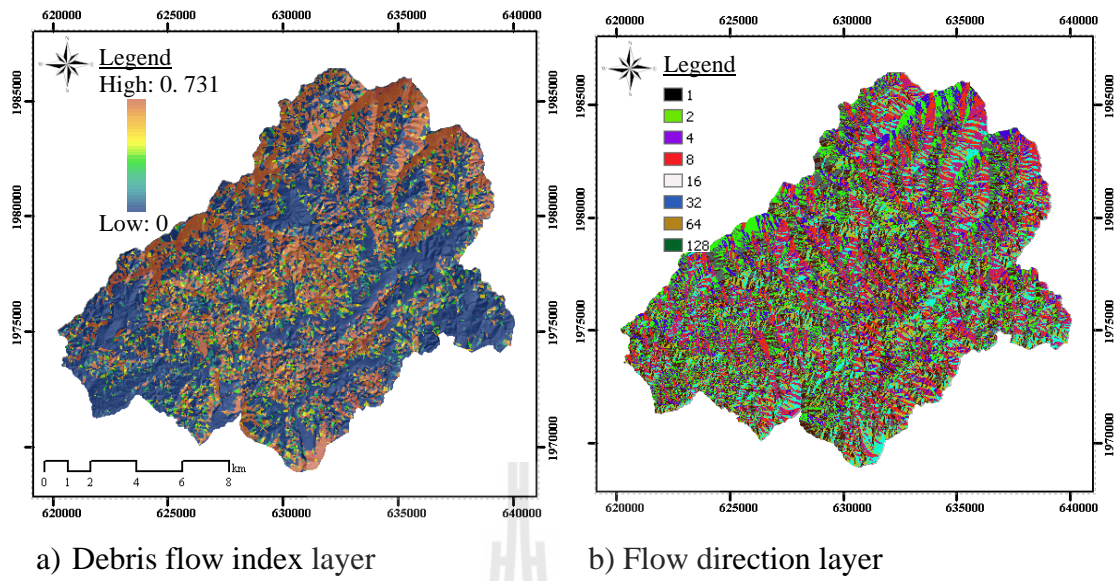


Figure 6.4 The input layers of flow accumulation process.

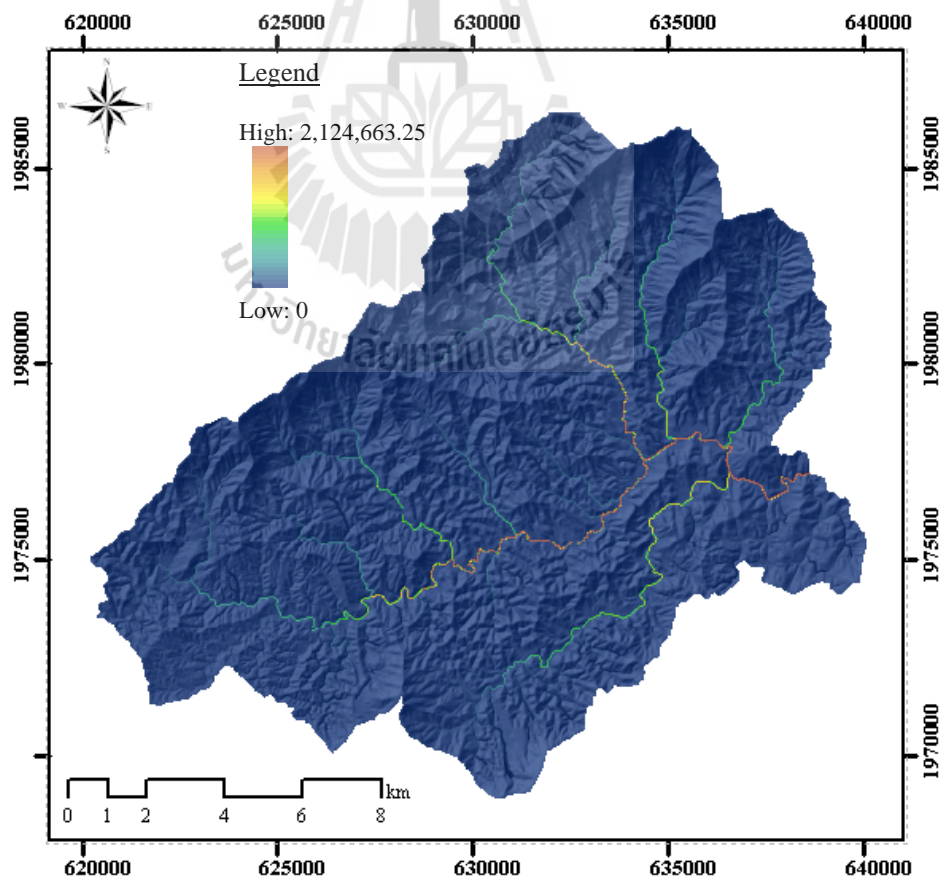


Figure 6.5 The distribution of DFAI of the study area.

6.4.2 Debris flow impact intensity index

Land surface damage or impact intensity is concentrated in flash flood area. The impact intensity is reflected by the interaction of DFAI and flood depth. The multiplication of interpolated DFAI (Figure 6.6 a)) and flood depth (Figure 6.6 b)) resulted in DFIII of the flood area of the event, shown in Figure 6.7. The indexes were normalized to be between 0-1. The area with higher index indicates higher damage capability to properties and infrastructures.

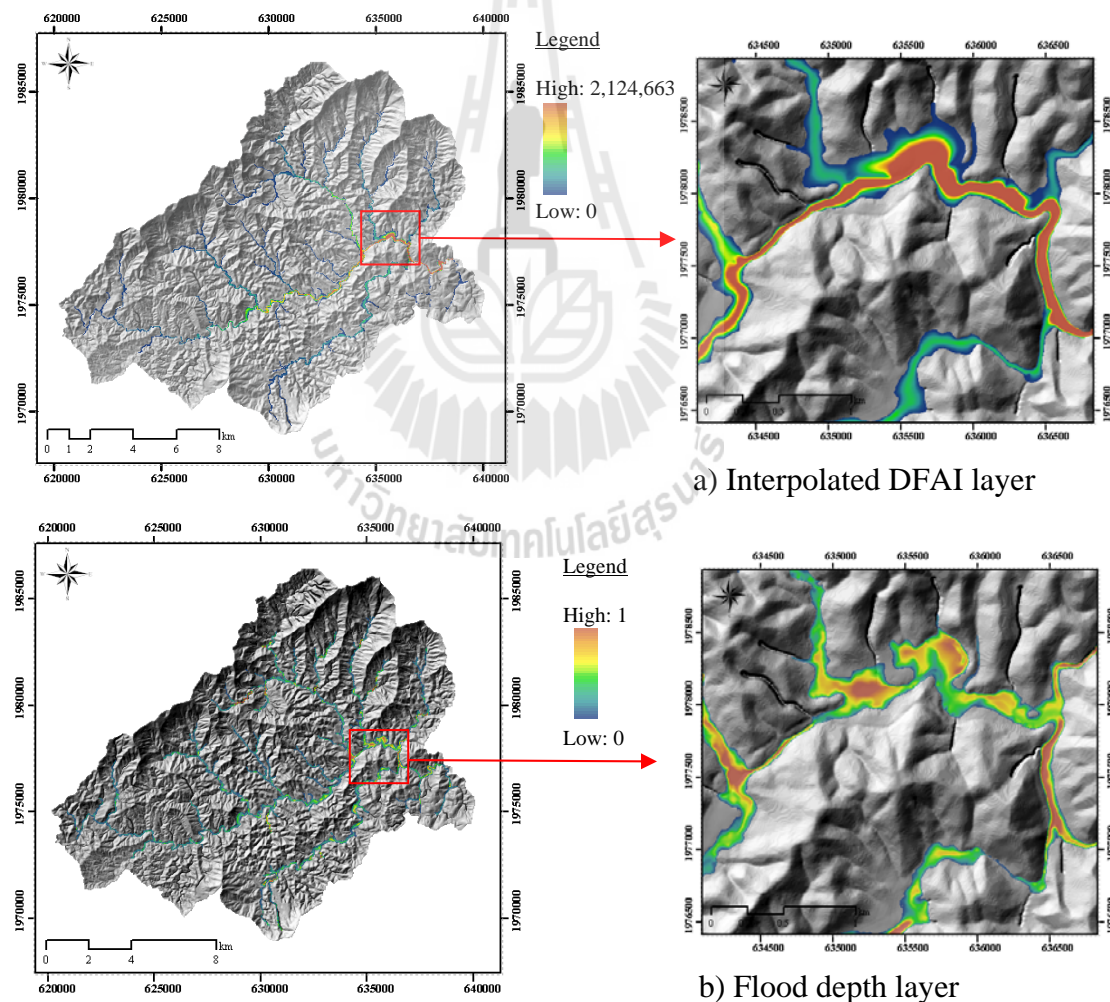


Figure 6.6 The interpolated DFAI and flood depth raster layers of the study area.

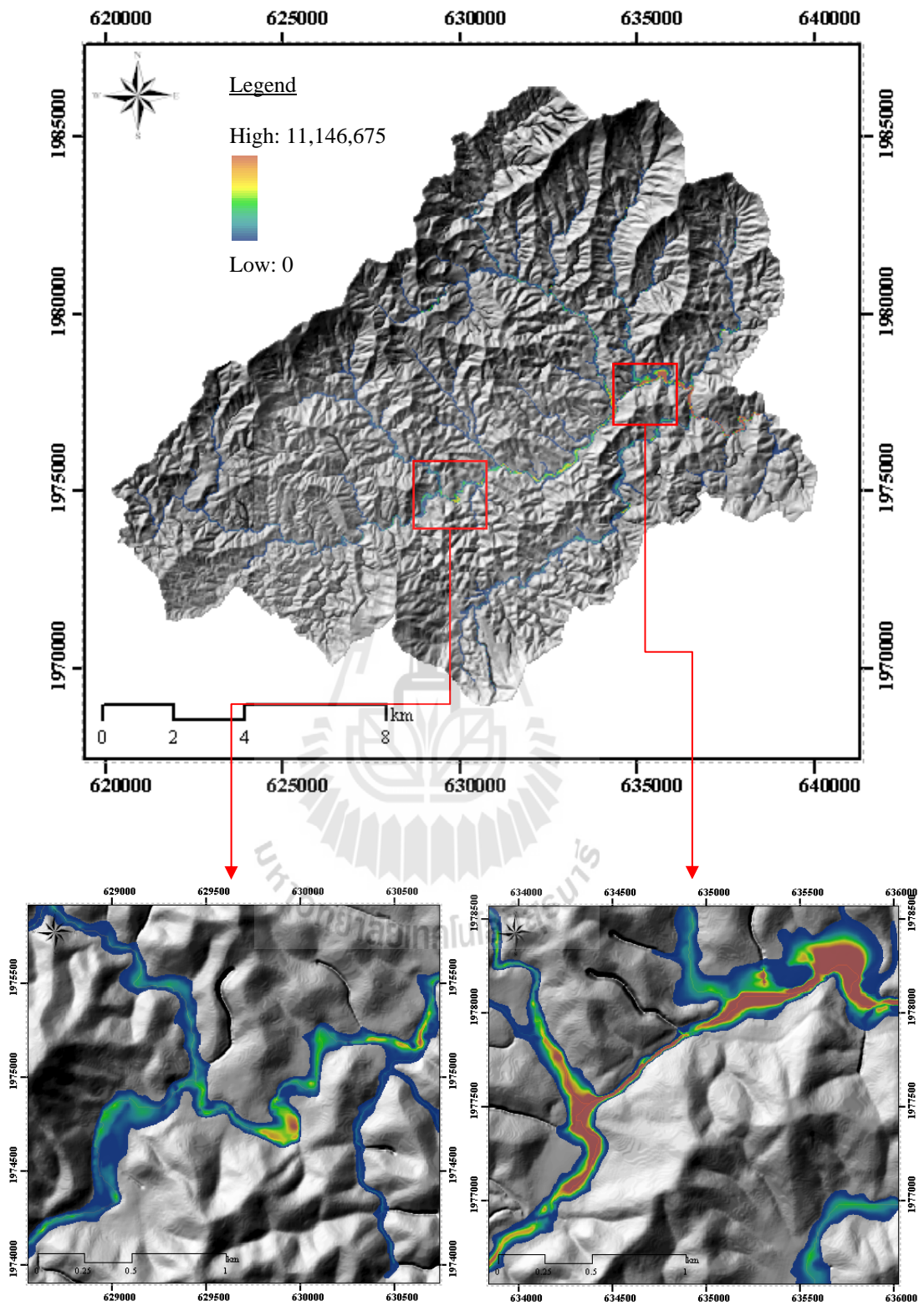
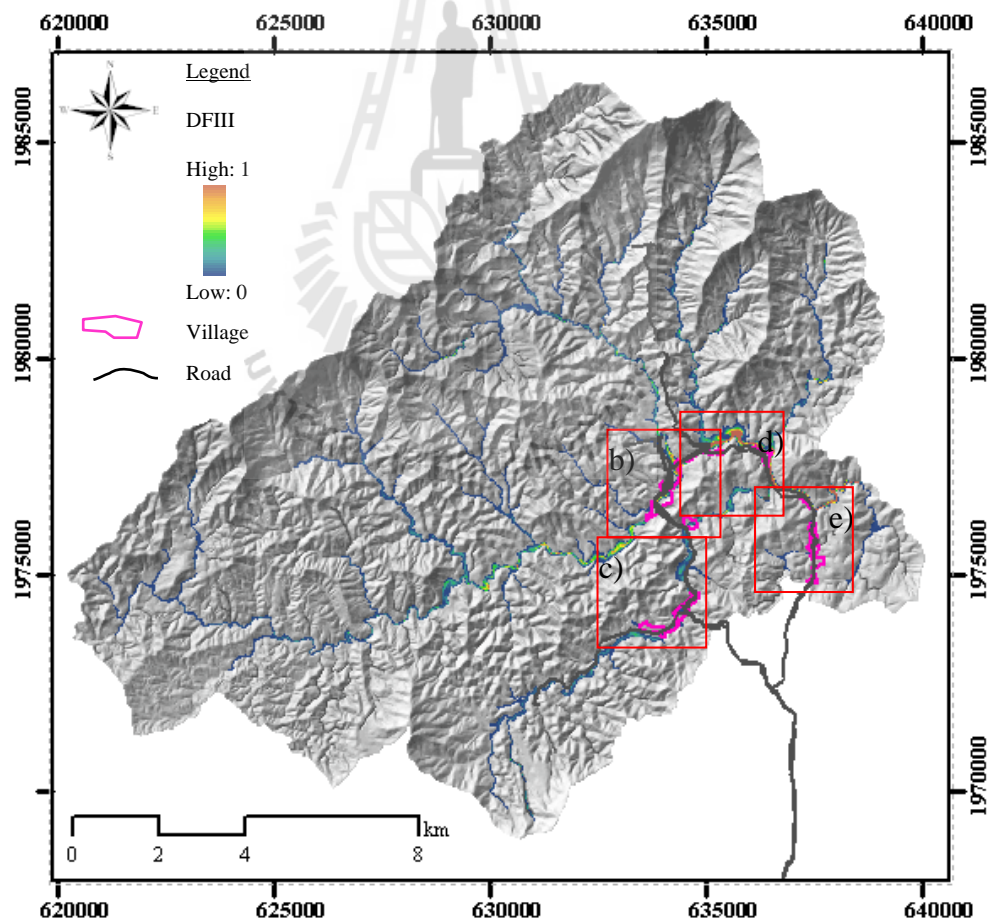


Figure 6.7 The distribution of Debris Flow Impact Intensity Index (DFIII).

After few months of the event field investigation to examine the damage was carried out. It can be concluded that there were damaged settlements located in 2 of 4 major flood areas. These included Ban Nam Ri (Figure 6.8 (b) and (c)) and Ban Nam Ta (Figure 6.8 (d)). Houses, bridges, infrastructures, and agriculture areas were badly damaged. Their locations were associated with high DFIII (0.0429-0.5420). Fortunately, there was no property located in other 2 major flood areas which were surrounded by the settlements of Ban Sai Ngam. Only small recreation area was damaged (Figure 6.8 (e)).



(a) 4 major settlements.

Figure 6.8 The 4 major settlements in the study area.

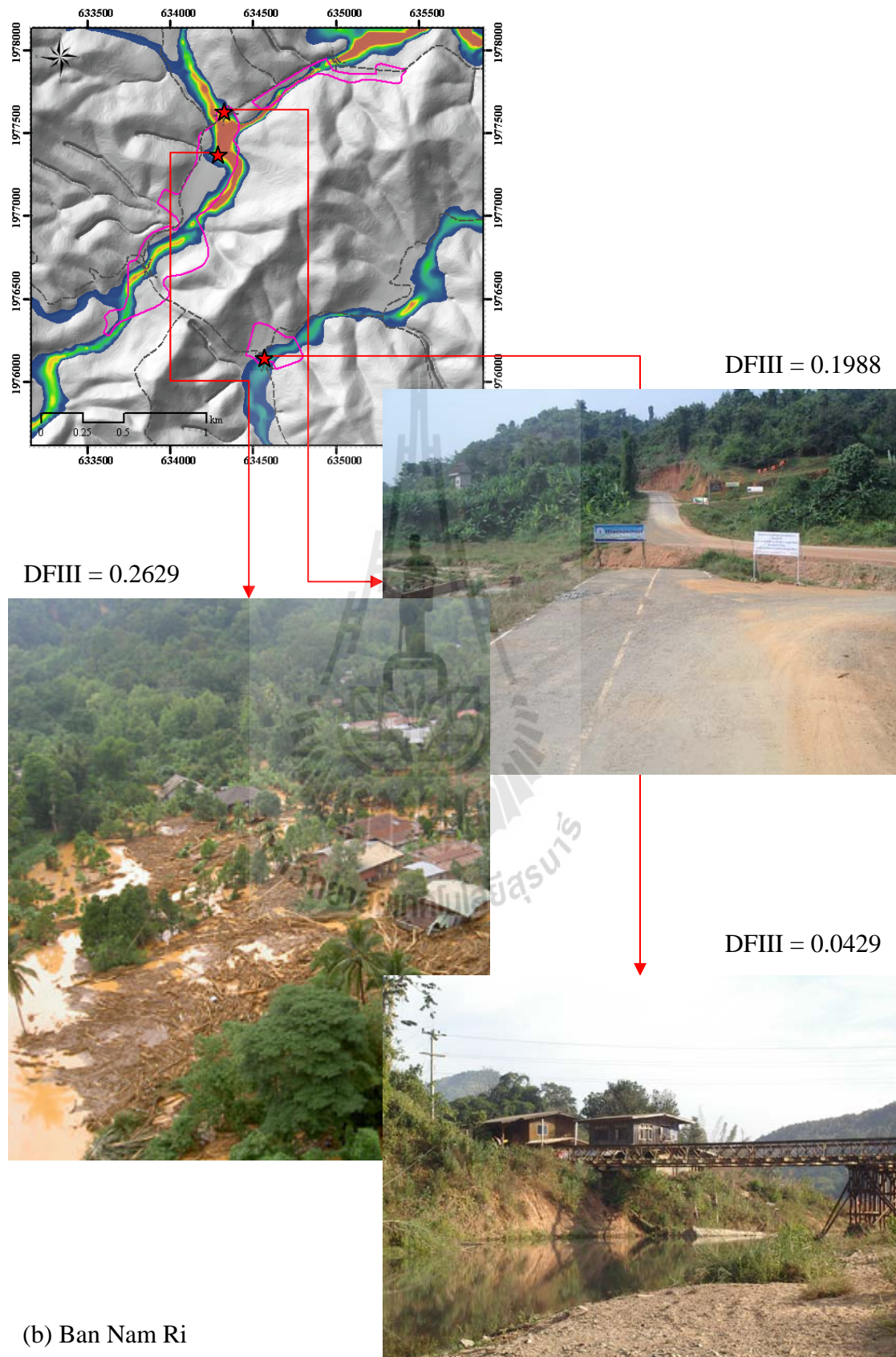


Figure 6.8 The 4 major settlements in the study area (Continued).

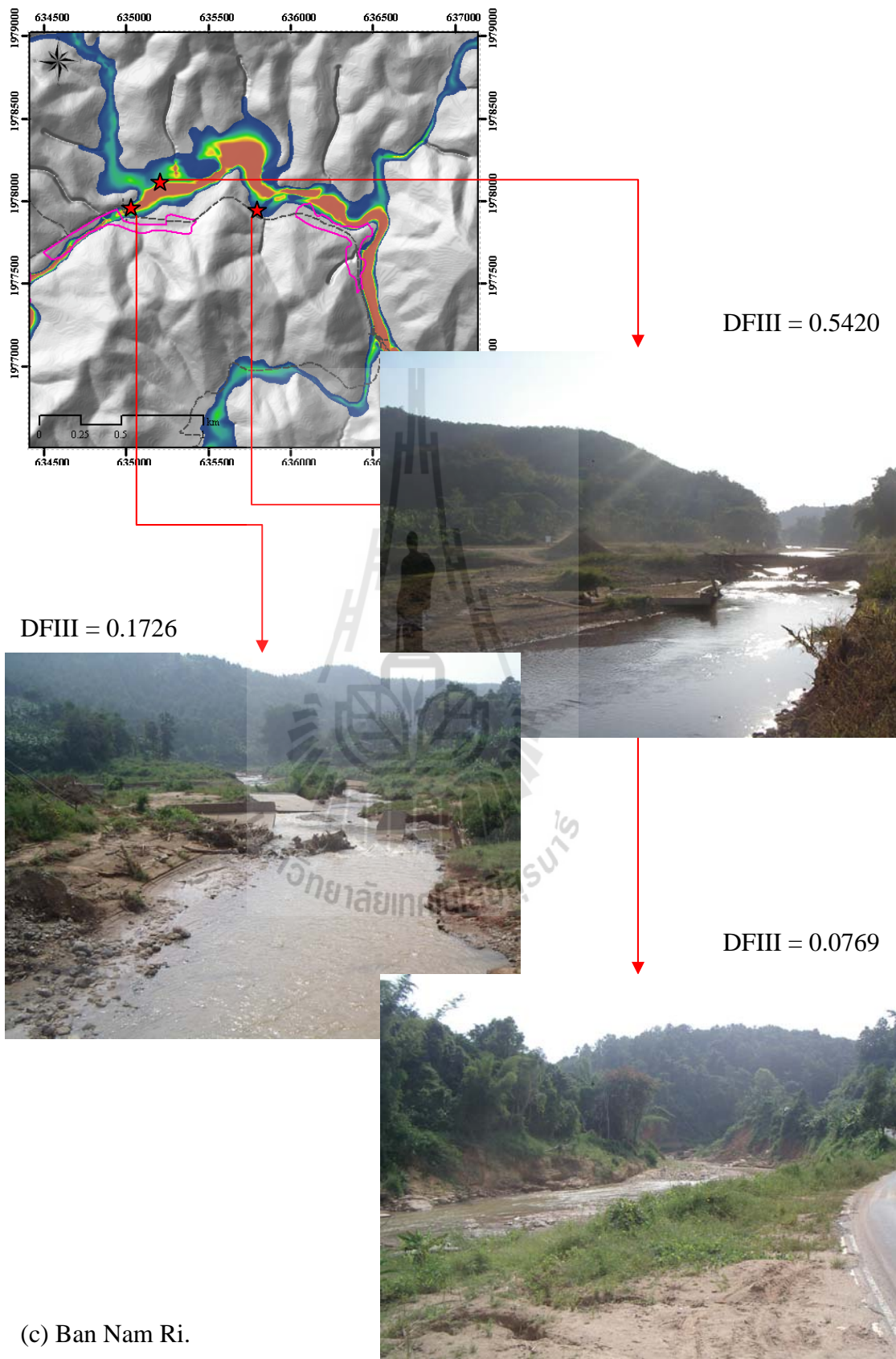


Figure 6.8 The 4 major settlements in the study area (Continued).

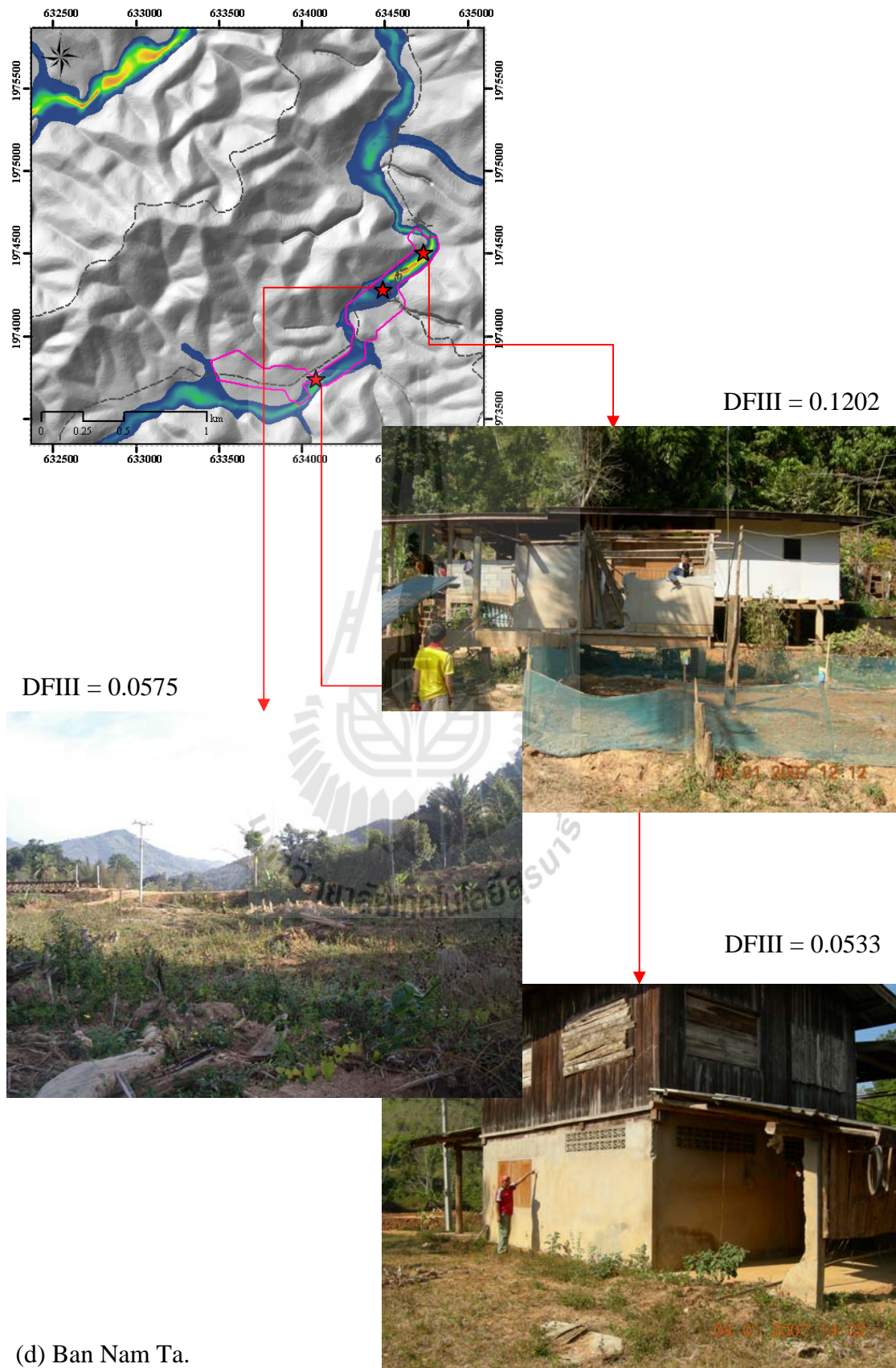


Figure 6.8 The 4 major settlements in the study area (Continued).

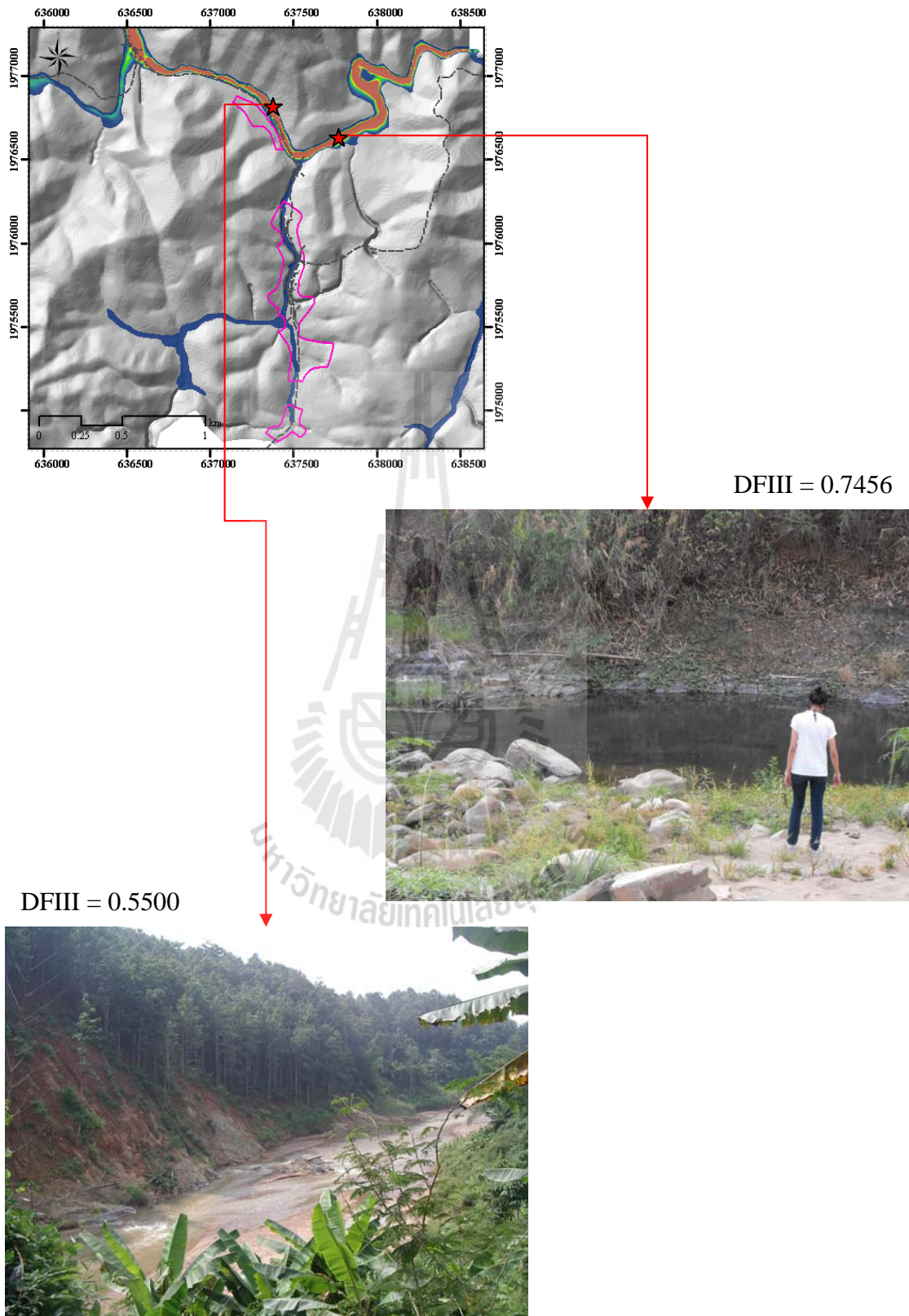
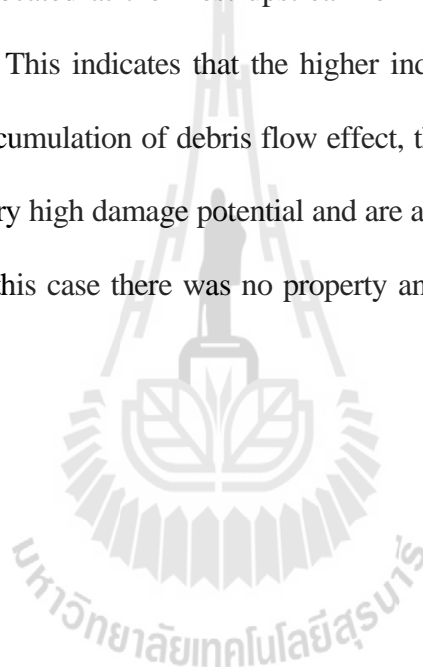


Figure 6.8 The 4 major settlements in the study area (Continued).

The evidences from field investigation showed that more damage was positively associated with the area of high DFIII as shown in Figure 6.9. The SE- NW cross section of Ban Nam Ri, where appeared the biggest damage, in term of DFIII is displayed in Figure 6.9 (a). The highest peak of DFIII is 0.1428 and was associated with the damaged bridge and the big deposit of debris flow product.

From the investigation, it revealed that some damaged properties (houses and agriculture land) located at the most upstream of Ban Nam Ta of which DFIII is approximately 0.0533. This indicates that the higher index from this can cause greater damage. Due to the accumulation of debris flow effect, the downstream areas both sides of main streams has very high damage potential and are always associated with very high index. Fortunately, in this case there was no property and infrastructure located in such area.





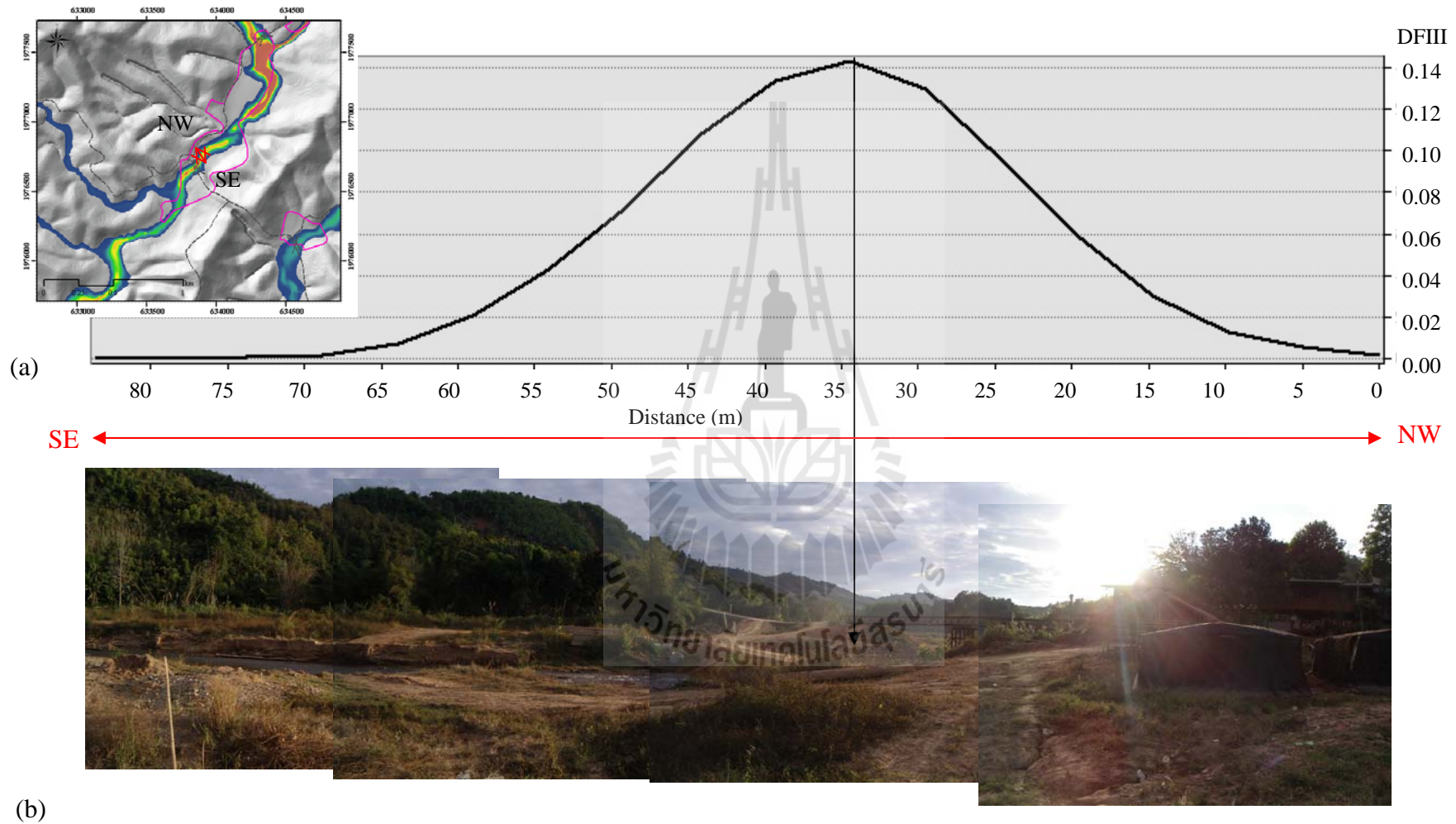


Figure 6.9 The SE-NW cross section of Huai Nam Li at Ban Nam Ri.



6.5 Conclusion

Land property damage particularly in the flood area resulted from the interaction of debris from landslide and the depth of excess water in form of flash flood. This impact was expressed as raster based DFIII layer. The indexes were the accumulation of interaction of debris and excess water using GIS facility. They were concentrated in downstream flood area where damage would occur when human settlement exists. The study revealed that the flood area with higher index indicate higher damage. The result was confirmed by the evidences from field investigation.

6.6 References

- Akapon Sumongkol. (2006). **Inundation and Landslide of Uttaradit Province 2549 B.E.**. The Department of Public works and Town & Country Planning Uttaradit Province [On-line]. Available: <http://www.dpt.go.th/stbd/files/uataradit1-10.pdf>.
- Chowdhury, R. (2000). An Assessment of flood forecasting in Bangladesh: The experience of the 1998 flood. **Natural Hazard**. 22: 139-163.
- Highland, L. M. and Bobrowsky, P. (2008). The Landslide Handbook –A guide to Understanding Landslides. Reston, Virginia: U.S. Geological Survey Circular 1325, Section I Part B. Page 16.
- Intaravichien, N. and Dasananda, S. (2011). Frequency ratio model based landslide susceptibility mapping in lower Mae Chaem watershed, Northern Thailand. **Environmental Earth Sciences**. 64(8):2271-2285.
- Lee, S. (2004). Application of likelihood ratio and logistic regression models to landslide susceptibility mapping using GIS. **Environmental Management**. 34(2): 223-232.

- Nutchanart Sriwongsitanon. (2010). Flood forecasting system development for the Upper Ping River basin. **Kasetsart Journal (Natural Science)**. 44(4): 717-731.
- Sombat Yumuang. (2005). **Evaluation of Potential for 2001 debris flow and debris flood in the Vicinity of Nam Ko area, Amphoe Lom Sak, Changwat Phetchabun, central Thailand**. Ph.D. Dissertation, Chulalongkorn University, Thailand.
- Sumangala. A. (2005). **Flood Inundation Mapping and 1-D Hydrodynamic Modelling Using Remote Sensing and GIS Technique**. Center of Space Science and Technology Education in Asia and the Pacific, IIRS Campus, India.
- Suree Teerarungsigul. (2006). **Landslide Prediction Model Using Remote Sensing, GIS and Field Geology: A Case Study of Wang Chin District, Phrae Province, Northern Thailand**. Ph.D. Geotechnology, Suranaree University of Technology, Thailand.

CHAPTER VII

CONCLUSION AND RECOMMENDATIONS

7.1 Conclusion

The objectives of the study are using geoinformatics technology and geological engineering data prepared in forms of GIS data to of the study area. All objectives of the study are achieved as explained and discussed in Chapter IV, V, and VI, respectively. In these Chapters, methodologies in detail were described, results from steps were enumerated and displayed in form of GIS raster layers, and discussions of results were also provided to respond to each objective. Evident by the results of the study, it is very important to confirm that remote sensing and GIS technology is a new approach and a capable tool in incorporating spatial models and geological engineering data for landslide, flash flood, and debris flow impact study.

The results in form of raster based GIS layers are presented to fit for planning and management of related geo-hazards and disasters in large-scale area. The results are more or less influenced by the scale of input data. Geology and land use data are in the scale of 1:50,000 while 5 m spatial resolution DEM data were generated from 1:4,000 contour map with 5 m interval. The model and process are mainly relied on GIS functions operating through all cells of input data. The results can be efficiently accepted for area planning and management. However, input data were acquired using area approach. Even though probability functions were applied to cover uncertain properties of any unit area, the accuracy of data can still be limited and varied from

point to point in a certain unit of classification. Therefore, the study results cannot be claimed to be comparable to the results from site investigation of which data are examined and measured in place.

To expect better results, detail mapping and application of other models are recommended to try. For example, input data of geology, land use, and engineering properties of soil and rock should be systematically investigated in more detail scale. Hydrological data of the area are very limited and can affect to some certain limit of the accuracy. Precipitation data used in the study were based on approximation of the surrounding stations. The area is also ungauged watershed. Application of other hydrological models and result comparison are recommended to perform.

7.2 Recommendations

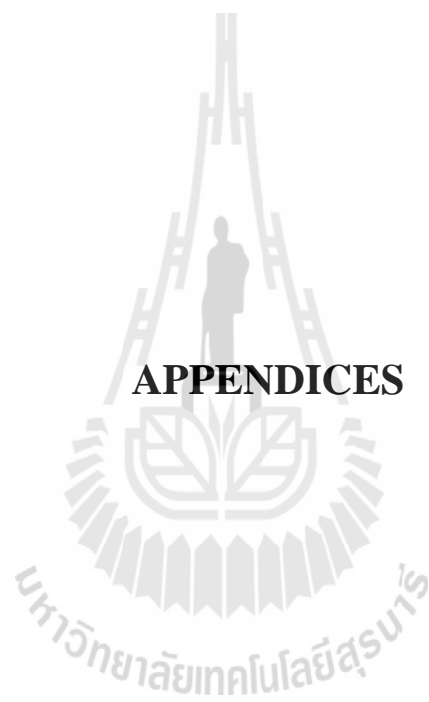
Although the methodology of landslide and flash flood susceptibility assessment is appropriated for identifying susceptibility area, parameters derivation and rare record of available data the limitation of accurate input. From the experience gained of this study, the recommendations for further study that could expect to better result are as follows.

- 1) The geologic unit based with scale 1:50,000 is the spatial complication of mixing kinds of rocks in a geological mapping unit. Its structure and any quantitative engineering property related to the landslide is not a single value. This geological map was modified based on field information and topographic. Therefore, the better spatial information of rock could be based on lithology of rock units which its physical characteristics are visible at outcrop.

2) Due to the limited time and budget, the engineering properties of rock consist of cohesion, average unit weight, and tangent of average friction angle were extract from literatures. Only C unit was tested by direct shear test in the engineering geological laboratory to prove properties from literatures. Moreover, by nature, each engineering property of a certain kind of rock will vary in a range, not a single value. Hence rock mechanic testing could be used to determine specified engineering properties of all rocks for slope stability analysis.

3) The precipitation for flash flood susceptibility assessment used daily rainfall which was regularly recorded at 7:00AM. Due to the definition of flash flood, it occurred and terminated very fast by heavy rainfall and the event often occurs less than 6 hours. The rainfall data for flash flood assessment could be high temporal and high spatial resolution. Many forest plantation camps in ungage area should have symmetric record rainfall from simple rain gage that can make by themselves. The telemeter of rainfall and water level could be installing in the high risk area for flash flood prediction and warning.

4) Although landslide and flash flood event in Nam Li watershed was never occurred previously, the hazardous intensity should compared with other event in the highland watershed.



APPENDICES

APPENDIX A

LANDSLIDE CLASSIFICATION

Table A.1 Classification of landslide suggested by Varnes (1978).

Type of movement	Type of material				
	Bedrock	Engineering soil			
		Predominantly coarse	Predominantly fine		
Falls		Rock fall	Debris fall	Earth fall	
Topples		Rock topple	Debris topple	Earth topple	
Slide	- Rotational	Few unit	Rock slump	Debris slump	Earth slump
	- Translational	Many unit	Rock block slide	Debris block slide	Earth block slide
Lateral spreads			Rock slide	Debris slide	Earth slide
			Rock spreads	Debris spreads	Earth spread
Flows			Rock flow (deep creep)	Debris flow	Earth flow (soil creep)
Complex	Combination of two or more principal types of movement				

Table A.2 Classification of landslide and down slope movements by Keller (2002).

Types of movement	Materials	
	Rock	Soil
Slides (variable water content and rate of movement)	Slump blocks	Slump blocks
Falls	Rock fall	Soil fall
	Rock creep	Soil creep
Flows	Unconsolidated materials (saturated)	
		Earth flow
		Mud flow
		Debris flow
		Debris avalanche
Subsidence	Rock	Soil
Complex	Combination of slides, slumping, and flowing	

Table A.3 Classification of landslide suggested by Hutchinson (1988).

Type of movement	Subdivision
A. Rebound Movement associated with	1. Man-made excavations. 2. Naturally eroded valleys.
B. Creep	1. Superficial, predominantly seasonal creep; mantle creep. 2. Deep-seated, continuous creep; mass creep. 3. Pre-failure creep; progressive creep. 4. Post-failure creep.
C. Sagging of mount slopes	1. Single-sided sagging associated with the initial stages of landsliding. 2. Double-sided sagging associated with the initial stages of double landsliding, leading to ridge spreading. 3. Sagging associated with multiple toppling.
D. Landslide	
1. Confined failures	a) In natural slope. b) In human-made slope.
2. Rotational failures	a) Single rotational slips. b) Successive rotational slips. c) Multiple rotational slips.
3. Compound failures (markedly non-circular, with listric or bi-planar slip)	a) Released by internal shearing towards the rear. b) Progressive compound slides.
4. Translational failures	a) Sheet slides. b) Slab slides. c) Peat slides. d) Rock slides (planar, stepped, and wedge). e) Slide of debris (debris slide, active layer slide, and sudden spreading failures)
E. Debris movement of flow-like form	
1. Mudslides	a) Sheets b) Lobes (lobate or elongate)
2. Periglacial mudslide	a) Sheets b) Lobes (lobate or elongate, active and relict)
3. Flow slides	a) In loose, cohesionless material. b) In lightly cemented, high porosity silts. c) In high porosity weak rock.
4. Debris flows Very to extremely rapid flows of wet debris	a) Involving weathered rock debris (except on volcanoes) (hillslope, channelized or mudflow). b) Involving peat, bog flow, bog bursts. c) Associated with volcanoes (hot lahars, cold lahars)
5. Rock avalanches/ stuzstroms Extremely rapid flows of dry debris	
F. Topples	1. Topples bounded by pre-existing discontinuities 2. Topples released by tension failure at rear of mass
G. Fall	1. Primary, involving fresh detachment of material; rock and soil falls. 2. Secondary, involving loose material, detached earlier; stone falls.
H. Complex slope movements	1. Cambering and valley-bulging 2. Block-type slope movements 3. Abandoned clay cliffs 4. Landslides breaking down into mudslides or flows at the toe 5. Slides caused by seepage erosion 6. Multi-tiered slides 7. Multi-storeyed slides

Table A.4 Classification of landslide suggested by EPOCH (1993).

Movement Type	Rock	Debris	Soil
Fall	Rock Fall	Debris Fall	Soil Fall
Topple	Rock Topple	Debris Topple	Soil Topple
Slide (Rotational)	single (slump) multiple successive	single multiple successive	single multiple successive
Slide (Translational) Non - rotational	Block Slide	Block Slide	Slab Slide
Planar	Rock Slide	Debris Slide	Mud Slide
Lateral Spreading	Rock Spreading	Debris Spread	Soil (Debris) Spreading
Flow	Rock Flow (Sackung)	Debris Flow	Soil Flow
Complex (with run-out or change of behaviour downslope; note that nearly all forms develop complex behaviour)	e.g. Rock avalanche	e.g. Flow Slide	e.g. Slump - earthflow

Note: A compound landslide is one that consist of more than one type e.g.. a rotational - translational slide. This should be distinguished from a complex slide where one form of failure develops into a second form of movement, i.e.. a change of behaviour downslope by the same material.

APPENDIX B

INFINITE SLOPE STABILITY ANALYSYS

For long slopes another potential failure mechanism is a failure plane, usually at relatively small depths, parallel to the material surface. The inter-slice force must cancel out and assuming the unit weight is the same above and below the water table. Then considering equilibrium, the forces act on the failure plane can write by

$$N = W \cos \beta = \gamma Z \cos \beta \quad \text{and} \quad T = W \sin \beta = \gamma Z \sin \beta, \quad (1)$$

where W is the weight of material, γ is the unit weight of material, Z is the thickness of slope material above sliding plane, and β is slope angle.

The normal and shear stresses on the assumed failure plane are given by

$$\sigma = \gamma Z \cos^2 \beta \quad \text{and} \quad \tau = \gamma Z \sin \beta \cos \beta. \quad (2)$$

The Mohr-Coulomb failure criterion given by

$$\tau = c + \sigma \tan \phi, \quad (3)$$

where τ is shear stress, c is the cohesion of material, σ is normal shear, and ϕ is the internal friction angle.

The water pressure can be determined from consideration of the flow as

$$u = \gamma_w Z_w \cos^2 \beta \quad (4)$$

The force due to water pressure on the failure surface is

$$U = \gamma_w Z_w \cos \beta \quad (5)$$

Where u is water pressure, γ_w is the unit weight of water, Z_w is the depth of water table, and U is the force due to water pressure. The normal and shear stresses on the assumed failure plane are thus given by when the force act on slope plane with β (degree) slope angle, the equations involved the Mohr-Coulomb failure criterion can be calculated FS by:

$$FS = \frac{c + (\gamma Z - \gamma_w Z_w) \cos^2 \beta \tan \phi}{\gamma Z \sin \beta \cos \beta} \quad (6)$$

where c is the cohesion (kN/m^2), γ is the unit weight of material (kN/m^3), γ_w is the unit weight of water (9.81 kN/m^3), Z is the thickness of slope material above sliding plane (m), Z_w is the thickness of saturated slope material above sliding plane (m), and ϕ is the internal friction angle (degree).

APPENDIX C

ROCK MECHANICS TESTING

C.1 Point Load Strength Index Testing

The point load strength index tests have been performed on-site. The test method and data reduction follow the American Society for Testing and Materials (ASTM) standard practice (ASTM D5731-95). Rock fragments (irregular lumps) with approximate sizes of 5×5×3 cm are loaded to failure. The point load strength index (I_s) is calculated by dividing the failure load by the fracture area. A total of 7 points have been tested with a minimum of 20 samples for each point. Appendix gives detailed results. The point load strength index is correlated to the uniaxial compressive strength (σ_c) by using a multiplied factor of 24 as suggested by the ASTM standard.

C.2 Direct Shear Testing

The direct shear tests are performed to determine the shear strength of the bedding planes in Phyllitic Shale/Bedded Chert Interbedded from Point C (SCAR). Four blocks containing bedding plane are transported to the GMR laboratory. Sample preparation, test method and data reduction follow the ASTM D5607 standard practice. The normal stresses of 100, 200, 300 and 400 MPa are used. Both peak and residual shear stresses are measured.

C.3 Slake Durability Index Testing

The slake durability index (SDI) test is performed on rock to predict the durability (strength) of the rock as a function of time. The sample preparation and test method follow the ASTM D4644 standard practice, except that up to two test cycles is performed, instead of two as suggested by the standards. The sample is prepared for testing under wet conditions. The results suggest that after rocks have been exposed to the surrounding environment, its strength will rapidly decrease. The method to predict the rock durability uses the concept proposed by Fuenkajorn (2008). The Δ SDI is a function of test cycles and time. The results suggest that after rock has been exposed to the surrounding environment, its strength will rapidly decrease. Water and fluctuation of temperatures accelerate the strength degradation. The exponential relation can best represent the change of rock durability with time. Under wet condition, rocks change from high durability rock to very low durability within 2 months.



APPENDIX D

THE FITTING RATIO CALCULATION

The FR is the fitting ratio of a number of cells obtained from intersect of PFI-1 (A) and scars cells (B) and the difference number of cells between the union of all PFI-1 and scar cells and the intersect of PFI-1 and scar cells $((A \cup B) - (A \cap B))$. $(A \cap B)$ is a number of PFI-1 cells falling in landslide scars which indicated the predicted accuracy while $(A \cup B) - (A \cap B)$ is the disagreement number of PFI-1 and landslide scar cells which indicated their discrepancy. The candidate LSI layer that could provide the best fitting or the highest ratio was identified to be the critical LSI.

Table D.1 The fitting ratio calculation of C unit.

LSI	A	B	$A \cap B$	$A \cup B$	$A \cup B - A \cap B$	FR
0.630	0	324245	0	324245	324245	-
0.700	0	324245	0	324245	324245	-
0.800	172	324245	0	324417	324417	-
0.900	22201	324245	6583	346446	339863	0.019
1.000	178940	324245	42689	503185	460496	0.093
1.100	543630	324245	104865	867875	763010	0.137
1.200	1097816	324245	177999	1422061	1244062	0.143
1.300	1662508	324245	231580	1986753	1755173	0.132
1.400	2137465	324245	265487	2461710	2196223	0.121
1.500	2476847	324245	285814	2801092	2515278	0.114
1.600	2734189	324245	298496	3058434	2759938	0.108
1.603	2734189	324245	298496	3058434	2759938	0.108

Table D.2 The fitting ratio calculation of P1 unit.

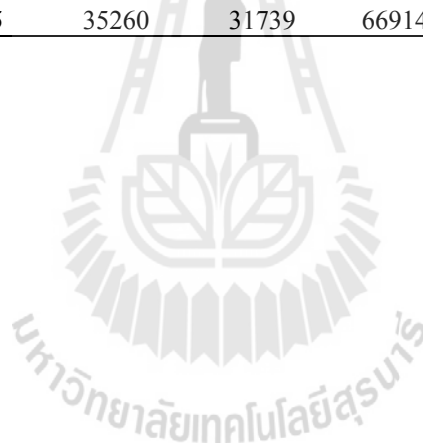
LSI	A	B	$A \cap B$	$A \cup B$	$A \cup B - A \cap B$	FR
0.926	0	70241	0	70241	70241	
1.000	402	70241	0	70643	70643	
1.100	901	70241	0	71142	71142	
1.200	3066	70241	166	73307	73141	0.002
1.300	12530	70241	1549	82771	81222	0.019
1.400	29712	70241	4181	99953	95772	0.044
1.500	86019	70241	9969	156260	146291	0.068
1.600	189007	70241	18739	259248	240509	0.078
1.700	316702	70241	29202	386943	357741	0.082
1.800	457238	70241	36259	527479	491220	0.074
1.900	607644	70241	43758	677885	634127	0.069
2.000	744687	70241	49471	814928	765457	0.065
2.100	873337	70241	53780	943578	889798	0.060
2.200	997765	70241	57433	1068006	1010573	0.057
2.300	1107769	70241	59807	1178010	1118203	0.053
2.400	1206130	70241	62364	1276371	1214007	0.051
2.480	1276644	70241	64229	1346885	1282656	0.050

Table D.3 The fitting ratio calculation of gr unit.

LSI	A	B	$A \cap B$	$A \cup B$	$A \cup B - A \cap B$	FR
1.026	0	10383	0	10383	10383	0.000
1.100	65	10383	47	10448	10401	0.005
1.200	1231	10383	690	11614	10924	0.063
1.300	1866	10383	838	12249	11411	0.073
1.400	3404	10383	1381	13787	12406	0.111
1.500	7785	10383	2036	18168	16132	0.126
1.600	16248	10383	3270	26631	23361	0.140
1.700	27902	10383	4147	38285	34138	0.121
1.800	41933	10383	4738	52316	47578	0.100
1.900	60989	10383	5362	71372	66010	0.081
2.000	85633	10383	6220	96016	89796	0.069
2.100	111065	10383	6625	121448	114823	0.058
2.200	139582	10383	7157	149965	142808	0.050
2.300	167974	10383	7639	178357	170718	0.045
2.400	192100	10383	7750	202483	194733	0.040
2.500	212625	10383	8105	223008	214903	0.038
2.600	241460	10383	8599	251843	243244	0.035
2.700	261649	10383	9065	272032	262967	0.034
2.800	278798	10383	9275	289181	279906	0.033
2.900	301364	10383	9366	311747	302381	0.031
3.000	317533	10383	9500	327916	318416	0.030
3.10	333727	10383	9644	344110	334466	0.029
3.196	349526	10383	9737	359909	350172	0.028

Table D.4 The fitting ratio calculation of Tr1 unit.

LSI	A	B	$A \cap B$	$A \cup B$	$A \cup B - A \cap B$	FR
0.768	0	35260	0	35260	35260	0.000
0.800	0	35260	0	35260	35260	0.000
0.900	0	35260	0	35260	35260	0.000
1.000	349	35260	120	35609	35489	0.003
1.100	737	35260	511	35997	35486	0.014
1.200	4554	35260	1737	39814	38077	0.046
1.300	11838	35260	3168	47098	43930	0.072
1.400	33527	35260	5527	68787	63260	0.087
1.500	63886	35260	8688	99146	90458	0.096
1.600	107668	35260	12554	142928	130374	0.096
1.700	168536	35260	16242	203796	187554	0.087
1.800	235106	35260	20206	270366	250160	0.081
1.900	302702	35260	22819	337962	315143	0.072
2.000	363596	35260	25652	398856	373204	0.069
2.100	429156	35260	27867	464416	436549	0.064
2.200	495432	35260	29200	530692	501492	0.058
2.300	557465	35260	31208	592725	561517	0.056
2.317	633885	35260	31739	669145	637406	0.050



APPENDIX E

RAINFALL DATA

E.1 The daily rainfall report of the Nam Li Watershed.

ข้อมูลปริมาณน้ำฝน
 สถานี...หน่วยจัดการต้นน้ำน้ำลิ...ตำบลน้ำหมื่น...อำเภอท่าปลา...จังหวัดอุตรดิตถ์.....
 ประจำเดือน.....พฤษภาคม.....พ.ศ. ...2549.....

วันที่	อุณหภูมิ (องศาเซลเซียส)			ปริมาณน้ำฝน (มม.)	การระเหย (มม.)	ความชื้น สัมพัทธ์ (%)	หมายเหตุ
	สูงสุด	ต่ำสุด	เฉลี่ย				
1				33.70			
2				-			
3				-			
4				-			
5				-			
6				25.02			
7				2.01			
8				-			
9				-			
10				22.00			
11				2.03			
12				-			
13				-			
14				26.70			
15				15.40			
16				1.08			
17				1.00			
18				2.00			
19				-			
20				3.70			
21				60.08			
22*				533.60			
23				40.00			
24				11.08			
25				-			
26				-			
27				-			
28				-			
29				-			
30				4.20			
31				3.60			
รวม				787.20			
เฉลี่ย				25.39			

ปริมาณน้ำฝนในรอบเดือน 787.20 มม. จำนวนวันที่ฝนตก 17 วัน
 ไล่เครื่องหมาย * ในวันที่ฝนตกมากที่สุด ลงนามผู้รายงาน.....

E.2 The 3 hours rainfall report of Uttaradit station.

ปริมาณฝน(มิลลิเมตร)

ราย 3 ชั่วโมง

ที่	รหัสสถานี-สถานี-จังหวัด	วันที่	เวลาทำการตรวจ								รวม	
			0100	0400	0700	1000	1300	1600	1900	2200		
486	351201-อุตรดิตถ์ จ.อุตรดิตถ์	1/5/2006	0	0	0	0	0	0	0	0	0	0
487	351201-อุตรดิตถ์ จ.อุตรดิตถ์	2/5/2006	0	0	0	0	0	0	0	0	0	0
488	351201-อุตรดิตถ์ จ.อุตรดิตถ์	3/5/2006	0	0	0	0	0	0	0	0	0	0
489	351201-อุตรดิตถ์ จ.อุตรดิตถ์	4/5/2006	0	0	0	0	0	0	0	0	0	0
490	351201-อุตรดิตถ์ จ.อุตรดิตถ์	5/5/2006	0	0	0	0	0	0	0	0	0	0
491	351201-อุตรดิตถ์ จ.อุตรดิตถ์	6/5/2006	0	0	0	0	0	0	0	0	0	0
492	351201-อุตรดิตถ์ จ.อุตรดิตถ์	7/5/2006	0	0.4	0	0	0	0	3.9	3.1	7.4	7.4
493	351201-อุตรดิตถ์ จ.อุตรดิตถ์	8/5/2006	0	0	0	0	0	0	4.4	2.9	7.3	7.3
494	351201-อุตรดิตถ์ จ.อุตรดิตถ์	9/5/2006	0	0	0	0	0	0	0	0	0	0
495	351201-อุตรดิตถ์ จ.อุตรดิตถ์	10/5/2006	0	0	0	0	0	0	0	0	0	0
496	351201-อุตรดิตถ์ จ.อุตรดิตถ์	11/5/2006	9.9	1.1	0	0	0	0	0	18.5	29.5	29.5
497	351201-อุตรดิตถ์ จ.อุตรดิตถ์	12/5/2006	0	0	0	0	0	0	0	0	0	0
498	351201-อุตรดิตถ์ จ.อุตรดิตถ์	13/5/2006	0	0	0	0	0	0	0	0	0	0
499	351201-อุตรดิตถ์ จ.อุตรดิตถ์	14/5/2006	0	0	T	0.1	0	0	0.4	17	17.5	17.5
500	351201-อุตรดิตถ์ จ.อุตรดิตถ์	15/5/2006	0.2	6.1	1.8	1.5	0.3	0	0	0	9.9	9.9
501	351201-อุตรดิตถ์ จ.อุตรดิตถ์	16/5/2006	2.6	9.2	3.8	0.5	0	0	0	0	16.1	16.1
502	351201-อุตรดิตถ์ จ.อุตรดิตถ์	17/5/2006	0	0	0	0	T	0	0	0	0	0
503	351201-อุตรดิตถ์ จ.อุตรดิตถ์	18/5/2006	0	0	0	0	T	0.3	0.7	0	1	1
504	351201-อุตรดิตถ์ จ.อุตรดิตถ์	19/5/2006	3	3.6	0.3	0	0	0	0	0	6.9	6.9
505	351201-อุตรดิตถ์ จ.อุตรดิตถ์	20/5/2006	0	0	0	0	0	0	0	0	0	0
506	351201-อุตรดิตถ์ จ.อุตรดิตถ์	21/5/2006	T	12	2.5	7	4.3	10.6	16	0.4	52.8	52.8
507	351201-อุตรดิตถ์ จ.อุตรดิตถ์	22/5/2006	41.9	39	1.2	4.8	5.7	11.8	35.2	59.7	199.3	199.3
508	351201-อุตรดิตถ์ จ.อุตรดิตถ์	23/5/2006	50.4	41.1	55	8.1	0	0	0	0	154.6	154.6
509	351201-อุตรดิตถ์ จ.อุตรดิตถ์	24/5/2006	0	0	0	0	0	0	0	0	0	0
510	351201-อุตรดิตถ์ จ.อุตรดิตถ์	25/5/2006	0	0	0	0	0	0	0	0	0	0
511	351201-อุตรดิตถ์ จ.อุตรดิตถ์	26/5/2006	0	0	0	0	0	0	0	0	0	0
512	351201-อุตรดิตถ์ จ.อุตรดิตถ์	27/5/2006	0	0	0	0	0	0	0	0	0	0
513	351201-อุตรดิตถ์ จ.อุตรดิตถ์	28/5/2006	0	0	0	0	0	0	0	0	0	0
514	351201-อุตรดิตถ์ จ.อุตรดิตถ์	29/5/2006	0	0	0	0	0	0	0	0	0	0
515	351201-อุตรดิตถ์ จ.อุตรดิตถ์	30/5/2006	2.5	0	0	0	0	0	0	16.7	19.2	19.2
516	351201-อุตรดิตถ์ จ.อุตรดิตถ์	31/5/2006	1.7	0	0.5	T	T	0	0	0	2.2	2.2

T = มีฝนแต่ไม่สามารถวัดได้ (Trace)

CURRICULUM VITAE

Name Mrs. Sirilak Tanang

Date of Birth July 4, 1969

Place of Birth Sungnoen Distric, Nakhorn Ratchasima, Thailand

Education 1994, B.Sc. (Geography), Department of Geography, Faculty of Education, Ramkhamhaeng University

Scholarship University Development Commission (UDC) Scholarship from the Commission on Higher Education

Position and Place of Work

Photogrammetrist in School of Remote Sensing, Institute of Science, Suranaree University of Technology

International Proceedings

Sunya Sarapirome and Sirilak Tanang. (2012). Probability of landslide occurrence mapping using probability density function: a case study of the Mae Tha Group in Nam Li watershed, Thailand. In **Proceeding of the 33rd Asian Conference on Remote Sensing**, November 26-30, 2012, Ambassador City Jomtien Hotel, Pattaya, Thailand.

Sirilak Tanang, Sunya Sarapirome, and Sasikarn Plaiklang. (2010). Landslide susceptibility map of Nam Li Watershed, Uttaradit, Thailand. In **Proceeding of the 31st Asian Conference on Remote Sensing**, November 1-5, 2010, the National Convention Center, Hanoi, Vietnam.